Universitat Autònoma de Barcelona

Tesi doctoral:

Estudi teòric de reaccions d'hidrogenació i d'oxidació en processos de catàlisi homogènia

Aleix Comas Vives

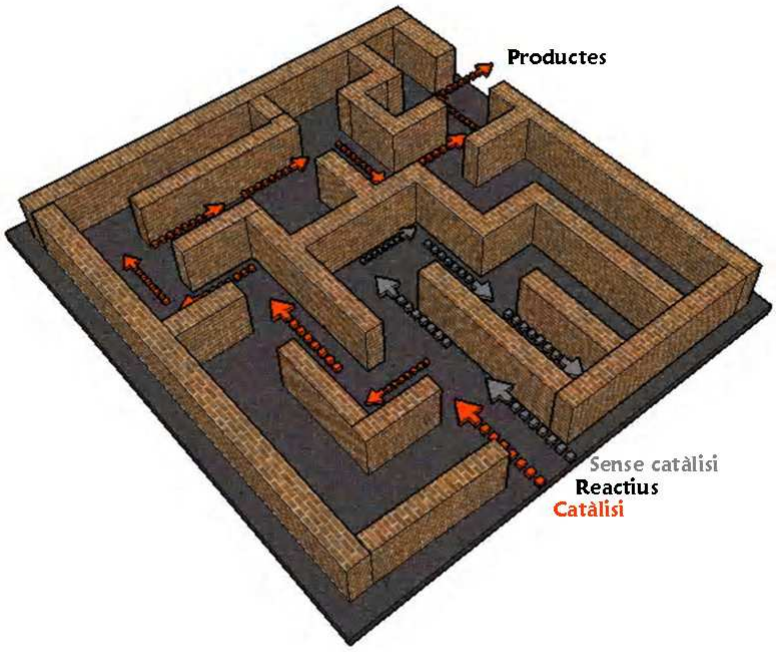

Directors: *Agustí Lledós Falcó i Gregori Ujaque Pérez*

Programa de doctorat: *Química Teòrica i Computacional*

Departament de Química, Facultat de Ciències

Universitat Autònoma de Barcelona

2009

Memòria presentada per aspirar al Grau de Doctor per

Aleix Comas Vives

Vistiplau,

Gregori Ujaque Pérez

Agustí Lledós Falcó

Bellaterra, 22/04/2009.

Al Francesc, a la Teresa,
a l'Anna i a la Marta

Universitat Autònoma de Barcelona

Tesi doctoral:

Estudi teòric de reaccions d'hidrogenació i d'oxidació en processos de catàlisi homogènia

Aleix Comas Vives

Directors: *Agustí Lledós Falcó i Gregori Ujaque Pérez*

Programa de doctorat: *Química Teòrica i Computacional*

Departament de Química, Facultat de Ciències

Universitat Autònoma de Barcelona

2009

Agraïments

Ara ja fa quatre anys i escaig del meu primer dia de treball a l'unitat. Aquell dia, en no haver-hi ningú al que havia de ser el meu despatx vaig entrar al que hi havia davant del nostre i un noi que després sabria que era conegut com a Prat i un altre que responia al nom d'Oriol em van donar la benvinguda i em van portar d'excursió. Van dir: "t'hem d'ensenyar... *quanta*!" I jo que em vaig preguntar: "què carai és *quanta*?" Llavors, em van portar a una porta blanca i a l'obrir-la hi vaig veure tot un seguit d'ordinadors connectats els uns als altres. Després, van dir amb un posat solemne: "Això és *quanta*." Jo em vaig quedar una mica xocat i vaig pensar que quina gent més rara, i em vaig dir:"on carai t'has fotut!" Després vaig entendre que allà (ara *spock*) era on enviàvem els càlculs de les reaccions químiques que modelitzàvem i és on vaig enviar el meu primer càlcul amb un *input* que em va ajudar a fer el Gregori. Després d'això han vingut un munt de càlculs, però també de *papers*, col·laboracions, cursos, *labmates*, congressos, xerrades, seminaris, estades, burocràcia (buff!), viatges...

El camí va començar quan vaig descobrir que hi havia gent que enlloc de fer reaccions al laboratori les feia als ordinadors estalviant-se així la toxicitat, les pudors, els experiments i tota la pesca. Vaig pensar que podia ser interessant i gràcies a l'interès que tenia per la química inorgànica, organometàl·lica i dels metalls de transició vaig anar a parlar amb el Gregori i l'Agustí, que dirigien el grup de modelització molecular de sistemes amb metalls de transició. Em van explicar el que feien i em va atreure i em vaig animar a començar el doctorat al seu grup. D'aquesta manera, vaig iniciar el llarg camí que ha dut a l'escriptura d'aquesta tesi que ara teniu a les mans. Així, el camí es va iniciar a Bellaterra, després va fer cap a Badajoz, on vaig assistir als cursos de doctorat, va tornar a Bellaterra, va fer via cap a Bristol, on vaig fer una estada al grup d'en Jeremy Harvey, va tornar un altre cop a Bellaterra, va prosseguir per Budapest, on vaig aprendre les vicissituds del mètode Car-Parrinello amb l'András Stirling, i finalment va tornar a Bellaterra, i així ha estat fins a dia d'avui.

Ha arribat el moment d'agrair a la bona gent que ha contribuït a fer aquesta tesi doctoral fos possible. En primer lloc, m'agradaria agrair als meus directors, Gregori i Agustí, la seva supervisió durant tot aquest temps. Al Gregori per les nombroses i

amenes discussions científiques que hem tingut, pel seu inestimable guiatge i perquè sempre millora tot el que li arriba a les mans. A l'Agustí perquè sempre hi és quan se'l necessita, perquè sempre et passa les referències clau i perquè sempre està al cas de tot. En l'apartat de recerca, també vull agrair a l'Avelino Corma i el seu grup i al Rinaldo Poli i el Rudy van Eldik i els seus respectius grups per les col·laboracions que han donat lloc als capítols 5 i 6 d'aquesta tesi doctoral, respectivament. També voldria agrair a l'András Stirling la seva contribució al darrer capítol d'aquesta tesi doctoral.

En segon lloc voldria agrair de manera particular a gent de la unitat. Al Max pels nombrosos cafès, tertúlia, consells i bones estones que hem compartit. Al Txarli, per tot el que vam viure durant els cursos de doctorat, per tota l'ajuda en les traves, burocràtiques o no, i per la seva manera de ser. Al Sergi per tots els croissants que ens ha arribat a portar i pels partits d'*squash* compartits, al Salva per les tasques d'*organizer* en congressos i al Gábor, hongarès catalanòfil de pro, per les seves lliçons magistrals de saviesa futbolística. També voldria agrair a gent que abans formava part del grup i que ha obert camí com la Maria, el Galí i l'Ainara. A l'Ainara i a la Maria per tot el que em van ajudar tan al despatx, com al despatx i a Bristol, respectivament. Al Galí per tota la seva ajuda en temes informàtics i de *linux* en particular. Altra gent de la unitat que voldria agrair personalment són la Raquel per la seva empatia i alegria, l'Edu pel seu bon rotllo, l'Erika pels seus dissenys, el Solans per les seves bromes monotemàtiques i el Marc per la seva ajuda com a tècnic informàtic. Seguidament, voldria agrair a la resta de gent de quimica física que ha contribuït a fer que la meva estada a la unitat fos d'allò més agradable i també als meus companys de Bristol i de Budapest.

En tercer lloc no em puc oblidar de la gent de Manresa, amb qui he compartit moltes coses més que caps de setmana: l'Helena, la Roser, la Vila, l'Enric, l'Oriol, la Gemma i l'Alba. I per acabar, no puc deixar-me aquella gent que més em fa ser com sóc. Els meus pares Francesc i Teresa, la meva germana Anna i la meva àvia Maria, per tot el que han fet per mi durant aquests vint-i-sis anys i escaig; i en darrer lloc la Marta, per tot el que hem viscut plegats i per estar sempre al meu costat.

A tothom, de debò, moltes gràcies. Bellaterra, abril del 2009.

Prefaci

"Es pot demostrar que aquesta història, del tot arbitrària, és veritat. Podria explicar innombrables històries diferents, i serien totes veritat: totes literalment veritat, en la natura dels traspassos, en l'ordre i en la data. El nombre dels àtoms es tan gran que sempre se'n trobaria un la història del qual coincidís amb una història qualsevol inventada a l'atzar. Podria explicar històries, i no acabaria mai, d'àtoms de carboni que es fan color o perfum a les flors; d'altres que, d'algues menudes a petits crustacis, a peixos cada vegada més grossos, es tornen de nou anhídrid carbònic a les aigües del mar, en una ronda perpètua i espantosa de vida i de mort, en què cada devorador és immediatament devorat; d'altres que arriben en canvi a una decorosa semieternitat a les pàgines esgrogueïdes d'algun document d'arxiu, o a la tela d'un pintor famós; d'aquells a qui tocà el privilegi de ser part d'un granet de pol·len, i deixaren la seva empremta fòssil a les roques per a la nostra curiositat; d'altres encara que baixaren fins a ser part dels misteriosos missatgers de forma del semen humà, i participaren en el subtil procés d'escissió, duplicació i fusió d'on cadascun de nosaltres és nat. N'explicaré en canvi només una altra, la més secreta, i l'explicaré amb la humilitat i la retenció de qui sap de bon començament que el seu tema és desesperat, els mitjans fluixos, i l'ofici de revestir els fets amb paraules fallit per la seva essència profunda. És altre cop entre nosaltres, en un got de llet. Està inserit en una llarga cadena, molt complexa, i tanmateix d'una mena que gairebé tots els seus anells són acollits pel cos humà. És engolit: i com que tota estructura vivent conté una desconfiança salvatge envers qualsevol aportació d'altre material d'origen vivent, la cadena és feta a trossos, i els trossos, un a un, acceptats o rebutjats. Un, aquell que ens toca, travessa el llindar intestinal i entra al corrent sanguini: migra, truca a la porta d'una cèl·lula nerviosa, hi entra i suplanta un altre carboni que en formava part. Aquesta cèl·lula pertany a un cervell, i aquest és el meu cervell, el meu, ara mentre escric, i la cèl·lula en qüestió, i en ella l'àtom en qüestió, està adscrita al meu escriure, en un joc gegantí i minúscul que encara ningú no ha descrit. És la que en aquest instant, fora d'una laberíntica trama de sís i de nos, fa que la meva mà corri seguint un cert camí sobre el paper, el senyali amb

aquestes volutes que són signes; un doble salt, cap amunt i cap avall, entre dos nivells d'energia condueix aquesta meva mà a imprimir damunt del paper aquest punt: aquest."

Primo Levi. El sistema periòdic.

Índex

Part I

Introducció

Capítol 1

Catàlisi

1.1 Què és la catàlisi?

El terme catàlisi (descompondre químicament)[†] fou introduït per Berzelius el 1836 per tal d'explicar vàries reaccions de descomposició i transformació. El terme encara contenia certes ressonàncies alquímiques ja que assumia que la catàlisi posseïa *poders especials* que podien influir en l'afinitat de les substàncies químiques. Actualment, la IUPAC defineix la catàlisi com l'acció d'una substància (catalitzador) que incrementa la velocitat d'una reacció sense modificar-ne la variació global d'energia de Gibbs estàndard (ΔG, veure figura 1.1).[1] Aquesta definició és molt similar a la que donà Ostwald[‡] l'any 1895: "*un catalitzador accelera una reacció química sense afectar la posició de l'equilibri*". Per tant, la clau de la catàlisi és que els catalitzadors afecten la cinètica i no la termodinàmica de les reaccions químiques; és a dir, que ΔG no varia mentre que l'energia de Gibbs d'activació ($\Delta G^{\ddagger}$) si que ho fa.

Les diferents etapes de reacció ens porten de reactius a productes tot recuperant el catalitzador inicial, fent que la catàlisi sigui un procés cíclic. Aquest conjunt d'etapes formen un *cicle catalític*.[2]

Un fet que no és del tot evident és que un catalitzador tan accelera la formació dels productes a partir dels reactius com la formació dels reactius a partir dels productes,[3] ja que ambdós processos passen pel mateix camí degut al *principi de reversibilitat*

[†]el mot prové del grec: "*kata*", que significa complet, i "*lysis*", que significa ruptura.

[‡]Premi Nobel de Química l'any 1909.

microscòpica.

Un catalitzador no sempre sortirà exitós de la seva contesa. Si l'enllaç entre qualsevol dels reactius i el catalizador és massa feble, hi haurà poca conversió. Tanmateix, si l'enllaç entre els catalitzadors i un dels reactius és massa fort, els altres reactius no estaran disponibles alhora de formar els productes.

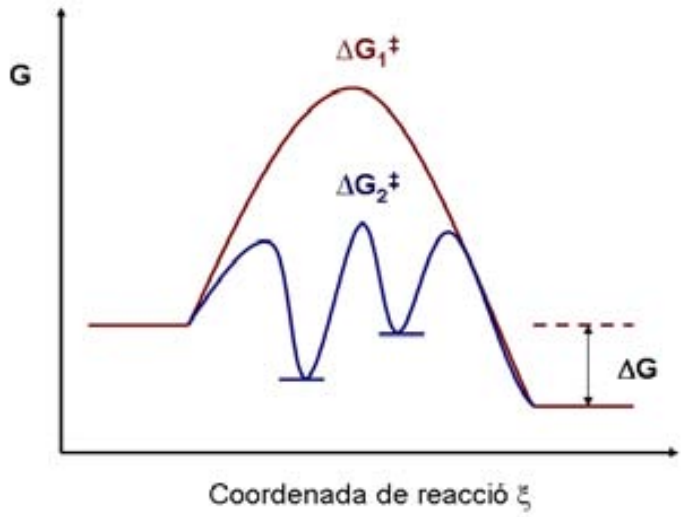

Figura 1.1: *Comparació entre l'energia de Gibbs d'activació d'una reacció no catalitzada ($\Delta G_1^{\ddagger}$) i la d'una reacció catalitzada ($\Delta G_2^{\ddagger}$). La termodinàmica de la reacció ve donada per ΔG.*

D'altra banda, si reactius o productes formen enllaços forts amb el catalitzador, la reacció pot esdevenir improbable provocant el que s'anomena enverinament degut a reactius o a productes. De la mateixa manera, si el producte s'enllaça massa fortament al catalitzador la reacció tampoc no pot prosperar perquè no s'allibera el

catalitzador per tal de què pugui prosseguir amb el cicle catalític produint l'anomenat enverinament degut al producte o als productes. Per tant, podríem dir que la millor combinació entre un catalitzador i els reactius és aquella que fa que els enllaços entre ambdós no siguin ni massa febles ni massa forts. Aquest concepte qualitatiu es coneix amb el nom de principi de Sabatier.[†]

Cal esmentar que, a banda d'accelerar reaccions químiques, els catalitzadors també ens permeten millorar la selectivitat dels processos; és a dir, obtenir productes desitjats enfront d'altres que no ho són: permetent formar certs productes químics enfront d'altres (quimioselectivitat), fent que la mateixa reacció química tingui lloc només en un lloc d'una molècula (regioselectivitat) o facilitant que es formi majoritàriament un diaestereoisòmer (diaestereoselectivitat) o un enantiòmer (enantioselectivitat).[2,4]

1.2 Tipus de catalitzadors

Els catalitzadors no són tots iguals ni actuen de la mateixa manera i, tot i que es poden classificar de diferents maneres, aquí els classificarem en base a l'estat d'agregació. A la figura 1.2 es pot veure una classificació esquemàtica dels diferents tipus de catalitzadors.[5] Així, si tan el catalitzador com els reactius i els productes es troben a la mateixa fase, parlem de catàlisi homogènia. Aquests, es poden dividir en catàlisi àcid-base, compostos de metalls de transició i organocatàlisi,[6] aquest darrer un camp emergent. D'altra banda, en catàlisi heterogènia els catalitzadors es troben a una fase diferent a la dels reactius. D'aquesta manera, els catalitzadors heterogenis generalment són sòlids que catalitzen reaccions de molècules en fase gas o en solució. També hi ha formes intermèdies com catalitzadors homogenis suportats (catalitzadors homogenis heterogenitzats). A més, hi ha els enzims, que en la nostra classificació es troben a mig camí entre els catalitzadors homogenis i els heterogenis, i un altre camp emergent com la nanocatàlisi. Per saber si per una reacció concreta ens cal un procés de catàlisi homogènia o heterogènia ens cal conèixer les característiques d'ambdós

[†]Paul Sabatier compartí amb Victor Grignard el premi Nobel de Química l'any 1912.

tipus de catàlisi. Així, els avantatges de la catàlisi homogènia són la selectivitat, l'elevada activitat, i les condicions suaus de reacció.

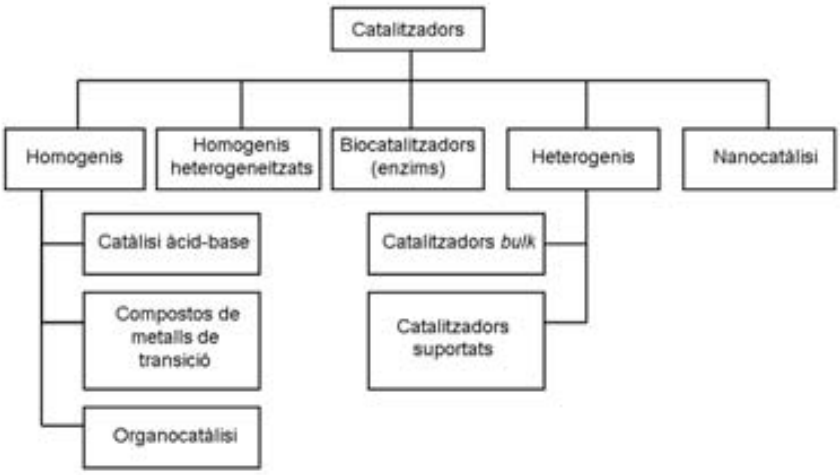

Figura 1.2: *Una classificació dels tipus de catalitzadors.*

Per contra, el major inconvenient de la catàlisi homogènia és la separació del catalitzador dels productes ja que es formen a la mateixa fase, fet que en limita l'aplicació industrial i, com a resultat, la majoria dels productes industrials s'obtenen mitjançant processos de catàlisi heterogènia.[5] En processos catalitzats per metalls de transició generalment es treballa a temperatures inferiors a 200 ℃.[7] En aquest rang de temperatures els catalitzadors homogenis es poden estabilitzar o modificar per l'addició dels lligands, essent l'efecte del solvent potencialment considerable.[5] Pel que fa a la catàlisi heterogènia, els reactius es poden separar amb facilitat, perquè com ja s'ha esmentat, els catalitzadors heterogenis generalment són sòlids que catalitzen reaccions de molècules en fase gas o en solució. Una altra diferència que presenten ambdues classes de catalitzadors és el grau de dispersió. Els catalitzadors homogenis presenten un grau de dispersió més alt que els catalitzadors heterogenis ja que cada molècula de catalitzador és potencialment activa. Per contra, en els catalitzadors heterogenis només els àtoms de la superficie són reactius, i en conseqüència, els catalitzadors homogenis exhibeixen una activitat més alta per unitat de massa que els catalitzadors heterogenis.[5] Això també permet usar una concentració de catalitzador

més baixa en catàlisi homogènia que en catàlisi heterogènia, a més de condicions de reacció més suaus. Una altra característica que diferencia la catàlisi homogènia de l'heterogènia i que és d'interès en aquesta tesi doctoral és que en catàlisi homogènia el lloc actiu és més conegut i, per tant, se solen esbrinar amb més precisió els mecanismes de reacció.

Pel que fa als biocatalitzadors, com ja hem dit, es troben a mig camí entre la catàlisi homogènia i la catàlisi heterogènia. En la majoria dels casos els biocatalitzadors són enzims, els quals són extremadament selectius i eficients. Un enzim és capaç de completar 1000 cicles catalítics en un segon mentre que, en comparació, els catalitzadors homogenis i heterogenis convencionals són lents i ineficients ja que solen completar entre 100 i 10000 cicles però per hora![2] A més a més, els enzims permeten treballar en condicions suaus, és a dir, a temperatura ambient, solució aquosa i pH proper a 7.[5] Per tant, no ha d'estranyar que els enzims resultin font d'inspiració pel disseny de nous catalitzadors!

En aquesta tesi, les reaccions que s'han estudiat formen part de la família de la catàlisi homogènia i en concret del subgrup de les reaccions catalitzades per compostos de metalls de transició.

1.3 Activitat i eficiència dels catalitzadors

Tot i que inicialment s'assumí que el catalitzador roman inalterat al llarg de la reacció[†] és evident que un catalitzador mai no es comporta idealment, ja que pot patir canvis que poden fer que la seva activitat esdevingui menor a mesura que transcorre la reacció, és a dir, que es desactivi.[5] Per tant, per tal de comparar els catalitzadors és cabdal obtenir magnituds que ens permetin mesurar la seva eficència.

El químic suec Svante August Arrhenius[‡] relacionà empíricament la constant de velocitat amb la temperatura per una reacció elemental mitjançant l'equació que porta el seu nom (Equació 1.1).[8] En principi, l'equació només és aplicable a reaccions

[†]es refereix a quan s'ha completat un cicle catalític.

[‡]premi Nobel de Química l'any 1903.

en fase gas tot i que sovint s'aplica de manera general:

$$k = Ae^{\frac{-E_a}{RT}} \tag{1.1}$$

on A és el factor prexponencial (també s'anomena factor de freqüència), E_a és l'energia d'activació, R és la constant universal dels gasos (8.314 $J{\cdot}mol^{-1}{\cdot}K^{-1}$) i T la temperatura absoluta (en graus Kelvin).[2,3,9,10] Malgrat que A sí que varia amb la temperatura, la seva dependència és normalment feble comparada amb la del terme exponencial i per tant generalment es pot negligir.[3] Com a regla general (aproximadament) cada 10 K es dobla la velocitat. Si la barrera és inferior a 5 $kcal{\cdot}mol^{-1}$, la reacció està controlada per difusió, mentre que si és superior diem que està controlada químicament.[2] L'energia d'activació és un paràmetre molt important en catàlisi ja que ens diu la barrera energètica que s'ha de superar per tal que una reacció donada tingui lloc. Així, partir de l'equació 1.1 podem arribar a l'equació 1.2, que ens diu que l'energia d'activació és un valor empíric que es pot determinar a partir de la variació de la constant de velocitat amb la temperatura:[9]

$$E_a = -R\frac{d\ln k}{d(\frac{1}{T})} = RT^2\frac{d\ln k}{dT} \tag{1.2}$$

L'energia d'activació també pot prendre valors negatius, cosa que significa que la constant de velocitat disminueix a l'augmentar la temperatura.[10]

Una teoria important alhora d'estudiar processos químics, aquesta de base teòrica, és la teoria de l'estat de transició (TET), la qual fou desenvolupada l'any 1935 per Eyring d'una banda[11] i per Evans i Polanyi de l'altra.[12] Hi poden haver diferents formulacions de la TET però aquí comentarem l'anomenada formulació termodinàmica.[9,13]

Imaginem que la reacció entre els reactius inicials A i B dongui lloc a una configuració dels àtoms tal que l'espècie activada $AB^{\ddagger}$ o estat de transició pugui donar lloc espontàniament tan als reactius inicials com al producte final i que, a més a més, estigui en equilibri amb els reactius inicials.

$$A + B \rightleftharpoons AB^{\ddagger} \rightarrow P \tag{1.3}$$

Degut a l'equilibri tenim una constant d'equilbri $K_c^{\ddagger}$ que la podem expressar de la següent manera:

$$K_c^{\ddagger} = \frac{[AB^{\ddagger}]}{[A][B]} \tag{1.4}$$

Se suposa que la concentració de l'espècie $AB^{\ddagger}$ és totalment menyspreable respecte les concentracions de les espècies A i B, de manera que es pot considerar que les concentracions de A i de B no varien. D'altra banda, la velocitat de la reacció la podem expressar en funció de la formació dels productes, on $k^{\ddagger}$ és la constant de velocitat que ens porta de $AB^{\ddagger}$ a productes:

$$\frac{d[P]}{dt} = k^{\ddagger}[AB]^{\ddagger} \tag{1.5}$$

El valor de $k^{\ddagger}$ ens el dóna la termodinàmica estadística i és igual a k_BT, on k_B és la constant de Boltzmann ($1.38{\cdot}10^{-23}$ $J{\cdot}K^{-1}$) i T la temperatura (en graus Kelvin).

Gràcies a les equacions 1.4 i 1.5 acabem obtenint:

$$\frac{d[P]}{dt} = \frac{k_BT}{h} K_c^{\ddagger}[A][B] \tag{1.6}$$

Finalment, la relació de van t'Hoff ens relaciona la constant d'equilibri amb la variació d'energia de estàndard Gibbs d'activació:

$$\Delta G_0^{\ddagger} = -RT \ln K_c^{\ddagger} \tag{1.7}$$

on $\Delta G_0^{\ddagger}$ és la diferència entre l'energia de Gibbs estàndard de l'estat de transició i la dels reactius A i B.

Per tant, acabem obtenint:

$$k = \frac{k_BT}{h} e^{-\frac{\Delta G_0^{\ddagger}}{RT}} \tag{1.8}$$

Com que $\Delta G_0^{\ddagger}$ es pot expressar en termes d'entalpia ($\Delta H_0^{\ddagger}$) i d'entropia ($\Delta S_0^{\ddagger}$) podem dividir l'equació 1.8 en dos termes:

$$\Delta G_0^{\ddagger} = \Delta H_0^{\ddagger} - T\Delta S_0^{\ddagger} \tag{1.9}$$

$$k = \frac{k_BT}{h} e^{\frac{\Delta S_0^{\ddagger}}{R}} e^{-\frac{\Delta H_0^{\ddagger}}{RT}} \tag{1.10}$$

Finalment, a partir de l'equació 1.2, tot substituïnt-hi l'equació 1.10 acabem obtenint la relació entre l'entalpia d'activació i l'energia d'activació:

$$E_a = \Delta H_0^{\ddagger} + RT \tag{1.11}$$

Ara, si es realitzen càlculs teòrics per tal d'estudiar reaccions químiques només ens faltarà saber la relació entre magnituds obtingudes experimentalment com ara E_a, $\Delta H^{\ddagger}$ i $\Delta G^{\ddagger}$, i l'energia potencial (E) obtinguda dels càlculs teòrics. Si a E hi afegim l'energia de punt zero i les correccions tèrmiques de l'energia interna obtenim l'energia interna a una temperatura donada (U(T)). A partir d'aquesta magnitud podem calcular l'entalpia i l'energia lliure de Gibbs a través de les fórmules:

$$H = U + PV \tag{1.12}$$

$$G = H - TS \tag{1.13}$$

Pel que fa a l'energia d'activació l'obtindrem a través de l'equació 1.11. D'aquesta manera, ja haurem obtingut valors per les magnituds experimentals E_a, $\Delta H^{\ddagger}$ i $\Delta G^{\ddagger}$ a partir de la E obtinguda dels càlculs teòrics.

Si finalment inserim l'equació 1.11 a l'equació 1.10 acabem relacionant l'equació d'Arrhenius amb la teoria de l'estat de transició tot obtenint una fórmula pel valor prexponencial de l'equació d'Arrhenius:

$$A = \frac{k_B T}{h} e^{(1+\frac{\Delta S_0^{\ddagger}}{R})} \tag{1.14}$$

Ara que hem definit paràmetres que ens permeten avaluar l'activitat dels catalitzadors passarem a descriure les propietats que ens permeten comparar l'eficiència dels catalitzadors: el "*turnover number*" (TON) i el "*turnover frequency*" (TOF).[2]

El TON són les voltes al cicle catalític que dóna el catalitzador fins que es desactiva, és a dir, el nombre de molècules de reactius que una molècula de catalitzador pot convertir a productes. Per tant, en un catalitzador ideal el TON fóra infinit. Pel que fa al TOF, és el TON dividit pel temps. Per tant, el TON és una mesura del temps de vida del catalitzador, mentre que el TOF és una mesura de l'activitat pròpiament

dita. De totes maneres, les definicions varien segons els tipus de catalitzadors. En catàlisi heterogènia, per exemple, el TON i el TOF es defineixen per lloc actiu o per gram de catalitzador ja que no se sap amb certesa quantes molècules de catalitzador hi ha a la superfície, mentre que en biocatàlisi (d'on prové el terme), el TON i el TOF es defineixen com la velocitat mesurada quan totes les molècules d'enzim estan complexades amb reactiu dividides per la concentració total d'enzim. Per tant, sempre que es treballi amb el TON i el TOF és important donar les unitats per tal que no hi hagi malentesos.

Capítol 2

Hidrogenacions i oxidacions de compostos insaturats en catàlisi homogènia

2.1 Hidrogenacions en catàlisi homogènia

En catàlisi homogènia el terme hidrogenació es refereix a una reacció química en la qual un o més hidrògens s'incorporen al producte(s) de reacció sota l'acció d'un catalizador dissolt a la mateixa fase que els reactius. L'hidrogen molecular no és l'única font d'hidrogen ja que també ho poden ser alcohols (normalment 2-propanol), glicols, aldehids, éters, amides o fins i tot hidrocarburs aromàtics. En aquest cas, parlem de reaccions de transferència d'hidrogen.[14]

2.1.1 Activació de l'hidrogen molecular

Començarem parlant de l'hidrogen com a font d'hidrogenació. En aquest cas, hem de trencar la molècula d'hidrogen, la qual no és gens reactiva, ja que tot i ser-ho més que d'altres molècules petites com ara el N_2 o el CO presenta una energia de dissociació de 104 kcal·mol^{-1}. Malgrat tot, la hidrogenació pot tenir lloc i pot ser catalitzada entre altres per compostos dels metalls de transició, una àmplia varietat dels quals són capaços d'actuar com a catalitzadors d'hidrogenació en condicions suaus.

Per tal que hi hagi reacció l'hidrogen s'ha d'activar i aquesta activació pot tenir lloc de dues maneres: mitjançant una activació homolítica o mitjançant una activació heterolítica tal i com es mostra a la figura 2.1:[15,16]

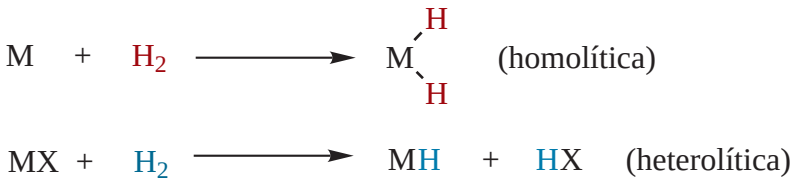

Figura 2.1: *Vies d'activació de l'hidrogen molecular.*

Ambdós processos poden ocórrer directament o bé a través de complexos dihidrogen no clàssics tipus $M(\eta^2 - H_2)$. La caracterització dels primers complexos de dihidrogen data de mitjans dels anys 80 i vingué de la mà de Kubas i col·laboradors amb complexos tipus $[M(CO)_3(PR_3)_2(\eta^2\text{-}H_2)]$ on M = Mo, W i R = Cy, ^{i}Pr.[17] L'enllaç en aquests compostos és anàleg al que s'usa per descriure l'enllaç amb l'etilè. L'orbital σ H-H dóna densitat electrònica a un orbital d buit de simetria σ. La interacció es reforça amb la retrodonació dels orbitals d ocupats del metall a l'orbital σ^* buit de l'hidrogen (figura 2.2).[18]

L'activació homolítica és una addició oxidant, ja que formalment dos electrons es transfereixen del metall als hidrògens i per tant aquest augmenta en dues unitats el seu estat d'oxidació. En conseqüència, per tal que l'activació homolítica tingui lloc, un metall en estat d'oxidació inicial (n) ha de tenir un estat d'oxidació (n + 2) estable, a més de ser capaç de tolerar un increment del nombre de coordinació en dues unitats i de ser capaç d'acceptar un parell d'electrons.[19]

En canvi, l'activació heterolítica no implica cap modificació de l'estat d'oxidació ni del nombre de coordinació de l'àtom metàl·lic. Implica que el grup acceptor, generalment un lligand, accepti un hidrogen en forma de protó mentre que l'altre hidrogen s'enllaci al metall en forma d'hidrur. L'habilitat de trencar l'hidrogen depèn de les propietats electròniques tan del metall com dels lligands[20] i està relacionada amb l'habilitat de poblar l'orbital σ^* del H_2. La retrodonació s'afavoreix en orbitals d difusos alts en energia ja que el forat d'energia entre els orbitals moleculars que

interaccionen és més petita i per tant el seu solapament és major. El trencament de l'hidrogen també es veu afectat per la naturalesa dels lligands (si són σ-donadors s'afavoreix en front de si són π-acceptors). Si el metall és ric en electrons, l'activació de l'hidrogen pot ocórrer més fàcilment per addició oxidant ja que pot retrodonar més densitat electrònica a l'orbital σ^* del H_2 tot facilitant el trencament de l'enllaç σ H-H. En canvi, per metalls poc rics en electrons l'activació heterolítica de l'hidrogen sol ser més freqüent i, per tant, és més habitual en metalls de la part esquerra del bloc *d*. No obstant, últimament s'ha vist que també pot ocórrer en metalls situats al centre i a la dreta del bloc *d*.[21–32]

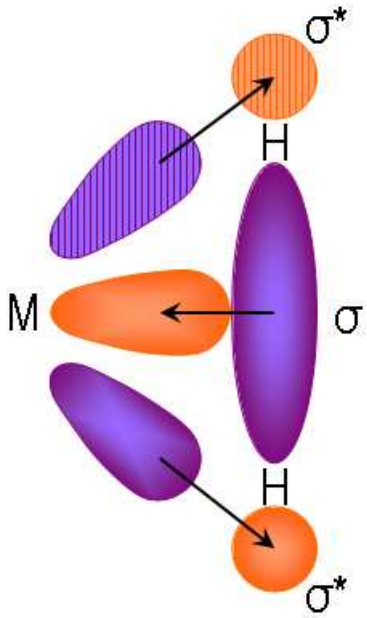

Figura 2.2: *Representació de la donació i retrodonació en els complexos de dihidrogen. El color lila és pels orbitals plens mentre que el color taronja és pels orbitals buits. D'altra banda, els orbitals tramats són de signe contrari als que no ho són.*

Darrerament, s'ha proposat que per diferents catalitzadors la hidrogenació heterolítica podia ésser assistida per solvents polars pròtics com ara alcohols.[33–37] En aquest cas, l'estat de transició del procés transcorre a través d'un anell de 6 membres

tal i com es mostra a la part dreta de la figura 2.3, en contraposició a la metàtesi σ [2 + 2] via un anell de 4 membres del procés no assistit, la qual es mostra a la part esquerra de la figura 2.3. Mitjançant càlculs teòrics també s'ha proposat que una base externa sigui capaç d'assistir el procés d'activació heterolítica en un mecanisme per passos; primer acceptant un protó d'un complex dihidrogen i després cedint-lo a un lligand acceptor.[38]

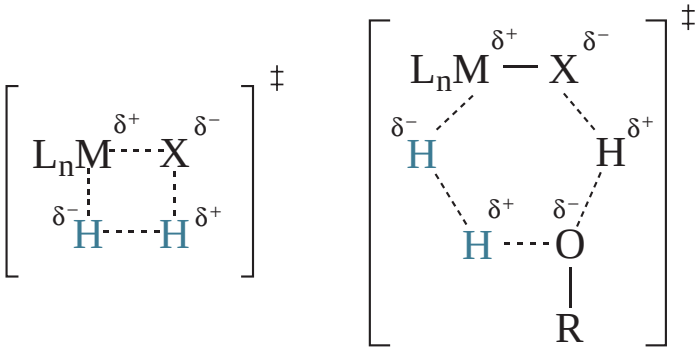

Figura 2.3: *Esquema dels estats de transició del trencament heterolític de l'hidrogen no assistit (a l'esquerra) i assistit per una molècula de solvent polar pròtic (a la dreta).*

2.1.2 Mecanismes d'inserció

L'activació de l'hidrogen genera hidrurs metàl·lics, és a dir, espècies amb almenys un enllaç M-H. Aquestes espècies s'anomenen així independentment de la polarització que presenti l'enllaç, ja sia H^-, H o H^+ i desenvolupen un paper important en cicles catalítics d'hidrogenació. En catàlisi homogènia, els catalitzadors clàssics d'hidrogenació sovint es basen en metalls de transició com ara Rh, Ir, Ru i Os.[14] Tot i això, tal i com es mostrarà al capítol 5 d'aquest treball, també complexos basats en d'altres metalls, com ara or amb lligands semi-salen, són capaços de catalitzar reaccions d'hidrogenació. De fet, tan el mecanisme d'hidrogenació de complexos d'or semi-salen com el de complexos anàlegs de pal·ladi han estat objecte d'estudi al capítol 5 d'aquesta tesi doctoral mitjançant càlculs teòrics mitjançant la teoria del funcional de la densitat (DFT). Un altre complex d'or, el $(AuCl)_2$[(R,R)-Me-Duphos], també és capaç d'hidrogenar enantioselectivament alquens i imines amb una activitat similar

als catalitzadors clàssics d'iridi o de platí.[39]

Pel que fa als mecanisme d'hidrogenació, molts d'aquests complexos operen a través de mecanismes d'inserció del substrat insaturat a l'enllaç M-H.[14,40] Per a la hidrogenació d'alquens, clàssicament es contemplen dues rutes possibles d'hidrogenació en funció del nombre d'hidrurs que continguin els catalitzadors: la ruta monohidrídica i la ruta dihidrídica. Els monohidrurs (d'aquí ruta monohidrídica), espècies amb un sol enllaç M-H, donen lloc a un cicle catalític com el que es mostra a la figura 2.4. És a dir, transcorren a través d'un intermedi M-alquil i la posterior entrada d'hidrogen molecular permet regenerar el monohidrur tot alliberant el producte final: l'alcà.

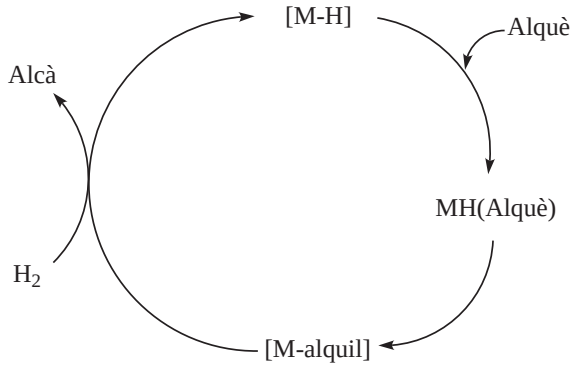

Figura 2.4: *Ruta a través del monohidrur.*

Com a exemple de complex que segueix la ruta monohidrídica hi ha el $RhH(CO)(PPh_3)_3$ en la hidrogenació d'alquens, essent la dissociació d'una fosfina una etapa necessària per tal de coordinar l'alquè.[41] Tal i com es veurà al capítol 5 d'aquesta tesi doctoral tan els complexos d'or amb lligands semi-salen com els compostos anàlegs de pal·ladi segueixen l'esquema general mostrat a la figura 2.4. Un altre complex que segueix la ruta monohidrídica és el catalitzador $RuCl_2(PPh_3)_3$ en la hidrogenació d'alquens terminals enfront d'alquens interns.[42] En aquest complex, l'activació de l'hidrogen es dóna heterolíticament donant lloc al complex $RuHCl(PPh_3)_3$ i a HCl.

Pel que fa a la ruta dihidrídica, aquesta dóna lloc a un cicle catalític on entren a l'esfera de coordinació primer la molècula d'hidrogen i després l'alquè o viceversa, per finalment eliminar l'alcà gràcies a la transferència dels dos hidrurs al substrat

(figura 2.5). El complex $[RhCl(PPh_3)_3]$ (també anomenat catalitzador de Wilkinson) és un exemple de compost que segueix la ruta dihidrídica, essent un dels casos més paradigmàtics i estudiats dels catalitzadors d'hidrogenació.

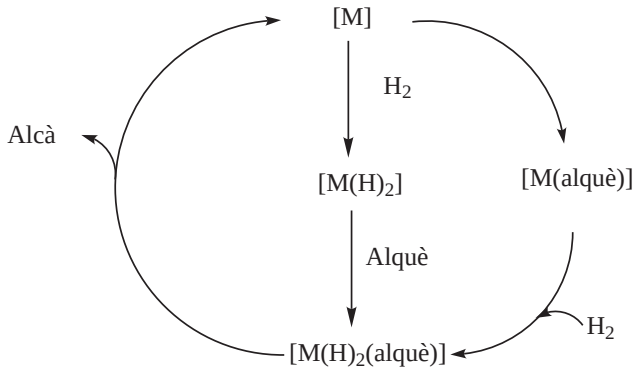

Figura 2.5: *Ruta a través del dihidrur.*

Aquest complex fou preparat per Bath i Vaska l'any 1963[43,44] i fou estudiat posteriorment per Wilkinson l'any 1965.[†,45,46] S'usa per hidrogenar una sèrie de compostos orgànics insaturats[‡] i segueix la ruta dihidrídica amb prèvia activació de la molècula d'hidrogen. La reacció té lloc en condicions suaus: temperatura ambient i pressió atmosfèrica del H_2. El mecanisme proposat que té més acceptació és el de Halpern provinent d'estudis cinètics[47–50] i estudis espectroscòpics de RMN i de IR.[51] Per aquest ordre tenen lloc: la dissociació d'un lligand, l'addició oxidant de la molècula de H_2, la coordinació d'una molècula d'etilè, la inserció de l'etilè a l'enllaç M-H, una isomerització i, finalment, l'eliminació reductiva, etapes que es mostren a la figura 2.6. Morokuma i col·laboradors proposaren el pas d'isomerització dins del cicle catalític mitjançant càlculs teòrics.[52,53] De fet, aquest treball fou el primer que estudià un cicle catalític complet mitjançant càlculs teòrics i es trobà una barrera pel pas determinant de la reacció (inserció + isomerització) d'unes 20 kcal·mol^{-1} a nivell Hartree-Fock (HF)[§] en concordança amb els resultats experimentals.[54–56] A

[†]premi Nobel de Química l'any 1973.

[‡]Tot i que normalment s'usa per hidrogenar enllaços C=C també s'ha fet servir per hidrogenar altres enllaços insaturats com ara enllaços C=O.

[§]Mitjançant càlculs puntuals MP2 la barrera calculada era superior, prenent un valor al voltant

més, aquest catalitzador té la particularitat que el seu mecanisme depèn de la font d'hidrogen, ja que en reaccions de transferència d'hidrogen a cetones fent servir 2-propanol com a font d'hidrogen s'ha proposat un mecanisme monohidrídic enlloc de dihidrídic.[57]

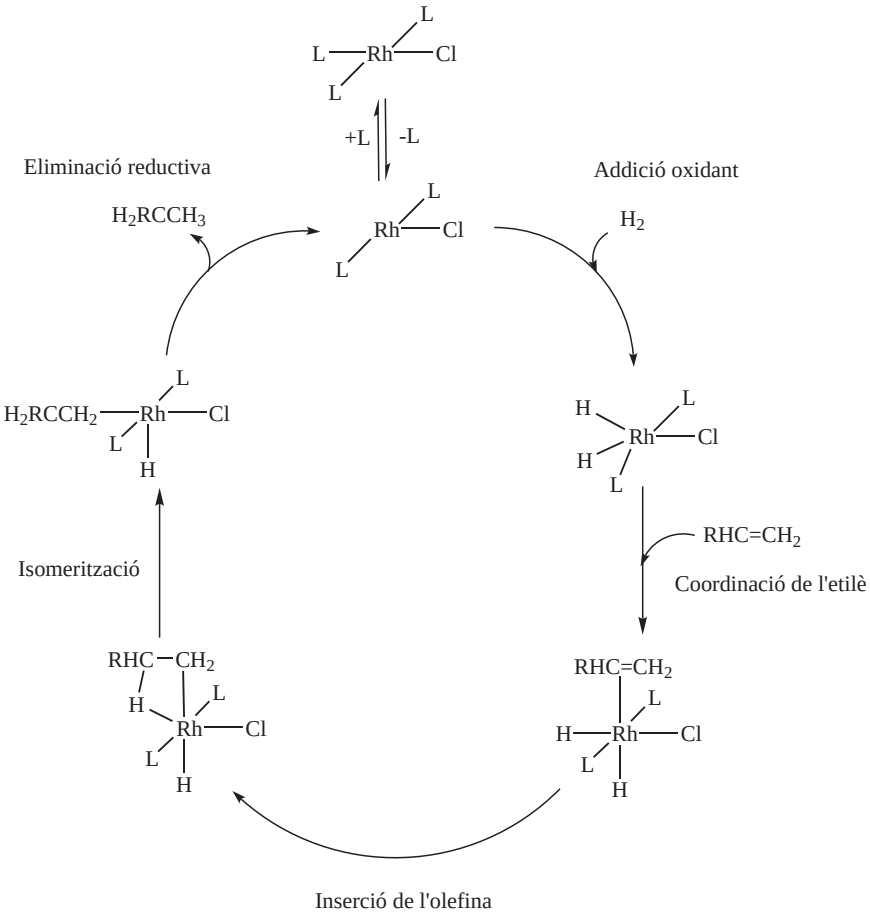

Figura 2.6: *Cicle catalític proposat pel catalitzador de Wilkinson.*

Pel que fa a d'altres substrats que no siguin alquens, com ara alquins, carbonils i imines, en alguns casos també s'han proposat mecanismes d'inserció anàlegs als observats a les figures 2.4 i 2.5. Per exemple, els complexos tipus $[OsHCl(CO)(PR_3)_2]$ ($PR_3 = P\textit{i}Pr_3$, $P\textit{t}Bu_2Me$) catalitzen la hidrogenació d'alquins mitjançant intermedis alquenil, essent la formació de l'alquè per reacció amb la molècula d'hidrogen el pas

d'unes 30 kcal/mol.

determinant de la velocitat de la reacció.[58]

També s'han desenvolupat catalitzadors d'hidrogenació en medi aquós. En alguns casos, el pH del medi s'ha vist que tenia una gran importància, fent que l'espècie activa fos un monohidrur o un dihidrur i donant lloc a regioselectivitat en la hidrogenació. Així, en la hidrogenació de α-β-aldehids insaturats amb H_2, complexos de Ru(II) de *m*tppms ((*m*-sulfonatofenil)difenilfosfina, lligands utilitzats per fer el catalitzador soluble en aigua) s'ha vist que en medi àcid catalitzaven la hidrogenació dels enllaços C=C mentre que en medi bàsic catalitzaven la hidrogenació dels enllaços C=O. Gràcies a estudis potenciomètrics i de RMN (^{1}H i ^{31}P) es detectà que el [RuHCl(mtppms)$_3$] era l'espècie majoritària en medi àcid mentre que el [RuH$_2$-(mtppms)$_4$] era l'espècie dominant en medi neutre i bàsic.[59,60] Posteriorment, prenent un model de l'espècie activa en cada cas (fent servir PH_3 com a lligands fosfínics) i mitjançant càlculs B3LYP i també en alguns casos metodologia ONIOM(B3LYP:UFF) (en aquest cas usant lligands PPh_3), es pogué explicar la regioselectivitat observada.[61,62] En medi àcid, on la hidrogenació de C=C és la que té preferència, es proposà la inserció del substrat a l'enllaç M-H i la formació del producte final per protonació gràcies a l'acidesa del medi.[61] L'efecte del solvent s'inclogué mitjançant clústers de tres aigües[†] per aquesta darrera etapa i també per l'etapa de regeneració de l'hidrur, la qual té lloc mitjançant la coordinació de l'hidrogen molecular al metall i la transferència d'un protó al clúster [$(H_2O)_3$]. En medi àcid, el pas que es proposà com a determinant de la regioselectivitat fou la inserció del substrat a l'enllaç M-H. Per contra, en l'estudi en medi bàsic mitjançant una aproximació anàloga, el pas que determina la regioselectivitat és la transferència protònica. En aquest cas, és l'aigua (ja que no hi ha hidronis al medi) la que ha de protonar el producte d'inserció del C=O o del C=C, essent termodinàmicament factible pel primer cas però no pel segon.[62] Delbecq i col·laboradors proposaren un mecanisme de transferència concertada de l'hidrur i del protó d'un lligand aquo coordinat al metall a l'enllaç C=O, però aquest mecanisme no sembla que tingui en compte la variació de la reactivitat en funció del pH.[65]

Per la hidrogenació de carbonils mitjançant el complex [Rh(diè)L$_2$]$^+$ també s'ha

[†]En estudis previs s'observà que mitjançant aquest model s'obtenia una bona descripció del sistema a un temps de càlcul raonable.[63,64]

proposat un mecanisme d'inserció a través d'intermedis alcòxid,[66] així com també pel complex $RuHCl(CO)(PPh_3)_3$,[67] mentre que per complexos com ara el $RuH_2(\eta^2\text{-}H_2)\text{-}(PPh_3)_3$ s'ha proposat la ruta dihidrídica per la hidrogenació de la ciclohexanona.[68]

Els mecanismes d'hidrogenació pels quals operen les imines són els menys estudiats de tots ja que se'n coneixen pocs catalitzadors.[41] Això probablement és degut al fet que la hidrogenació d'imines és només lleugerament exotèrmica (aproximadament 15 kcal·mol^{-1}) en comparació amb la hidrogenació d'alquens (aproximadament 30 kcal·mol^{-1}), a que la hidrogenació requereix una coordinació η^2 del substrat (si bé el mode de coordinació habitual de les imines és η^1) i a que les amines resultants poden arribar a enverinar el catalitzador degut a que generalment són força bons lligands.[41]

En conseqüència, tal i com s'ha vist pels exemples mostrats fins ara i independentment del substrat i del catalitzador, s'observen per quasi bé tots els casos dos processos clau. El primer és la coordinació del substrat insaturat al metall, essent necessària una vacant de coordinació a l'esfera de coordinació del metall via la marxa d'un lligand o bé via una reorganització de l'estructura del catalitzador. El segon és la inserció d'aquesta espècie a l'enllaç M-H.

Tot i això, hi ha alternatives mecanístiques que no requereixen ni la coordinació del substrat al metall ni la inserció del substrat a l'enllaç M-H. Es tracta del mecanisme iònic i del mecanisme d'esfera externa. El mecanisme d'esfera externa, si bé també es pot donar quan la font d'hidrogen és hidrogen molecular, s'explicarà dins l'apartat 2.1.4 dedicat a les reaccions de transferència d'hidrogen.

2.1.3 Mecanisme iònic

El terme mecanisme iònic s'aplica a aquells sistemes on es transfereixen un protó i un hidrur al substrat.[40,69] La suma d'ambdues espècies dóna com a resultat hidrogen molecular i, en conseqüència, té lloc una hidrogenació. La reacció transcorre mitjançant l'esquema mostrat a la figura 2.7. Inicialment té lloc l'addició oxidant de l'hidrogen molecular, posteriorment es dóna la transferència del protó i finalment ocorre la transferència de l'hidrur donant lloc al producte final. Una sèrie de complexos de Mo i W de fórmula $[W(Cp)(CO)_2(PR_3)(O{=}CEt_2)]BAr_4$' [Ar=3,5-bis(trifluorometil)fenil] es va veure que eren precursos catalítics de la hidrogenació iònica de cetones. En

la majoria dels casos el pas limitant de la velocitat de reacció era el desplaçament de la cetona (o l'alcohol) per H_2 per tal de formar el dihidrur.[70,71] Posteriorment, se sintetitzaren els complexos de fórmula $[MoH(CO)_2\{\eta^5{:}\eta^1\text{-}C_5H_4(CH_2)_2PR_2\}]$ (R = Ph, Cy, tBu) amb $Ph_3C^+BAr_4{}'^-$ que milloraren l'activitat dels complexos anteriors.[72] Un mecanisme d'hidrogenació iònica anàleg al de la figura 2.7 també fou proposat per la hidrogenació iònica de cations iminis mitjançant un complex de Ru amb fosfines quirals. En aquest cas, la transferència de l'hidrur era l'etapa determinant de la velocitat i de l'enantioselectivitat.[73]

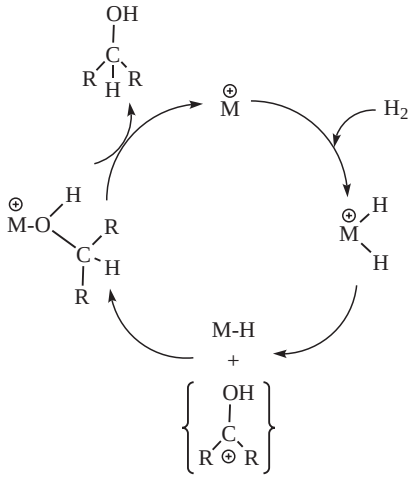

Figura 2.7: *Mecanisme iònic per a la hidrogenació de cetones.*

Encara que la font d'hidrogen sigui hidrogen molecular, els anomenats catalitzadors bifuncionals (*vide infra*) sovint també s'han inclòs dins del terme d'hidrogenació iònica ja que el catalitzador acaba aportant H_2 com a suma d'un protó i d'un hidrur tal i com passa en els mecanismes iònics.[40,69]

2.1.4 Reaccions de transferència d'hidrogen i mecanismes associats

Pel que fa a les reaccions de transferència d'hidrogen, el seu esquema general es mostra a la figura 2.8. En aquestes reaccions una espècie donadora $\mathbf{DH_2}$ dóna hidrogen molecular mentre que una espècie acceptora **A** l'accepta. Les reaccions de trans-

ferència d'hidrogen són més freqüents per a dobles enllaços polars com ara cetones i imines que no pas per a alquens i alquins, si bé també se'n coneixen alguns casos.[74–78] Aquests processos són una opció molt atractiva en la hidrogenació de dobles enllaços polars ja que comparada amb la hidrogenació habitual permeten condicions de reacció suaus, una elevada selectivitat, una concentració de reductor (generalment alcohols) elevada i, a més, presenten altres avantatges com ara que els reductors són fàcils de manejar a més d'ambientalment sostenibles.[79]

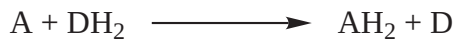

Figura 2.8: *Esquema general de les reaccions de transferència d'hidrogen.*

Els mecanismes per a aquests processos es poden subdividir en dos grups: un mecanisme directe del donador a l'acceptor anomenat mecanisme de Meerwein-Ponndorf-Verley (MPV)[80–82] i un mecanisme indirecte que transcorre a través d'una espècie metall-hidrur tal i com s'ha vist pels mecanismes d'inserció. El mecanisme MPV és habitual pels elements dels grups principals i transcorre a través d'un estat de transició de sis membres tal i com es mostra a la figura 2.9.

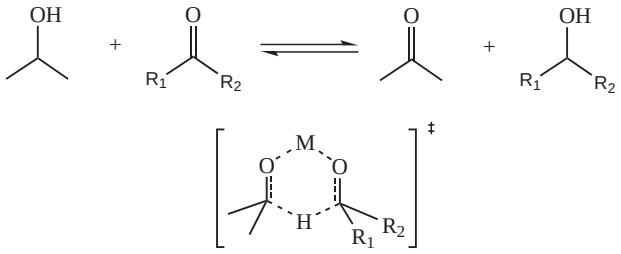

Figura 2.9: *Mecanisme de Meerwein-Ponndorf-Verley (MPV) per la transferència d'hidrogen.*

Generalment, el mecanisme MPV està catalitzat per àcids de Lewis com ara isopropòxids d'alumini o sals de lantànids,[12,83,84] però també s'ha proposat per metalls de transició.[85–87] Pel que fa al mecanisme que transcorre a través de la via hídridica, aquest és el preferit pels metalls de transició, ja que aquests mostren més afinitat per formar hidrurs que no pas els elements dels grups principals. La ruta hidrídica es pot

dividir en dues rutes: la que procedeix a través d'un monohidrur i la que procedeix a través d'un dihidrur, de forma anàloga a la subdivisió dels mecanismes d'inserció. Així, en reaccions de transferència d'hidrogen, apart del complex de Wilkinson(*vide supra*), també transcorren a través de la ruta monohidrídica catalitzadors com ara el $(bipy)_2Rh_2Cl_2$, el $(PPh_3)_3RhCl$, el $Mo_2(OH)_2Cp_4$, el $[Ir(COD)(bipy)]BF_4$, el $Ir_2Cl_2(dppp)_2$, el $Ir(COD)(bipy)]BF_4$ i el $[Ir(COD)(dppp)]BF_4$.[57,88,89] Per complexos tipus $[MH(\eta^2\text{-}H_2)PP_3]^+$ M = Fe,Ru,Os; $PP_3 = P(CH_2CH_2PPh_2)_3$ també s'ha proposat un mecanisme monohidrídic.[90,91] D'altra banda, per complexos com ara el $RuCl_2(PPh_3)_3$[92] o el complex $Ru(diamino)Cl_2(PPh_3)_2$[57] s'ha proposat el mecanisme dihidrídic. A tall d'exemple, els mecanismes d'hidrogenació de carbonils mitjançant els complexos $RhCl(PPh_3)_3$ i $RuCl_2(PPh_3)_3$ es mostren a les figures 2.10 i 2.11, respectivament.

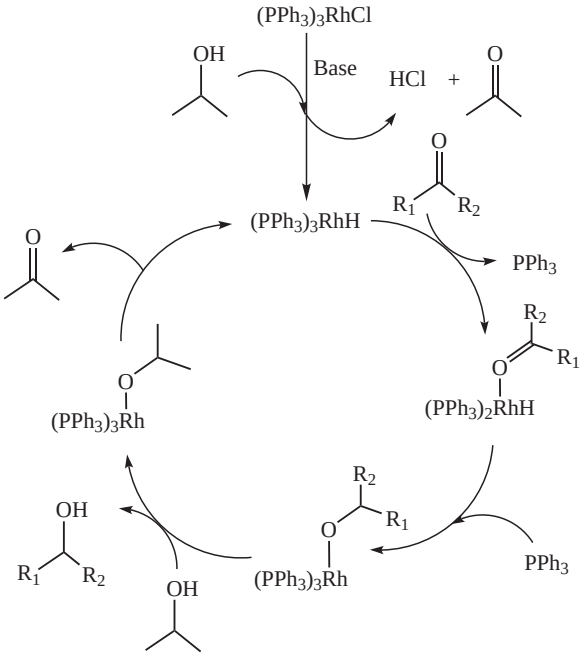

Figura 2.10: *Cicle catalític proposat per la hidrogenació de carbonils mitjançant el complex $RhCl(PPh_3)_3$. Mecanisme monohidrídic.*

Bäckvall i col·laboradors han desenvolupat un experiment que permet distingir la ruta monohidrídica de la dihidrídica i que consisteix en racemitzar un alcohol

òpticament actiu a la posició α. Així, si la ruta dihidrídica té lloc, el deuteri s'hauria de trobar deslocalitzat entre el carboni i l'oxigen, mentre que si la ruta monohidrídica té lloc, el deuteri hauria d'estar en la posició α de l'alcohol racemitzat.[57,93]

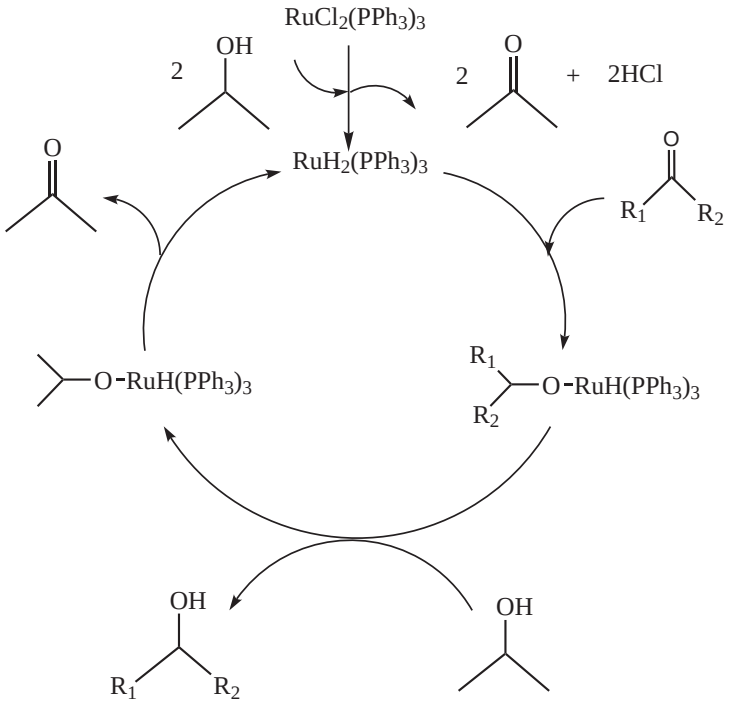

Figura 2.11: *Cicle catalític proposat per la hidrogenació de carbonils mitjançant el complex de $RuCl_2(PPh_3)_3$. Mecanisme dihidrídic.*

Pel que fa a la ruta monohidrídica dins d'aquesta s'han proposat dues subrutes addicionals. La primera és com la que s'ha vist anteriorment i requereix la coordinació del substrat prèvia a l'inserció a l'enllaç M-H i també s'anomena d'esfera interna en contraposició al mecanisme d'esfera externa que exposarem a continuació. La segona és diferent als mecanismes vistos fins ara i consisteix en la transferència concertada de l'hidrur i del protó fora de l'esfera de coordinació del metall. És per això que també s'anomena mecanisme d'esfera externa i se'n mostra l'esquema a la figura 2.12, essent una variant mecanística molt habitual pels anomenats catalitzadors bifuncionals. Aquest terme fou proposat per Noyori† per aquells catalitzadors

†Ryoji Noyori fou premi Nobel de Química l'any 2001 pel seu treball en reaccions d'hidrogenació

que contenen un hidrogen amb caràcter hidrídic enllaçat al metall i un hidrogen amb caràcter pròtic enllaçat a un lligand que alhora està coordinat al metall.[94]

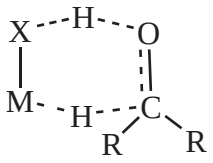

Figura 2.12: *Mecanisme de transferència concertada de l'hidrur i del protó fora de l'esfera de coordinació del metall.*

A la figura 2.13 es mostren exemples de catalitzadors bifuncionals per una bona colla de metalls de transició.[34,94–101]

Les reaccions de transferència d'hidrogen també s'han estudiat mitjançant càlculs teòrics. Així, mitjançant càlculs teòrics BLYP en complexos com ara el Ir(COD)(aminoalcohol) i Ir(COD)(aminosulfit) s'ha proposat el mecanisme MPV[85] i pel complex $RhH(C_2H_4)_2[N(CH_3)_3]_2$ s'ha vist mitjançant càlculs teòrics que aquest mecanisme era factible, tot presentant una barrera energètica de 22 kcal·mol^{-1}. Per aquest catalitzador, el mecanisme MPV ha permès explicar l'absència d'enantioselectivitat quan amines terciàries enlloc d'amines primàries i secundàries estaven coordinades al metall.[87]

La suma del complex $[RuCl_2(\eta^6\text{-benzè})]_2$, N-tosiletilendiamina o etanolamina, i KOH formen un catalitzador actiu en reaccions de transferència d'hidrogen entre alcohols i carbonils.[94,102,103] En un estudi pioner, Noyori i col·laboradors mostraren mitjançant càlculs teòrics que pel catalitzador Ru(η^6-benzè)($NHCH_2CH_2Y$) (Y=O, NH) el mecanisme concertat fora de l'esfera de coordinació del metall presentava una barrera de 15.8 kcal·mol^{-1}.[104] Posteriorment s'aconseguí explicar l'origen de l'enantioselectivitat a través d'aquest mecanisme.[105] El mecanisme concertat també s'ha mostrat més favorable en la hidrogenació de carbonils en reaccions de transferència d'hidrogen en d'altres estudis teòrics per un complex de Ru anàleg al de Noyori[106] i per d'altres compostos com ara el Ru(difosfina)(diamina)[107,108] (també permetent explicar l'enantioselectivitat),[109–111] i també experimentalment

en catàlisi asimètrica. El premi el compartí amb K. Barry Sharpless i William S. Knowles.

mitjançant estudis d'efectes cinètics d'isòtop (KIEs) pel complex tipus [*p*-(Me2CH)C_6H_4Me]Ru(NHCHPhCHPhN$SO_2C_6H_4$-*p*-CH_3) en la hidrogenació de carbonils.[112] Per un complex similar, el Ru(η^6-arene)(NHCHPhCHPhNHTs), també s'ha proposat el mateix mecanisme per a la hidrogenació d'imines.[94] Per altres catalitzadors, com ara el RhH(COD)diamina[86] i el IrH_3[(^{i}Pr$_2$PC_2H_4)$_2$NH],[113] càlculs teòrics també mostraren que el procés complet de transferència d'hidrogen també procedeix a través del mecanisme concertat fora de l'esfera de coordinació del metall.

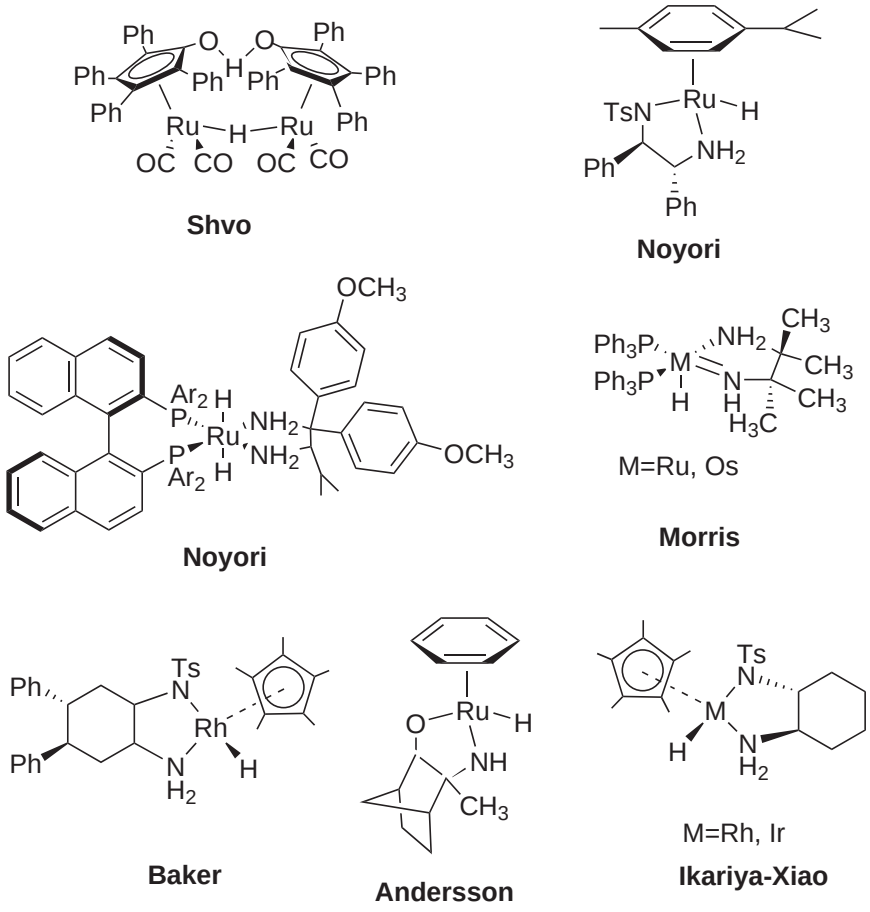

Figura 2.13: *Exemples de catalitzadors bifuncionals amb els grups que els han sintetitzat.*

Pel que fa al mecanisme d'esfera interna, s'ha estudiat teòricament per força compostos però en pocs s'ha proposat com el mecanisme operatiu de la reacció. Com ja s'ha comentat, la coordinació del substrat implica canvis a l'esfera de coordina-

ció del metall. Pel compost Ru(η^6-benzè)($NHCH_2CH_2Y$) (Y=O, NH) de Noyori, càlculs B3LYP han mostrat que la coordinació del substrat carbonílic requereix el desplaçament de l'anell de η^6 a η^2.[†] Aquest pas, en l'estudi de Noyori, es mostrà força menys favorable que el mecanisme d'esfera externa ja que presentava una barrera energètica aproximadament 10 kcal·mol^{-1} superior.[104] Pel que fa a complexos d'iridi, com ara el Ir(COD)(aminoalcohol) i el Ir(COD)(aminosulfit), la coordinació del carbonil tenia lloc gràcies a l'hemilabilitat proporcionada per la part alcohol i sulfit dels lligands aminoalcohol i aminosulfit, respectivament. Pel complex Rh(COD)(diamina)hidrur, la coordinació del carbonil es donava gràcies a la descoordinació d'un lligand amina. En aquest cas, el pas determinant de la velocitat de reacció era la β-eliminació, amb una barrera energètica de 23.6 kcal·mol^{-1} deguda bàsicament a l'elevada estabilitat de l'intermedi alcòxid. Aquest pas permetia regenerar l'hidrur tot generant l'espècie carbonílica final.[114]

Un complex pel qual sí que s'ha proposat el mecanisme d'esfera interna és el [RuH(i-PrOH)(CH_3-CONH)(CO)(PCy_3)$_2$], el qual és capaç d'hidrogenar cetones i imines. En aquest cas es proposà un mecanisme amb dissociació inicial d'un lligand PCy_3 degut a que l'addició de PCy_3 inhibeix la velocitat de reacció. Els següents passos, degut a l'observació d'efectes cinètics d'isòtop inversos, foren la ràpida transferència, primer del protó i després de l'hidrur.[115]

Per tant, fins ara podem concloure que, dins de la via hidrídica, la majoria de complexos metàl·lics prefereixen el mecanisme d'esfera externa enfront del mecanisme d'esfera interna i del mecanisme MPV. Perquè el mecanisme MPV i el mecanisme d'esfera interna siguin competitius en les reaccions de transferència d'hidrogen és necessària la labilitat d'algun dels lligads per tal de permetre la coordinació del substrat. Un altre fet que limita l'operativitat del mecanisme d'esfera interna (en el cas dels carbonils) és l'elevada estabilitat de l'intermedi alcòxid[‡], fet que dificulta el pas següent de la reacció que no és altre que la generació del producte final.

Un dels catalitzadors bifuncionals més versàtils degut a la seva àmplia aplicació en processos de transferència d'hidrogen és el catalitzador de Shvo (veure figura 2.13).[95,96,116] Permet usar tant hidrogen molecular com alcohols com a font d'hidro-

[†]En càlculs MP4 el desplaçament de l'anell conduïa a una coordinació η^4.

[‡]Això en cas que la vacant que queda lliure al transferir l'hidrur es cobreixi una altra vegada.

gen (generalment 2-propanol) i ha estat aplicat en moltes reaccions de transferència d'hidrogen com ara la hidrogenació de carbonils,[117] imines[118] i alquins,[119] l'oxidació d'alcohols[120] i d'amines[121,122] i en resolució cinètica dinàmica d'alcohols secundaris[123,124] i amines primàries[125] en combinació amb lipases. El seu mecanisme en reaccions de transferència d'hidrogen ha generat una forta controvèrsia ja que durant força temps s'ha polemitzat sobre si aquest catalitzador operava a través d'un mecanisme d'esfera interna o bé a través d'un mecanisme d'esfera externa sobretot en la hidrogenació de carbonils[126,127] i en la hidrogenació d'imines.[128–134] El seu mecanisme ha estat objecte d'estudi al capítol 4 d'aquesta tesi doctoral per a la hidrogenació de cetones, imines, alquens i alquins.

2.2 Oxidacions en catàlisi homogènia

Una oxidació implica la pèrdua d'un o més electrons d'una entitat molecular i un increment del nombre d'oxidació de qualsevol àtom del substrat. Per tal que puguem parlar d'oxidació, aquests dos criteris s'han de complir. Un tercer criteri, que es compleix moltes vegades però no sempre, és el guany d'oxigen i/o pèrdua d'hidrogen per part d'un substrat orgànic.[1] A continuació, es comentaran breument les característiques generals de les reaccions d'oxidació d'olefines en catàlisi homogènia que s'han estudiat en aquesta tesi doctoral: l'epoxidació mitjançant compostos tipus Cp*Mo(VI) i el procés de Wacker.

2.2.1 Epoxidacions en catàlisi homogènia

Un procés de gran importància industrial és l'epoxidació d'olefines ja que és una via relativament fàcil de funcionalització d'olefines. Com a exemple, l'òxid de propilè té una producció anual de 4 milions de tones i és un intermedi clau en la indústria química ja que es fa servir per a la síntesi de propilenglicol, poliuretans i resines.[135] La meitat de la producció anual d'aquest compost encara se sintetitza mitjançant la ruta de la clorhidrina malgrat que aquesta ruta usi Cl_2 i generi 2 kg de $CaCl_2$ per cada kg d'òxid de propilè produït i, per tant, tingui un fort impacte ambiental.[136]

D'aquí neix la importància del desenvolupament de catalitzadors per a l'epoxidació d'olefines. En el nostre cas ens centrarem en els catalitzadors homogenis.

A finals dels anys 60, les empreses Halcon i Arco desenvoluparen una ruta d'epoxidació fent servir catalitzadors homogenis de Mo(VI) per tal de sintetitzar òxid d'etilè emprant *tert*-butilhidroperòxid (TBHP) com a font oxidant. D'aleshores ençà, nombrosos complexos de metalls de transició s'han emprat per a epoxidacions, com ara triòxids de Re i diòxids de Mo i W,[137–140] complexos bisperòxids de Mo i W amb fórmula $[MO(O_2)_2(L_1(L_2)]$,[141] polioxometal·lats[142–144] i una gran varietat d'òxids generats *in situ* a partir de complexos de Fe i Mn amb lligands porfirina, salen i altres tipus de lligands.[145–148] Com que molts peròxids de Mo i W s'han pogut caracteritzar, s'ha proposat que aquestes espècies són les que són capaces de transferir un àtom d'oxigen a l'etilè. En conseqüència, varen sorgir dues propostes mecanístiques per tal d'explicar l'epoxidació: la de Mimoun,[149] que proposà un mecanisme pel qual es forma un cicle de cinc membres, i la de Sharpless,[150] en la qual té lloc la transferència d'oxigen sense coordinació de l'olefina al metall.

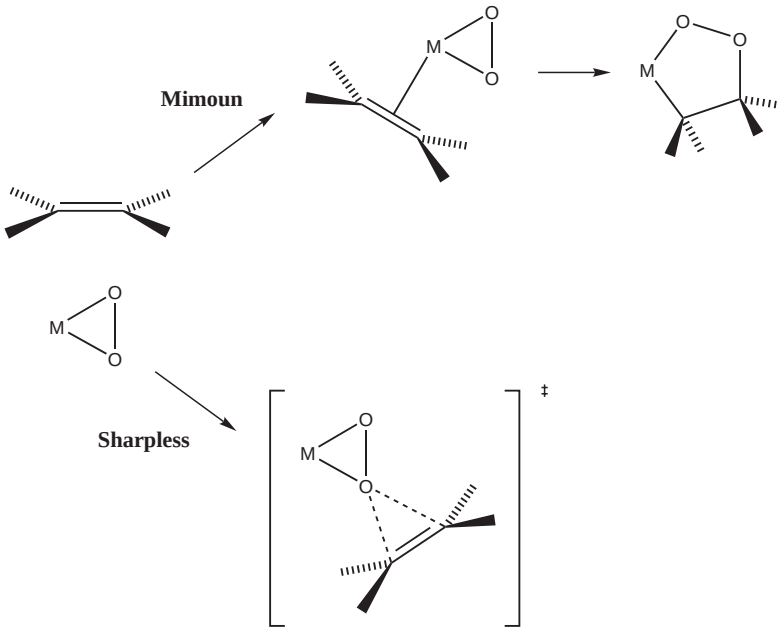

Figura 2.14: *Mecanismes proposats per Mimoun i Sharpless per a l'epoxidació d'olefines.*

La majoria d'estudis teòrics han avalat la preferència del mecanisme de Shar-

pless.[151–159] Així, càlculs DFT a nivell B3LYP han conclòs que l'epoxidació estequiomètrica d'olefines mitjançant complexos tipus Mimoun [$MoO(\eta^2\text{-}O_2)_2(OPR_3)$] procedeix a través del mecanisme de Sharpless amb una barrera energètica de 15 kcal·mol^{-1}, mentre que el mecanisme de Mimoun a través de la formació d'un metal·lacicle de 5 membres condueix a la formació d'aldehids i no pas a la formació d'epòxids.[152] Altres estudis teòrics amb complexos tipus Herrmann [$ReO(\eta^2\text{-}O_2)_2Me$][160] amb peròxids de Cr, Mo i W[151] i amb el complex $[VO(O_2)_2(\text{imidazol})]^-$[158] també han proposat el mecanisme de Sharpless. Pel que fa al caràcter electrònic de l'estat de transició resultant s'ha proposat que l'olefina actua com a nucleòfil mentre que el peroxo ho fa com a electròfil, ja que s'ha mostrat que la interacció dominant és entre l'orbital HOMO de l'etilè i l'orbital antienllaçant σ^*(O-O) del peròxid.[152]

Pel que fa a les epoxidacions catalítiques, es poden donar altres mecanismes si hi ha més d'una espècie reactiva. Això ha fet que els peròxids es poguessin activar mitjançant la protonació, ja sigui intramolecularment per la transferència d'un protó des d'un lligand aquo o des de la protonació intermolecular mitjançant àcids de Brönsted. Així, mitjançant càlculs teòrics en complexos de Re(VII) es trobà que aquesta protonació era endotèrmica, mentre que en complexos de Mo(VI) era exotèrmica i l'epoxidació resultant presentava una barrera lleugerament més elevada que la del peròxid. Per tant, apart del lligand η^2-O_2, el lligand η^1-OOH també era capaç de transferir un àtom d'oxigen. Per exemple, en el cas de catalitzadors bifàsics tipus Mimoun [$MoO(O_2)_2(OPR_3)$], l'energia d'activació de l'epoxidació es veigué dràsticament disminuïda amb la protonació del peròxid, amb barreres de 3 a 1 kcal·mol^{-1}, en funció de si hi havia o no un lligand aquo addicional, respectivament.[161]

D'altra banda, Thiel proposà un mecanisme alternatiu degut a que des d'un complex tipus $[MoO(O_2)_2(L_1)(L_2)]$ la reacció no tenia lloc si no s'hi afegia TBHP.[162–164] En conseqüència, l'oxigen que atacava l'etilè havia de provenir de l'hidroperòxid i no pas del peròxid. En aquesta proposta mecanística, primer es donava l'activació de l'hidroperòxid tot transferint-se el protó al grup peròxid i coordinant-se el grup OOR al metall. Seguidament, es donava l'epoxidació pròpiament dita de manera similar al mecanisme proposat per Sharpless i, finalment, tenia lloc l'eliminació de l'epòxid, la regeneració del peròxid i la formació de l'alcohol ROH per transferència del protó (figura 2.15). Pel que fa a l'oxidant emprat, quan la reacció no és catalitzada per metalls

de transició normalment s'usen peràcids i dioxirans.[165] Malgrat que l'ús de TBHP presenta avantatges a nivell industrial, darrerament estan cobrant gran importància aquells que usen peròxid d'hidrogen com a font oxidant, ja que l'únic subproducte que s'obté és aigua i, per tant, és una via molt a tenir en compte des d'un punt de vista ambiental.

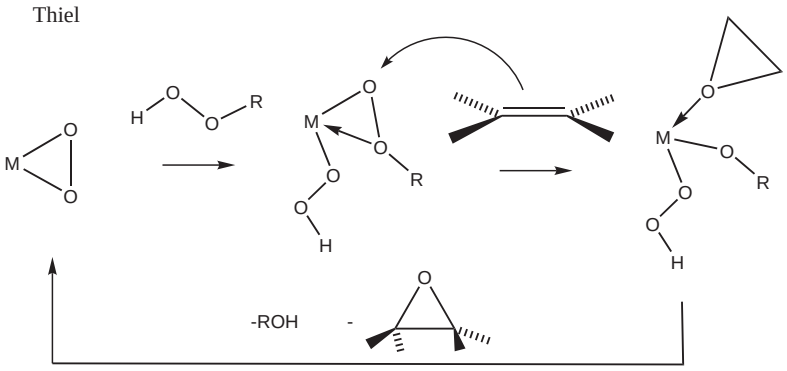

Figura 2.15: *Mecanisme proposat per Thiel per a l'epoxidació d'olefines.*

A més a més, el peròxid d'hidrogen presenta un major percentatge d'oxigen disponible respecte d'altres oxidants.[136] Entre els diversos intents d'usar el peròxid d'hidrogen com a oxidant, destaquen els basats en el complex de CH_3ReO_3 de Herrmann i col·laboradors[166,167] o els basats en complexos de Mo(VI) modificats de Sundermeyer.[168]

Pel que fa a la química dels metalls en estats d'oxidació alts, tot i que generalment han estat restringits a solvents no aquosos, l'ús d'aigua com a solvent ha guanyat força interès ja que no és tòxica, és barata i és de fàcil accés. Així, una part d'aquesta tesi doctoral s'emmarca en la naturalesa de l'especiació en solució aquosa del complex $[Cp^*MoO_2]^+$, així com la seva posterior aplicació en l'epoxidació d'olefines, on s'han avaluat els diferents mecanismes exposats en aquesta secció (capítol 6).

2.2.2 Procés de Wacker

Les reaccions d'oxidació en fase homogènia han estat molt estudiades des del punt de vista mecanístic. El cas més paradigmàtic és l'anomenat procés de Wacker, ja que

fou la primera oxidació catalítica organometàl·lica que es coneix. Aquest procés és d'una gran importància industrial, ja que avui en dia es produeixen al voltant de 4 milions de tones a l'any d'aldehids a partir d'alquens mitjançant aquest procés.[19] La reacció global del procés es mostra a la figura 2.16.

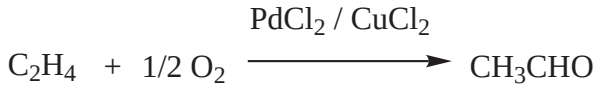

Figura 2.16: *Reacció global del procés de Wacker.*

De fet, des de finals del segle XIX se sabia que el $PdCl_2$ aquós era capaç d'oxidar estequiomètricament l'etilè a acetaldehid tot dipositant Pd(0) metàl·lic. Com que el $PdCl_2$ era massa car per tal d'usar-se estequiomètricament a nivell industrial, la clau perquè el procés fos viable econòmicament era la catàlisi. El procés catalític fou desenvolupat a finals de la dècada dels 50 per J. Smidt, de l'empresa alemanya Wacker Chemie.[169,170] La reacció que en resultà es pot subdividir en tres etapes (figura 2.17).

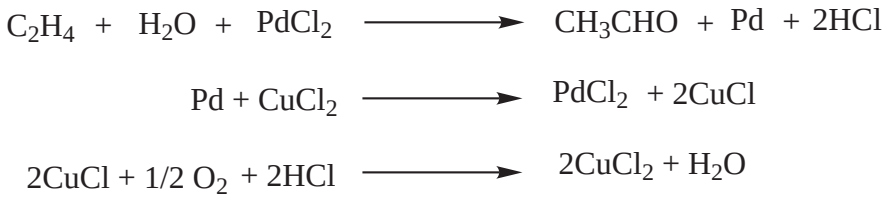

Figura 2.17: *Etapes del procés de Wacker.*

La primera implica l'oxidació pròpiament dita d'etilè a acetaldehid, mentre que la segona capta el Pd(0) mitjançant $CuCl_2$ abans no precipiti, tot regenerant el $PdCl_2$ i formant CuCl. Com que el CuCl és sensible a l'aire, en la tercera i última etapa aquest complex és reoxidat mitjançant oxigen molecular tot regenerant el $CuCl_2$. El cicle catalític sencer del procés de Wacker es mostra a la figura 2.18. Aquest cicle parteix del $PdCl_4^{2-}$, que és l'espècie catalítica inicial en medi aquós. Inicialment, s'ha proposat la substitució d'un clorur per l'etilè i a continuació té lloc l'etapa que ha generat més controvèrsia: l'atac nucleòfil d'una molècula d'aigua a l'etilè. Per

aquesta etapa s'han proposat dos mecanismes. En el primer, després de la coordinació d'un lligand aquo gràcies a la marxa d'un clorur, es desprotona el lligand aquo i a continuació es dóna l'atac nucleòfil en *syn* de l'hidroxil a l'etilè. Aquest mecanisme també s'anomena d'esfera interna ja que el nucleòfil està coordinat al metall. Pel que fa al segon mecanisme, es dóna l'atac nucleòfil fora de l'esfera de coordinació del metall (és per això que aquest mecanisme també s'ha anomenat d'esfera externa) en *anti* d'una molècula d'aigua del medi, amb l'alliberació simultània d'un protó i d'un clorur.

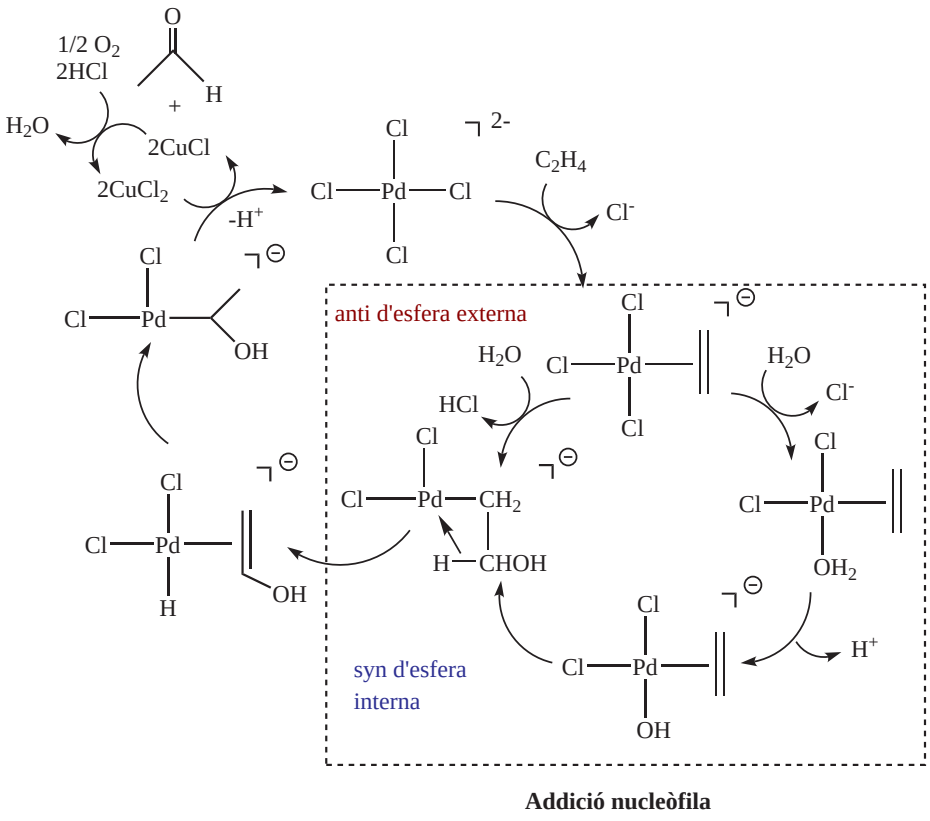

Figura 2.18: *Cicle catalític proposat pel procés de Wacker amb les dues addició nucleòfiles possibles: en* syn *i en* anti.

Tan estudis experimentals[171–178] com teòrics[179–185] han estudiat l'atac nucleòfil, el qual s'acabarà d'explicar i d'abordar al capítol 7 d'aquesta tesi doctoral. En aquest capítol s'ha estudiat aquesta etapa mitjançant dinàmiques moleculars de primers

principis (veure el capítol següent) situant el complex metàl·lic en una caixa de 26 molècules d'aigua.

Un cop ha tingut lloc l'atac nucleòfil, la reacció pot procedir mitjançant la β-eliminació d'un hidrogen seguida de l'inserció del doble enllaç resultant a l'enllaç Pd-H, mentre que mitjançant el $CuCl_2$ i l'alliberament d'un protó es regenera l'espècie activa del catalitzador ($PdCl_4^{2-}$). L'eliminació final del producte també ha estat objecte de controvèrsia pel procés de Wacker. Per aquesta etapa, clàssicament s'ha proposat un mecanisme d'eliminació de l'hidrur en β,[19] tot i que també s'havia suggerit el desplaçament α de l'hidrur.[171,186] Els estats de transició corresponents a les dues propostes respectives es mostren a la figura 2.19.

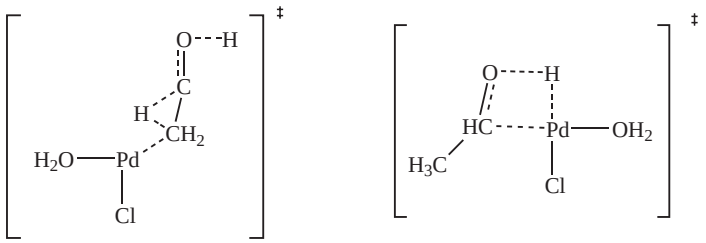

Figura 2.19: *Estats de transició del desplaçament α de l'hidrur i de la β-eliminació de l'hidrur.*

En un estudi recent, Goddard i col·laboradors proposaren mitjançant càlculs teòrics DFT una eliminació reductiva directa assistida per una molècula d'aigua (figura 2.20).[187]

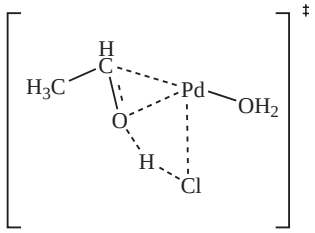

Figura 2.20: *Estat de transició de l'eliminació reductiva directa assistida per una molècula d'aigua.*

Mecanismes similars (però sense assistència d'una molècula d'aigua) ja havien estat prèviament proposats en altres estudis.[188,189] Tot i que la β-eliminació reductiva també s'ha vist que podia ésser assistida per una molècula d'aigua, la barrera energètica associada seguia essent més gran que per a l'eliminació reductiva directa motiu pel qual es proposà aquest pas per l'etapa de finalització del cicle catalític.

Capítol 3

Aproximació teòrica a la catàlisi homogènia

3.1 Aplicació dels càlculs teòrics a la catàlisi homogènia

Tal i com hem vist al primer capítol, un procés catalític eficient és aquell que procedeix ràpidament sense canvis energètics abruptes. Això fa que en el millor dels casos la detecció i caracterització experimental d'intermedis sigui difícil. A més, els cicles catalítics poden arribar a presentar moltes etapes. Per tant, els càlculs teòrics són una opció molt a tenir en compte alhora d'estudiar mecanismes de reacció en catàlisi homogènia.[56,190] En aquests estudis és clau el concepte de superfície d'energia potencial (PES) perquè permet la determinació d'intermedis de reacció i barreres d'activació.

El concepte de PES sorgeix d'aplicar l'aproximació de Born-Oppenheimer,[191] que considera que el moviment dels nuclis és negligible respecte el moviment dels electrons ja que els primers són molt més pesats i per tant l'estructura electrònica s'adapta instantàniament a qualsevol reorganització nuclear. Al resoldre l'equació d'Schrödinger electrònica trobem l'energia per una determinada configuració nuclear, però per tal d'obtenir la superfície d'energia potencial completa aquesta s'hauria de resoldre per totes les possibles configuracions nuclears. Per sort, amb alguns punts de la superfície

d'energia potencial ja en tenim prou per l'estudi de la reactivitat química i aquests punts són aquells en els quals l'energia és estacionària respecte les coordenades nuclears: els mínims i els estats de transició (punts de sella d'ordre 1). La localització dels estats de transició és la part més difícil del procés i, tot i que hi ha algunes metodologies que ens permeten localitzar els estats de transició de forma sistemàtica, generalment la cerca d'aquestes estructures es fonamenta en la intuïció química. Hi ha qui diu que cercar estats de transició és un art i possiblement tingui bona part de raó.

Un cop hem localitzat els mínims i els estats de transició obtenim un perfil d'energia potencial per la reacció d'estudi i, en conseqüència, podem conèixer l'energia de reacció (ΔE) i també la seva barrera energètica ($\Delta E^{\ddagger}$). No s'ha de confondre l'alçada de la barrera energètica $\Delta E^{\ddagger}$ que obtenim dels càlculs teòrics amb l'energia d'activació E_a, ja que la darrera és una quantitat empírica.[3] Com s'ha comentat al capítol 1, a partir de l'energia potencial dels càlculs podem obtenir l'energia lliure de Gibbs de la reacció estudiada. Tanmateix, calcular el perfil d'energia lliure de Gibbs d'aquesta manera té força limitacions, sobretot en processos associatius i dissociatius. Així, si en una dissociació en fase gas passem d'un fragment a dos el terme entròpic creix bàsicament gràcies a les components translacionals i rotacionals de l'entropia. En solució aquest increment entròpic no pot ser tal, ja que les molècules de solvent restringiran el moviment dels dos fragments. Per tant, els processos dissociatius s'obtenen més favorables del que haurien de ser mentre que pels processos associatius passa justament el contrari.[192] Alguns autors han proposat tenir en compte només la component vibracional de l'entropia,[193–195] però si la primera aproximació peca per excés aquesta generalment peca per defecte. És per això que en gran part dels càlculs d'aquesta tesi s'ha preferit usar ΔE i $\Delta E^{\ddagger}$ pels mecanismes avaluats de les reaccions estudiades enlloc de ΔG i $\Delta G^{\ddagger}$. Posteriorment, s'ha inclòs l'efecte del solvent.

Malgrat tot, existeixen mètodes que ens permetran obtenir una estimació raonable de l'energia lliure. Per tal d'aconseguir-ho, en aquesta tesi doctoral s'han usat metadinàmiques acoblades a dinàmiques moleculars de Car-Parrinello. Aquesta metodologia, la qual es descriurà a la secció 3.2.4, s'ha aplicat satisfactòriament en processos de catàlisi homogènia[85,196–198] i ens resultarà útil al capítol 7, on hem estudiat el procés de Wacker.

3.2 Metodologia

En aquesta secció es descriu breument la metodologia que s'ha usat durant aquesta tesi doctoral. En primer lloc es descriu la teoria del funcional de la densitat (DFT), la qual s'ha usat per tal d'obtenir l'energia electrònica.† Posteriorment es comenten els mètodes que ens permeten incloure l'efecte del solvent, i finalment s'exposa breument la dinàmica molecular Car-Parrinello i la metadinàmica acoblada a aquesta dinàmica.

3.2.1 Teoria del Funcional de la Densitat (DFT)

La DFT és la metodologia que hem usat per tal d'obtenir l'energia electrònica. Aquest mètode permet calcular l'energia d'un sistema introduïnt la correlació electrònica de manera alternativa als mètodes post Hartree-Fock a un cost computacional raonable. La teoria es basa en el teorema de Hohenberg i Kohn,[200] que enuncia que l'energia electrònica de l'estat fonamental d'un sistema queda completament determinada per la densitat electrònica ρ, o el que és el mateix, que l'energia és un funcional de la densitat i la podem expressar de la següent manera:

$$E[\rho] = T[\rho] + E_{en}[\rho] + E_{ee}[\rho] \tag{3.1}$$

on T és l'energia cinètica, E_{en} l'energia d'interacció electró-nucli i E_{ee} l'energia d'interacció electró-electró. Malauradament, el problema d'aquest formulisme és que l'expressió del funcional que relaciona la densitat i l'energia es desconeix. Per tant, l'objectiu dels mètodes DFT consisteix en dissenyar funcionals que relacionin la densitat electrònica amb l'energia.

El gran impuls pel que fa a l'aplicabilitat i desenvolupament dels mètodes DFT vingué amb la consideració de Kohn i Sham,[201] la qual suposa que la densitat del sistema real és la d'un sistema de N electrons que no interaccionen entre sí que es mouen sota l'acció d'un potencial extern. D'aquesta manera, la densitat la podem

†Quasi bé tots els càlculs realitzats en aquesta tesi doctoral han emprat la DFT. És per això que, malgrat que en un estudi s'han realitzat càlculs puntuals a nivell MP2 i CCSD(T), la descripció d'aquests mètodes no s'ha trobat pertinent incloure-la. Aquesta descripció es pot trobar a qualsevol llibre general de química quàntica.[199]

escriure com a combinació d'un conjunt funcions monoelectròniques, els anomenats orbitals de Kohn-Sham (Ψ_i de l'equació 3.2):

$$\rho_s(r) = \sum_i |\Psi_i(r)|^2 \tag{3.2}$$

D'aquesta manera, l'equació (3.1) passa a ser:

$$E[\rho] = T_s[\rho] + E_{en}[\rho] + J[\rho] + E_{xc}[\rho] \tag{3.3}$$

on T_s és una aproximació a l'energia cinètica real T i correspon a l'energia cinètica d'un sistema d'electrons independents que té la mateixa densitat que el sistema real:

$$T_s[\rho] = \sum_{i=1}^{N} \langle \Psi_i | \frac{1}{2} \nabla^2_{(1)} | \Psi_i \rangle \tag{3.4}$$

D'altra banda, E_{en} és l'energia d'interacció electró-nucli, J és l'energia d'interacció coulòmbica electró-electró i E_{xc} és l'energia de correlació-intercanvi.

L'*únic* que ens queda per conèixer és el terme E_{xc}. Aquest terme, es pot subdividir en dos. El primer (T_c) inclou la diferència entre l'energia cinètica del sistema real (T) i l'energia cinètica del sistema de N electrons independents (T_s), mentre que el segon (W_{xc}) inclou la diferència entre la interacció electró-electró (E_{ee}) i l'energia d'interacció coulòmbica electró-electró (J). Aquest darrer terme s'anomena energia d'interacció no clàssica electró-electró (W_{xc}).

$$E_{xc}[\rho] = T[\rho] - T_s[\rho] + E_{ee}[\rho] - J[\rho] = T_c[\rho] - W_{xc}[\rho] \tag{3.5}$$

És en aquest terme E_{xc} on hi ha la *clau* dels mètodes DFT, ja que hi ha compreses totes les contribucions a l'energia per les quals no tenim una expressió senzilla en funció de la densitat electrònica. Per tant, la dificultat fonamental dels mètodes DFT rau en el fet de trobar una expressió adient per E_{xc}.
Si assumim que l'expressió per E_{xc} és coneguda, el que s'ha de fer és determinar el conjunt d'orbitals ψ_i que minimitzin l'energia, amb el requeriment que siguin ortogonals. Les equacions que en resulten són les equacions de Kohn-Sham:

$$\hat{h}_{KS}(1)\Psi_i = [-\frac{1}{2}\nabla^2_{(1)} + \hat{v}_{ef}(1)]\Psi_i = \varepsilon_i \Psi_i \tag{3.6}$$

on

$$\hat{v}_{ef}(1) = \hat{V}_{en}(1) + 2\sum_{i=1}^{N} \hat{J}_i(1) + \hat{V}_{xc}(1) \tag{3.7}$$

v_{ef} és un potencial efectiu que inclou el potencial d'atracció electró-nucli V_{en},

$$\sum_{i=1}^{N} J_i(1) \tag{3.8}$$

el terme de repulsió electró-electró clàssic i

$$\hat{V}_{xc} = \frac{\delta E_{xc}}{\delta \rho(r)} \tag{3.9}$$

que és el potencial de correlació-intercanvi. Com que $v_{ef}(1)$ depèn de la densitat electrònica total, la determinació dels orbitals ψ_i s'ha de realitzar iterativament. Si es conegués exactament $E_{xc}[\rho]$, de la resolució de les equacions n'obtindríem l'energia exacta de l'estat fonamental del sistema amb tota la correlació electrònica inclosa. Però com que per tal de trobar E_{xc} hem de realitzar aproximacions, depenent de quina és l'aproximació que fem servir parlem de diferents classes de funcionals.[202]

En primer lloc, hi ha els funcionals LDA (aproximació de la densitat local) que usen la densitat d'un gas uniforme d'electrons. Aquests mètodes, tot i que s'usaren en els primers compassos de l'aplicació dels càlculs DFT a la catàlisi homogènia[203] es descartaren aviat en la química dels metalls de transició degut a que subestimen l'energia d'intercanvi i sobreestimen en excés l'energia de correlació, donant lloc a energies d'enllaç massa grans.

A continuació vénen els funcionals GGA (aproximació de gradient generalitzat) que incorporen correccions usant el mòdul del gradient de la densitat i ja suposaren una notable millora. En un dels estudis d'aquesta tesi doctoral (capítol 7) s'ha usat un funcional GGA: HCTH/120.[204] Aquest funcional, desenvolupat per Handy i col·laboradors, es basa en l'ajustament de mínims quadrats de propietats de 120 sistemes i descriu de manera raonable les propietats estructurals de l'aigua líquida en dinàmiques de Car-Parrinello. Per tant, és un bon mètode per tractar sistemes aquosos.[205]

Una altra classe de funcionals són els anomenats mètodes híbrids, que incorporen una part de l'energia d'intercanvi exacte de Hartree-Fock (E_x^{HF}). Per a la gran majoria d'estudis d'aquest treball, s'ha usat un funcional híbrid molt extès tan en sistemes

orgànics com en sistemes que contenen metalls de transició: el B3LYP. Aquest funcional ve donat per la combinació del funcional d'intercanvi B3 (de Becke)[206] amb el funcional de correlació LYP (de Lee, Yang i Parr)[207] i presenta la següent expressió:[208]

$$E_{xc}^{B3LYP} = (1 - a_0)E_x^{LSDA} + a_0 E_x^{HF} + a_x \Delta E_x^{B88} + a_c \Delta E_c^{LYP} + (1 - a_c)E_c^{VWN} \quad (3.10)$$

on els valors dels quoficents a_0, a_x i a_c vénen donats per l'ajustament a un seguit de dades termodinàmiques experimentals. El B3LYP és molt popular en el camp de la química, ja que apareix un 80 per cent de vegades en els estudis que han usat funcionals de la densitat entre els anys 1990 i 2006 segons l'*Isi Web of Science* de l'any 2007. Malgrat aquest fet, sembla que les coses estan començant a canviar. Així, per propietats tan importants per la reactivitat química com les barreres de reacció sembla que el B3LYP les subestima tot sovint mentre que el funcional meta-GGA híbrid (*vide infra*) BB1K presenta major exactitud.[209]

Els funcionals meta-GGA depenen de gradients de la densitat d'ordre superior o de la densitat d'energia cinètica, la qual involucra derivades dels orbitals de Kohn-Sham ocupats. Finalment, hi ha els mètodes meta-GGA híbrids que depenen de l'intercanvi de Hartree-Fock, de la densitat electrònica i del seu gradient i de la densitat d'energia cinètica.

El nombre i sofisticació dels funcionals de la densitat s'ha incrementat tan ràpidament últimament que l'any 2000 Perdew mostrà la seva visió de l'evolució en el camp fent una analogia amb l'escala de Jacob (veure figura 3.1):

> "Jacob va sortir de Beerxeba cap a la ciutat d'Haran. Quan el sol ja s'havia post, va arribar en un indret i s'hi quedà per fer-hi nit. Va prendre una pedra, se la posà per capçal i va dormir en aquell lloc. Tot somiant, va veure una escala que des de terra, anava fins al cel. Els àngels de Déu hi pujaven i baixaven."†

Aquesta escala conté 5 generacions de funcionals de la densitat on els usuaris serien els àngels que pugen i baixen l'escala d'acord amb les seves necessitats de precisió i d'eficiència computacional. Per tant, per a la majoria de propietats que vulguem calcular, pujar un esglaó significa augmentar la qualitat dels resultats però també el

†Bíblia, Gènesi 28, 10-12.

cost computacional. Tot i això, encara hi ha propietats químiques on fins i tot els funcionals més sofisticats tenen limitacions: sobretot en les interaccions no-enllaçants en les quals la dispersió és la major font d'atracció.

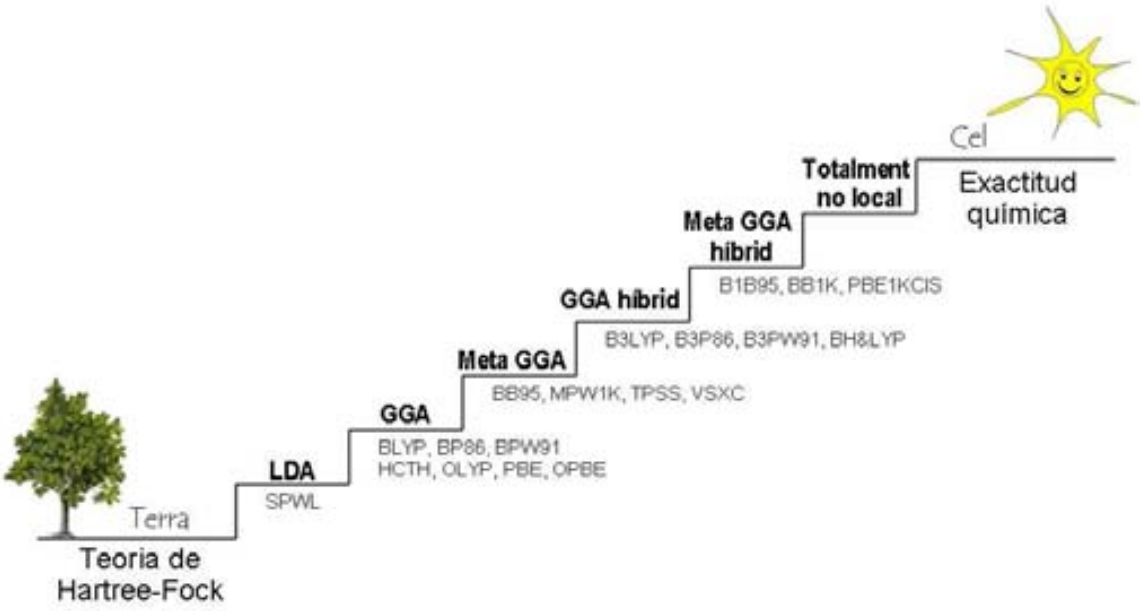

Figura 3.1: *Escala de Jacob de les 5 generacions de funcionals DFT segons Perdew, amb els funcionals més habituals de cada rang.*

3.2.2 Tractament del solvent

Fins ara hem parlat de càlculs en fase gas però la catàlisi homogènia generalment té lloc en solució. Per tant, la naturalesa del solvent pot afectar molt la reacció d'estudi i, en conseqüència, l'hem de tenir en compte en les reaccions que vulguem estudiar. En química computacional bàsicament hi ha dues estratègies per tal d'incorporar l'efecte del solvent: els models continus o implícits i els models explícits. A la figura 3.2 es mostren ambdós models.

En el primers es considera el solut dins d'una cavitat envoltat d'un continu polaritzable caracteritzat per una constant dielèctrica ε, que és la del dissolvent on es troba el nostre solut. La distribució de càrrega del solut és la font de la polarització

del dielèctric i així es produeix la interacció de tipus electrostàtic entre la distribució de càrrega del solut i el dielèctric polaritzat. Aquests mètodes tenen l'avantatge que són senzills, tenen un cost computacional baix i permeten tenir en compte a nivell qualitatiu els efectes bàsics de la solvatació. Per contra, el desavantatge més gran que presenten és que no tenen en compte ni les interaccions intermoleculars ni la possible participació del solvent en la reacció d'estudi.

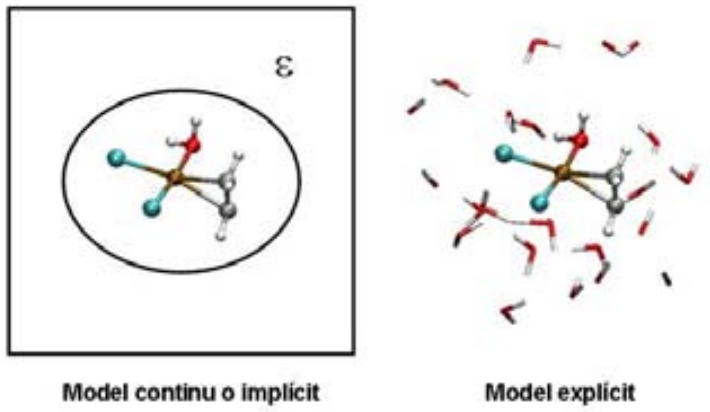

Figura 3.2: *Representació dels models de solvatació: model continu o implícit i model explícit.*

En aquesta tesi doctoral s'han usat dos mètodes continus àmpliament usats en química computacional: el PCM[210] i el CPCM.[211,212] A l'afegir l'energia lliure de solvatació a l'energia potencial en fase gas obtindrem per les reaccions d'estudi una ΔE i una $\Delta E^{\ddagger}$ en solució. Cal esmentar que no podem parlar d'energia lliure en solució, ja que no estem tenint en compte la contribució entròpica del solut.

Pel que fa als mètodes explícits, aquests són aparentment més simples, ja que consisteixen en afegir molècules de solvent a les del solut. És necessari usar aquests mètodes quan el solvent participa en la reacció d'estudi. El problema és que anar introduint a nivell de mecànica quàntica molècules de solvent augmenta força el cost computacional a més d'incorporar una variable conformacional important. Per tant, tot sovint s'ha d'usar metodologia QM/MM (mecànica quàntica/mecànica molecu-

lar) i càlculs de dinàmica molecular. En funció del problema d'estudi en aquesta tesi doctoral s'han usat mètods continus (capítols 4 i 5), la combinació de mètodes continus i mètodes explícits amb molècules de solvent descrits a nivell QM (capítols 5 i 6) i metadinàmiques acoblades a dinàmiques moleculars Car-Parrinello (*vide infra*) on el solut s'ha situat en una caixa amb molècules de solvent (capítol 7).

3.2.3 Dinàmica molecular Car-Parrinello

La dinàmica molecular Car-Parrinello (CPMD) és una dinàmica molecular de primers principis basada en la teoria del funcional de la densitat (DFT).[213] En dinàmica molecular el procediment habitual consta de tres passos: en primer lloc es resol el problema electrònic per una configuració nuclear donada, a continuació se'n calcula el gradient i finalment es resolen les equacions de moviment tot obtenint unes noves configuracions nuclears. Si se segueix aquest procediment parlem de dinàmica molecular de Born-Oppenheimer. El problema d'aquest mètode és que és molt car ja que implica haver de resoldre el problema electrònic a cada pas.

En canvi, en dinàmiques moleculars Car-Parrinello això s'evita mitjançant la inclusió dels orbitals de Kohn-Sham en les equacions de moviment com a nous graus de llibertat. Així, al resoldre les equacions de moviment obtenim una noves coordenades nuclears (R_i) i uns nous orbitals electrònics (Ψ_i). L'esquema resultant que segueix una dinàmica molecular Car-Parrinello es mostra a la figura 3.3. Per tant, no només es mouen els nuclis sinó que també ho fan els electrons i això és precisament el que evita haver de resoldre el problema electrònic a cada pas de simulació.

Pel que fa a la descripció del mètode ve descrit pel lagrangià següent, on els graus de llibertat electrònics es tracten com a partícules clàssiques:

$$L_{CPMD} = \mu \sum_i \int |\dot{\Psi}|^2 dr + \frac{1}{2} \sum_I M_I \dot{R}_I^2 - E_{KS}[\Psi_i, R_I] + \sum_{ij} \Lambda_{ij} \left(\int \Psi_i^* \Psi_i dr - \delta_{ij} \right) \tag{3.11}$$

on el primer terme correspon a l'energia cinètica *fictícia* electrònica, essent μ la massa electrònica *fictícia*; el segon terme correspon a l'energia cinètica nuclear, essent M_I i R_I les masses i les posicions dels nuclis respectivament, E_{KS} és l'energia obtinguda a nivell DFT i Λ_{ij} són els multiplicadors de Lagrange que imposen l'ortonormalitat

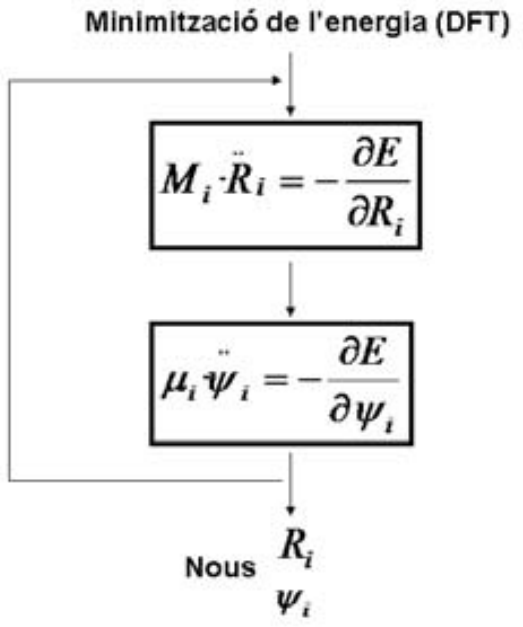

Figura 3.3: *Esquema de la dinàmica molecular Car-Parrinello.*

dels orbitals electrònics.

3.2.4 Metadinàmica acoblada a la dinàmica molecular Car-Parrinello

Tot i que gràcies al mètode CPMD podem realitzar càlculs de dinàmica molecular de primers principis, la potencialitat d'aquesta per tal de descriure reaccions químiques està fortament limitada pel temps de simulació que és necessari per tal que les reaccions químiques que volem descriure tinguin lloc. Això és degut a que la probabilitat de passar d'un mínim a una altre tot superant la barrera energètica que els separa depèn exponencialment de la barrera i excedeix fàcilment el temps de simulació que la tecnologia computacional ens proporciona avui en dia. En altres paraules, en aquesta escala de temps és molt difícil que la reacció que vulguem descriure tingui lloc espontàniament. Per tant, cal cercar alternatives i una d'aquestes alternatives és la metadinàmica.

La metadinàmica ens permet explorar la superfície d'energia lliure, essent una dinàmica artificial en l'espai definit per unes variables col·lectives (CVs) s_α.[214,215] Aquestes variables estan associades a alguns moviments col·lectius que seleccionem del sistema i ens permeten descriure el camí de reacció que ens interessi, com ara el trencament o la formació d'un enllaç. Són exemples de variables col·lectives la distància entre dos àtoms, els angles dièdres, els nombres de coordinació o qualsevol altra funció de les coordenades atòmiques. En aquesta tesi doctoral nosaltres hem fet ús dels nombres de coordinació. Cal remarcar que en aquest cas, nombre de coordinació es refereix al nombre d'enllaços entre dues espècies i no al terme d'acceptació comú en química organometàl·lica que es refereix al nombre de lligands coordinats al centre metàl·lic. El nombre de coordinació (CN) es defineix com una funció contínua de valors R_{ij} (la distància entre els àtoms i i j):

$$CN_i = \sum_{j=1}^{n} \left(\frac{1 - (\frac{R_{ij}}{d_0})^p}{1 - (\frac{R_{ij}}{d_0})^q} \right) \tag{3.12}$$

on i és l'àtom de referència, j corre sobre tots els àtoms coordinats a l'àtom de referència, d_0 és la distància de referència i p i q marquen el decreixement de la corba CN. El més important d'una variable col·lectiva és que ens permeti diferenciar els reactius dels productes de la reacció química que volem estudiar. El sistema complet de variables nuclears, electròniques i col·lectives ve donat per la lagrangiana extesa:

$$L = L_{CPMD} + \frac{1}{2}\sum_\alpha M_\alpha \dot{s}_\alpha^2 - \frac{1}{2}\sum_\alpha k_\alpha (s_\alpha(R) - s_\alpha)^2 - V(t,s) \tag{3.13}$$

on L_{CPMD} és la lagrangiana de Car-Parrinello descrita a la secció anterior. El primer terme afegit respecte la lagrangiana de Car-Parrinello és l'energia cinètica *fictícia* del conjunt de variables col·lectives s_α. M_α és la massa *fictícia* corresponent a les variables col·lectives. El segon terme és un potencial que força que els graus iònics de llibertat[†] es moguin conjuntament amb les variables col·lectives. En darrer lloc hi ha un terme potencial que depèn del temps i que augmenta el mostratge de l'espai configuracional, tot permetent que el sistema visiti zones de la superfície d'energia

[†]En dinàmiques moleculars Car-Parrinello el terme iònic equival a atòmic.

lliure que encara no s'han visitat mitjançant l'addició de termes de potencial repulsiu en forma de gaussianes localitzades. Cada gaussiana està caracteritzada per la seva amplada i alçada. Si aquestes gaussianes es posen suficientment a poc a poc, el potencial omple el pou d'energia lliure del reactiu de manera que el sistema es pot escapar via l'estat de transició més baix al següent mínim local. Això és el que es mostra a la figura 3.4 per un perfil de potencial en funció de la variable col·lectiva s, on la pilota vermella mostra la zona de l'estat de transició.

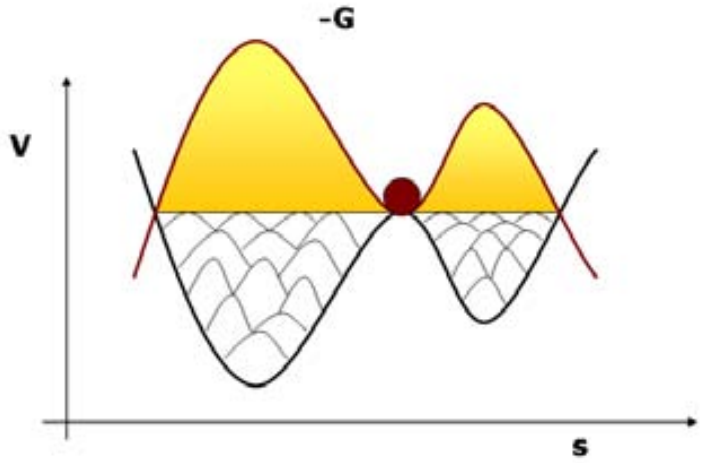

Figura 3.4: *Reconstrucció del perfil d'energia lliure (G) a partir del potencial afegit (V).*

El potencial que anem afegint és una estimació de l'energia lliure en funció de la variable col·lectiva s (figura 3.4). La trajectòria d'una metadinàmica no té sentit físic, però sí que en tenen en canvi els punts pels quals passem, ja siguin mínims o estats de transició. En una metadinàmica, hi ha diferents paràmetres que són importants de controlar: les constants d'acoblament k_α i les masses *fictícies* M_α de les variables col·lectives que hem definit, el *time step* i la temperatura i l'alçada i l'amplada de les gaussianes que anem afegint. Com a guia pràctica per tal de modificar k_α i M_α cal tenir en compte que com més gran és M_α més es desacoblen adiabàticament els graus de llibertat iònics i col·lectius però per contra més lenta és l'evolució de la variable col·lectiva corresponent, és a dir, que s'explora més lentament la superfície d'energia lliure. Pel que fa a k_α, com més gran és més juntes van $S_\alpha(r)$ i s_α i més petit és

el "*time step*" que s'ha d'utilitzar. Ensing proposà recentment una recepta per tal d'escollir tots aquests paràmetres.[216] Finalment, per tal d'obtenir major resolució, i per tant valors més acurats d'energia lliure hem d'anar afegint gaussianes cada vegada més i més petites. En aquesta mateixa línia, Parrinello i col·laboradors estimaren en un treball l'exactitud de la metadinàmica.[217]

Part II

Estudi teòric de la hidrogenació homogènia de compostos insaturats

Capítol 4

Hidrogenació mitjançant el catalitzador de Shvo

4.1 El catalitzador de Shvo

L'any 1985 el grup de Shvo sintetitzà el considerat primer catalitzador metall-lligand bifuncionalitzat: el qual s'ha anomenat catalitzador de Shvo (complex **1** de la figura 4.1).[95] Aquest complex organometàl·lic deu la seva versatilitat a l'equilibri que es mostra a la figura 4.1. Quan s'escalfa el complex bimetàl·lic **1** es forma l'espècie **A**, activa en hidrogenacions, i l'espècie **B** activa en oxidacions. Gràcies a l'hidrur enllaçat al Ru i el protó del grup OH de l'espècie **A** es pot donar la transferència d'hidrogen. Depenent de com aquesta transferència tingui lloc obtindrem els diferents mecanismes d'hidrogenació. Un cop ha tingut lloc la hidrogenació, l'espècie **A** es pot regenerar per reacció de l'espècie **B** i l'espècie donadora d'hidrogen i així es pot completar el cicle catalític. Casey i Cui mostraren mitjançant càlculs teòrics que aquesta regeneració es dóna heterolíticament quan l'hidrogen molecular és la font d'hidrogen i que pot ésser assistida per H_2O, etanol o la pròpia espècie saturada **A**.[218] Tal i com s'ha dit a la introducció, aquest catalitzador és capaç d'hidrogenar tan dobles enllaços polars (carbonils i imines) com també dobles i triples enllaços apolars (alquens i alquins). Tanmateix, la hidrogenació és més eficient pels enllaços polars, ja que la hidrogenació d'aquests es pot donar per sota de temperatura ambient mentre que la hidrogenació

d'alquins i d'alquens requereix temperatures més elevades.

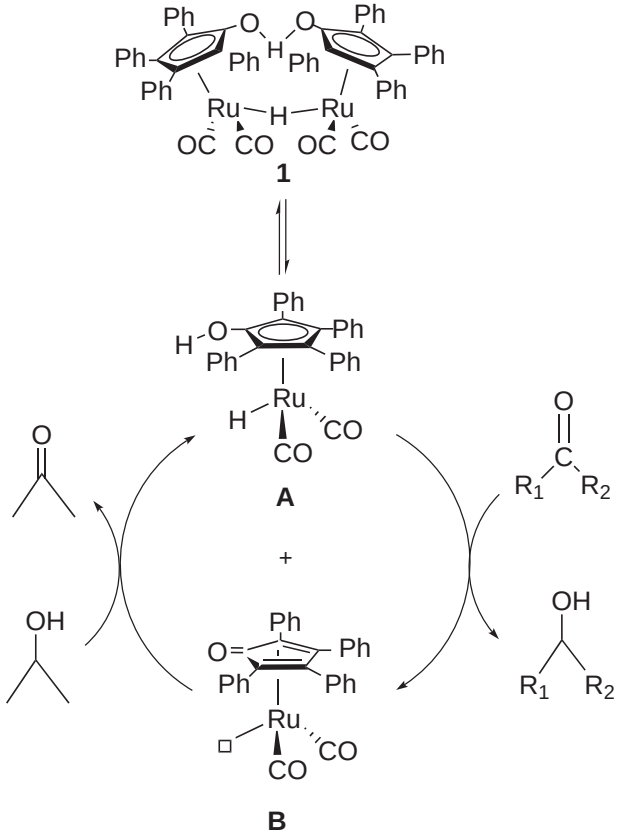

Figura 4.1: *Equilibri del catalitzador de Shvo amb la posterior transferència d'hidrogen. Un carbonil actua com a grup acceptor mentre que l'isopropanol actua com a grup donador.*

4.2 Controvèrsia experimental

El mecanisme d'hidrogenació dels carbonils mitjançant el catalitzador de Shvo era font de controvèrsia entre els grups de Casey i Bäckvall.[126,127] El primer proposava un mecanisme concertat de l'hidrur i del protó fora de l'esfera de coordinació del metall (veure part superior de la figura 4.2). La seva proposta es basava en efectes cinètics d'isòtop (KIEs) per a la hidrogenació de PhCHO fent servir una variant del catalitzador de Shvo: [2,5-Ph_2-3,4-Tol_2(η^5-C_4OH)]$Ru(CO)_2H$. Casey també s'ajudà de càlculs

teòrics DFT, tot mostrant la viabilitat energètica de la seva proposta mecanística, tot calculant-ne una barrera de 13.8 kcal·mol^{-1}.[128] En canvi, Bäckvall, basant-se en una aproximació similar en la deshidrogenació d'alcohols mitjançant l'espècie **B** també proposà un mecanisme concertat, però en aquest cas d'esfera interna. És a dir, amb coordinació prèvia del substrat, la qual era possible gràcies al desplaçament $\eta^5 \rightarrow \eta^3$ de l'anell de CpOH (veure part inferior de la figura 4.2).

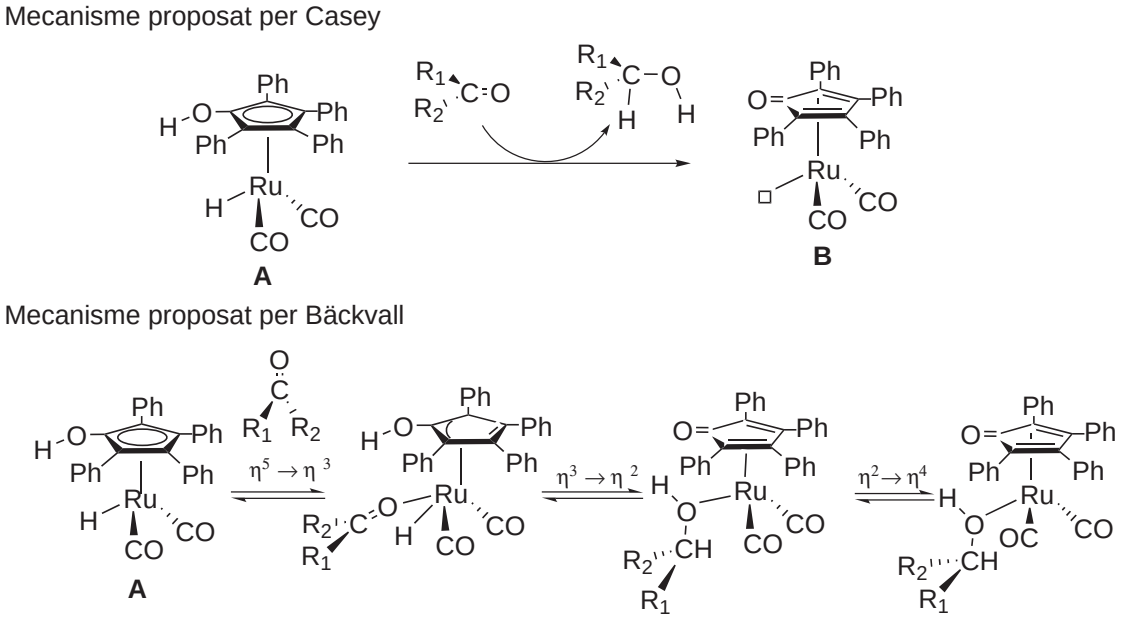

Figura 4.2: *Mecanismes d'hidrogenació dels carbonils mitjançant el catalitzador de Shvo proposats per Casey i Bäckvall, respectivament.*

La controvèrsia entre ambdós autors també es donava en el cas de les imines.[128–134] Tot i això, el cas de les imines presentava una complexitat superior ja que Casey proposà un canvi en el pas limitant de la velocitat de reacció de la hidrogenació depenent del substituent al nitrogen imínic en base a KIEs.[130] Proves d'atrapament d'imines que contenien una amina enllaçada al nitrogen imínic també estaven d'acord amb un mecanisme d'esfera externa.[128,219] D'altra banda, Bäckvall proposà un mecanisme d'esfera interna per les imines que és anàleg al mostrat a la figura 4.2 pels carbonils. Mitjançant KIEs,[131,132] Bäckvall també detectà canvis en l'etapa limitant de

la velocitat en funció de l'imina i mitjançant experiments d'atrapament trobà dades concordants amb el mecanisme d'esfera interna.[133]

En el cas de les imines, Casey i Bäckvall també realitzaren càlculs teòrics per tal de verificar els mecanismes que proposaven. Així, Casey trobà una barrera energètica de 4.8 kcal·mol^{-1} pel mecanisme d'esfera externa en la hidrogenació de H_2C=N-CH_3, prenent un model del catalizador complet i incloent l'efecte del solvent (THF) mitjançant un mètode continu (IEF-PCM).[128] Anàlogament, Bäckvall, Privalov i Samec analitzaren llur proposta mecanística prenent una imina electrodonadora ($(CH_3)_2$C=N-CH_3) i el catalitzador complet, tot incloent l'efecte del solvent mitjançant càlculs PCM i molècules de solvent explícites (CH_2Cl_2 en aquest cas). Trobaren una barrera energètica pel mecanisme d'esfera interna de 15 kcal·mol^{-1}, essent la coordinació de l'imina per desplaçament de l'anell de CpOH el pas limitant de la velocitat de la reacció, si be les etapes posteriors presentaven una energia molt similar.[134] La hidrogenació d'alquins Shvo proposà un cicle catalític on el trencament de la molècula d'hidrogen es dóna homolíticament i que s'inicia amb el desplaçament de l'anell de CpOH (veure figura 4.3).[119] La hidrogenació d'alquins té la particularitat que té un TON significativament baix en comparació amb les altres espècies insaturades. Shvo atribuí aquest fet a la formació d'una espècie molt estable (**D** de la figura 4.3) que enverinava el catalitzador. En el mateix treball, Shvo suggerí que per la hidrogenació d'alquens es pot considerar un mecanisme anàleg al mecanisme dels alquins. Per la mateixa reacció, Casey suggerí un mecanisme amb dissociació d'una molècula de CO seguida de la coordinació de l'alquè, la inserció a l'enllaç M-H i el trencament final de l'intermedi Ru-alquil mitjançant la molècula de H_2 amb l'alliberament de l'alcà com a producte final.[220]

4.3 El nostre estudi: resultats i discussió

Donada tota la controvèrsia experimental existent pel mecanisme d'hidrogenació mitjançant el catalitzador de Shvo, ens proposàrem comparar mitjançant càlculs teòrics DFT els mecanismes d'esfera interna i els mecanismes d'esfera externa per la hidrogenació de carbonils, imines, alquens i alquins. Realitzàrem optimitzacions mitjançant el funcional híbrid B3LYP i càlculs puntuals CPCM en solució (THF).

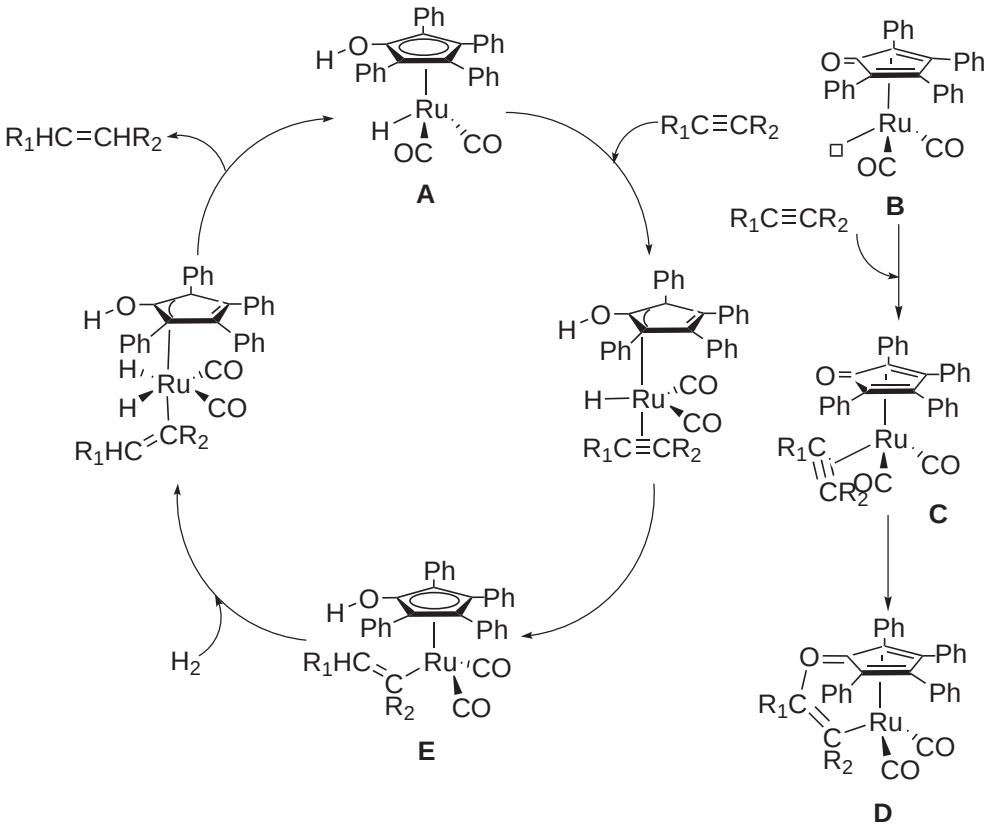

Figura 4.3: *Cicle catalític proposat per Shvo per a la hidrogenació d'alquins i ruta d'enverinament del catalitzador.*

Els valors d'energies presentats seran els dels càlculs puntuals en solució a no ser que es digui el contrari. En el cas dels carbonils també avaluàrem els KIEs. Inicialment, substituïrem els fenils del lligand [$Ph_5(\eta^5$-$C_4H_4COH)$] del catalitzador per hidròdens i, posteriorment, en alguns casos que ja es comentaran, es van incloure els substituents fenílics. Com a substrats, usàrem les espècies més simples amb enllaços C=O, C=N, C=C i C≡C: formaldehid, metanimina, etilè i acetilè, respectivament. En el cas de les imines també realitzàrem algunes optimitzacions en solució i càlculs amb l'imina substituïda H_3C-N=$C(CH_3)_2$.

4.3.1 Hidrogenació de carbonils

El procés global d'hidrogenació del formaldehid presentava un balanç energètic de -3.5 kcal·mol^{-1} en solució. Tot i que la controvèrsia a nivell experimental era la que s'ha descrit anteriorment, també es van avaluar altres mecanismes d'esfera interna: el mecanisme que involucrava la marxa d'un CO i permetia la coordinació del substrat i un altre mecanisme que incloïa el desplaçament $\eta^5 \rightarrow \eta^2$ de l'anell de CpOH, tal i com es mostra a la figura 4.4. Així doncs, es van avaluar tres mecanismes d'esfera interna a més del mecanisme d'esfera externa. Per tant, a continuació es descriuen els mecanismes avaluats d'esfera interna i d'esfera externa per la hidrogenació de carbonils .

Mecanismes d'esfera interna

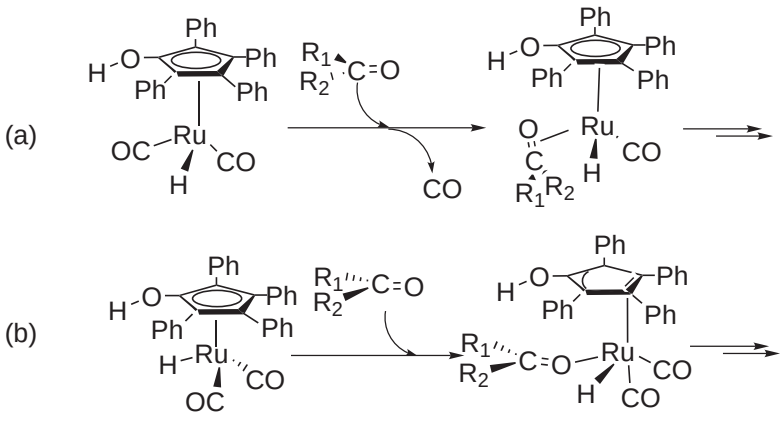

Figura 4.4: *Etapes inicials dels mecanismes d'esfera interna amb marxa del CO (a) i amb desplaçament $\eta^5 \rightarrow \eta^2$ de l'anell (b).*

La marxa del CO era endotèrmica en 45.7 kcal·mol^{-1} mentre que la substitució del grup de CO per un carbonil ho era en 26.8 kcal·mol^{-1}. D'aquesta manera, la marxa del CO era l'etapa limitant de la velocitat d'aquest mecanisme ja que els passos posteriors presenten barreres inferiors. Per tant, el cost energètic d'aquest procés era significativament elevat i això ens portà a descartar aquest mecanisme com a

mecanisme operatiu de reacció. La dificultat d'aquest procés també la detectà Casey, mostrant que l'intercanvi de CO per ^{13}CO es donava molt lentament a no ser que la reacció tingués lloc sota llum fluorescent.[126]

El següent mecanisme avaluat d'esfera interna fou el que implicava el desplaçament $\eta^5 \rightarrow \eta^2$ de l'anell de CpOH (figura 4.4 (b)). Aquest mode de coordinació de l'anell de Cp també s'havia mostrat com el més estable en altres compostos de metalls de transició[221,222] i també s'havia observat en estats de transició durant l'etapa de coordinació d'un lligand.[223] En aquest cas, el mecanisme proposat implicava la coordinació del substrat via el ja esmentat desplaçament de l'anell,[†] la posterior inserció del carbonil a l'enllaç Ru-H i la transferència del protó a l'oxigen del carbonil. Totes les etapes d'aquest mecanisme de reacció es mostren a la figura 4.5.

El desplaçament $\eta^5 \rightarrow \eta^2$ de l'anell presentava una barrera de 19.7 kcal·mol^{-1} i donava com a resultat l'intermedi **co-2b**. En aquesta etapa es donava simultàniament la coordinació η^1 de l'atom d'oxigen del carbonil al ruteni. Seguidament, es donava el canvi de coordinació de η^1 a η^2 del carbonil, endotèrmica en 5.8 kcal·mol^{-1} (**co-3b**). Les posteriors transferències de l'hidrur i del protó, estaven localitzades al perfil energètic 25.7 i 24.8 kcal·mol^{-1} per sobre dels reactius inicials, respectivament. La barrera global d'aquest mecanisme era de 33.0 kcal·mol^{-1} en solució respecte el mínim inicial entre el catalitzador i el substrat (des de **co-1a** fins a **co-ts2a** de la figura 4.6).

Per tant, aquest mecanisme d'esfera interna, si bé era més favorable que el que es dóna mitjançant la marxa del CO (45.7 kcal·mol^{-1}) encara era massa elevat (33.0 kcal·mol^{-1}) per ésser el mecanisme operatiu de la reacció d'hidrogenació.

Un mecanisme inesperat que es trobà durant la realització d'aquest estudi fou el mecanisme d'esfera interna, en el qual la transferència de l'hidrur i del protó es dóna concertadament però amb prèvia coordinació del substrat al metall. En aquest cas, el desplaçament de l'anell de CpOH era de η^5 a η^3. Aquest mode de coordinació només s'observà per a l'estat de transició d'aquest procés, si bé també s'havia observat per altres metalls de transició durant processos de substitució de lligands.[223] El perfil energètic d'aquest mecanisme presentava una barrera energètica de 34.6 kcal·mol^{-1} (des de **co-1b** fins a **co-ts1c** de la figura 4.7).

[†]El mode de coordinació η^2 es donava tan a l'estat de transició com al producte resultant.

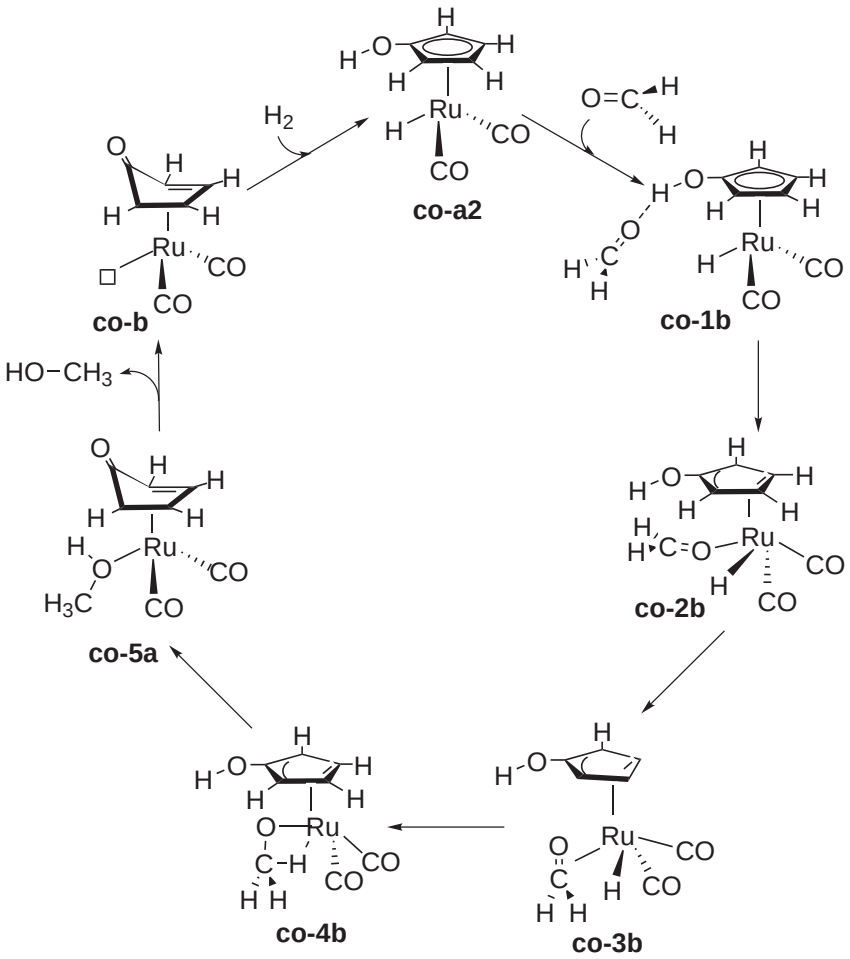

Figura 4.5: *Etapes del mecanisme d'hidrogenació dels carbonils amb desplaçament* $\eta^5 \rightarrow \eta^2$ *de l'anell de CpOH.*

Pel mecanisme més favorable dels mecanismes d'esfera interna avaluats (el que inclou el desplaçament $\eta^5 \rightarrow \eta^2$ de l'anell de CpOH), avaluàrem l'efecte d'incloure els substituents fenílics al catalitzador. El resultat fou que el mínim més estable presentava una energia de 20.7 kcal·mol^{-1} en fase gas respecte els reactius inicials. Per aquest mecanisme també s'avaluà l'efecte cinètic d'isòtop combinat RuD-OD i obtinguérem un valor de 0.8, el qual difereix significativament del valor trobat per Casey i col·laboradors en toluè: 3.6 ± 0.25.[224]

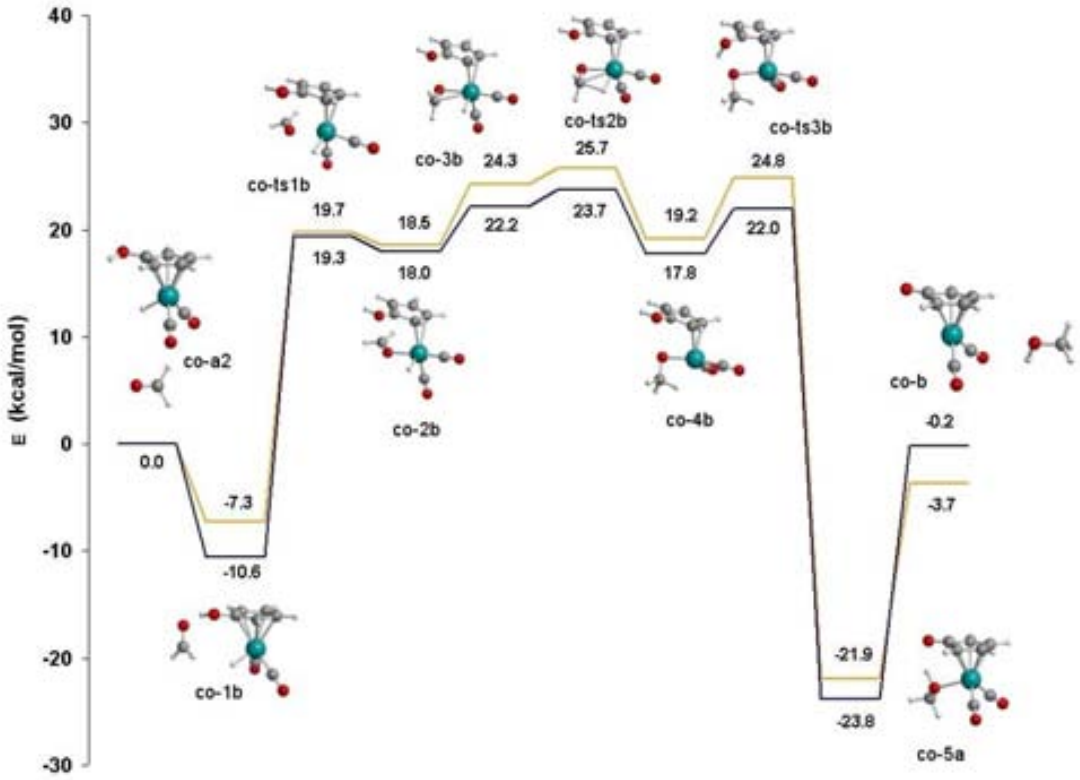

Figura 4.6: *Perfil energètic en fase gas (blau) i en solució (taronja) pel mecanisme d'hidrogenació dels carbonils amb desplaçament $\eta^5 \rightarrow \eta^2$ de l'anell de CpOH.*

Mecanisme d'esfera externa

Pel que fa al mecanisme concertat d'esfera externa, presentava una barrera energètica de 7.7 kcal·mol^{-1}. Casey i col·laboradors havien calculat pel mateix procés una barrera de 13.8 kcal·mol^{-1} mitjançant càlculs teòrics.[128] La inclusió dels fenils en el catalitzador no varià significativament el valor de la barrera energètica: 8.0 kcal·mol^{-1}. La geometria d'ambdós estats de transició amb les distàncies més significatives es mostra a la figura 4.8. Aquest valor estava d'acord amb dades experimentals del grup de Casey ja que per a la hidrogenació de PhCHO en THF-d_8 amb 0.1 mol·L^{-1} de H_2O o D_2O trobaren una $\Delta H^{\ddagger} = 12.0 \pm 1.5$ kcal·mol^{-1},[126] mentre que en THF-d_8

sec trobaren una $\Delta H^{\ddagger} = 11.2 \pm 0.9$ kcal·mol^{-1}.[†,224] Una altra dada que podíem comparar amb dades experimentals era el KIE combinat Ru-OD, pel qual Casey trobà un valor experimental de 3.6 ± 0.25.[224]

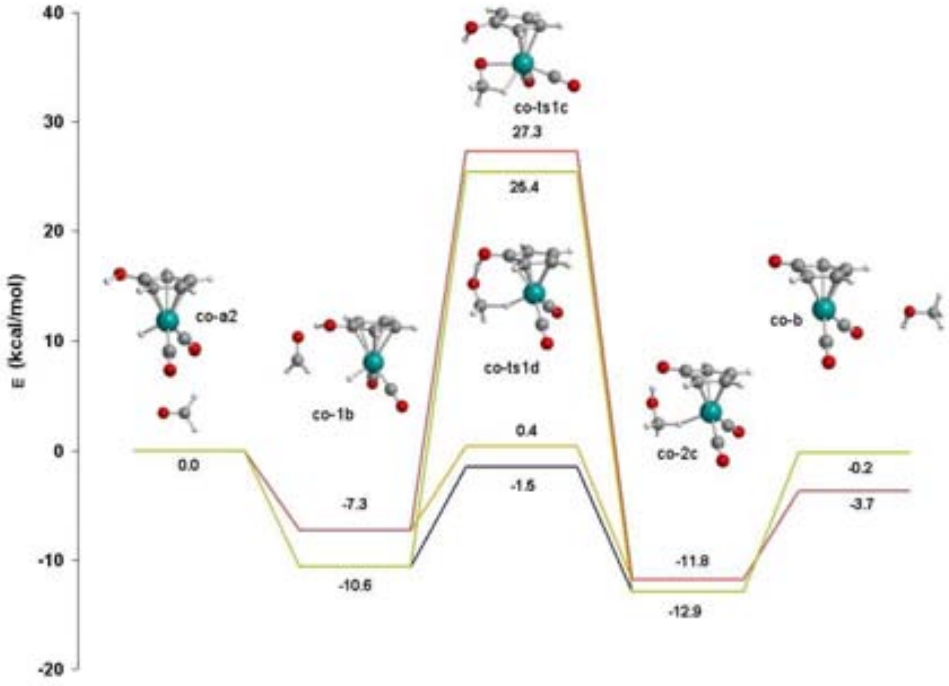

Figura 4.7: *Perfils energètics en fase gas i en solució pels mecanismes concertats d'esfera interna i d'esfera externa d'hidrogenació dels carbonils. El mecanisme concertat d'esfera interna es mostra en verd en fase gas i en vermell en solució mentre que el mecanisme concertat d'esfera externa es mostra en blau en fase gas i en taronja en solució.*

Per tant, vam calcular el KIE d'una forma aproximada mitjançant les equacions 4.1 i 4.2 a 298.15 K de temperatura i a 1 atm de pressió.

$$KIE = \frac{k_H}{k_D} = e^{\frac{(\Delta G_D^{\ddagger} - \Delta G_H^{\ddagger})}{RT}} \tag{4.1}$$

$$\Delta G_X^{\ddagger} = G_X^{\ddagger} - G_X^{Adducte} \qquad X = H, D \tag{4.2}$$

[†]Ambdós valors són per l'anàleg del catalitzador de Shvo: [2,5-Ph_2-3,4-Tol_2(η^5-C_4OH)]$Ru(CO)_2H$.

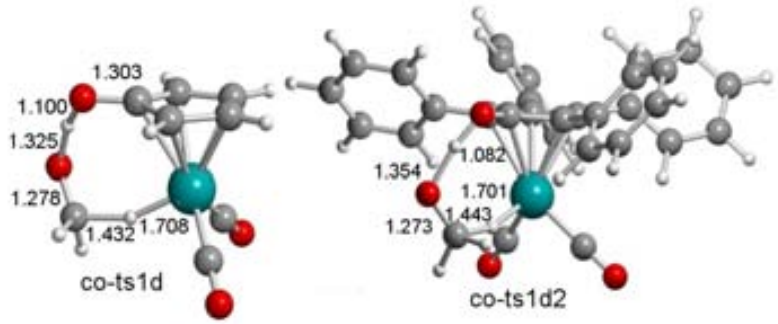

Figura 4.8: *Geometries dels estats de transició del mecanisme concertat d'esfera externa pel sistema model i pel sistema complet. Distàncies en Å.*

D'aquesta manera, vam obtenir un valor pel KIE combinat RuD-OD pel mecanisme d'esfera externa concertat de 3.8 pel sistema model i de 3.5 pel sistema complet (incloent els substituents fenílics). Per contra, el mecanisme concertat d'esfera interna presentava un valor de 0.8. Per tant, el KIE calculat pel mecanisme d'esfera externa era molt similar a l'obtingut experimentalment i en conseqüència els KIEs també suggerien que el mecanisme d'esfera externa concertat era un candidat adient com a mecanisme operatiu de la reacció.

4.3.2 Hidrogenació d'imines

El mecanisme d'hidrogenació de la metanimina presentava un balanç energètic de -9.0 kcal·mol^{-1}. En aquest cas només es va avaluar el mecanisme d'esfera interna amb desplaçament $\eta^5 \rightarrow \eta^2$ de l'anell, ja que el mecanisme que involucrava la marxa del CO es descartà inicialment degut a l'elevat cost energètic que suposava. D'altra banda, també s'avaluà el mecanisme d'esfera externa proposat per Casey.

Mecanisme d'esfera interna

El mecanisme amb desplaçament $\eta^5 \rightarrow \eta^2$ de l'anell és anàleg al trobat en el cas dels carbonils. Pel desplaçament inicial de l'anell calculàrem una barrera relativa de 26.3 kcal·mol^{-1}. El mínim resultant estava situat a 4.6 kcal·mol^{-1} respecte els reactius inicials i presentava una geometria amb l'imina coordinada al metall mitjançant una coordinació η^1. Els següents passos són la rotació de la imina i el canvi de coordinació de la imina de η^1 a η^2, endotèrmica en 19.0 kcal·mol^{-1}. Posteriorment, tenia lloc la transferència de l'hidrur i del protó al carboni i al nitrogen imínics, respectivament. Ambdós passos són els punts més alts en energia del perfil energètic: 27.8 i 29.6 kcal·mol^{-1}, respectivament. La barrera global d'aquest mecanisme és de 39.7 kcal·mol^{-1} en solució (des de **cn-1d** fins a **cn-ts3d** de la figura 4.9). Com que per aquest mecanisme Bäckvall i col·laboradors proposaren que la inclusió dels substituents fenílics ajudava al desplaçament del lligand aromàtic,[134] incloguérem els fenils i reoptimitzàrem en solució quasi bé tots els mínims mostrats a la figura 4.9. El perfil energètic obtingut no varià significativament i, per tant, el sistema model i els càlculs puntuals en solució són adients per a la descripció d'aquest mecanisme. Cal remarcar que la barrera global d'aquest mecanisme (40.4 kcal·mol^{-1}) difereix significativament del valor obtingut per Privalov i Bäckvall (15 kcal·mol^{-1}).[134]

Pel que fa al mecanisme d'esfera interna amb desplaçament $\eta^5 \rightarrow \eta^3$ de l'anell de CpOH, el qual fou localitzat en el cas dels carbonils, no fórem capaços de localitzarlo en el cas de les imines. Probablement això significa que, en cas d'existir, aquest mecanisme és massa costós energèticament per ésser un camí de reacció raonable.

Mecanisme d'esfera externa

Pel que fa al mecanisme concertat d'esfera externa, calculàrem una barrera energètica de 9.6 kcal·mol^{-1} en solució. La inclusió dels fenils al catalitzador i la reoptimització en solució provocà una lleugera disminució de la barrera energètica: 6.8 kcal·mol^{-1}. Pel que fa a la geometria de l'estat de transició, la inclusió dels fenils i del solvent provocà que el protó estigués més transferit al nitrogen imínic i que l'hidrur estigués menys transferit al carboni imínic. Això portat a l'extrem obriria la porta a un mecanisme per passos amb transferència inicial del protó i amb posterior transferència

de l'hidrur. Pel que fa a l'optimització en solvent del procés d'hidrogenació de l'espècie $(CH_3)_2C{=}N\text{-}CH_3$, presentava una barrera inferior: 4.0 kcal·mol^{-1}.

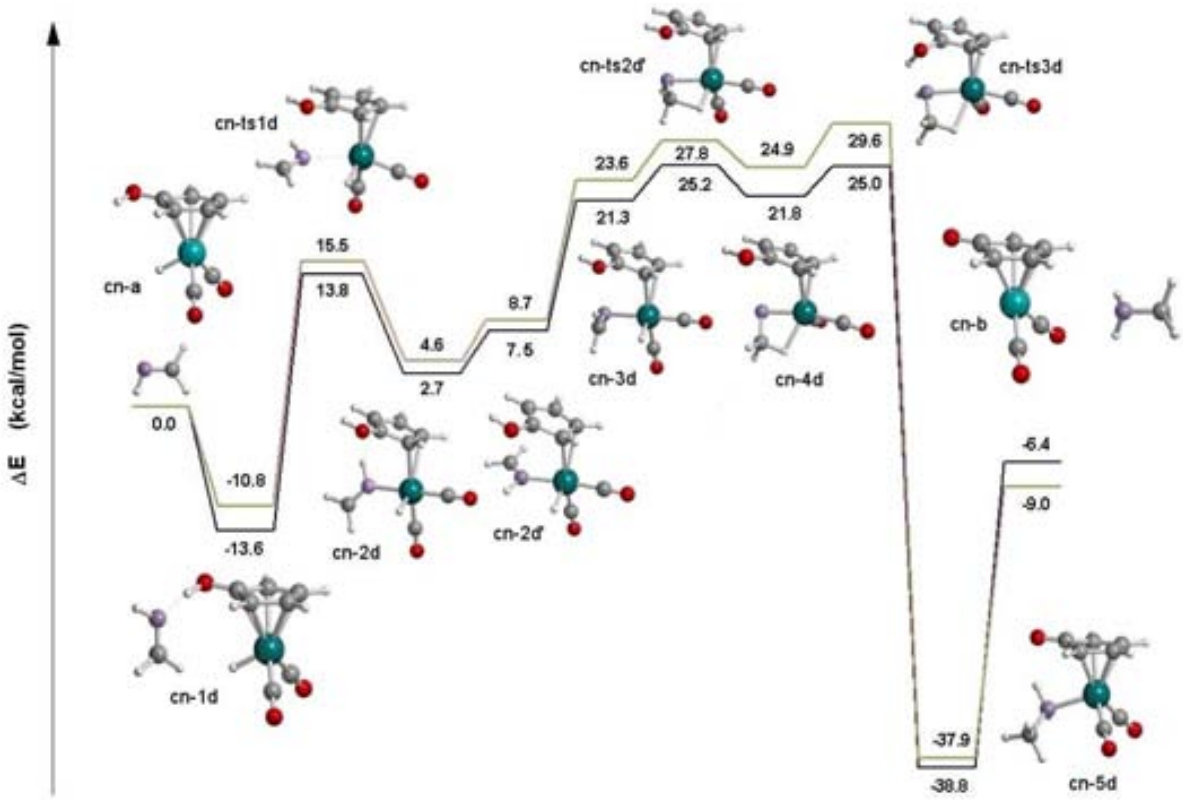

Figura 4.9: *Perfil energètic en fase gas (blau) i en solució (taronja) pel mecanisme d'hidrogenació de les imines amb desplaçament $\eta^5 \rightarrow \eta^2$ de l'anell de CpOH.*

Les estructures dels estats de transició de la hidrogenació de $H_2C{=}NH$ pel sistema model optimitzat en fase gas i de la hidrogenació de $(CH_3)_2C{=}N\text{-}CH_3$ pel sistema complet optimitzat en solució es mostren a la figura 4.10. A l'augmentar la basicitat de la imina, torna a augmentar una altra vegada l'asincronia entre la transferència del protó i de l'hidrur. Pel que fa als valors obtinguts per les barreres calculades, els nostres resultats estan d'acord amb el valor de 4.8 kcal·mol^{-1} obtingut per Casey i Cui mitjançant càlculs puntuals MP2 en solució (PCM) sobre geometries optimitzades a nivell B3LYP.[128]

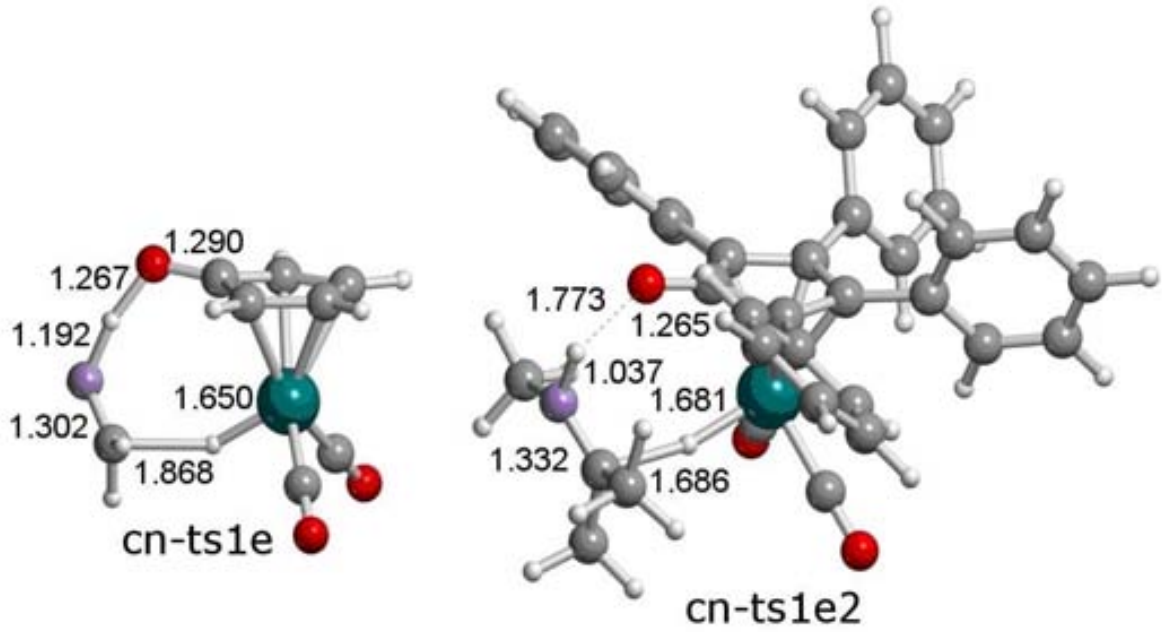

Figura 4.10: *Estats de transició de la hidrogenació de H_2C=NH (**cn-ts1e**) pel sistema model optimitzat en fase gas i de la hidrogenació de $(CH_3)_2C$=N-CH_3 pel sistema complet (**cn-ts1e2**) optimitzat en solució. Distàncies en Å.*

Cal remarcar que la barrera energètica del mecanisme d'esfera externa és més de 10 kcal·mol^{-1} més favorable en energia que la barrera obtinguda per Privalov i Bäckvall pel seu mecanisme d'esfera interna (15 kcal·mol^{-1}).[134] D'altra banda, la barrera obtinguda pel nostre estudi pel mecanisme d'esfera interna presenta un valor molt superior (40.4 kcal·mol^{-1}).

4.3.3 Hidrogenació d'alquens i alquins

El balanç energètic de la hidrogenació d'alquins i alquens presenta valors de -28.9 i -17.7 kcal·mol^{-1}, respectivament. Per aquests processos, s'avaluà el mecanisme

d'esfera interna amb desplaçament $\eta^5 \rightarrow \eta^2$ de l'anell i el mecanisme d'esfera externa proposat per Casey, ja que el mecanisme d'esfera interna amb marxa del CO proposat per Casey es descartà inicialment degut a l'elevat cost energètic que suposava.

Mecanismes d'esfera interna

Les etapes avaluades per la hidrogenació dels alquins es mostren a la figura 4.11. Pels alquins, l'etapa de desplaçament $\eta^5 \rightarrow \eta^2$ de l'anell de CpOH amb coordinació de l'acetilè presentava una barrera relativa de 26.3 kcal·mol^{-1} en solució i donava lloc a l'espècie **cc-2f**. La posterior transferència de l'hidrur presentava una barrera relativa de 8.2 kcal·mol^{-1} produint l'intermedi **cc-3f**. Aquest, era el punt més alt del perfil energètic, essent la barrera global del mecanisme de 32.3 kcal·mol^{-1}. La transferència del protó presentava una barrera relativa molt gran després de la recoordinació η^5 de l'anell (des de **cc-4f** a **cc-5f**), de 33.0 kcal·mol^{-1} en solució. Així, en aquest cas, fou necessària la inclusió d'una molècula d'hidrogen que per metàtesis de l'enllaç σ de l'hidrogen produïa l'alquè i la regeneració del catalitzador (des de l'espècie **cc-3f** a la **cc-7f** passant per **cc-6f**). Aquesta etapa prenia una barrera relativa raonable de 7.4 kcal·mol^{-1}, donant lloc a un cicle catalític menys abrupte. La proposta de Shvo que el trencament de l'hidrogen fós homolític (a través d'una espècie de Ru(IV))[119] la descartàrem, ja que no localitzàrem l'estructura resultant a la superfície d'energia de potencial.

Pels alquens s'analitzà un mecanisme anàleg al mostrat a la figura 4.11 per la hidrogenació dels alquins. Així, s'obtingué una barrera relativa pel desplaçament $\eta^5 \rightarrow \eta^2$ de l'anell amb coordinació de l'alquè de 24.3 kcal·mol^{-1} en solució. La posterior transferència de l'hidrur presentava una barrera relativa de 9.0 kcal·mol^{-1}. Aquest era el punt més alt del perfil energètic (28.0 kcal·mol^{-1}), el qual presentava una barrera global de 29.6 kcal·mol^{-1} en solució. Altra volta, la transferència del protó era massa elevada des de la coordinació η^5, ja que presentava una barrera relativa de 43.0 kcal·mol^{-1}.[†] La barrera per a aquesta etapa, tan pels alquens com pels alquins,

[†]A diferència dels alquins, on només es localitzà la transferència amb coordinació η^5 de l'anell, pels alquens aquesta transfèrencia es localitzà tan des de la coordinació η^2 de l'anell (amb una barrera relativa de 33.6 kcal·mol^{-1}) com des de la coordinació η^5.

era significativament major que la trobada pels dobles enllaços polars (carbonils i imines).

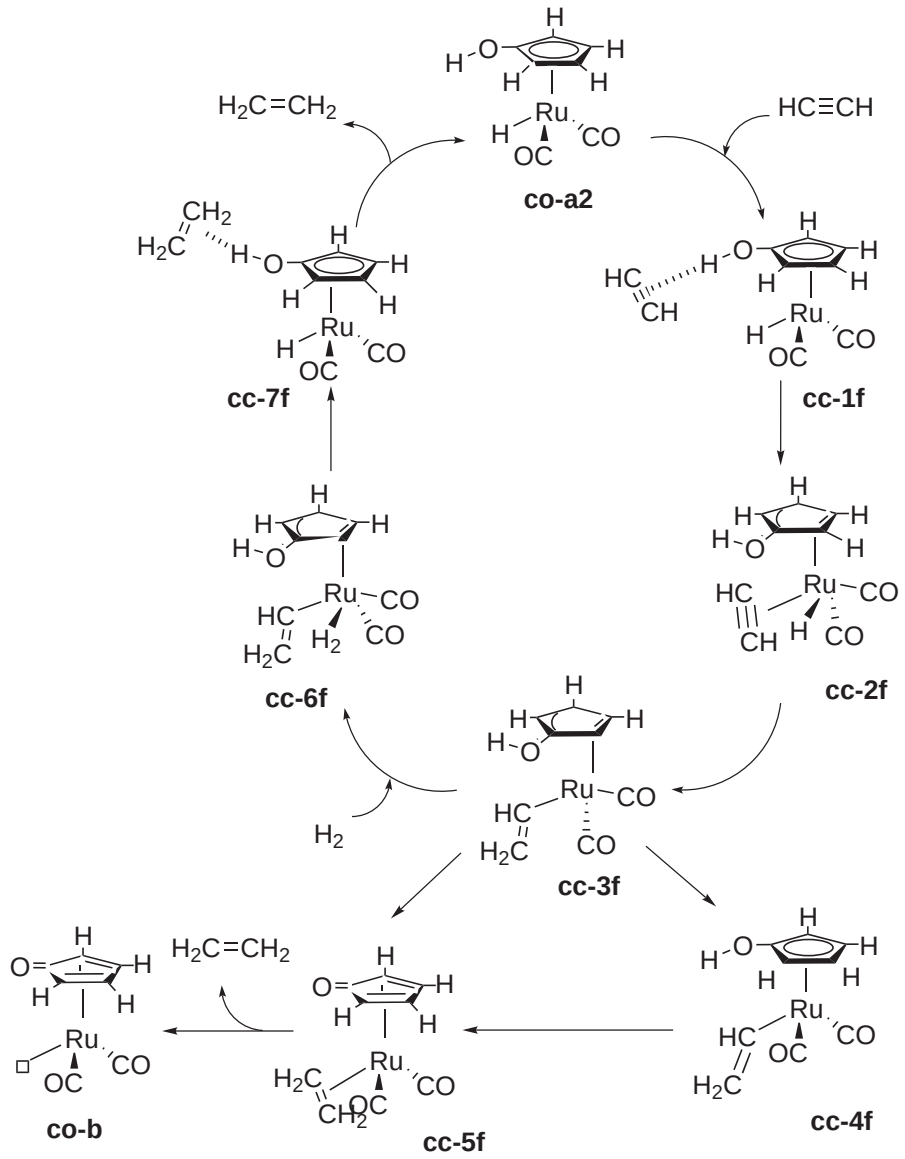

Figura 4.11: *Etapes pel mecanisme d'esfera interna amb desplaçament* $\eta^5 \rightarrow \eta^2$ *per la hidrogenació d'alquins. Pels alquens es trobà un mecanisme anàleg que s'inicia amb l'intermedi* ***cc-7f****.*

Aquesta diferència energètica es podia explicar per la menor basicitat que presen-

ten els alquens i els alquins respecte carbonils i les imines. Quedant descartada la transferència pròtica com a alternativa, només quedava per avaluar la metàtesi σ de la molècula d'hidrogen, la qual presentava una barrera relativa de 8.0 kcal·mol^{-1} en solució.

Mecanisme d'esfera externa

Pel què fa al mecanisme concertat d'esfera externa pels alquins, trobàrem una barrera de 18.5 kcal·mol^{-1}, mentre que el mecanisme anàleg pels alquens presentava una barrera de 17.9 kcal·mol^{-1}.[†] Aquestes barreres eren al voltant d'unes 10 kcal·mol^{-1} superiors a les barreres anàlogues de carbonils i imines. En conseqüència, això permetia explicar la quimioselectivitat observada pels dobles enllaços polars enfront els enllaços múltiples carboni-carboni.

En darrer lloc, fórem capaços d'avaluar la ruta de desactivació proposada per Shvo per la hidrogenació d'alquins (espècie **D** de la figura 4.3), essent un procés amb una barrera energètica de 23.4 kcal·mol^{-1} i termodinàmicament molt afavorit: exotèrmic en 34.8 kcal·mol^{-1}. Per aquest mateix procés també localitzàrem un intermedi metall-alquenil molt estable al llarg del cicle catalític (-35.2 kcal·mol^{-1}). Això concordava amb l'elevada estabilitat que trobà Shvo per aquest intermedi.

4.4 Conclusions

S'han avaluat mitjançant càlculs teòrics DFT mecanismes d'hidrogenació d'esfera interna i d'esfera externa per la hidrogenació de carbonils, imines, alquens i alquins mitjançant el catalitzador de Shvo. Els resultats obtinguts han permès concloure que:

- El sistema model del catalitzador (substituïnt fenils per hidròsgens al lligand aromàtic) és adequat per descriure computacionalment la reacció d'hidrogenació del catalitzador de Shvo. L'efecte dels substituents fenílics s'ha mostrat energèticament poc significatiu en els casos on s'ha tingut en compte.

[†]Aquestes barreres d'energia són clarament inferiors a les trobades pels mecanismes d'esfera interna.

D'altra banda, l'efecte del solvent (THF) també s'ha mostrat poc rellevant energèticament, ja que afecta poc les barreres de reacció obtingudes.

- El mecanisme d'esfera externa és el mecanisme de transferència d'hidrogen més favorable per tots i cadascun dels substrats en base a les barreres energètiques de reacció obtingudes. A més, en el cas dels carbonils, el KIE calculat pel mecanisme d'esfera externa és el que més concorda amb el KIE experimental.

- L'elevada asincronicitat de l'estat de transició del procés d'hidrogenació de l'imina [H_3C-N=$C(CH_3)_2$] obre la porta a la possibilitat que un mecanisme per passos amb transferència del protó i transferència posterior de l'hidrur sigui factible a l'augmentar la basicitat de l'imina.

- Pels enllaços múltiples apolars (alquens i alquins), la barrera energètica del mecanisme d'esfera externa és aproximadament 10 kcal·mol^{-1} més elevada que per dobles enllaços polars (carbonils i imines). Aquest fet permet explicar la quimioselectivitat observada experimentalment.

- En el cas dels alquins, la ruta de desactivació del catalitzador proposada per Shvo s'ha vist que podia ser energèticament competitiva amb la reacció d'hidrogenació.

Capítol 5

Hidrogenació d'alquens mitjançant complexos de Au(III) i Pd(II)

5.1 Catàlisi mitjançant complexos d'or i compostos anàlegs de pal·ladi

Durant dècades l'ús de l'or com a catalitzador en catàlisi homogènia havia estat obviat per la comunitat científica degut a l'extès *prejudici* entre els químics que el fet de ser un metall intert el convertia en un metall poc atractiu com a catalitzador. Tanmateix, darrerament les coses han canviat i s'han trobat nombroses reaccions on l'or actua eficaçment, tan en processos de catàlisi heterogènia com en processos de catàlisi homogènia.[225–235] Podem destacar les reaccions d'oxidació, les addicions nucleòfiles a sistemes π, les reaccions de *cross-coupling* i les hidrogenacions d'alquens i d'imines entre d'altres. A més a més, recentment s'han estudiat teòricament nombroses reaccions catalitzades per complexos d'or.[236–246]

D'altra banda, resultats experimentals de Corma i col·laboradors mostraren que complexos de Au(III) eren capaços d'hidrogenar olefines a elevats TOFs. La síntesi i l'estructura d'aquests catalitzadors homogenis d'or es mostra la figura 5.1 (complexos **2Au**, **3Au**, **4Au**, **5Au**). També se sintetitzaren complexos anàlegs de Pd(II), dels quals s'esperava que es comportéssin de manera similar als complexos de Au(III) ja que les dues famílies de complexos són isoelectròniques (d^8). En ambdós casos, su-

portar els catalitzadors sobre un substrat polar (MCM-41) incrementava el TOF dels catalitzadors. Si posteriorment s'augmentava l'acidesa de la superfície per substitució de Si per Al (MCM-41, Si/Al = 50) el TOF dels catalitzadors encara augmentava més. La taula 5.1 mostra els valors de TOF corresponent a la hidrogenació mitjançant el complex 2 d'or (**2Au**) i del seu anàleg de pal·ladi (**2Pd**) de la figura 5.1, per les diferents situacions ja esmentades.

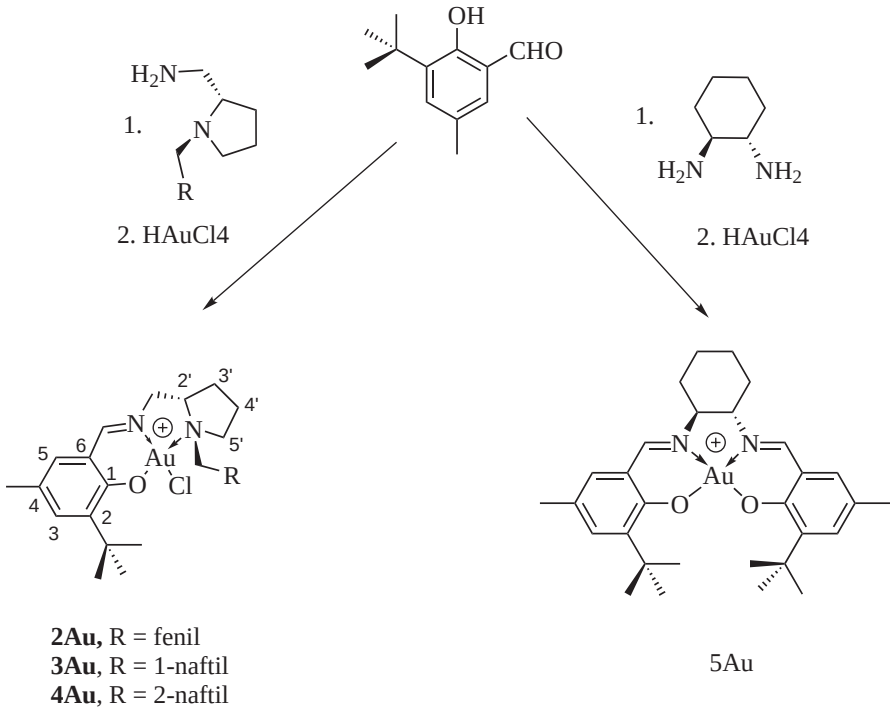

2Au, R = fenil
3Au, R = 1-naftil
4Au, R = 2-naftil

5Au

Figura 5.1: *Síntesi dels catalitzadors homogenis d'or.*

Aquests resultats suggerien l'activació heterolítica de l'hidrogen ja que en aquest cas es forma un hidrur neutre i un protó, i aquest fet permetria explicar l'increment de l'activitat catalítica quan augmenta la polaritat i l'acidesa del substrat.

5.2 El nostre estudi: resultats i discussió

El nostre objectiu era trobar un mecanisme d'hidrogenació viable per la hidrogenació d'alquens mitjançant els complexos de Au(III), ja que fins llavors no hi havia cap

proposta mecanística per la hidrogenació homogènia mitjançant complexos d'or.

Taula 5.1: *TOFs ($mmol_{substrat} \cdot mmol^{-1}_{catalitzador} \cdot h^{-1}$) per la hidrogenació catalítica de dietilitaconat ($(EtO_2C\text{-}CH_2)(EtO_2C)C{=}CHPh$) en EtOH mitjançant el complex **2Au** i el complex **2Pd** sense suportar i suportats sobre els substrats MCM-41 i MCM-41,Si/Al=50, en condicions de 4 bar de H_2, 40 ºC i amb una ratio substrat/catalitzador igual a 1000).*

Estructura	Au^{III}	Pd^{II}
2	3430	3360
2-(MCM-41)	4920	4980
2-(MCM-41,Si/Al=50)	6730	6000

A més, també ens proposàrem avaluar el mecanisme d'hidrogenació mitjançant complexos de Pd(II) per tal de veure si operava mitjançant el mateix mecanisme de reacció. Per tal de fer-ho, combinàrem els estudis cinètics realitzats per Corma i col·laboradors i els càlculs teòrics. Així, pel que fa als càlculs teòrics, realitzàrem optimitzacions mitjançant el funcional híbrid B3LYP i càlculs puntuals PCM en solució (EtOH). Tots els valors presentats en aquest capítol són en solució a no ser que es digui el contrari. Per tal de minimitzar el cost computacional, escollírem un dels catalitzadors (complex **2Au** i el seu anàleg de pal·ladi), prenguérem un model d'aquest (**1Au** i **1Pd** de la figura 5.2) tan per l'or com pel pal·ladi i usàrem etilè com a substrat de la reacció.

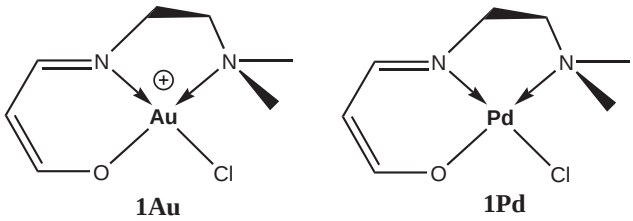

Figura 5.2: *Sistema model pel complex **2Au** (**1Au**). Pel cas del pal·ladi usàrem el complex anàleg que es mostra (**1Pd**).*

5.2.1 Hidrogenació mitjançant complexos d'or

En aquesta secció es descriuen breument les etapes de reacció avaluades mitjançant els càlculs teòrics per la hidrogenació utilitzant el model **1Au**, tot comparant-les amb les dades cinètiques obtingudes per Corma i col·laboradors. Cadascuna de les etapes del mecanisme de reacció es comenta en un subapartat diferent.

Activació de l'hidrogen

En primer lloc, s'havia de trobar una via per tal d'activar l'hidrogen molecular. Com ja s'ha comentat a la introducció, l'activació de l'hidrogen podia tenir lloc homolíticament o heterolítica i, per tant, s'avaluaren ambdós processos d'activació.

El primer es descartà, ja que el producte de l'activació homolítica era aproximadament 50 kcal·mol^{-1} més inestable que els reactius corresponents (en fase gas). Això es podia explicar per la dificultat de l'or d'assolir l'estat d'oxidació Au(V).

Pel que fa a l'activació heterolítica, aquesta dóna com a resultat la formació d'un enllaç M-H i la formació d'un protó. La destinació del protó és el que distingeix els diferents trencaments heterolítics. Així doncs, s'avaluà que el protó anés a parar als següents lligands del complex: al grup oxo, al nitrogen de l'amina i al clorur, trobant barreres pels trencaments heterolítics de l'hidrogen de 47.4, 53.4 i 37.8 kcal·mol^{-1}, respectivament. Aquestes etapes es mostren a la figura 5.3 juntament amb les estructures dels estats de transició corresponents i els valors de les barreres associades a cada procés. Aquestes barreres encara eren massa elevades perquè formessin part del mecanisme operatiu de reacció. Així doncs, avaluàrem la possible influència del solvent (EtOH) a través d'un estat de transició de sis membres, on el solvent assistiria al trencament heterolític de l'hidrogen, tal i com ja s'ha esmentat a la introducció. Així, calculàrem els mecanismes assistits pel trencament heterolític sobre el grup oxo i el clorur i trobàrem barreres de reacció molt més baixes: 31.5 i 26.8 kcal·mol^{-1} respecte els reactius inicials, la qual cosa significava una disminució en 16 i 11 kcal·mol^{-1} de cada barrera de reacció. Els estats de transició d'aquests dos processos es mostren a la figura 5.4. Com que el trencament heterolític de l'hidrogen sobre el clorur és el més favorable dels camins de reacció avaluats prenguérem aquesta etapa com el pas que genera l'espècie activa del cicle catalític. Aquesta etapa dóna com a productes

l'espècie metall-hidrur, $EtOH_2^+$ i Cl^- tal i com es mostra a la figura 5.5.

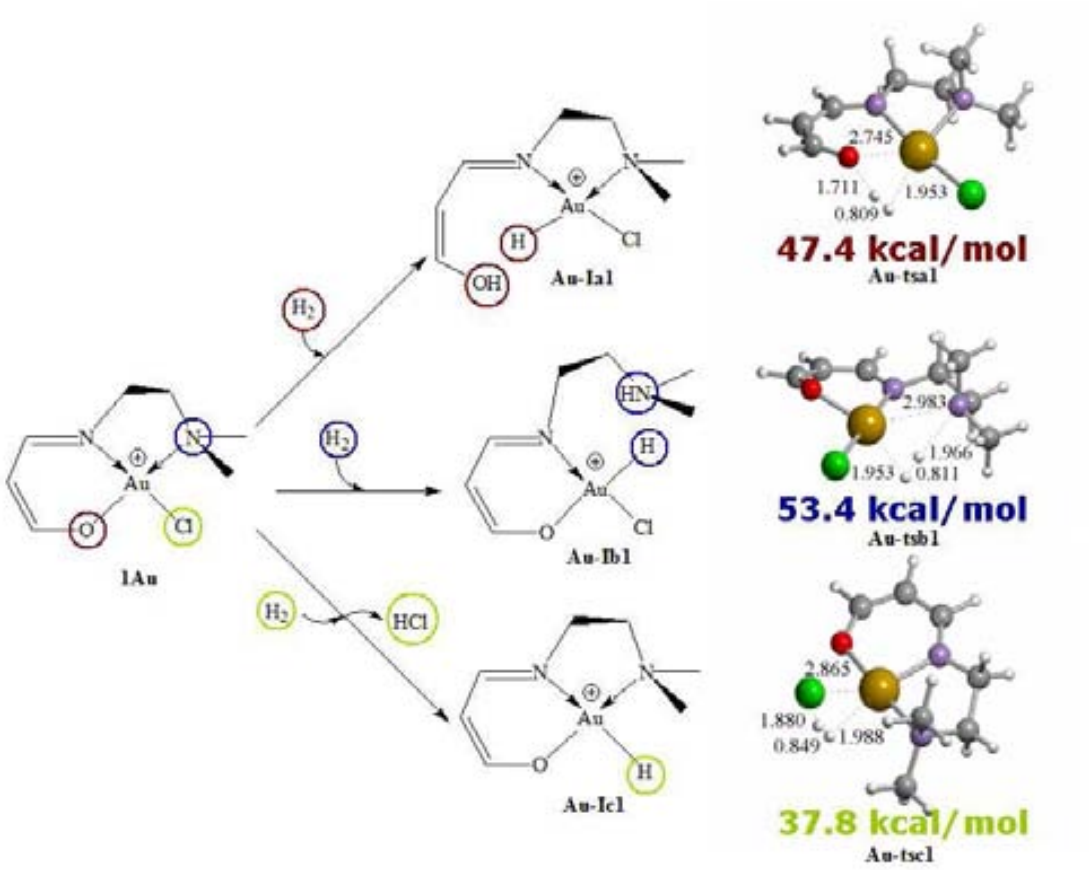

Figura 5.3: *Etapes dels trencaments heterolítics sobre els lligands oxo, amino i clorur, respectivament. També es mostren les estructures dels estats de transició corresponents i els valors de les barreres associades a cada procés. Distàncies en Å.*

Els resultats teòrics implicaven que el solvent jugava un paper clau en el mecanisme de reacció. Per tal de confirmar aquest fet, vam proposar als nostres col·laboradors que provessin la reacció en un solvent apròtic però de polaritat similar (acetona) i... eureka! La comparació entre la hidrogenació en un solvent polar pròtic com l'etanol i un solvent polar apròtic com l'acetona revelà que la velocitat inicial d'hidrogenació disminuïa dràsticament al passar d'etanol a acetona, tal i com es mostra a la figura 5.6.

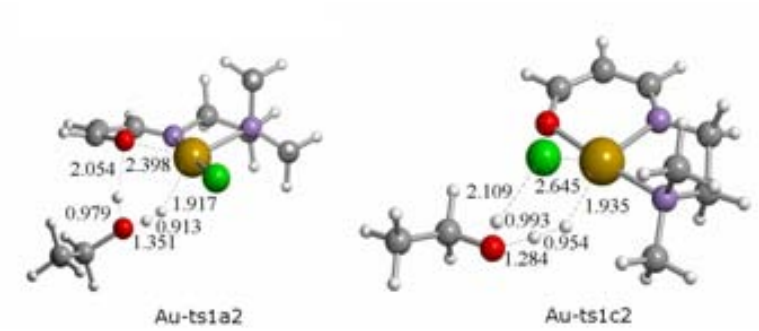

Figura 5.4: *Estats de transició pel trencament heterolític de l'hidrogen assistit per la molècula de dissolvent (EtOH) sobre els lligands oxo (**Au-ts1a2**) i clorur (**Au-ts1c2**). Distàncies en Å.*

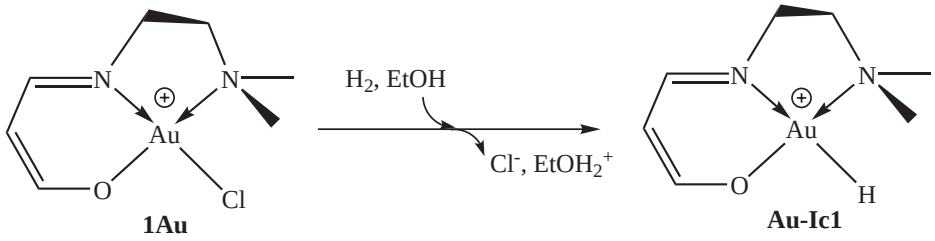

Figura 5.5: *Etapa inicial que genera l'espècie activa del cicle catalític, l'espècie metall-hidrur (**Au-Ic1**).*

Coordinació de l'etilè al catalitzador i inserció a l'enllaç Au-H

Un cop activat l'hidrogen, el següent pas implicava l'entrada de l'etilè al cicle catalític. Per aquesta etapa tinguérem en compte dues possibilitats. La primera consistia en el desplaçament del lligand amina permetent d'aquesta manera la coordinació de l'etilè (**Au-Ic2a** de la figura 5.7). Aquesta etapa presentava una barrera de 21.8 kcal·mol^{-1}. Pel que fa a la segona possibilitat, implicava la coordinació de l'etilè donant lloc a un complex amb estructura de bipiràmide trigonal (**Au-Ic2bis** de la figura 5.7). Aquesta etapa presentava una barrera significativament més elevada: 34.7 kcal·mol^{-1}.

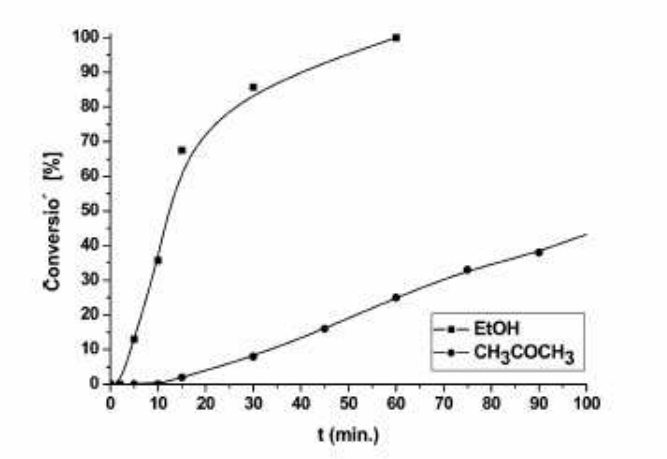

Figura 5.6: *Comparació de la velocitat inicial d'hidrogenació per l'etanol i l'acetona en la hidrogenació de benzilidèsuccinat en les condicions de reacció exposades a la taula 5.1 mitjançant el complex* ***2Au****.*

Per tant, la primera etapa era clarament més favorable que la segona i es postulava com el següent pas de la reacció.

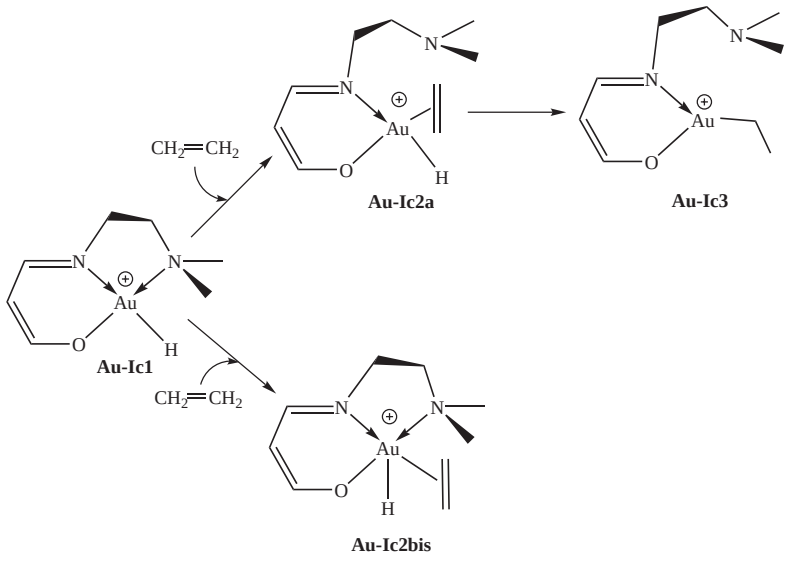

Figura 5.7: *Modes de coordinació de l'etilè al complex* ***1Au*** *que s'han avaluat i etapa d'inserció de l'etilè a l'enllaç Au-H.*

L'etapa postulada era similar a la que proposaren Vrieze, van Leeuwen i col·laboradors per la reacció d'inserció de CO a l'enllaç Pd-C en complexos amb lligands terdentats de nitrogen, on també es proposà que un dels lligands nitrogen terminals se substituïa per una molècula entrant de CO.[247] Altres estudis també observaren substitucions similars.[248]

Un cop l'olefina era dins l'esfera de coordinació del catalitzador podia tenir lloc la inserció de l'alquè a l'enllaç Au-H, la qual es donava al mateix temps que la rotació de l'olefina. Aquesta etapa presentava una barrera relativa al voltant d'aproximadament 4 kcal·mol^{-1} i donava com a resultat l'intermedi metall-alquil (**Au-Ic3** de la figura 5.7).

Finalització del cicle catalític

Per tal de finalitzar el cicle catalític, formalment s'havia de transferir un protó a l'intermedi metall-alquil i així generar el producte final: età. Per tant, vàrem considerar que aquest protó podia venir d'espècies presents al medi com àcid acètic o l'espècie $EtOH_2^+$[†] tal i com s'havia proposat a la literatura[249–251] o bé d'una molècula addicional d'hidrogen (veure figura 5.8).

Pel que fa al primer cas, prèviament podia tenir lloc la recoordinació del lligand amina que s'havia descoordinat per tal de permetre l'entrada de l'etilè formant **Au-Ic4bis**. Aquesta etapa és molt favorable termodinàmicament, essent exotèrmica en 37.2 kcal·mol^{-1}. La posterior transferència protònica per part de l'àcid acètic (ruta a **Au-Ic51bis**) o l'espècie $EtOH_2^+$ (ruta a **Au-Ic52bis**) presentaven barreres de reacció massa elevades per ésser etapes de reacció favorables, 57.5 i 37.5 kcal·mol^{-1}, respectivament. L'alternativa era que l'hidrogen molecular acabés transferint el protó a l'intermedi metall-alquil. Per a la coordinació de l'hidrogen a l'intermedi metall-alquil vam considerar dues alternatives: un procés on la molècula de dihidrogen es coordinava a la vacant de coordinació (**Au-Ic4**) o un procés on el lligand amina es recoordinava i després la molècula d'hidrogen es coordinava a l'or tot formant un complex pentacoordinat (**Au-Ic42**). Aquesta espècie pentacoordinada no fou possible de localitzar a la superfície d'energia potencial, fet que suggeria que en cas

[†]Aquesta espècie és l'espècie més àcida que pot existir en una solució d'etanol.

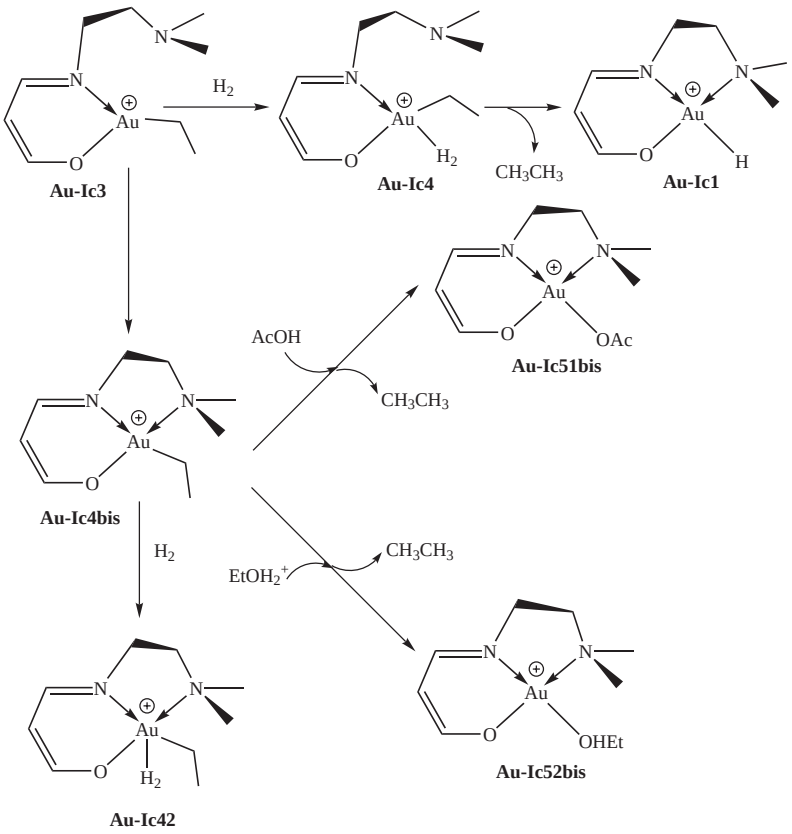

Figura 5.8: *Modes de finalització del cicle catalític.*

d'existir aquest intermedi seria molt elevat en energia.

Per tant, prosseguírem l'estudi analitzant la coordinació de la molècula d'hidrogen a la vacant de coordinació, la qual era lleugerament exotèrmica: -2.9 kcal·mol^{-1}. El posterior trencament de la molècula d'hidrogen regenerava l'hidrur i formava el producte final (età) a través de la metàtesi σ de la molècula d'hidrogen mitjançant un estat de transició de quatre membres. La barrera per aquesta etapa de reacció era raonable (15 kcal·mol^{-1}) i era una manera elegant i senzilla de finalitzar el cicle catalític. Un pas anàleg pel trencament de l'hidrogen fou proposat per Morokuma, Musaev i col·laboradors en la polimerització d'etilè mitjançant catalitzadors de níquel i de pal·ladi.[252] Aquesta etapa també s'ha suggerit per processos d'intercanvi d'hidrur.[253]

Mecanisme global de la reacció: cicle catalític complet

En base als resultats previs es va obtenir el cicle catalític complet que es mostra a la figura 5.9.

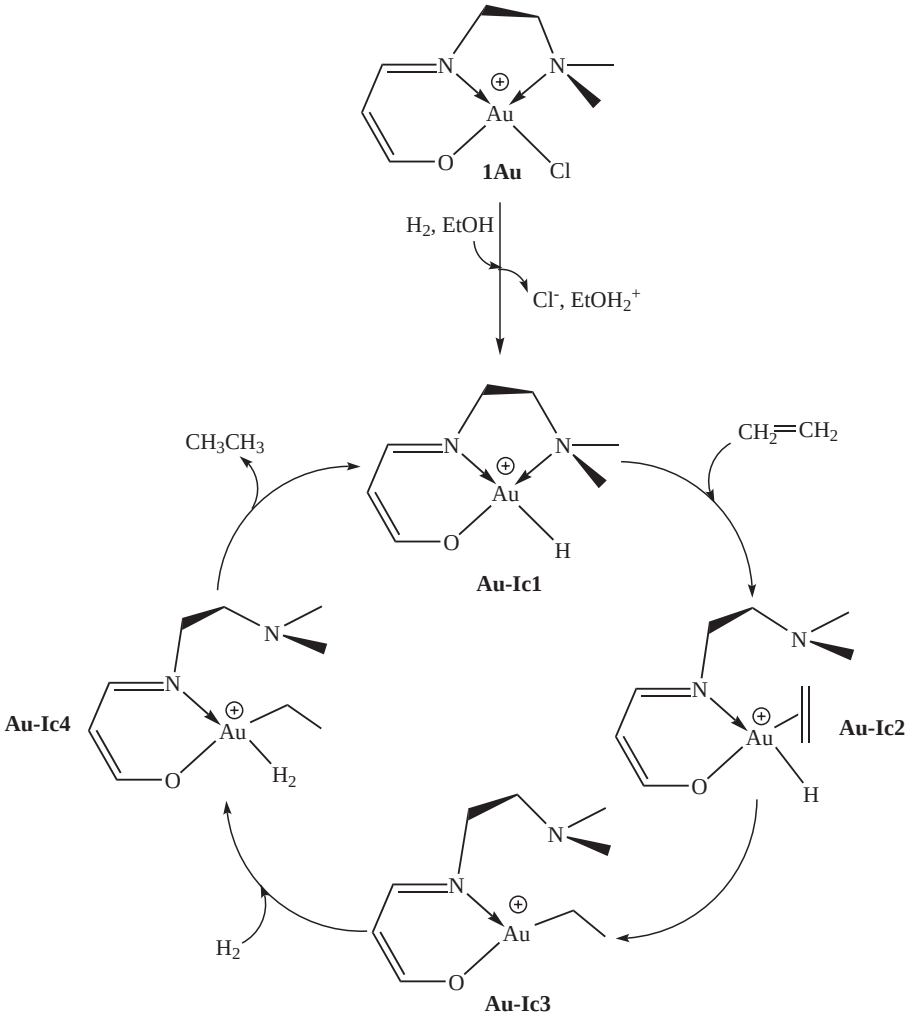

Figura 5.9: *Cicle catalític complet per la hidrogenació d'etilè mitjançant el complex* ***1Au****.*

Com ja s'ha comentat, el primer pas correspon a la formació de l'hidrur mitjançant el trencament heterolític de l'hidrogen sobre el clorur amb l'assistència de l'etanol. Això està d'acord amb el fet que el període d'inducció trobat experimentalment sigui més gran a temperatures baixes i també que aquest disminueixi a l'augmentar la

pressió parcial de l'hidrogen de 2 a 4 bar. Un cop s'ha format l'hidrur s'inicia el cicle catalític pròpiament dit ja que aquesta és l'espècie activa del catalitzador. Dins del cicle catalític l'etapa amb la barrera relativa més alta correspon a l'entrada de l'etilè dins l'esfera de coordinació. Això està d'acord amb el fet experimental que després del període d'inducció la velocitat de la reacció s'incrementi a l'augmentar la concentració d'olefina fins a un valor en el qual la saturació dels llocs actius i el pseudo-ordre de la reacció esdevingui zero respecte l'olefina. Pel que fa al perfil energètic global, aquest presenta una barrera d'unes 20 kcal·mol^{-1} (des de l'intermedi **Au-Ic1** fins a l'estat de transició **Au-ts3** de la figura 5.10).

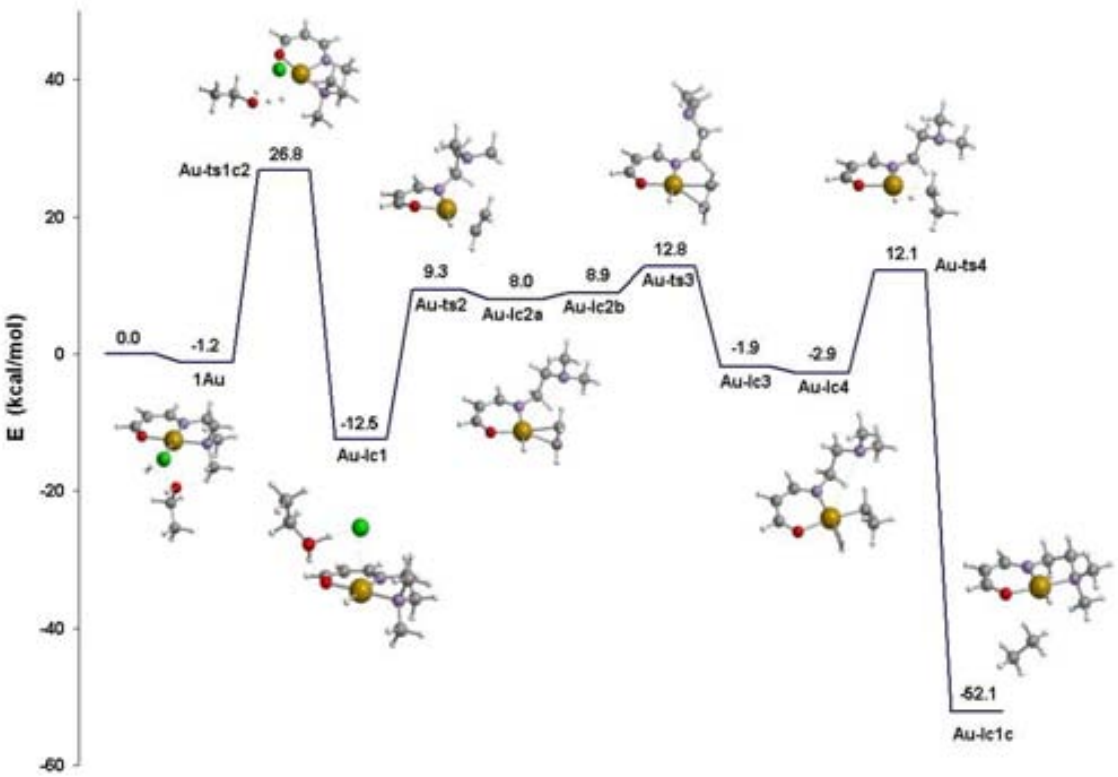

Figura 5.10: *Perfil energètic pel mecanisme d'hidrogenació proposat per la hidrogenació d'etilè mitjançant el complex* ***1Au***.

5.2.2 Hidrogenació mitjançant complexos de pal·ladi

En aquesta secció es descriuen breument les etapes de reacció avaluades mitjançant els càlculs teòrics per a la hidrogenació del model **1Pd**, tot comparant-les amb les dades obtingudes per la hidrogenació de l'or i amb les dades cinètiques obtingudes per Corma i col·laboradors. Com en el cas anterior, les diferents etapes es comenten als subapartats següents.

Activació de l'hidrogen

L'activació de la molècula d'hidrogen es podia donar de forma homolítica o heterolítica. Pel que fa a l'activació homolítica el producte resultant presentava un valor de 37.9 kcal·mol^{-1} els respecte reactius inicials. Això mostrava l'elevat cost d'assolir l'estat d'oxidació Pd(IV) i, per tant, el descartàrem com a camí de reacció favorable. Pel que fa a l'activació heterolítica descartàrem inicialment la possibilitat del trencament heterolític sobre el nitrogen amínic ja que era la que mostrava la barrera més elevada pel cas de l'or. En conseqüència, avaluàrem el trencament heterolític sobre el lligands oxo i clorur del catalitzador. Aquests presentaven barreres de reacció respectives de 32.7 kcal·mol^{-1} i de 19.2 kcal·mol^{-1} en solució. En el darrer cas, la inclusió de l'efecte del solvent mitjançant els càlculs puntuals PCM disminuí fortament la barrera de reacció ja que en fase gas la barrera de reacció era de 28.1 kcal·mol^{-1}. L'elevat increment de la càrrega de Mulliken a l'àtom de clorur d'aquest estat de transició respecte els reactius inicials (-0.314) indicava que possiblement era la polaritat del solvent (EtOH) el que feia disminuir la barrera d'activació en 9 kcal·mol^{-1}. L'augment de càrrega sobre el lligand oxo fou considerablement inferior. Ambdós estats de transició corresponents al trencament heterolític de l'hidrogen sobre els grups oxo i clorur es mostren a la figura 5.11. Anàlogament al cas de l'or, avaluàrem la participació activa de molècules de dissolvent assistint al trencament heterolític de l'hidrogen mitjançant un estat de transició de sis membres. En aquest cas, i a diferència del cas de l'or, la barrera pràcticament no es veigué afectada: 32.8 i 18.6 kcal·mol^{-1} pels trencaments heterolítics sobre els grups oxo i clorur, respectivament. Així doncs, pels complexos de Pd(II) l'assistència del solvent no era necessària pel trencament heterolític de l'hidrogen. Això quedà confirmat experimentalment per

Corma i col·laboradors, ja que en el cas del pal·ladi en etanol la reacció era tan sols lleugerament més ràpida que en acetona tal i com es mostra a la figura 5.12.

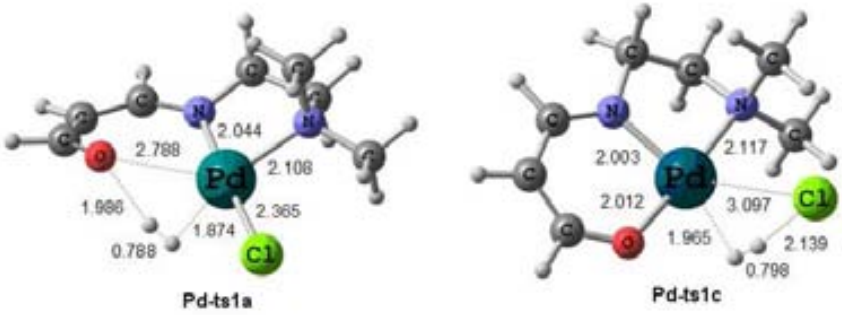

Figura 5.11: *Estats de transició dels trencaments heterolítics de l'hidrogen sobre el grup oxo (**Pd-ts1a**) i el grup clorur (**Pdts1c**). Distàncies en Å.*

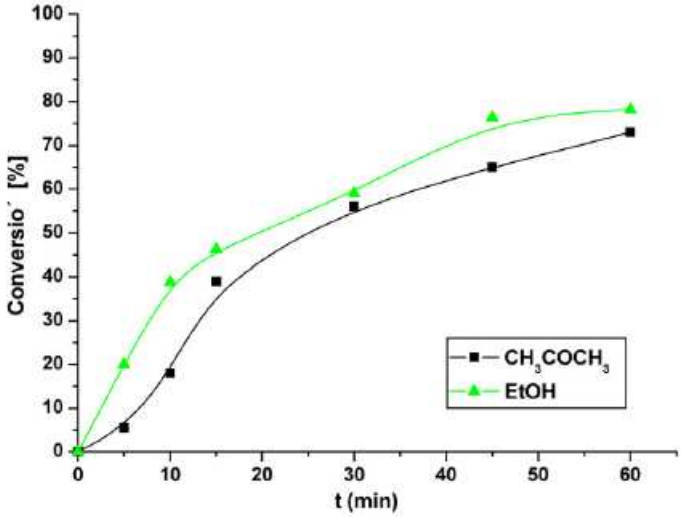

Figura 5.12: *Comparació de la velocitat inicial d'hidrogenació per l'etanol i l'acetona en la hidrogenació de benzilidèsuccinat en les condicions de reacció exposades a la taula 5.1 mitjançant el complex **2Pd**.*

Aquests resultats es poden comparar amb els obtinguts pel complex d'or (figura

5.6). Així, pels complexos de pal·ladi el trencament heterolític sobre el clorur era el que presentava la barrera energètica més favorable. Els productes d'aquesta etapa eren l'intermedi metall-hidrur i HCl tal i com es mostra a la figura 5.13. A diferència del cas de l'or, l'assistència del solvent no era necessària per tal que la reacció seguís el seu curs.

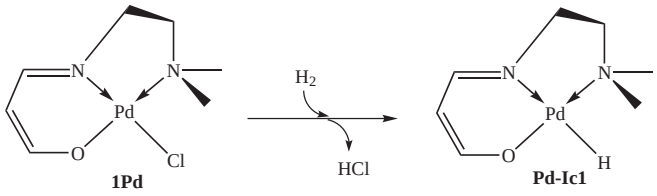

Figura 5.13: *Etapa inicial que genera l'espècie activa del cicle catalític, l'espècie metall-hidrur (**Pd-Ic1**).*

Coordinació de l'etilè al catalitzador i inserció a l'enllaç Pd-H

El següent pas del cicle catalític involucrava la coordinació de l'etilè al pal·ladi. En aquest cas, i a diferència del cas de l'or localitzàrem dues estructures on l'etilè estava coordinat al pal·ladi i on el complex presentava una geometria de bipiràmide trigonal. La més estable de les estructures estava localitzada 14.6 kcal·mol^{-1} per sobre dels reactius inicials (**Pd-Ic2** de la figura 5.14). Des d'aquesta estructura, el següent pas consistia en la marxa del lligand amino per formar una estructura planoquadrada (**Pd-Ic3a,b**). Aquesta etapa era molt favorable, ja que presentava una barrera relativa de tan sols 0.4 kcal·mol^{-1}. Posteriorment podia tenir lloc la inserció de l'etilè a l'enllaç M-H, la qual es donava al mateix temps que la rotació de l'olefina. Aquesta etapa presentava una barrera relativa de 5.0 kcal·mol^{-1} i produïa un agòstic entre el metall i l'enllaç C-H acabat de formar (**Pd-Ic4a,b**). Des de la segona estructura amb geometria de bipiràmide trigonal (**Pd-Ic2bis**) localitzàrem un estat de transició on la inserció de l'etilè a l'enllaç Pd-H es donava al mateix temps que la marxa del lligand amino. Aquest camí de reacció presentava una barrera de 9.6 kcal·mol^{-1} i per tant era menys favorable que la ruta per passos prèviament explicada (5.0 kcal·mol^{-1}). Aquest resultat estava d'acord amb estudis de Hoffmann i Thorn, que trobaren que

l'inserció de l'etilè a l'enllaç M-H era més difícil en una estructura de bipiràmide trigonal que en una estructura planoquadrada.[254] D'altra banda, tot i que s'avaluà, no fou possible localitzar un estat de transició on la transferència de l'hidrur i la marxa del lligand amino tinguessin lloc al mateix temps des de la primera de les estructures amb geometria de bipiràmide trigonal (fletxa discontínua de la figura 5.14).

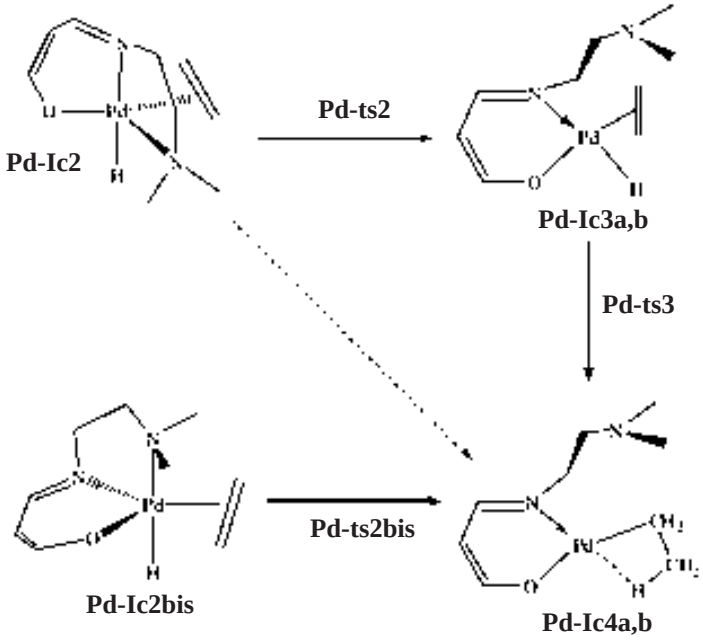

Figura 5.14: *Diversos camins de reacció per obtenir l'intermedi metall-alquil (**Pd-Ic4a,b**) a partir dels isòmers **Pd-Ic2** i **Pd-Ic2bis**. Les lletres **a,b** per **Pd-Ic3** i **Pd-Ic4** es refereixen als diferents confòrmers que presenta cada espècie.*

Finalització del cicle catalític

Per tal de finalitzar el cicle catalític s'havia de transferir un hidrogen a l'intermedi metall-alquil acabat de formar. Pel que fa a la possibilitat que una espècie àcida del medi transferís un protó al grup etil per donar l'età la descartàrem inicialment ja que en el cas de l'or localitzàrem barreres de reacció molt elevades per aquesta etapa. En canvi, vàrem considerar que l'hidrogen molecular fos capaç de transferir aquest protó al grup etil. Per tal que el protó es pogués transferir, primer s'havia de coordinar la

molècula d'hidrogen, etapa per la qual vam considerar les dues alternatives considerades pel complex **1Au**. Com en el cas d'aquest complex, l'espècie pentacoordinada on l'hidrogen estava coordinat al pal·ladi no es va localitzar a la superfície d'energia potencial. En canvi, sí que es va localitzar el camí de reacció on la molècula de dihidrogen es coordinava al metall amb previ trencament de l'agòstic entre l'enllaç C-H i el metall, tot donant lloc a un complex amb geometria planoquadrada (**Pd-Ic5** de la figura 5.15).

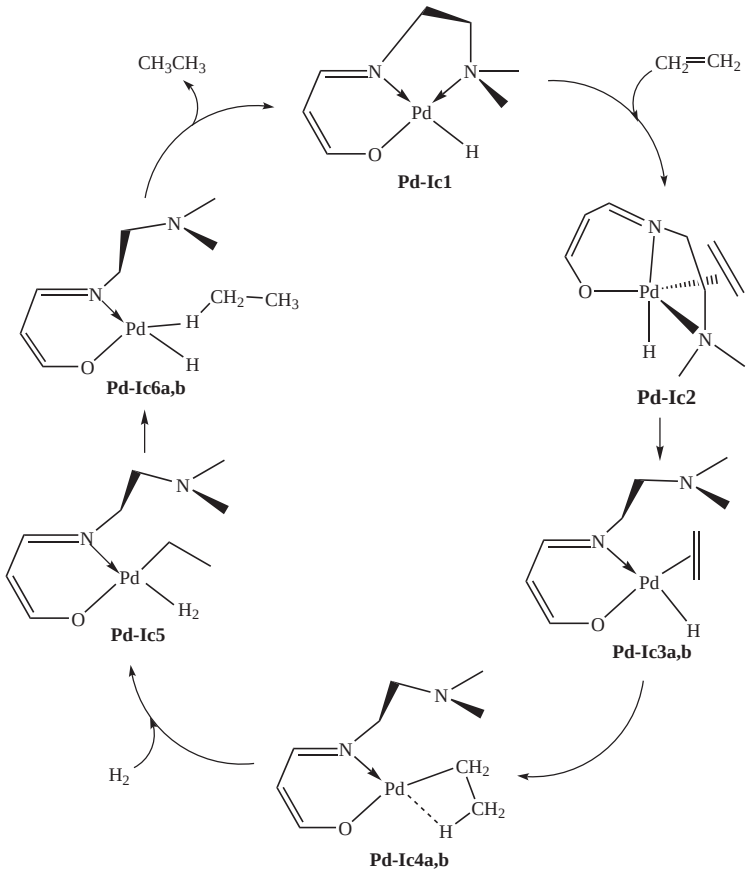

Figura 5.15: *Cicle catalític complet per a la hidrogenació d'etilè mitjançant el complex* ***1Pd****.*

El trencament de l'agòstic entre l'enllaç C-H i el metall permetia la coordinació de la molècula d'hidrogen a la vacant de coordinació, essent exotèrmica en 4.0 kcal·mol^{-1} (**Ic5**), mentre que el posterior trencament de la molècula d'hidrogen re-

generava l'hidrur i formava el producte final (età) a través de la metàtesi σ de la molècula d'hidrogen mitjançant un estat de transició de quatre membres. Aquesta etapa presentava una barrera de 12.1 kcal·mol^{-1}. En aquesta estructura, l'età formava un agòstic a través d'un enllaç C-H amb l'àtom metàl·lic (**Ic6a,b**). Finalment, l'última etapa rellevant consistia en la marxa de l'età al mateix temps que es coordinava l'amina, amb una barrera relativa de tan sols 0.2 kcal·mol^{-1}. Aquesta etapa regenerava l'hidrur format durant el trencament heterolític inicial de l'hidrogen, tancant d'aquesta manera el cicle catalític.

Mecanisme global de la reacció: cicle catalític complet

Un cop es trenca l'hidrogen mitjançant l'activació heterolítica sobre el clorur s'inicia el cicle catalític pròpiament dit (figura 5.15) ja que es forma l'espècie activa del catalitzador: l'intermedi metall-hidrur (**Pd-Ic1**). El perfil energètic del cicle catalític es mostra a la figura 5.16.

L'activació de l'hidrogen és la barrera més elevada que s'ha trobat (19.2 kcal·mol^{-1}), fet que s'ha comprovat experimentalment gràcies a l'observació de període d'inducció a la corba cinètica, si bé en aquest cas i a diferència del cas de l'or, el període d'inducció sols disminueix lleugerament quan la pressió parcial d'hidrogen s'incrementa de 2 a 4 bar, suggerint que aquest pas no és tan rellevant per a la velocitat de reacció com en el cas de l'or. Pel que fa al cost global del procés (figura 5.16), aquest és de 15.0 kcal·mol^{-1} i correspon a l'etapa on es dóna l'entrada de l'etilè a l'esfera de coordinació del pal·ladi.

5.3 Conclusions

Mitjançant càlculs DFT s'ha fet una proposta mecanística per la hidrogenació d'alquens mitjançant complexos de Au(III) i Pd(II). Els resultats obtinguts han permès concloure que:

- Tan per l'or com pel pal·ladi el mecanisme avaluat inclou com a etapa inicial més favorable el trencament heterolític de l'hidrogen sobre el clorur, la qual genera l'espècie activa del catalitzador: l'intermedi metall-hidrur.

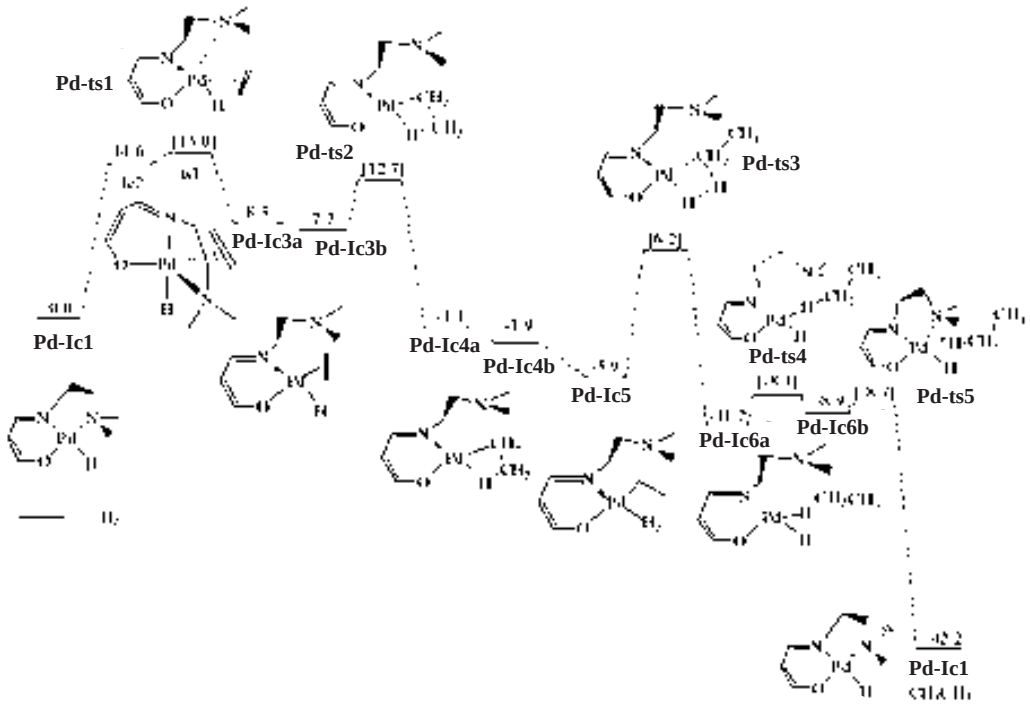

Figura 5.16: *Perfil energètic pel cicle catalític d'hidrogenació proposat pel complex 1Pd. Energies en kcal·mol*$^{-1}$.

- En la hidrogenació mitjançant complexos de Au(III), el solvent juga un paper important assistint al trencament heterolític de l'hidrogen, essent el trencament heterolític sobre el clorur l'etapa més favorable. Això quedà avalat experimentalment per la reducció de la velocitat observada per l'acetona en comparació amb l'etanol i per la disminució del període d'inducció a l'augmentar la pressió parcial de l'hidrogen.

- En el trencament heterolític de l'hidrogen mitjançant complexos de pal·ladi, l'efecte del solvent és important pel que fa a la polaritat però no pel que fa al seu caràcter pròtic i per tant no es dóna l'assistència del solvent en el procés de trencament heterolític. Això queda confirmat experimentalment, ja que el període d'inducció es veu poc afectat si se substitueix etanol per acetona com a solvent.

- Un cop generada l'espècie activa comença el cicle catalític pròpiament dit. Els passos següents consisteixen en la substitució del lligand amino per etilè, la inserció de l'etilè a l'enllaç M-H i la regeneració de l'hidrur gràcies al trencament heterolític de la molècula d'hidrogen.

- El pas limitant de la velocitat de reacció és el mateix tan pel complex d'or com pel complex de pal·ladi un cop s'ha format l'espècie catalíticament activa (l'intermedi metall-hidrur). Aquesta etapa correspon a la coordinació de l'olefina al catalitzador.

Part III

Estudi teòric de l'oxidació homogènia d'alquens

Capítol 6

Naturalesa del compost $Cp^*MoO_2^+$ en aigua i epoxidació d'olefines mitjançant complexos tipus Cp*Mo(VI) en cloroform i aigua

6.1 Complexos tipus Cp*Mo(VI) en aigua i aplicacions en epoxidació d'olefines

Els complexos de Mo amb lligands oxo amb estats d'oxidació elevats s'han emprat en diverses reaccions catalítiques com ara l'epoxidació d'olefines, les oxidacions selectives d'alcohols a aldehids, la deshidrogenació i isomerització d'alquens i fins i tot en processos de reducció com ara la hidrosililació de carbonils.[255] Pel que fa a la versió organometàl·lica d'aquests sistemes, aquesta s'ha mostrat força activa sobretot en reaccions d'epoxidació d'olefines.[256–259]

El grup de R. Poli (Tolouse) ha estudiat complexos d'aquest tipus centrant-se en derivats tipus Cp*Mo per diversos estats d'oxidació (VI, V, IV i clústers de valències mixtes).[260] Era força interessant adaptar aquests sistemes perquè poguessin operar en medi aquós i aquí rau la importància de conèixer la naturalesa del complex $[Cp^*MoO_2]^+$ en aigua. La formació del compost $[Cp^*MoO_2(H_2O)]^+$ (**2a**) per proto-

nació a partir del complex [Cp*MoO_2(OH)] era d'ordre 1 en concentració de protons ([H^+])[261] i això suggeria dos mecanismes possibles. El primer (opció (a) de la figura 6.1) involucra un equilibri ràpid per donar l'aquo-oxo isòmer (**2a**), seguit de la pèrdua d'una molècula d'aigua que seria el pas determinant de la velocitat. Pel que fa al segon (opció b) de la figura 6.1), involucra la isomerització intramolecular del complex dihidroxo (**1a**) al complex aquo-oxo (**2a**) com a pas determinant de la velocitat de reacció.

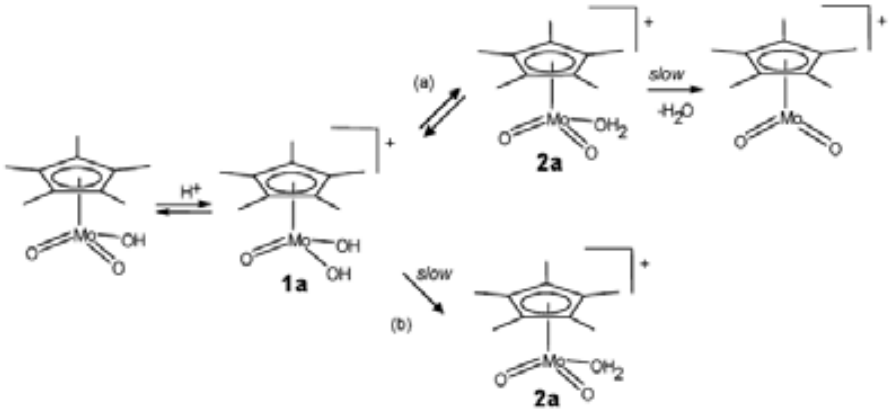

Figura 6.1: *Protonació del complex [Cp*MoO_2OH] i possibles mecanismes de formació del [Cp*MoO_2(H_2O)]$^+$ (**2a**).*

Experimentalment, els grups de Poli i van Eldik van realitzar cinètiques de *stopped-flow* a pH's baixos i van mostrar que l'energia lliure de la tautomerització entre els compostos **2a** i **1a** afavoria la formació del primer en 6.5 kcal·mol^{-1}. A més, els paràmetres d'activació per la protonació i isomerització del complex [Cp*MoO_2(OH)] fins a [Cp*MoO_2(H_2O)]$^+$ (**2a**) eren igual a $\Delta H^\ddagger$ = 5.1 ± 0.1 kcal·mol^{-1}, $\Delta S^\ddagger$ = -37 ± 1 cal·mol^{-1}K^{-1} i $\Delta V^\ddagger$ = -9.1 ± 0.2 cm^3·mol^{-1}. Aquests valors negatius per l'entropia i el volum d'activació suggerien un procés en el qual o bé hi havia una important formació d'enllaç o bé tenia lloc un procés de creació de càrrega, i per tant suggerien que la reacció seguia l'opció (b) de la figura 6.1. D'altra banda, la presència d'un equilibri per la dissociació de l'aigua permetia explicar la baixa acidesa observada pel

complex **2a** ($pK'_{a1} = 4.19$).

Pel que fa al mecanisme d'epoxidació mitjançant complexos de molibdè, estudis experimentals amb complexos de fórmula $MoO_2X_2L_2$ i *t*-BuOOH (TBHP) com a oxidant mostraren que la font d'oxigen per l'epoxidació era el TBHP i no pas els lligands peròxid.[262] D'altra banda Romão i col·laboradors trobaren que complexos tipus [$Cp^{\#}Mo_2O_5$] i [$Cp^{\#}MoO_2Cl$] ($Cp^{\#}$ = ciclopentadienil substituït) eren actius en solució aquosa amb TBHP però no amb H_2O_2 com a oxidant.[258] Per la seva banda Trost i Bergman, en el primer estudi catalític fent servir un oxo derivat de molibdè van mostrar que el binomi [Cp*Mo(O_2)Cl]/TBHP era efectiu en l'epoxidació d'olefines mentre que el compost anàleg de peròxid [Cp*MoO(O_2)Cl] era catalíticament inactiu.[263] Per tant, l'existència i estabilitat dels grups peròxid havia d'estar relacionada amb processos secundaris com ara la desprotonació dels lligand hidroperòxid M-OOH. De fet, en un estudi teòric on es modelava el *t*-BuOOH com a MeOOH s'ha proposat un mecanisme que s'assembla al proposat per Thiel (figura 2.15 del capítol 2) excepte en què el que rep el dipositari del protó és un lligand oxo.[262,264] Aquest mecanisme es mostra a la figura 6.2 i s'assembla el mecanisme proposat per Mimoun (figura 2.14 del capítol 2) ja que té lloc la inserció de l'alquè a l'enllaç metall-peroxo. Tot i això, per l'estat de transició corresponent a la inserció de l'alquè es calculà una barrera de 52 kcal·mol^{-1}. És raonable pensar que en base al valor d'aquesta barrera obtinguda aquesta és massa elevada per un procés catalític i que, per tant, és necessària una nova investigació del mecanisme d'epoxidació.

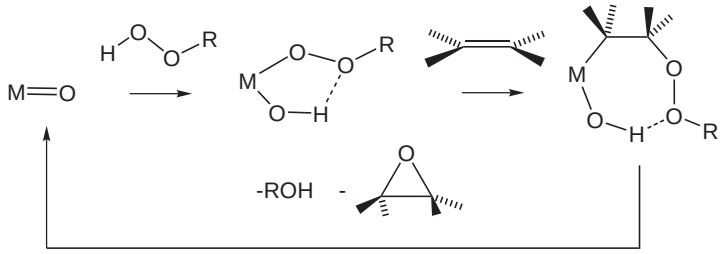

Figura 6.2: *Proposta mecanística de Calhorda i col·laboradors.*

6.2 El nostre estudi: resultats i discussió

Mitjançant càlculs teòrics es volia establir si el nombre d'aigües coordinades al complex $[Cp^*MoO_2(H_2O)_n]^+$ era n=0 o n=1, es volia saber el mecanisme que duia a la formació d'aquest i es volien entendre els factors que regulaven l'energia relativa dels tautòmers dihidroxo i aquo-oxo. A més, es volia calcular un mecanisme d'epoxidació viable mitjançant el complex $[Cp^*MoO_2^+]$, es volia entendre la diferència d'activitat entre els derivats oxo i peroxo dels complexos de Trost i Bergman $[Cp^*MoO_2Cl]$ i $[Cp^*MoO(O_2)Cl]$ i es volia saber perquè el TBHP era millor oxidant que el H_2O_2. Com que el complex Cp^*MoO_2Cl era isoelectrònic dels compostos tipus $[MoO_2X_2L_2]$ els resultats obtinguts es podrien extrapolar a aquesta classe de complexos.

D'aquesta manera, vam realitzar càlculs a nivell DFT (B3LYP) incloent l'efecte del solvent mitjançant càlculs puntuals CPCM usant etilè com a substrat i H_2O_2 com a oxidant en el cas de la reacció d'epoxidació. En el cas del $[Cp^*MoO_2]^+$, el solvent usat fou aigua mentre que en el cas dels complexos de Trost i Bergman era cloroform. Els valors que es presenten en aquest capítol són en solució a no ser que es digui el contrari.

6.2.1 Naturalesa en medi aquós del complex $[Cp^*MoO_2]^+$

Addició d'aigua al complex $[Cp^*MoO_2]^+$

Inicialment vam calcular el resultat d'afegir una molècula d'aigua al complex $[Cp^*MoO_2]^+$, procés exotèrmic en 10.1 kcal·mol^{-1} en solució. Això contrastava amb el resultat en fase gas (exotèrmic en 39.7 kcal·mol^{-1}) ja que en solució s'estabilitzava notablement el complex catiònic $[Cp^*MoO_2]^+$.

Transferència intramolecular del protó

El procés d'anar del complex dihidroxo (**1a**) a l'aquo-oxo (**2a**) era endotèrmic en 7.2 kcal·mol^{-1} i la barrera energètica per passar de l'un a l'altre prenia un valor força elevat, 43.9 kcal·mol^{-1}. Aquesta barrera probablement estava relacionada amb l'elevada tensió de la geometria de l'estat de transició, on l'enllaç O-Mo-O presentava un

angle de 71.3 °. El perfil energètic d'aquest procés i l'estat de transició corresponent (**ts1a**) es mostren a les figures 6.3 i 6.4, respectivament.

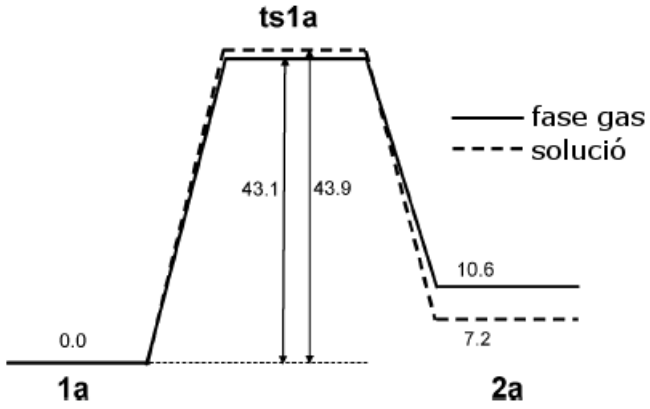

Figura 6.3: *Perfil energètic per a la transferència protònica intramolecular entre el dihidroxo (**1a**) i l'aquo-oxo (**2a**). Energies en kcal·mol*$^{-1}$.

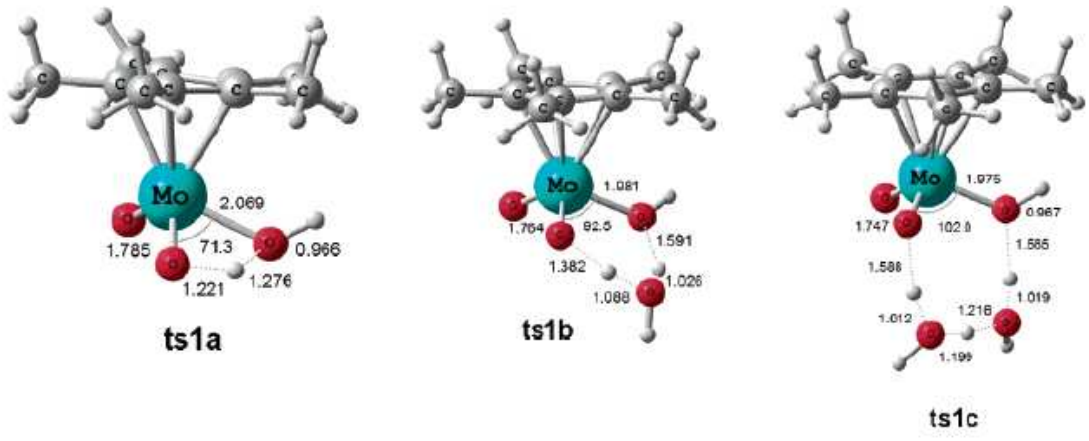

Figura 6.4: *Estats de transició per la transferència protònica intramolecular sense assistir (**ts1a**), assistida per una molècula d'aigua (**ts1b**) i assistida per dues molècules d'aigua (**ts1c**). Distàncies en Å.*

Per tal d'estudiar si aquesta transferència protònica podia ésser assistida per altres molècules d'aigua es van realitzar càlculs afegint 1 i 2 molècules d'aigua, respectivament. Altres estudis teòrics ja havien suggerit la participació activa de cadenes d'aigua en processos de tautomerització[265–269] i d'intercanvi de protó.[270,271] A l'afegir una molècula d'aigua la diferència energètica entre el complex dihidroxo (**1b**) i el complex aquo-oxo (**2b**) passava a ser sols de 4.0 kcal·mol^{-1} a favor del primer mentre que la barrera que els separava prenia un valor de tan sols 10.3 kcal·mol^{-1}. El perfil energètic corresponent es mostra a la figura 6.5

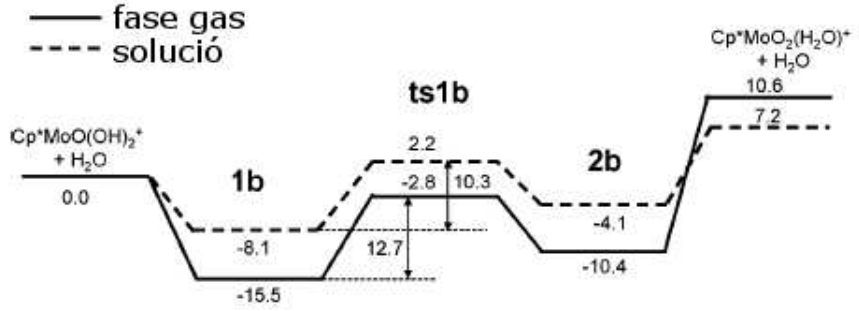

Figura 6.5: *Perfil de la transferència protònica intramolecular assistida per una molècula d'aigua entre el dihidroxo (**1b**) i l'aquo-oxo (**2b**). Energies en kcal·mol^{-1}.*

Això quedava reflectit a l'angle de l'enllaç O-Mo-O ja que ara prenia un valor més gran (92.5 °) i per tant la geometria de l'estat de transició estava més relaxada (**ts1b** de la figura 6.4). Aquest estat de transició mostra certa analogia amb el que s'ha mostrat al capítol 5 per l'activació heterolítica de l'hidrogen assistida per l'etanol. Finalment, vam avaluar el procés en el qual dues molècules d'aigua assistien la transferència protònica a través d'un estat de transició de vuit membres. En aquest cas, l'estat de transició que va del dihidroxo (**1c**) a l'aquo-oxo (**2c**) prenia un valor en solució inferior al mínim previ. Això probablement era degut a l'error inherent del mètode CPCM, ja que en fase gas la barrera prenia un valor de tan sols 1.3 kcal·mol^{-1}. El perfil energètic corresponent es mostra a la figura 6.6. En aquest cas, l'angle O-Mo-O a l'estat de transició era encara més obert: 102.0 °(**ts1c** de la figura 6.4). A més, ara la diferència d'energia entre ambdós isòmers ja era lleugerament

favorable a l'isòmer aquo-oxo en 0.4 kcal·mol^{-1}.

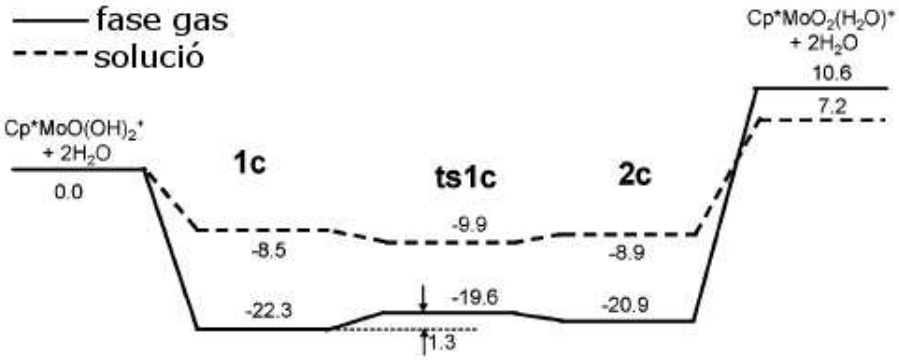

Figura 6.6: *Perfil de la transferència protònica intramolecular assistida per dues molècules d'aigua entre el dihidroxo (**1c**) i l'aquo-oxo (**2c**). Energies en kcal·mol^{-1}.*

Per tant, el fet d'anar afegint molècules d'aigua explícites al sistema millorava la descripció de la solvatació en aigua, tot mostrant una tendència que estava d'acord amb l'estabilitat relativa obtinguda experimentalment, on l'aquo-oxo isòmer era més estable que el dihidroxo en 6.5 kcal·mol^{-1}. Finalment, vam afegir una tercera molècula d'aigua al nostre sistema i la diferència a favor del complex aquo-oxo s'ampliava fins a 1.8 kcal·mol^{-1}, si bé ambdos mínims, **1d** i **2d**, formalment eren més aviat el complex [Cp*MoO_2(OH)] interaccionant amb el clúster $H_7O_3^+$. Així, degut a l'acidesa d'ambdós isòmers ja observada experimentalment es transferia un dels protons al medi.

Com que ambdues espècies predominen en medi àcid, per tal de tenir una idea de l'efecte que tenia baixar el pH vam usar el clúster $[H_3O(H_2O)_2]^+$ com a model. La naturalesa de l'hidroni en solució i la seva esfera de solvatació han inspirat nombrosos treballs teòrics.[272–275] Aquest model de clúster ja s'ha fet servir per modelar l'hidroni en solució en altres reaccions de complexos de metalls de transició, tal i com s'ha explicat al capítol 2.[61,63,64] Així, s'obtingueren cinc mínims que es mostren a la figura 6.7, on en dos dels quals (**1e** i **2e**) l'hidroni està situat a la segona esfera de coordinació mentre en els altres tres (**1e2**, **1e3** i **2e2**) està siutat a la primera esfera

de coordinació. Tal i com era d'esperar, en aquest cas no es transfereix el protó al medi ja que hi hauria un excés de càrrega positiva. Pel que fa a l'estabilitat relativa, la configuració més estable dels mínims de l'isòmer dihidroxo (**1e**) és més estable que la configuració més estable de l'isòmer aquo-oxo (**2e**) en 5.3 kcal·mol^{-1}. Aquesta estabilitat relativa, que és contrària a l'experimental, probablement mostra com la descripció de la solvatació de les espècies catiòniques encara no és òptima i que força més molecules d'aigua serien necessàries per tal de descriure correctament els cations aquo-oxo i dihidroxo interaccionant amb el catió hidroni.

6.2.2 Epoxidació

Les dues primeres seccions avaluen l'epoxidació d'olefines mitjançant els complexos [Cp*MoO_2Cl] i [Cp*Mo(O_2)OCl] per tal d'esbrinar perquè el segon és inactiu per aquest procés. Pel que fa a l'última secció és on s'estudia l'epoxidació d'olefines mitjançant el complex [Cp*MoO_2]$^+$.

Epoxidació d'olefines mitjançant el complex [Cp*MoO_2Cl]

En base a altres treballs teòrics en epoxidació d'olefines catalitzada per compostos de molibdè,[151,153,154,156,158,159,262,264,276–280] la primera etapa estudiada fou la d'activació de l'oxidant. Per tant, el primer pas corresponia a la coordinació i activació de la molècula de H_2O_2 per transferència protònica a un dels grups oxo i coordinació del lligand hidroperòxid, la qual presentava una barrera de 24.3 kcal·mol^{-1}. En aquest cas, ni l'assistència d'una molècula de H_2O_2 addicional ni d'una molècula d'aigua no canviava significativament la barrera de reacció: 25.0 i 21.9 kcal·mol^{-1}, respectivament.

Aquesta poca variació de la barrera energètica probablement és deguda a que l'angle O-Mo-OOH no canvia substancialment en els processos assistits (80.2 °i 74.9 °) respecte el procés no assistit (65.8 °). El perfil energètic corresponent a tot el procés d'epoxidació es mostra a la figura 6.8 mentre que els estats de transició corresponents es mostren a la figura 6.9.

El pas següent correspon a la transferència de l'oxigen a l'etilè per part de l'oxigen en α respecte el metall del grup hidroperòxid, la qual presenta una barrera de 12.7

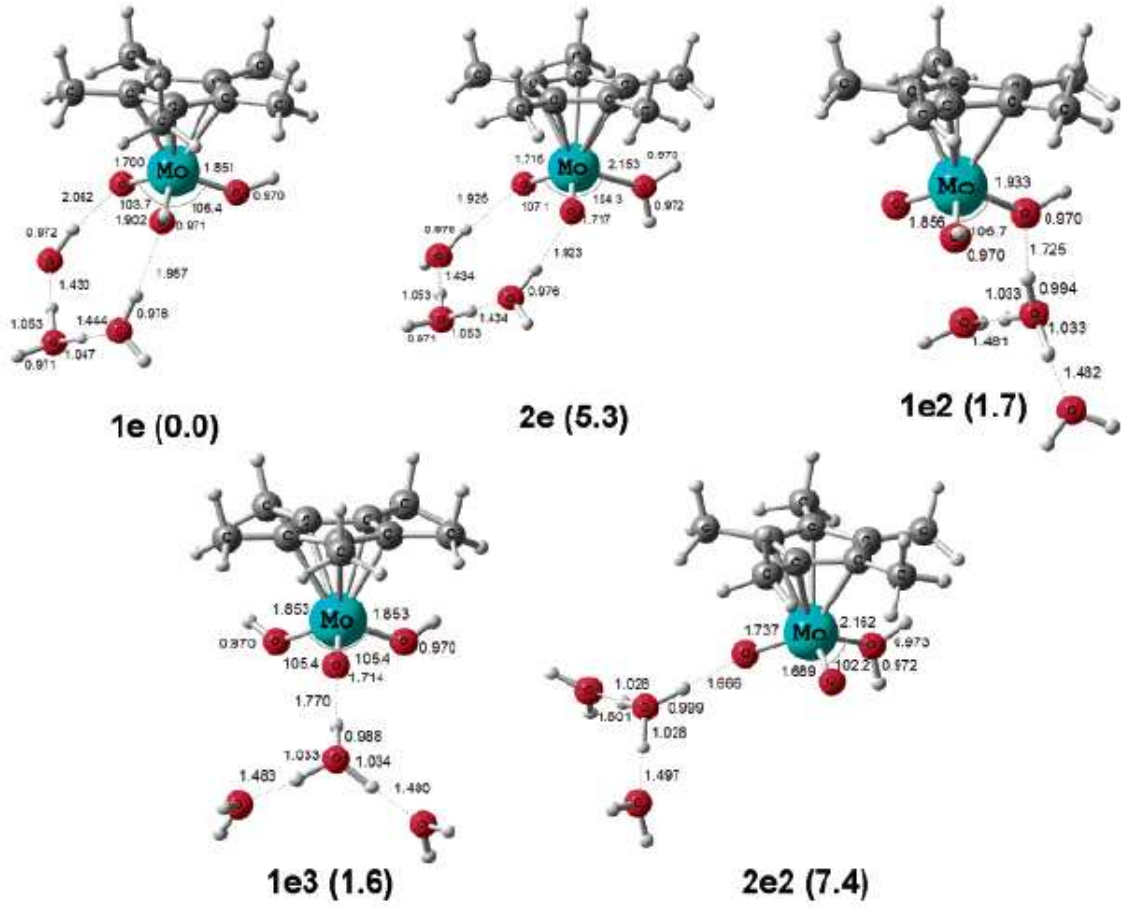

Figura 6.7: *Geometries optimitzades dels complexos $[Cp^*MoO(OH)_2]^+$ i $[Cp^*MoO_2(H_2O)]^+$ interaccionant amb el clúster $[(H_3O)(H_2O)_2]^+$. Distàncies en Å.*

kcal·mol^{-1} en $CHCl_3$, essent una barrera molt inferior a la calculada per Calhorda i col·laboradors (52 kcal·mol^{-1}).[262,264] Finalment, el cicle catalític es tanca amb l'eliminació d'una molècula d'aigua, etapa amb una barrera relativa de 16.0 kcal·mol^{-1} en $CHCl_3$. Pel que fa al pas limitant de la velocitat de reacció, tot i que la barrera més alta correspon a l'activació del H_2O_2, l'estat de transició corresponent a l'etapa d'epoxidació presenta una barrera molt similar.

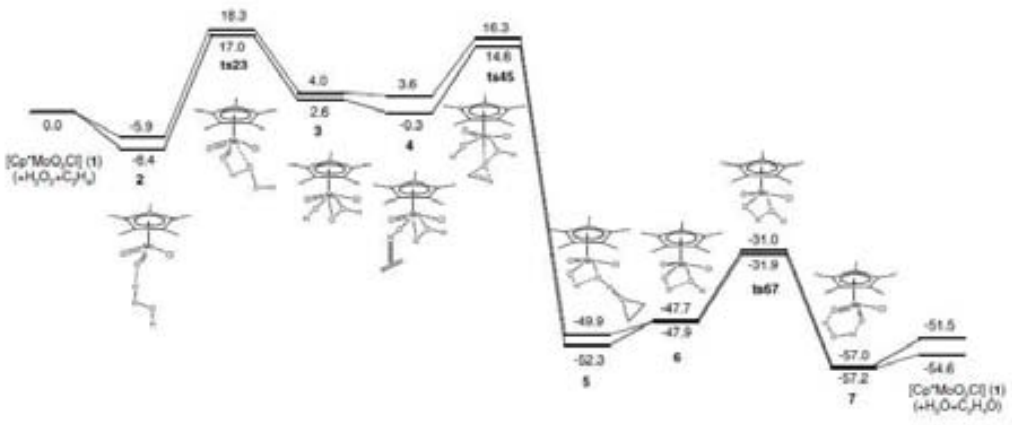

Figura 6.8: *Perfil energètic per a l'activació de H_2O_2 i l'epoxidació de l'etilè mitjançant el complex [Cp*MoO_2Cl] en fase gas (línia discontinua) i en $CHCl_3$ (línia contínua). Energies en kcal·mol^{-1}.*

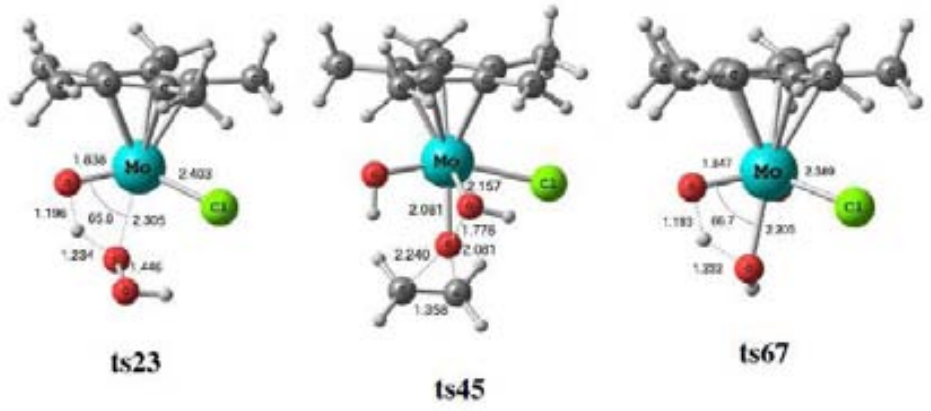

Figura 6.9: *Estats de transició involucrats en el procés d'epoxidació mitjançant el complex [Cp*MoO_2Cl]. Distàncies en Å.*

Epoxidació d'olefines mitjançant el complex [Cp*Mo(O_2)OCl]

Pel que fa a l'epoxidació d'olefines mitjançant el complex [Cp*Mo(O_2)OCl], vam calcular la barrera de la transferència d'un oxigen del lligand η^2-O_2 a l'etilè, la qual presentava una barrera de 22.2 kcal·mol^{-1} en $CHCl_3$ i per tant era aproximadament

unes 10 kcal·mol^{-1} més alta que en el cas del lligand hidroperoxo.

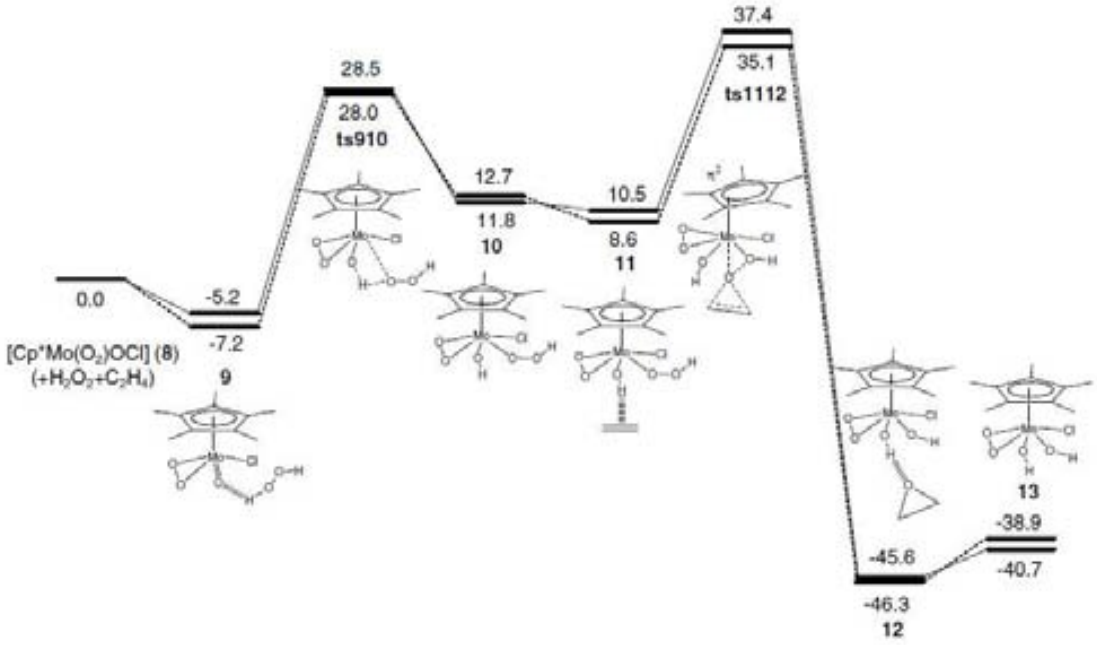

Figura 6.10: *Perfil energètic per a l'activació de H_2O_2 i l'epoxidació de l'etilè mitjançant el complex [Cp*Mo(O_2)OCl] en fase gas (línia discontinua) i en $CHCl_3$ (línia contínua). Energies en kcal·mol^{-1}.*

En un estudi teòric previ, Rösch i col·laboradors ja van concloure que els mecanismes mitjançant hidroperòxid eren competitius i fins i tot superiors als mecanismes mitjançant peròxid.[280]

Per tal de comprovar teòricament si aquesta espècie era catalíticament inactiva vam avaluar un mecanisme on el lligand peroxo rebia un protó provinent de l'activació de H_2O_2 com en el camí de reacció proposat per Thiel[162–164] (figura 2.15 del capítol 2). El perfil energètic corresponent es mostra a la figura 6.10 i com es pot observar els estats de transició corresponents a l'activació del H_2O_2 i a l'epoxidació de l'etilè presenten barreres significativament més elevades que en el cas del complex [Cp*MoO_2Cl]. La situació de l'estat de transició corresponent a l'etapa d'epoxidació (**ts1112**) és significativament més elevada que en l'altre perfil energètic (**ts45**). Les

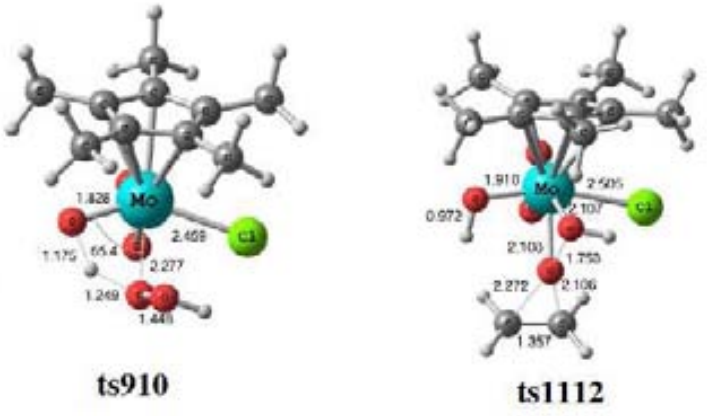

Figura 6.11: *Estats de transició corresponents al procés d'epoxidació mitjançant el complex [Cp*Mo(O_2)OCl]. Distàncies en Å.*

estructures dels estats de transició es mostren a la figura 6.11. Els resultats anteriors permeten racionalitzar perquè els complexos tipus [$Cp^{\#}MoO_2X$] ($Cp^{\#}$ = ciclopentadienil substituït) i els complexos isoelectrònics $MoO_2X_2L_2$ són eficients quan s'usa TBHP com a oxidant i no quan s'usa H_2O_2. Això és degut a que en aquest cas l'activació de H_2O_2 formaria el complex [$Cp^{\#}MoO(OH)(OOH)X$], el qual podria eliminar aigua i formar el complex [$Cp^{\#}MoO_2(O)X$] que és menys actiu que els complexos hidroperòxid d'acord amb els resultats prèviament exposats.

Epoxidació d'olefines mitjançant el complex [Cp*MoO_2]$^+$

En medi aquós el complex [$Cp^*_2Mo_2O_5$] genera els complexos [Cp*$MoO_2(H_2O)$]$^+$ i [Cp*MoO_3]$^-$. El complex catiònic [Cp*$MoO_2(H_2O)$]$^+$ estudiat a la primera secció d'aquest capítol també és capaç d'epoxidar i l'anàlisi del mecanisme es presenta a continuació. Si es pren aquest complex com l'origen d'energies el pas inicial correspon a la substitució del lligand aquo per H_2O_2. Considerant un procés dissociatiu inicialment té lloc la marxa de l'aigua, etapa endotèrmica en 10.1 kcal·mol^{-1} i posteriorment ocorre l'entrada del H_2O_2, situada a 6.7 kcal·mol^{-1} al perfil energètic corresponent (figura 6.12). A continuació, pot tenir lloc l'activació de l'oxidant, la qual presenta una barrera de 28.1 kcal·mol^{-1} (**ts1617**). En aquest procés, un protó de

H_2O_2 migra a un lligand oxo mentre el lligand OOH s'enllaça al metall donant lloc a l'espècie **17a**. L'estat de transició corresponent a aquesta etapa presenta un angle O-Mo-O significativament estret (68.8 °), fet que suggereix que una molècula d'aigua pugui assistir l'activació de H_2O_2 tal i com hem vist entre els complexos dihidroxo i aquo-oxo a l'estudiar la naturalesa del complex $[Cp^*MoO_2]^+$ en aigua.

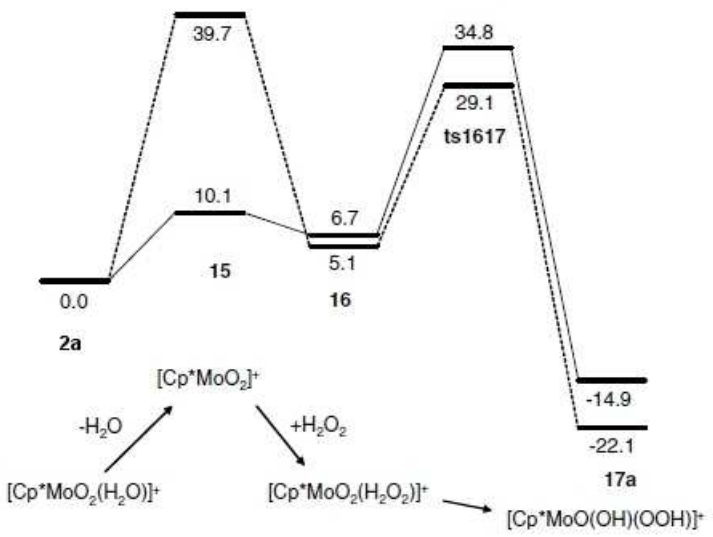

Figura 6.12: *Perfil energètic de la substitició de H_2O per H_2O_2 i de la posterior activació de H_2O_2 mitjançant el complex $[Cp^*MoO_2]^+$. Energies en kcal·mol^{-1}.*

A l'incloure la molècula d'aigua addicional, la barrera queda reduïda a tan sols 1.0 kcal·mol^{-1}, tal i com es mostra al perfil de la figura 6.13.

En aquest cas, l'angle O-Mo-O ja era força més ample (94.8 °). Ambdós estats de transició es mostren a la figura 6.14.

D'aquesta manera l'etapa limitant del procés d'activació de H_2O_2 passava a ser la dissociació de l'aigua (10.1 kcal·mol^{-1}).

Pel que fa a l'activació del TBHP és d'esperar un procés anàleg. Pel que fa al procés d'epoxidació vam localitzar dos processos de transferència de l'oxigen. En el primer, es transferia l'oxigen en α respecte el metall del lligand hidroperòxid (**ts2122**) mentre que en l'altre es transferia l'oxigen en β (**ts1819**). El perfil energètic d'ambdós processos es mostra a la figura 6.15 partint del complex $[Cp^*MoO(OH)(OOH)]^+$

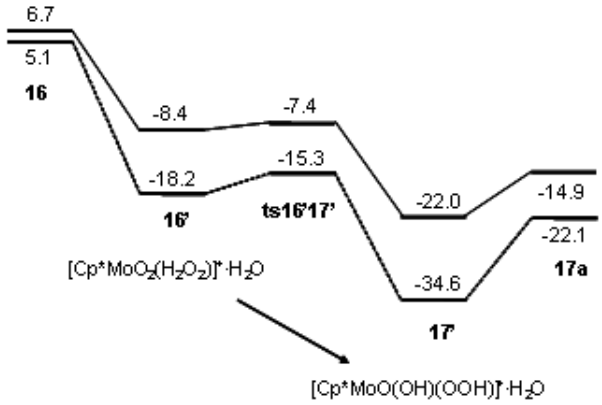

Figura 6.13: *Perfil energètic de l'activació de H_2O_2 assistida per una molècula d'aigua mitjançant el complex $[Cp^*MoO_2]^+$. Energies en kcal·mol^{-1}.*

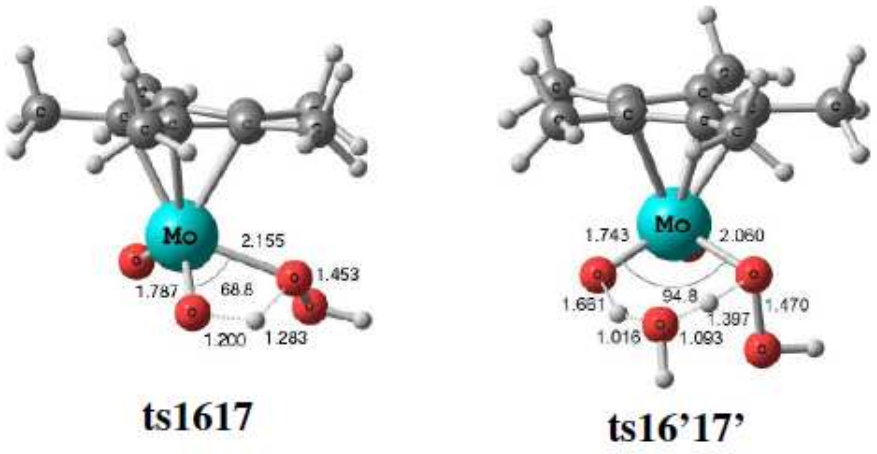

Figura 6.14: *Estats de transició del procés d'activació de H_2O_2 mitjançant el complex $[Cp^*MoO_2]^+$ no assistit (**ts1617**) i assistit (**ts16'17'**) per una molècula d'aigua. Distàncies en Å.*

(**17a**). En el primer cas, abans de l'atac en α té lloc la reorientació del grup OOH d'una posició perpendicular a una posició paral·lela, etapa que és endotèrmica en

7.2 kcal·mol^{-1}. Posteriorment, tindria lloc la transferència de l'oxigen en α a l'etilè, situada 14.0 kcal·mol^{-1} per sobre del mínim **17a**. Durant l'atac de l'oxigen en β també té lloc la transferència del protó de l'oxigen en β a l'oxigen en α. La barrera relativa d'aquest procés pren un valor de 15.2 kcal·mol^{-1} respecte **18**. Cal esmentar que només el procés de l'atac de l'oxigen en α (**ts2122**) pot ésser adaptat a l'oxidació mitjançant TBHP, ja que en aquest cas el de l'atac de l'oxigen en β **ts1819** involucraria la transferència del grup *t*-Bu enlloc de la transferència del protó. Ambdós estats de transició es mostren a la figura 6.16.

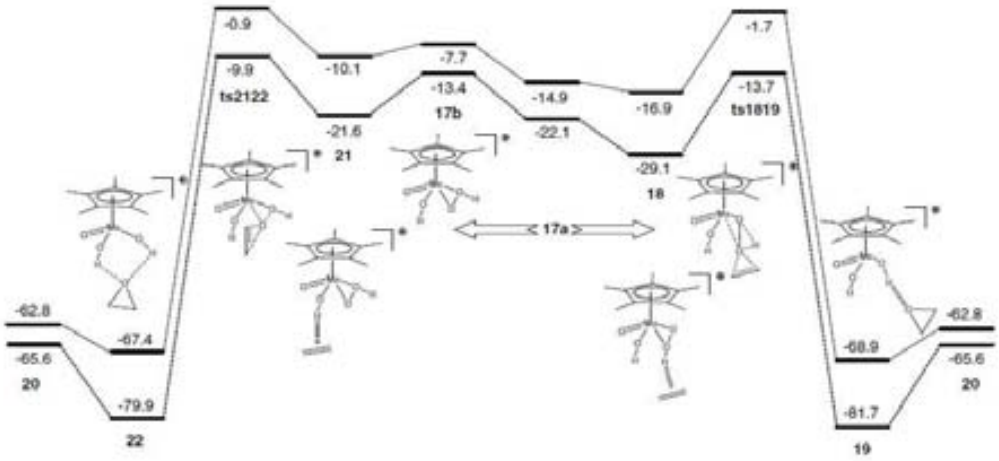

Figura 6.15: *Perfil energètic pels dos processos d'epoxidació a partir del producte de l'activació del H_2O_2: $[Cp^*MoO(OH)(OOH)]^+$ (**17a**). Energies en kcal·mol^{-1}.*

Seguidament, ens disposàrem a estudiar la possibilitat de formació dels complexos $[Cp^*Mo(O_2)(OH)_2]^+$ o $[Cp^*MoO(O_2)(H_2O)]^+$ per transferència del protó del grup OOH a partir del complex $[Cp^*MoO(OH)(OOH)]^+$ als lligands oxido i hidroxido, respectivament. Aquests processos els vàrem estudiar perquè isomeritzacions que portessin a grups peròxid inactius permetrien explicar la manca d'activitat d'aquest sistema quan s'usa H_2O_2 com a oxidant[258] ja que el TBHP no pot isomeritzar per transferència del grup *t*-Bu. Com que en el cas de l'estudi de la naturalesa del $[Cp^*MoO_2]^+$ en aigua va quedar palesa la importància d'afegir molècules d'aigua

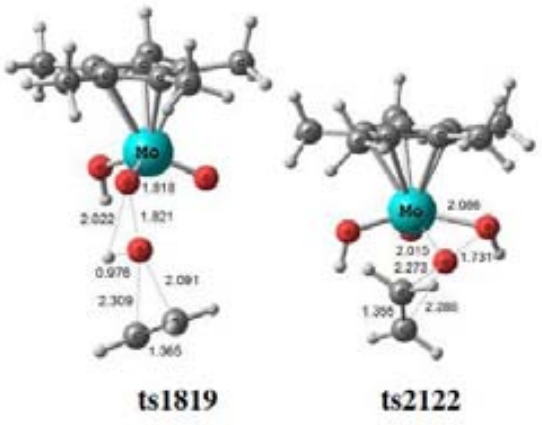

Figura 6.16: *Estats de transició del procés d'epoxidació d'olefines a partir del complex* ***17a****. Distàncies en Å.*

explícites al sistema en aquest cas també vam utilitzar una aproximació similar. D'aquesta manera, vam localitzar cinc mínims amb tres molècules addicionals d'aigua (figura 6.17).

Així, vam localitzar dues estructures pel complex $[Cp^*MoO(OH)(OOH)]^+$ (**17a(**H_2O**)$$_3$**-1** i **17a(**$H_2O$**)$$_3$**-2**), una pel complex $[Cp^*Mo(O_2)(OH)_2]^+$ (**23(**H_2O**)$$_3$**) i dues pel complex $[Cp^*MoO(O_2)(H_2O)]^+$ (**24(**H_2O**)$$_3$**-1** i **24(**$H_2O$**)$$_3$**-2**). En tots els casos un protó de cada sistema es transfereix al clúster d'aigües donant lloc a l'espècie $(H_7O_3)^+$. Pel que fa a l'estabilitat dels complexos (**24**, **23**, **17a**), aquesta segueix l'ordre relatiu d'acidesa decreixent (Mo-OH_2, Mo-OH, Mo-OOH). Cal esmentar que els complexos peròxid formats (**23** i **24**) són més estables que el complex hidroperòxid (**17a**). Per tant, la ruta de formació del peròxid és favorable termodinàmicament. Per tal de verificar que els complexos peròxid formats són menys actius vam calcular la barrera d'activació de la transferència d'oxigen a l'etilè del grup peròxid per part dels isòmers **23** i **24** (**ts2320** i **ts2414**, figura 6.18).

Les dues barreres d'activació calculades des dels reactius separats presenten valors de 10.7 kcal·mol^{-1} (**ts2320**) i 19.1 kcal·mol^{-1} (**ts2414**). Així doncs, la primera barrera és similar a l'observada pel complex hidroperòxid (12.3 kcal·mol^{-1} també respecte reactius separats) mentre que la segona és significativament superior. Per

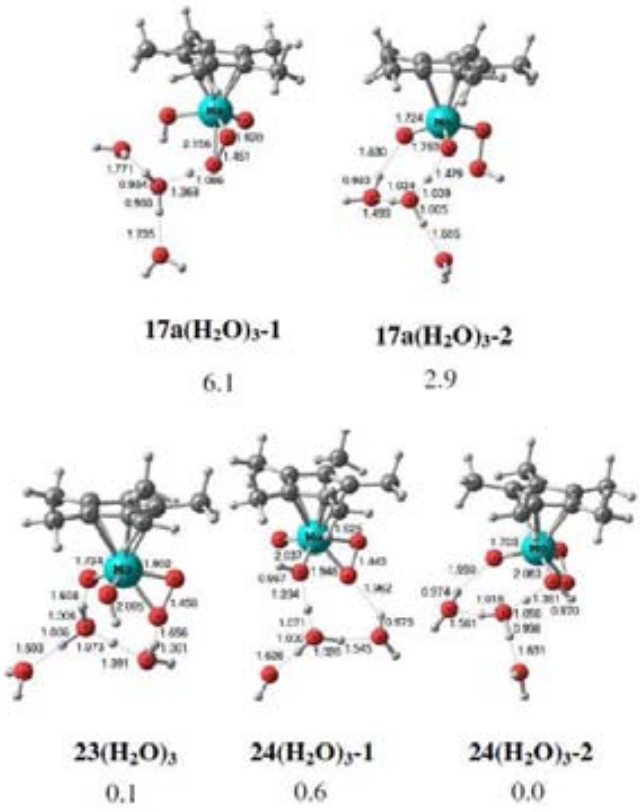

Figura 6.17: *Geometries optimitzades pels complexos* ***17a(H$_2$O)$_3$****,* ***23(H$_2$O)$_3$*** *i* ***24(H$_2$O)$_3$*** *amb la seva energia relativa (en kcal·mol^{-1}) corresponent en solució. Distàncies en Å.*

tant, la formació de grups peròxid sí que suposa una disminució de l'activitat si bé no en tots els casos. Finalment, vam avaluar la marxa del lligand aquo del complex **24** per tal de donar lloc a l'espècie $[Cp^*MoO(O_2)]^+$ i la posterior transferència d'un oxigen del grup peròxid a l'etilè. En aquest cas, la dissociació del lligand aquo tenia un cost de 24.4 kcal·mol^{-1} mentre que la posterior transferència de l'oxigen presentava una barrera de 20.5 kcal·mol^{-1} (**ts2515** de la figura 6.18) i per tant mostrava una altra vegada que la menor activitat dels grups peròxid conduïa a sistemes catalíticament menys actius.

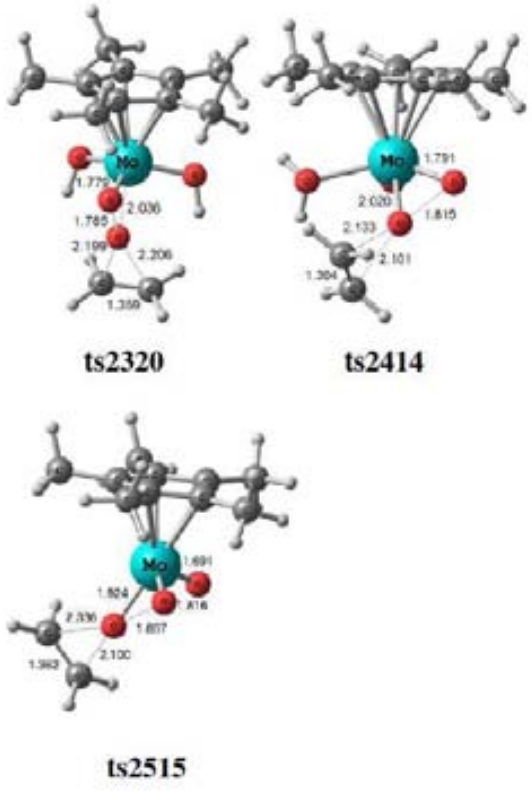

Figura 6.18: *Geometries optimitzades pels processos d'epoxidació mitjançant els complexos [Cp*Mo(O$_2$)(OH)$_2$]$^+$ (**ts2320**), [Cp*MoO(O$_2$)(H$_2$O)]$^+$ (**ts2414**) i [Cp*MoO(O$_2$)]$^+$ (**ts2515**). Distàncies en Å.*

6.3 Conclusions

Mitjançant càlculs DFT s'ha estudiat la naturalesa del [Cp*MoO_2]$^+$ en aigua i la posterior aplicació de complexos de Mo(VI) en l'epoxidació d'olefines. Els resultats obtinguts han permès concloure que:

- La descoordinació del lligand aquo del complex [Cp*$MoO_2(H_2O)$]$^+$ pren un valor de tan sols 10.1 kcal·mol^{-1} en solució, fet que mostra la facilitat de l'intercanvi del lligand aquo en solució.

- L'addició successiva de molècules d'aigua explícites (fins a tres) al sistema [Cp*MoO_2]$^+$ suposa una millora de la descripció energètica d'aquest (l'isòmer

$[Cp^*MoO_2(H_2O)]^+$ resulta més estable que l'isòmer $[Cp^*MoO(OH)_2]^+$ en 1.8 kcal·mol^{-1}).

- La transferència intramolecular protònica per passar de $[Cp^*MoO(OH)_2]^+$ a $[Cp^*MoO_2(H_2O)]^+$ presenta una barrera d'activació molt elevada: 43.9 kcal·mol^{-1}. Tanmateix, la barrera d'activació disminueix dràsticament a l'afegir una molècula d'aigua explícita al sistema (10.3 kcal·mol^{-1}) i és pràcticament negligible a l'afegir-ne dues, fet que suggereix la participació activa del solvent en el procés de tautomerització.

- L'estabilitat obtinguda pels complexos $[Cp^*MoO_2(H_2O)]^+$ i $[Cp^*MoO(OH)_2]^+$ en medi àcid mitjançant el clúster $[H_3O(H_2O)_2]^+$ és diferent a l'obtinguda experimentalment, ja que el complex dihidroxo és més estable que l'aquo-oxo en 5.3 kcal·mol^{-1}. Això probablement és degut al fet que calguin un nombre superior de molècules d'aigua per tal de descriure adequadament el medi àcid.

- Pel procés d'epoxidació mitjançant el complex $[Cp^*MoO_2Cl]$ proposem un mecanisme que inclou l'activació de H_2O_2 per formar el lligand hidroperòxid, la transferència de l'oxigen en α del grup OOH a l'etilè i la transferència protònica que allibera H_2O i que permet la regeneració del catalitzador inicial. En concordança amb els resultats experimentals, la transferència de l'oxigen per part del complex $[Cp^*Mo(O_2)OCl]$ (catalíticament inactiu) presenta una barrera d'epoxidació que és unes 10 kcal·mol^{-1} superior.

- Pel procés d'epoxidació mitjançant el complex $[Cp^*MoO_2(H_2O)]^+$ proposem un mecanisme favorable que s'inicia amb l'activació del H_2O_2. S'han estudiat les transferències de l'oxigen a l'etilè tan des de l'oxigen en α del grup hidroperòxid com des de l'oxigen en β, si bé la segona transferència només pot tenir lloc quan l'oxidant és H_2O_2 i no quan és TBHP, ja que es transfereix un protó durant la transferència de l'oxigen.

- La formació de grups peròxid per desprotonació del lligand hidroperòxid del complex $[Cp^*MoO(OH)(OOH)]^+$ permet racionalitzar la diferència d'activitat entre el H_2O_2 i el TBHP, si bé el complex $[Cp^*MoO_2(OH)_2]^+$ també pot ésser

catalíticament competitiu amb el complex $[Cp^*MoO(OH)(OOH)]^+$. Per tant, un sistema catalític d'epoxidació d'olefines que volgúes utilitzar H_2O_2 només hauria de proveïr un lloc basic per a la transferència de tan sols un dels dos protons del H_2O_2 ja que si en tingués dos es formaria un lligand peròxid que donaria lloc a un complex menys actiu d'epoxidació.

Capítol 7

Procés de Wacker

7.1 Etapa d'addició nucleòfila del procés de Wacker

La reacció de Wacker consisteix en l'oxidació d'etilè a acetaldahid mitjançant oxigen catalitzada per $PdCl_2$ i $CuCl_2$. Com ja s'ha comentat al capítol 2, el pas de la reacció de Wacker que havia generat més controvèrsia era l'addició nucleòfila o hidroxipal·ladació de l'etilè. La controvèrsia principal es basava en si l'addició nucleòfila de l'aigua a l'etilè es donava a través d'un mecanisme d'esfera interna mitjançant una molècula d'aigua coordinada al pal·ladi (addició en *syn*) o a través d'un mecanisme d'esfera externa (addició en *anti*) mitjançant una molècula d'aigua provinent del medi. Ambdós processos es mostren a la figura 7.1 dins del cicle catalític del procés. Tanmateix, cal esmentar que el mecanisme d'addició nucleòfila també es veia afectat per les condicions de reacció, com $[Cl^-]$ i $[CuCl_2]$.[176–178,281,282]

El mecanisme d'esfera externa era el que es desprenia d'estudis d'estereoquímica,[172,174,175] mentre que el mecanisme d'esfera interna es proposava en base a estudis cinètics i d'efecte cinètic d'isòtop.[171,173] Hoffmann i Eisenstein mitjançant la teoria d'orbitals moleculars van mostrar que el desplaçament de η^2 a η^1 de l'etilè era la força que dirigia l'atac nucleòfil extern,[179] mentre que mitjançant una aproximació similar Fujimoto i Yamasaki proposaren l'addició en *trans* de l'hidroxil.[180] El procés de Wacker també fou estudiat per Siegbahn,[182–184] el qual va descriure de

forma implícita i explícita el medi (afegint fins a quatre molècules d'aigua)[184] tot proposant el mecanisme d'esfera externa. D'altra banda fent servir un model similar Eshtiagh-Hosseini trobà resultats comparables[185] encara que algunes de les seves conclusions s'hagin qüestionat darrerament.[283]

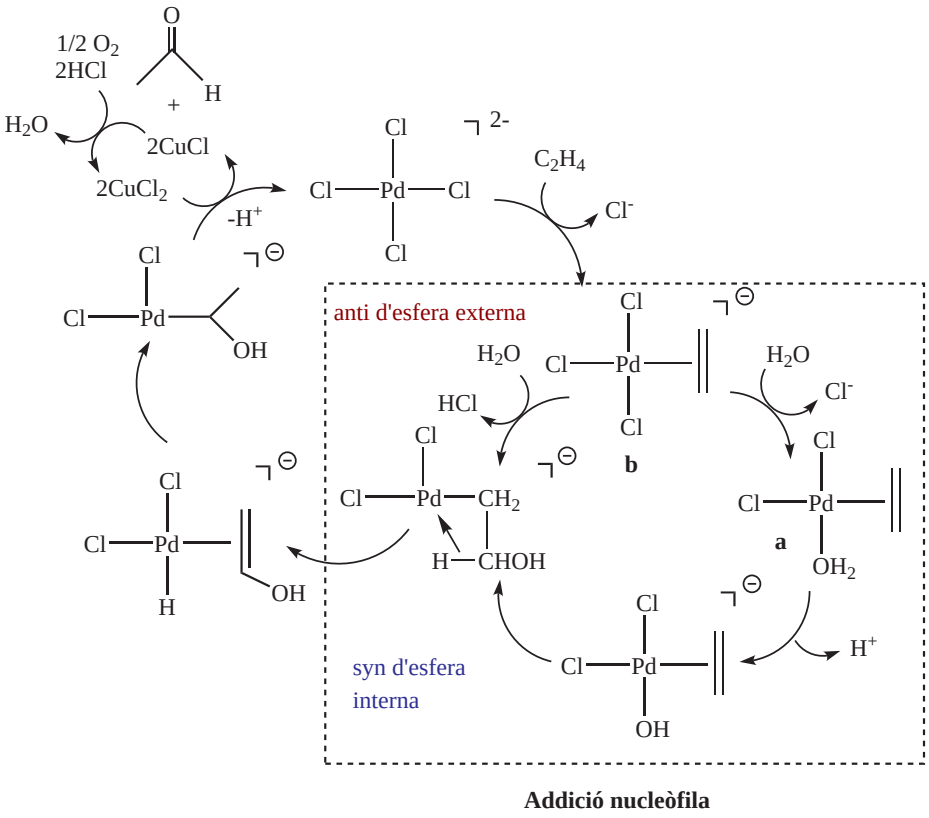

Figura 7.1: *Cicle catalític proposat pel procés de Wacker amb les dues addició nucleòfiles possibles: en* syn *i en* anti.

Finalment, Goddard i col·laboradors també estudiaren el procés de Wacker,[181,187] tot racionalitzant la dependència del mode d'addició en funció de les condicions de reacció ($[Cl^-]$ i $[CuCl_2]$) en base a càlculs teòrics.[181] Tanmateix, hagueren d'incloure una correcció empírica als càlculs teòrics per tal d'obtenir barreres de reacció raonables per aquells passos on s'alliberava un protó al medi. D'aquesta manera, tot i la valuosa informació obtinguda mitjançant la combinació de models implícits i explícits per a la descripció del solvent, aquesta aproximació encara té certes limitacions, com

ara l'escàs nombre de molècules d'aigua afegides a les simulacions o la necessitat d'haver d'incloure correccions empíriques.

7.2 El nostre estudi: resultats i discussió

Com que les molècules de solvent participen activament en la reacció, una descripció apropiada del medi aquós era crucial en l'etapa d'addició nucleòfila. Així, el nostre objectiu era avaluar aquesta etapa mitjançant dinàmica molecular de primers principis acoblada amb metadinàmica per tal de descriure la reactivitat de les molècules d'aigua provinents del medi. D'aquesta manera, s'estudiaren les dues alternatives principals per l'etapa d'addició nucleòfila: el mecanisme d'esfera interna i el mecanisme d'esfera externa. Es va partir dels dos intermedis des d'on podria tenir lloc l'atac nucleòfil: l'intermedi $[PdCl_2(H_2O)(CH_2{=}CH_2)]$ (**a** de la figura 7.1) i l'intermedi $[PdCl_3(CH_2{=}CH_2)]^-$ (**b** de la figura 7.1). Per tal de fer-ho, es realitzaren càlculs de dinàmica molecular Car-Parrinello acoblats a metadinàmiques. S'usà el HCTH/120 com a funcional de la densitat i pseudopotencials amb un conjunt d'ones planes expandides fins a 70 Ry. Per tal de descriure la solvatació, els intermedis **a** i **b** se situaren juntament amb 26 molècules d'aigua en cel·les de simulació de 9.86x9.86x9.86 Å a una temperatura de 300 K. A més se substituïren hidròdens per deuteris per tal de poder usar un *time step* de 7 u. a. i un valor 1000 u. a. per a la massa electrònica fictícia. Abans de realitzar la metadinàmica, es realitzaren dinàmiques moleculars Car-Parrinello a 600 K durant 1 ps seguides d'*annealing* fins a una temperatura de 300 K per tal d'equilibrar el sistema.

7.2.1 Variables col·lectives seleccionades

En primer lloc, vam seleccionar les variables col·lectives pels processos que volíem accelerar i pels quals volíem obtenir barreres d'energia lliure. Per a l'intermedi **a** vam seleccionar les següents variables col·lectives: el nombre de coordinació (CN) de l'oxigen del lligand aquo respecte els hidròdens (**CV1**), el CN dels carbonis de l'etilè respecte l'oxigen del lligand aquo (**CV2**), el CN del Pd respecte els àtoms de clor (**CV3**), el CN entre els carbonis de l'etilè i tots els oxígens (**CV4**), el CN del Pd

respecte tots els àtoms d'oxigen (**CV5**) i el CN del Pd respecte l'oxigen del lligand aquo (**CV6**). Per **b** es van usar variables col·lectives anàlogues a **CV3**, **CV4** i **CV5**: **CV3'**, **CV4'** i **CV5'**. Per tal d'avaluar la hidroxipal·ladació es van analitzar sis conjunts de variables col·lectives (**S1-S6**) tal i com es mostren a la figura 7.2.

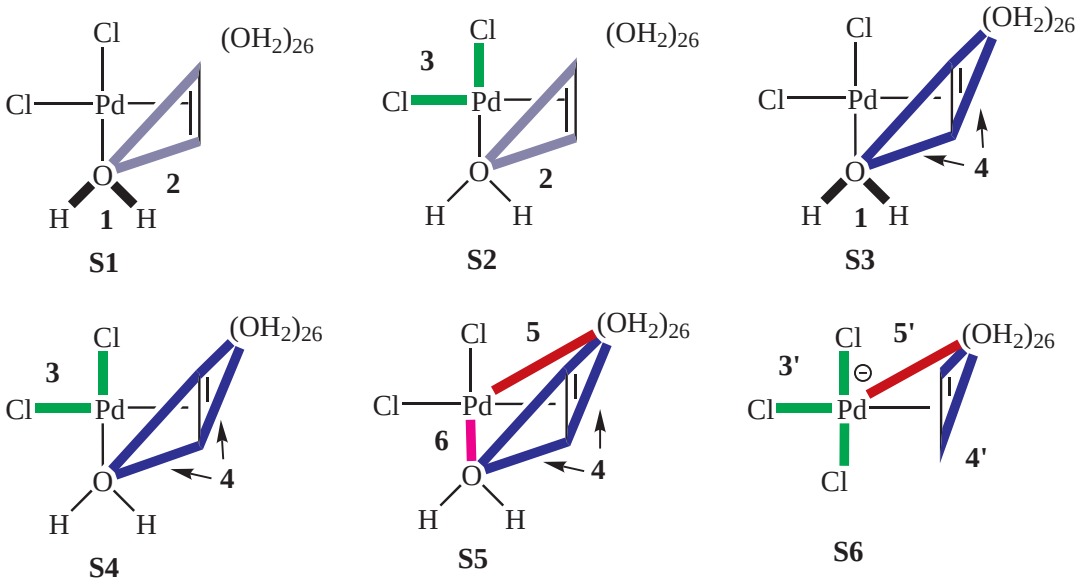

Figura 7.2: *Conjunt de variables col·lectives seleccionades pels complexos* ***a*** *(**S1-S5**) i* ***b*** *(**S6**).*

Cadascun d'aquests conjunts conté dues o tres variables col·lectives. En primer lloc, vam analitzar processos químics que podien afectar l'esfera de coordinació de l'espècie **a**. Així, vam calcular que l'intercanvi Cl^--H_2O tenia una barrera de 14 kcal·mol^{-1} mentre que la barrera per l'intercanvi del segon lligand prenia un valor de 35 kcal·mol^{-1}. Pel que fa a l'intercanvi degenerat H_2O-H_2O, la barrera prenia un valor de 25 kcal·mol^{-1}. També vam trobar que la transferència d'un protó al medi del lligand aquo prenia un valor de 10 kcal·mol^{-1}, mentre que la barrera per la protonació del lligand aquo presentava un valor de 13 kcal·mol^{-1}. Tenint en compte que el valor experimental per la barrera de l'addició nucleòfila presentava un valor de 22.4 kcal·mol^{-1} podíem concloure que els processos exposats anteriorment podien alterar l'estequiometria del catalitzador abans que la reacció d'addició tingués lloc i que, per tant, les simulacions havien d'incloure aquestes possibilitats.

7.2.2 Addició nucleòfila d'esfera interna

Les simulacions **S1** i **S2** tenien per objectiu simular el mecanisme d'esfera interna. A la primera metadinàmica (**S1**) s'observà l'addició nucleòfila d'esfera interna (**CV2**) precedida d'un parell d'intercanvis de protons amb el medi (**CV1**). Així, l'aigua coordinada es desprotonava ràpidament formant un lligand hidroxil que posteriorment reaccionava amb l'etilè. A la figura 7.3 es mostra un fotograma representatiu d'aquest procés.

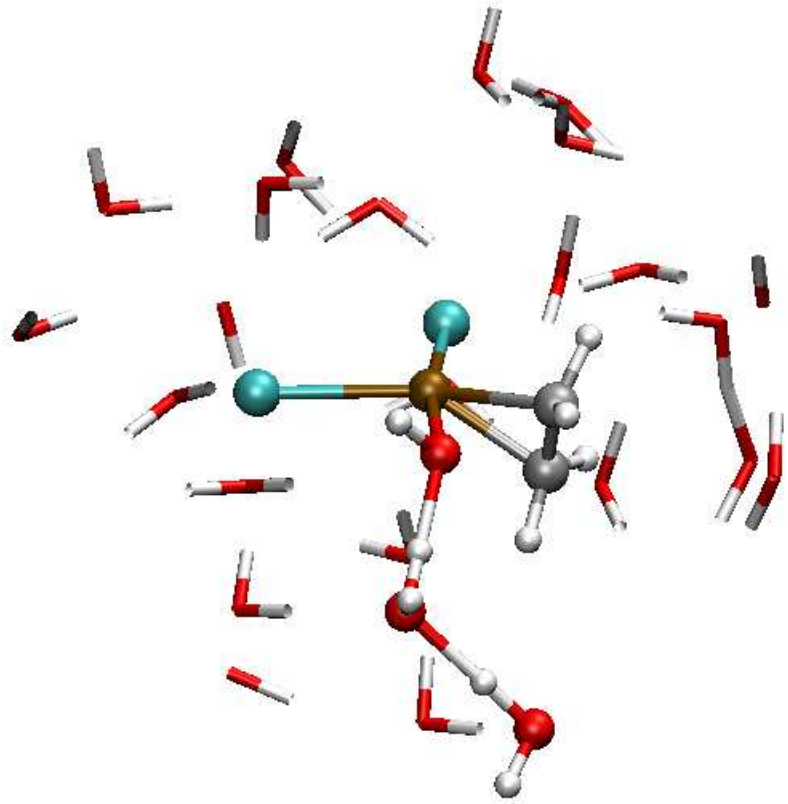

Figura 7.3: *Fotograma representatiu de la simulació **S1** on es dóna l'addició nucleòfila d'esfera interna del lligand hidroxil a l'etilè.*

Aquest pas presentava una barrera d'energia lliure de 60 kcal·mol^{-1} produïnt el producte d'addició en *syn*. És, doncs, una barrera significativament més gran que l'obtinguda experimentalment.

La segona metadinàmica (**S2**) incloïa la coordinació del Cl al voltant del Pd (**CV3**) juntament amb l'addició nucleòfila d'esfera interna (**CV2**). La simulació mostrà que la mobilitat dels clorurs és força alta, havent-hi dissociacions d'aquests prèviament a l'addició nucleòfila d'esfera interna. Pel que fa a l'addició nucleòfila d'esfera interna la barrera prenia un valor de 48 kcal·mol^{-1}, essent massa elevada si es comparava amb la barrera experimental. Per tant, amb els resultats obtinguts mitjançant les simulacions **S1** i **S2** podíem concloure que el mecanisme d'esfera interna no era compatible amb la barrera d'energia lliure experimental.

7.2.3 Addició nucleòfila d'esfera externa

Per tal de simular l'addició nuclèofila d'esfera externa vam realitzar les quatre simulacions següents (**S3**-**S6**). La simulació **S3** incloïa les variables col·lectives **CV1** i **CV4** per tal d'observar l'intercanvi de protó del lligand aquo amb el medi i l'atac nucleòfil a l'etilè, respectivament. Cal esmentar que en aquest cas, a diferència del que passava amb **S1**, qualsevol de les aigües del sistema podien atacar l'etilè. Durant la simulació, en primer lloc es donava la transferència d'un protó entre un lligand aquo i la solució gràcies a la baixa barrera d'activació associada a aquest procés. A continuació, tenia lloc l'addició nucleòfila d'esfera externa, i aquesta es donava quan una molècula d'aigua estava coordinada al pal·ladi, la qual presentava una barrera d'energia lliure de 24 kcal·mol^{-1} que concordava amb el resultat experimental. A la figura 7.4 es mostra un fotograma de l'atac de la molècula d'aigua a l'etilè en el qual es forma l'enllaç C-O i al mateix temps es dóna la transferència protònica d'aquesta molècula d'aigua a una molècula d'aigua adjacent. En la simulació **S4** també s'avaluà el rol dels lligands clorur en l'addició nucleòfila d'esfera externa mitjançant les variables col·lectives **CV3** i **CV4**. En aquest cas, l'addició nucleòfila d'esfera externa era simultània a l'alliberació al medi d'un dels protons de la molècula d'aigua que ataca a l'etilè. L'addició nucleòfila es donava després de la descoordinació parcial d'un clorur, amb una barrera de 22 kcal·mol^{-1}, un valor molt similar a l'obtingut per

S3 usant unes altres variables col·lectives i en concordança amb el valor experimental. Això mostrava que la mobilitat del clorur no afectava a la hidroxipal·ladació d'esfera externa.

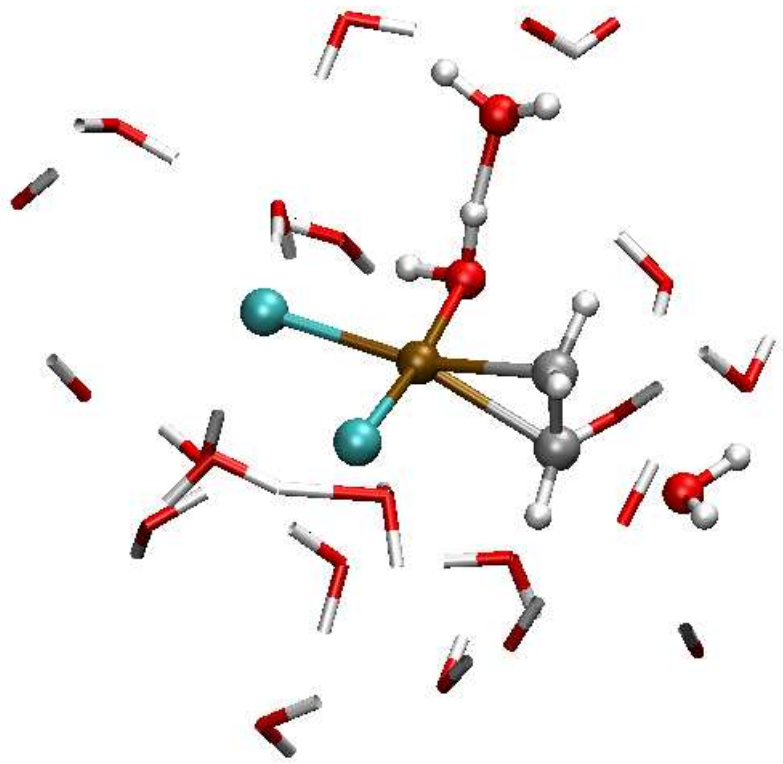

Figura 7.4: *Fotograma representatiu de la simulació **S3** on es dóna l'addició nucleòfila d'esfera externa d'una molècula d'aigua a l'etilè amb alliberament d'un protó al medi.*

Pel que fa a la simulació **S5**, es va usar la combinació de tres variables col·lectives: **CV4**, **CV5** i **CV6** d'aquesta manera podent-se obtenir informació de l'intercanvi de lligands aquo al voltant del Pd(II) (**CV5** i **CV6**). Així, durant la simulació, l'atac d'esfera interna no tenia lloc degut a l'elevada barrera que presentava i en canvi l'atac d'esfera externa sí que s'observà, tot presentant una barrera de 22 kcal·mol^{-1} en bona concordança amb el valor experimental. La simulació també va permetre observar altres etapes de reacció amb barreres més baixes, com ara l'intercanvi Cl^{-}-H_2O o la

transferència protònica espontània d'un protó de l'aigua que atacava l'etilè durant l'etapa d'addició nucleòfila. Cal esmentar que la recoordinació d'un lligand clorur dissociat té lloc en posició *trans* respecte l'altre clorur. A més a més, també s'observà intercanvi del lligand aquo a l'intermedi $[PdCl(H_2O)_2(C_2H_4)]^+$.

Des de l'intermedi **b** només pot tenir lloc l'atac nucleòfil d'esfera externa a no ser que hi hagi una substitució Cl^--H_2O. D'aquesta manera, per la simulació **S6** s'han usat les variables col·lectives corresponents a la coordinació dels clorurs (**CV3'**), al nombre de molècules d'aigua coordinades al pal·ladi (**CV5'**) i al nombre d'aigües coordinades a l'etilè per tal de descriure la hidroxipal·ladació (**CV4'**). Durant la metadinàmica, primer s'observà la substitució del lligand Cl^- *trans* per una molècula d'aigua. A continuació s'observà l'atac nucleòfil d'una molècula d'aigua de la solució a l'etilè, juntament amb la transferència protònica al medi, procés que presentava una barrera d'energia lliure de 19 kcal·mol^{-1}. Malgrat que aquesta barrera és una mica inferior a les obtingudes per l'intermedi **a** segueix estant d'acord amb el valor experimental de la barrera i fins i tot dins del marge d'error de les simulacions, que és de 2.6 kcal·mol^{-1}.[217]

D'aquesta manera, els resultats obtinguts mostren la viabilitat de l'addició nucleòfila d'esfera externa en *anti* en contraposició a l'addició nucleòfila d'esfera interna. Cal esmentar que les varibles col·lectives que hem seleccionat no distingeixen entre els atacs en *anti* i en *syn* sinó entre els atacs d'esfera externa i d'esfera interna. Per tant, l'atac d'esfera externa en *syn* no es pot descartar si bé com que en les simulacions de **S3** a **S6** no s'ha observat l'atac en *syn*, aquest ha de presentar necessàriament una barrera més alta que l'atac en *anti*. En les simulacions prèvies el solvent jugava un paper important ja que en tots els casos l'addició nucleòfila d'esfera externa tenia lloc simultàniament a la transferència d'un protó al medi provinent de l'aigua que protagonitzava l'atac nucleòfil. Això es mostra a la figura 7.5, on es pot observar que la formació de l'enllaç C-O i la transferència protònica te lloc simultàniament (simulació **S4**). L'el·lipse indica la zona de l'estat de transició. Per les altres simulacions també s'han observat corbes similars. Aquest comportament concertat mostra la importància de les molècules d'aigua veïnes, ja que la transferència protònica amb la corresponent separació de càrrega associada es veu afavorida per la polaritat del medi aquós.[184] Això mostra com la inclusió explícita de molècules d'aigua és clau en

les simulacions per tal que es doni de forma apropiada el procés concertat d'addició nucleòfila i de transferència protònica.

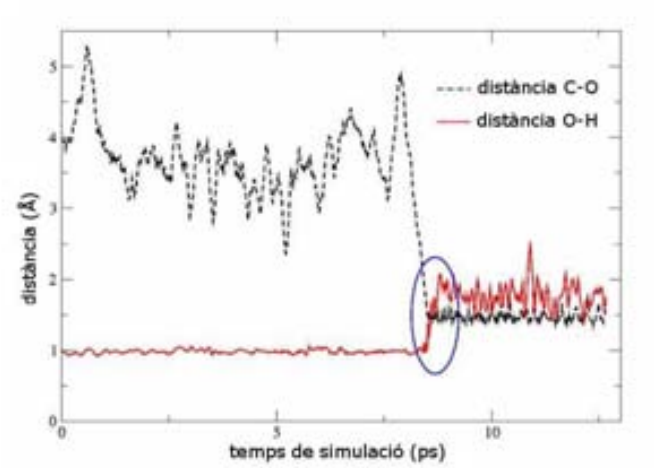

Figura 7.5: *Evolució de l'enllaç C-O i d'un dels enllaços O-H de l'aigua reactiva durant la simulació* ***S4****. Les corbes representen configuracions preses a cada pas de metadinàmica, és a dir, cada 13.6 fs.*

7.3 Conclusions

Mitjançant dinàmiques moleculars basades en la teoria del funcional de la densitat s'han estudiat les addicions nucleòfiles d'esfera interna i d'esfera externa d'una molècula d'aigua a l'etilè pels complexos **a** $[PdCl_2(H_2O)(CH_2{=}CH_2]$ i **b** $[PdCl_3(CH_2{=}CH_2)]^-$. Els resultats obtinguts han permès concloure que:

- Processos com l'intercanvi Cl^--H_2O, l'intercanvi H_2O-H_2O i la desprotonació o protonació del lligand aquo poden afectar l'estequiometria del catalitzador

abans que la reacció d'addició tingui lloc i, per tant, s'han de tenir en compte durant les simulacions.

- El mecanisme d'addició nucleòfila d'esfera externa des de l'intermedi **a** $[PdCl_2(H_2O)(CH_2{=}CH_2]$ és clarament més favorable al mecanisme d'addició nucleòfila d'esfera interna. Per l'addició d'esfera externa s'han obtingut barreres d'energia lliure entre 22 i 24 kcal·mol^{-1} mentre que per l'addició d'esfera interna s'han obtingut valors de 48 i 60 kcal·mol^{-1}. Els valors obtinguts per l'addició nucleòfila d'esfera externa concorden amb el valor obtingut experimentalment (22.4 kcal·mol^{-1}).

- L'atac nucleòfil partint de l'intermedi **b** $[PdCl_3(CH_2{=}CH_2)]^-$ ha donat lloc a una barrera d'energia lliure de 19 kcal·mol^{-1}. Aquesta etapa ve precedida per una substitució *trans* Cl^--H_2O. Això indica que l'espècie que pateix l'atac nucleòfil és l'espècie neutra $[PdCl_2(H_2O)(CH_2{=}CH_2)]$.

- L'addició en *anti* és preferible a l'addició en *syn*, ja que si bé els càlculs pressuposen cap de les dues opcions en tots els casos s'ha observat l'addició en *anti*, fet que mostra que l'addició en *syn* ha de presentar una energia necessàriament superior. D'aquesta, manera el mecanisme de la reacció d'addició proposat és l'addició nucleòfila en *anti* d'esfera externa.

Part IV

Conclusions

Capítol 8

Conclusions

Els resultats obtinguts durant la realització d'aquesta tesi doctoral han permès extreure les següents conclusions:

- L'estudi del catalitzador de Shvo com a exemple de catalitzador metall-lligand bifuncionalitzat (capítol 4) ha mostrat que el mecanisme d'hidrogenació més favorable és el mecanisme que inclou la transferència concertada de l'hidrur i del protó fora de l'esfera de coordinació del metall independentment de quin sigui el substrat (cetones, imines, alquens o alquins). Aquest mecanisme permet explicar la quimioselectivitat observada experimentalment (dobles enllaços polars més reactius que els enllaços múltiples apolars).

- En reaccions d'hidrogenació d'olefines mitjançant complexos de Au(III) i de Pd(II) (capítol 5) el mecanisme de la reacció prossegueix dins l'esfera de coordinació del metall amb un cicle catalític que s'inicia gràcies al trencament heterolític de la molècula d'hidrogen. El cicle catalític pròpiament dit inclou l'entrada de l'etilè a l'esfera de coordinació gràcies a la marxa d'un lligand amino (etapa determinant de la velocitat de reacció), la posterior inserció a l'enllaç M-H i la regeneració de l'hidrur (espècie activa) gràcies al trencament heterolític d'una altra molècula d'hidrogen.

- Els processos d'epoxidació de l'etilè mitjançant els complexos [Cp*MoO_2Cl] i [Cp*$MoO_2(H_2O)]^+$ s'inicien amb l'activació del H_2O_2. Posteriorment té lloc la

transferència de l'oxigen α o β del lligand hidroperòxid a l'etilè tot obtenint-se l'epòxid i, finalment, té lloc la transferència protònica que regenera l'espècie activa del catalitzador.

- En el procés de Wacker, l'etapa d'addició nucleòfila d'una molècula d'aigua sobre l'etilè té lloc mitjançant un atac en *anti* d'esfera externa. En tots els casos aquest procés es dóna sobre l'espècie neutra [$PdCl_2(H_2O)(CH_2{=}CH_2)$].

- Les reaccions d'hidrogenació mitjançant el catalitzador de Shvo (capítol 4), les epoxidacions mitjançant compostos tipus Cp*Mo(VI) (capítol 6) i l'addició nucleòfila del procés de Wacker (capítol 7) prossegueixen a través de mecanismes que es donen fora de l'esfera de coordinació del metall.

- La participació del solvent s'ha observat que juga un paper determinant en la majoria dels processos estudiats. Així, en el cas dels complexos de Au(III) (capítol 5) l'etapa de trencament heterolític de l'hidrogen era assistida pel solvent (etanol), la tautomerització dihidroxo aquo-oxo pels complexos tipus Cp*Mo(VI) es donava a través de cadenes d'aigua, i l'addició de molècules d'aigua ajudava a la descripció de la naturalesa en aigua dels complexos Cp*Mo(VI) (capítol 6). Finalment, en l'etapa d'addició nucleòfila del procés de Wacker (capítol 7), el solvent participava tan en l'atac nucleòfil com en l'estabilització del protó alliberat durant l'etapa esmentada.

- La química computacional és una eina molt útil alhora d'estudiar mecanismes de reacció en processos de catàlisi homogènia tal i com s'ha vist en les nombroses reaccions estudiades durant aquesta tesi doctoral. Tanmateix, és important determinar amb quin grau de rigorositat es modelitza el solvent en funció de les necessitats del problema d'estudi.

Bibliografia

[1] A. D. McNaught and A. Wilkinson, editors. *IUPAC. Compendium of Chemical Terminology. (the "Gold Book").* Blackwell Scientific Publications, Oxford, 1997.

[2] G. Rothenberg. *Catalysis: Concepts and Green Applications.* Wiley-VCH, Weinheim, 2008.

[3] I. Chorkendorff and J. W. Niemantsverdriet. *Concepts of Modern Catalysis and Kinetics.* Wiley-VCH, Weinheim, 2007.

[4] P. W. van Leeuwen. *Homogeneous Catalysis: Understanding the Art.* Kluwer Academic Publishers, Dordrecht, 2004.

[5] J. Hagen. *Industrial Catalysis: A Practical Approach.* Wiley-VCH, Weinheim, 2006.

[6] B. List. *Chem. Rev.*, 107:5413, 2007.

[7] S. A. Moya. *Fundamentos y aplicaciones de la Catálisis Homogénea.* Zaragoza, 2000.

[8] S. Arrhenius. *Zeit. Phys. Chem.*, 28:317, 1899.

[9] S. R. Logan. *Fundamentos de Cinética Química.* Addison Wesley Iberoamericana, Madrid, 2000.

[10] P. Atkins and J. de Paula. *Atkins' Physical Chemistry.* Oxford University Press, New York, 2002.

[11] H. Eyring. *J. Chem. Phys.*, 3:107, 1935.

[12] M. G. Evans and M. Polanyi. *Trans. Faraday Soc.*, 31:875, 1935.

[13] J. I. Steinfeld, J. S. Francisco, and W. L. Hase. *Chemical Kinetics and Dynamics.* Prentice Hall, Inc., New Jersey, 1989.

[14] P. A. Chaloner, M. A. Esteruelas, F. Joó, and L. A. Oro. *Homogeneous Hydrogenation.* Kluwer Academic Publishers, Dordrecht, 1994.

[15] B. R. James. *Homogeneous Hydrogenation.* Wiley, New York, 1973.

[16] P. J. Brothers. *Prog. Inorg. Chem.*, 28:1, 1981.

[17] G. J. Kubas, R. R. Ryan, B. I. Swanson, P. J. Vergamini, and H. J. Wasserman. *J. Am. Chem. Soc.*, 106:451, 1984.

[18] D. M. Heinekey and W. J. Oldham. *Chem. Rev.*, 93:913, 1993.

[19] R. H. Crabtree. *The Organometallic Chemistry of the Transition Metals*. Wiley-Interscience, New York, 2001.

[20] Y. Jean, O. Eisenstein, F. Volatron, B. Maouche, and F. Sefta. *J. Am. Chem. Soc.*, 108:6587, 1986.

[21] A. J. Lough, S. Park, R. Ramachandran, and R. H. Morris. *J. Am. Chem. Soc.*, 116:8356, 1994.

[22] R. H. Crabtree, P. E. M. Siegbahn, O. Eisenstein, A. L. Rheingold, and T. F. Koetzle. *Acc. Chem. Res.*, 29:348, 1996.

[23] S. Niu and M. B. Hall. *Chem. Rev.*, 100:353, 2000.

[24] F. Hutschka, A. Dedieu, and W. Leitner. *Angew. Chem. Int. Ed.*, 34:1742, 1995.

[25] F. Hutschka, A. Dedieu, M. Eichberger, R. Fornika, and W. Leitner. *J. Am. Chem. Soc.*, 119:4432, 1997.

[26] A. Milet, A. Dedieu, G. Kapteijn, and van Koten. G. *Inorg. Chem.*, 36:3223, 1997.

[27] A. Dedieu, S. Humbel, J. E. Cornelis, and C. Grauffel. *Theor. Chem. Acc.*, 112:305, 2004.

[28] D. G. Musaev, R. D. J. Froese, K. Morokuma, S. Strömberg, K. Zetterberg, and P. E. M. Siegbahn. *Organometallics*, 16:1933, 1997.

[29] D. G. Musaev, R. D. J. Froese, and K. Morokuma. *Organometallics*, 17:1850, 1998.

[30] D. Sellmann, F. Geipel, and M. Moll. *Angew. Chem. Int. Ed.*, 39:561, 2000.

[31] Y. Musashi and S. Sakaki. *J. Am. Chem. Soc.*, 122:3867, 2000.

[32] G. Zampella, M. Bruschi, P. Fantucci, and L. De Gioia. *J. Am. Chem. Soc.*, 127:13180, 2005.

[33] M. Ito, M. Hirakawa, K. Murata, and T. Ikariya. *Organometallics*, 20:379, 2001.

[34] C. A. Sandoval, T. Ohkuma, K. Muñiz, and Noyori R. *J. Am. Chem. Soc.*, 125:13490, 2003.

[35] V. Rautenstrauch, X. Hoang-Cong, R. Churlaud, K. Abdur-Rashid, and R. H. Morris. *Chem. Eur. J.*, 9:4954, 2003.

[36] C. P. Casey, J. B. Johnson, S. W. Singer, and Q. Cui. *J. Am. Chem. Soc.*, 127:3100, 2005.

[37] C. Hedberg, K. Källström, P. I. Arvidsson, P. Brandt, and P. G. Andersson. *J. Am. Chem. Soc.*, 127:15083, 2005.

[38] F. Hutschka and A. Dedieu. *J. Chem. Soc., Dalton Trans.*, 1899, 1997.

[39] C. González-Arellano, A. Corma, M. Iglesias, and F. Sánchez. *Chem. Commun.*, 3451, 2005.

[40] R. M. Bullock. *Chem. Eur. J.*, 10:2366, 2004.

[41] L. A. Oro. *Fundamentos y aplicaciones de la Catálisis Homogénea.* INO Reproducciones, S.A., Zaragoza, 2000.

[42] D. Evans, J. A. Osborn, F. H. Jardine, and G. Wilkinson. *Nature*, 32:265, 1965.

[43] S. S. Bath and L. Vaska. *J. Am. Chem. Soc.*, 85:3500, 1965.

[44] L. Vaska. *Inorg. Nucl. Chem. Lett.*, 1:89, 1965.

[45] D. Evans, G. Yagupsky, and G. Wilkinson. *J. Chem. Soc. A*, 2660, 1968.

[46] M. Yagupsky, C. K. Brown, G. Yagupsky, and G. Wilkinson. *J. Chem. Soc. A*, 937, 1970.

[47] J. A. Osborn, F. H. Jardine, J. F. Young, and G. Wilkinson. *J. Chem. Soc. A*, 1711, 1966.

[48] S. Montelatici, A. van der Ent, J. A. Osborn, and G. Wilkinson. *J. Chem. Soc. A*, 1054, 1968.

[49] C. O'Connor and G. Wilkinson. *J. Chem. Soc. A*, 2665, 1968.

[50] F. H. Jardine, J. A. Osborn, and G. Wilkinson. *J. Chem. Soc. A*, 1574, 1967.

[51] C. A. Tolman, P. Z. Meakin, D. L. Lindner, and J. P. Jesson. *J. Am. Chem. Soc.*, 96:2762, 1974.

[52] N. Koga, C. Daniel, J. Han, X. Y. Fu, and K. Morokuma. *J. Am. Chem. Soc.*, 109:3455, 1987.

[53] C. Daniel, N. Koga, J. Han, X. Y. Fu, and K. Morokuma. *J. Am. Chem. Soc.*, 110:3773, 1988.

[54] J. Halpern. *Inorg. Chim. Acta*, 50:11, 1981.

[55] J. Halpern, T. Okamoto, and A. Zakhariev. *J. Mol. Catal.*, 2:65, 1976.

[56] F. Maseras and A. Lledós, editors. *Computational Modeling of Homogeneous Catalysis.* Kluwer Academic Publishers, Dordrecht, 2002.

[57] O. Pàmies and J. E. Bäckvall. *Chem. Eur. J.*, 7:5052, 2001.

[58] A. Andriollo, M. A. Esteruelas, U. Meyer, L. A. Oro, R. Sánchez-Delgado, E. Sola, C. Valero, and H. Werner. *J. Am. Chem. Soc.*, 111:7431, 1989.

[59] F. Joó, J. Kovács, A. C. Bényei, and Á. Kathó. *Angew. Chem. Int. Ed.*, 37:969, 1998.

[60] F. Joó, J. Kovács, A. C. Bényei, and Á. Kathó. *Catal. Today*, 42:441, 1998.

[61] G. Kovács, G. Ujaque, A. Lledós, and F. Joó. *Organometallics*, 25:862, 2006.

[62] A. Rossin, G. Kóvacs, G. Ujaque, A. Lledós, and F. Joó. *Organometallics*, 25:5010, 2006.

[63] G. Kovács, G. Schubert, F. Joó, and I. Pápai. *Organometallics*, 24:3059, 2005.

[64] G. Kovács, G. Schubert, F. Joó, and I. Pápai. *Catal. Today*, 115:53, 2006.

[65] J. Joubert and F. Delbecq. *Organometallics*, 25:854, 2006.

[66] R. R. Schrock and J. A. Osborn. *J. Chem. Soc., Chem. Commun.*, 567, 1970.

[67] R. A. Sánchez-Delgado, N. Valencia, R. L. Márquez-Silva, A. Andriollo, and M. Medina. *Inorg. Chem.*, 25:1106, 1986.

[68] D. E. Linn and J. Halpern. *J. Am. Chem. Soc.*, 109:2969, 1987.

[69] H. Guan, M. Iimura, M. P. Magee, J. R. Norton, and G. Zhu. *J. Am. Chem. Soc.*, 127:7805, 2005.

[70] R. M. Bullock and M. H. Voges. *J. Am. Chem. Soc.*, 122:12594, 2000.

[71] M. H. Voges and R. M. Bullock. *J. Chem. Soc., Dalton Trans.*, 759, 2002.

[72] B. F. M. Kimmich, P. J. Fagan, E. Hauptman, and R. M. Bullock. *Chem. Commun.*, 1014, 2004.

[73] M. P. Magee and J. R. Norton. *J. Am. Chem. Soc.*, 123:1778, 2001.

[74] P. Hauwert, G. Maestri, J. W. Sprengers, M. Catellani, and C. J. Elsevier. *Angew. Chem. Int. Ed.*, 47:3223, 2008.

[75] A. G. Campanya, R. E. Estévez, N. Fuentes, R. Robles, J. M. Cuerva, E. Buñuel, D. Cárdenas, and J. E. Oltra. *Org. Lett.*, 9:2195, 2007.

[76] D. Gnanamgari, A. Moores, E. Rajaseelan, and R. H. Crabtree. *Organometallics*, 26:1226, 2007.

[77] K. Tani, A. Iski, and T. Yamagata. *Chem. Commun.*, 1821, 1999.

[78] K. Tani, N. Ono, S. Okamoto, and F. Sato. *Chem. Commun.*, 386, 1993.

[79] D. Klomp, U. Hanefeld, and J. A. Peters. *Handbook of Homogeneous Hydrogenation*, volume 2. Wiley-VCH, Weinheim, 2007.

[80] H. Meerwein and R. Schmidt. *Justus Liebigs Ann. Chem.*, 444:221, 1925.

[81] A. Verley. *Bull. Soc. Chim. Fr.*, 37:537, 1925.

[82] W. Ponndorf. *Angew. Chem.*, 29:138, 1926.

[83] A. L. Wilds. *Org. React.*, 2:178, 1944.

[84] J. L. Namy, J. Souppe, J. Collin, and H. B. Kagan. *J. Org. Chem.*, 2045:178, 1984.

[85] J. W. Handgraaf, J. N. H. Reek, and E. V. Meijer. *Organometallics*, 22:3150, 2003.

[86] P. Gamez, F. Fache, and M. Lemaire. *Tetrahedron: Asymmetry*, 6:705, 1995.

[87] V. Guiral, F. Delbecq, and P. Sautet. *Organometallics*, 20:2207, 2001.

[88] L. Y. Kuo, D. M. Finigan, and N. N. Tandros. *Organometallics*, 22:2422, 2003.

[89] G. Mestroni, G. Zassinovich, A. Camus, and F. Martinelli. *J. Organomet. Chem.*, 198:87, 1980.

[90] C. Bianchini, E. Farnetti, M. Graziani, M. Peruzzini, and A. Polo. *Organometallics*, 12:3753, 1993.

[91] C. Bianchini, M. Peruzzini, E. Farnetti, J. Kaspar, and M. Graziani. *J. Organomet. Chem.*, 488:91, 1995.

[92] A. Aranyos, G. Csjernyik, K. J. Szabó, and J. E. Bäckvall. *Chem. Commun.*, 51, 1999.

[93] J. S. M. Samec, J. E. Bäckvall, P. G. Andersson, and P. Brandt. *Chem. Soc. Rev.*, 35:237, 2006.

[94] R. Noyori and S. Hashiguchi. *Acc. Chem. Res.*, 30:97, 1997.

[95] Y. Blum, D. Czarkie, Y. Rahamim, and Y. Shvo. *Organometallics*, 4:1459, 1985.

[96] Y. Shvo, D. Czarkie, and Y. Rahamim. *J. Am. Chem. Soc.*, 108:7400, 1986.

[97] R. Noyori and T. Ohkuma. *Angew. Chem. Int. Ed.*, 40:40, 2001.

[98] A. Fujii, S. Hashiguchi, N. Uematsu, T. Ikariya, and R. Noyori. *J. Am. Chem. Soc.*, 118:2521, 1996.

[99] N. Uematsu, A. Fujii, S. Hashiguchi, T. Ikariya, and R. Noyori. *J. Am. Chem. Soc.*, 118:4916, 1996.

[100] X. Wu, D. Vinci, T. Ikariya, and J. Xiao. *Chem. Commun.*, 4447, 2005.

[101] S. E. Clapham and R. H. Morris. *Organometallics*, 24:479, 2005.

[102] J. Takehara, S. Hashiguchi, A. Fujii, S. Inoue, T. Ikariya, and R. Noyori. *Chem. Commun.*, 233, 1996.

[103] S. Hashiguchi, A. Fujii, J. Takehara, T. Ikariya, and R. Noyori. *J. Am. Chem. Soc.*, 117:7562, 1995.

[104] M. Yamakawa, H. Ito, and R. Noyori. *J. Am. Chem. Soc.*, 122:1466, 2000.

[105] M. Yamakawa, I. Yamada, and R. Noyori. *Angew. Chem. Int. Ed.*, 40:2818, 2001.

[106] D. A. Alonso, P. Brandt, S. J. M. Nordin, and P. G. Andersson. *J. Am. Chem. Soc.*, 121:9580, 1999.

[107] K. Abdur-Rashid, S. E. Clapham, A. Hadzovic, J. N. Harvey, A. J. Lough, and R. H. Morris. *J. Am. Chem. Soc.*, 124:15104, 2002.

[108] D. Di Tommaso, S. A. French, and C. R. A. Catlow. *J. Mol. Struct.*, 812:39, 2007.

[109] S. A. French, D. Di Tommaso, A. Zanotti-Gerosa, F. Hancock, and C. R. A. Catlow. *Chem. Commun.*, 2381, 2007.

[110] D. Di Tommaso, S. A. French, A. Zanotti-Gerosa, F. Hancock, E. J. Palin, and C. R. A. Catlow. *Inorg. Chem.*, 47:2674, 2008.

[111] T. Leyssens, D. Peeters, and J. N. Harvey. *Organometallics*, 27:1514, 2008.

[112] C. P. Casey and J. B. Johnson. *J. Org. Chem.*, 68:1998, 2003.

[113] S. Bi, Q. Xie, X. Zhao, Y. Zhao, and X. Kong. *J. Organomet. Chem.*, 693:633, 2008.

[114] V. Guiral, F. Delbecq, and P. Sautet. *Organometallics*, 19:1589, 2000.

[115] C. S. Yi, Z. He, and I. A. Guzei. *Organometallics*, 20:3641, 2001.

[116] R. Karvembu, R. Prabhakaran, and K. Natarajan. *Coord. Chem. Rev.*, 249:911, 2005.

[117] N. Menashe, E. Salant, and Y. Shvo. *J. Organomet. Chem.*, 514:97, 1996.

[118] J. S. M. Samec and Bäckvall J. E. *Chem. Eur. J.*, 8:2955, 2002.

[119] Y. Shvo, I. Goldberg, D. Czierke, D. Reshef, and Z. Stein. *Organometallics*, 16:133, 1997.

[120] G. Csjernyk, A. H. Éll, L. Fadini, B. Pugin, and J. E. Bäckvall. *J. Org. Chem.*, 67:1657, 2002.

[121] J. S. M. Samec, A. H. Éll, and J. E. Bäckvall. *Chem. Eur. J.*, 11:2327, 2005.

[122] A. H. Éll, J. S. M. Samec, C. Brasse, and J. E. Bäckvall. *Chem. Commun.*, 1144, 2002.

[123] A. L. E. Larsson, B. A. Persson, and J. E. Bäckvall. *Angew. Chem. Int. Ed.*, 36:1211, 1997.

[124] B. A. Persson, A. L. E. Larsson, M. L. Ray, and J. E. Bäckvall. *J. Am. Chem. Soc.*, 121:1645, 1999.

[125] J. Paetzold and J. E. Bäckvall. *J. Am. Chem. Soc.*, 127:17620, 2005.

[126] C. P. Casey, S. W. Singer, D. R. Powell, R. K. Hayashi, and M. Kavana. *J. Am. Chem. Soc.*, 123:1090, 2001.

[127] J. B. Johnson and J. E. Bäckvall. *J. Org. Chem.*, 68:7681, 2003.

[128] C. P. Casey, G. A. Bikzhanova, Q. Cui, and I. A. Guzei. *J. Am. Chem. Soc.*, 127:14062, 2005.

[129] C. P. Casey, G. A. Bikzhanova, and I. A. Guzei. *J. Am. Chem. Soc.*, 128:2286, 2006.

[130] C. P. Casey and Johnson. J. B. *J. Am. Chem. Soc.*, 127:1883, 2005.

[131] J. S. M. Samec, A. H. Éll, and J. E. Bäckvall. *Chem. Commun.*, 2748, 2004.

[132] A. H. Éll, J. B. Johnson, and J. E. Bäckvall. *Chem. Commun.*, 1652, 2003.

[133] J. S. M. Samec, A. H. Éll, J. B. Åberg, T. Privalov, L. Eriksson, and J. E. Bäckvall. *J. Am. Chem. Soc.*, 128:14293, 2006.

[134] T. Privalov, J. S. M. Samec, and J. E. Bäckvall. *Organometallics*, 26:2840, 2007.

[135] K. Weissermel and H. J. Arpe. *Industrial Organic Chemistry.* Wiley, New York, 2003.

[136] R. A. Sheldon. *Chem. Commun.*, 3352, 2008.

[137] F. E. Kühn, A. M. Santos, and W. A. Herrmann. *J. Chem. Soc., Dalton Trans.*, 2483, 2005.

[138] C. Freund, M. Abrantes, and F. E. Kühn. *J. Organomet. Chem.*, 691:3718, 2006.

[139] F. E. Kühn, A. M. Santos, and M. Abrantes. *Chem. Rev.*, 106:2455, 2006.

[140] C. Freund, W. Herrmann, and F. E. Kühn. *Topics Organomet. Chem.*, 22:39, 2007.

[141] M. H. Dickman and M. T. Pope. *Chem. Rev.*, 94:569, 1994.

[142] N. Mizuno, K. Yamaguchi, and K. Kamata. *Coord. Chem. Rev.*, 249:1944, 2005.

[143] V. Nardello, J. M. Aubry, D. E. De Vos, R. Neumann, W. Adam, R. Zhang, J. E. Ten Elshof, Witte P. T., and P. L. Alsters. *J. Mol. Catal. A*, 251:185, 2006.

[144] J. M. Bregeault, M. Vennat, L. Salles, J. Y. Piquemal, Y. Mahha, E. Briot, P. C. Bakala, A. Atlamsani, and R. Thouvenot. *J. Mol. Catal. A*, 250:177, 2006.

[145] T. Katsuki. *Coord. Chem. Rev.*, 140:189, 1995.

[146] C. Dalton, K. M. Ryan, V. M. Wall, C. Bousquet, and D. G. Gilheany. *Topics Cat.*, 5:75, 1998.

[147] E. M. Mcgarrigle and D. G. Gilheany. *Chem. Rev.*, 105:1563, 2005.

[148] E. Rose, B. Andrioletti, S. Zrig, and M. Quelquejeu-Etheve. *Chem. Soc. Rev.*, 34:573, 2005.

[149] H. Mimoun, I. S. De Roch, and L. Sajus. *Tetrahedron*, 26:37, 1970.

[150] K. B. Sharpless, J. M. Townsend, and D. R. Williams. *J. Am. Chem. Soc.*, 94:295, 1972.

[151] C. Di Valentin, P. Gisdakis, I. V. Yudanov, and N. Rösch. *J. Org. Chem.*, 65:2996, 2000.

[152] D. V. Deubel, J. Sundermeyer, and Frenking G. *J. Am. Chem. Soc.*, 122:10101, 2000.

[153] D. V. Deubel, J. Sundermeyer, and G. Frenking. *Eur. J. Inorg. Chem.*, 1819, 2001.

[154] D. V. Deubel, Frenking G., P. Gisdakis, W. A. Herrmann, N. Rösch, and J. Sundermeyer. *Acc. Chem. Res.*, 37:645, 2004.

[155] D. V. Deubel. *J. Phys. Chem. A*, 105:4765, 2001.

[156] I. V. Yudanov, C. Di Valentin, P. Gisdakis, and N. Rösch. *J. Mol. Chem. A*, 158:189, 2000.

[157] P. Gisdakis, I. V. Yudanov, and N. Rösch. *Inorg. Chem.*, 40:3755, 2001.

[158] M. Bühl, R. Schurhammer, and P. Imhof. *J. Am. Chem. Soc.*, 126:3310, 2004.

[159] L. Salles, J. Y. Piquemal, R. Thouvenot, C. Minot, and J. M. Bregeault. *J. Mol. Catal. A*, 117:375, 1997.

[160] P. Gisdakis, S. Antonczak, S. Köstlmeier, W. A. Herrmann, and N. Rösch. *Angew. Chem. Int. Ed.*, 37:2211, 1998.

[161] D. V. Deubel, J. Sundermeyer, and G. Frenking. *Org. Lett.*, 3:329, 2001.

[162] W. R. Thiel and T. Priermeier. *Angew. Chem. Int. Ed.*, 34:1737, 1995.

[163] W. R. Thiel. *J. Mol. Catal. A*, 117:449, 1997.

[164] W. R. Thiel and J. Eppinger. *Chem. Eur. J.*, 3:696, 1997.

[165] J. W. Schwesinger and T. Bauer. *Stereoselective synthesis.* Houbel Weil Thieme, 1995.

[166] W. A. Herrmann, R. W. Fischer, and D. W. Marz. *Angew. Chem. Int. Ed.*, 30:1638, 1991.

[167] W. A. Herrmann and F. E. Kühn. *Acc. Chem. Res.*, 30:169, 1997.

[168] G. Wahl, D. Kleinhenz, A. Schorm, J. Sundermeyer, R. Stowasser, C. Rummey, G. Bringmann, C. Fickert, and W. Kiefer. *Chem. Eur. J.*, 1999.

[169] J. Smidt, W. Hafner, R. Jira, J. Sedlmeier, R. Sieber, R. Ruttinger, and H. Kojer. *Angew. Chem. Int. Ed.*, 71:176, 1959.

[170] J. Smidt, J. Sedlmeier, W. Hafner, R. Sieber, A. Sabel, and R. Jira. *Angew. Chem. Int. Ed.*, 74:93, 1962.

[171] P. M. Henry. *J. Am. Chem. Soc.*, 86:3246, 1964.

[172] J. K. Stille and D. E. James. *J. Organometallic Chemistry*, 108:401, 1976.

[173] M. Kosaki, M. Isemura, Y. Kitaura, S. Shinoda, and Y. Saito. *J. Mol. Catal.*, 2:351, 1977.

[174] J. E. Backvall, B. Akermark, and S. O. Ljunggreen. *J. Am. Chem. Soc.*, 101:2411, 1979.

[175] J. K. Stille and R. Divakaruni. *J. Organometallic Chemistry*, 169:239, 1979.

[176] O. Hamed, C. Thompson, and P. M. Henry. *J. Org. Chem.*, 62:7082, 1997.

[177] N. Gregor, K. Zaw, and P. M. Henry. *Organometallics*, 3:1251, 1984.

[178] J. W. Francis and P. M. Henry. *J. Mol. Catal. A*, 112:317, 1996.

[179] O. Eisenstein and R. Hoffmann. *J. Am. Chem. Soc.*, 103:4308, 1981.

[180] H. Fujimoto and T. Yamasaki. *J. Am. Chem. Soc.*, 108:578, 1986.

[181] J. A. Keith, R. J. Nielsen, J. Oxgaard, and W. A. Goddard III. *J. Am. Chem. Soc.*, 129:12342, 2007.

[182] P. E. M. Siegbahn. *Struct. Chem.*, 6:271, 1995.

[183] P. E. M. Siegbahn. *J. Am. Chem. Soc.*, 117:5409, 1995.

[184] P. E. M. Siegbahn. *J. Phys. Chem.*, 100:14672, 1996.

[185] S. A. Beyramabadi, H. Eshtiagh-Hosseini, M. R. Housaindokht, and A. Morsali. *Organometallics*, 27:72, 2008.

[186] C. N. Cornell and M. S. Sigman. *J. Am. Chem. Soc.*, 127:2796, 2005.

[187] J. A. Keith, J. Oxgaard, and W. A. Goddard III. *J. Am. Chem. Soc.*, 128:3132, 2006.

[188] D. J. Nelson, R. B. Li, and C. Brammer. *J. Am. Chem. Soc.*, 123:1564, 2001.

[189] J. Tsuji. *New J. Chem.*, 24:127, 2000.

[190] K. Morokuma and D. G. Musaev, editors. *Computational Modeling for Homogeneous and Enzymatic Catalysis: A Knowledge-Base for Designing Efficient Catalysis*. Wiley-VCH, Weinheim, 2008.

[191] M. Born and J. R. Oppenheimer. *Ann. Physik*, 84:457, 1927.

[192] A. A. C. Braga, G. Ujaque, and F. Maseras. *Organometallics*, 25:3647, 2006.

[193] M. Sumimoto, N. Iwane, T. Takahama, and S. Sakaki. *J. Am. Chem. Soc.*, 126:10457, 2004.

[194] H. Tamura, H. Yamasaki, H. Sato, and S. Sakaki. *J. Am. Chem. Soc.*, 125:16114, 2003.

[195] S. Sakaki, T. Takayama, M. Sumimoto, and M. Sugimoto. *J. Am. Chem. Soc.*, 126:3332, 2004.

[196] A. Stirling, M. Iannuzzi, M. Parrinello, F. Molnar, V. Bernhart, and G. A. Luinstra. *Organometallics*, 24:2533, 2005.

[197] C. Michel, A. Laio, F. Mohamed, M. Krack, M. Parrinello, and A. Milet. *Organometallics*, 26:1241, 2007.

[198] A. Magistrato, A. Togni, U. Rothlisberger, and T. K. Woo. *Computational Modeling of Homogeneous Catalysis*. Kluwer Academic Publishers, Dordrecht, 2002.

[199] A. Szabo and N. S. Ostlund. *Modern Quantum Chemistry: Introduction to Advanced Electronic Structure Theory*. Dover Publications, Inc., Mineola, New York, 1996.

[200] P. Hohenberg and W. Kohn. *Phys. Rev. B*, 136, 1964.

[201] W. Kohn and L. J. Sham. *Phys. Rev. A*, 140:1133, 1965.

[202] W. Koch and M. C. Holthausen. *A Chemist's Guide to Density Functional Theory*. Wiley-VCH, Weinheim, 2000.

[203] T. Ziegler. *Chem. Rev.*, 91:651, 1991.

[204] A. D. Boese, N. L. Doltsinis, N. C. Handy, and M. Sprik. *J. Chem. Phys.*, 112:1670, 2000.

[205] S. Izvekov and G. A. Votha. *J. Chem. Phys.*, 123:44505, 2005.

[206] A. D. Becke. *J. Chem. Phys.*, 98:5648, 1993.

[207] C. T. Lee, W. T. Yang, and R. G. Parr. *Phys. Rev. B*, 37:785, 1988.

[208] P. J. Stephens, F. J. Devlin, C. F. Chabalowski, and M. J. Frisch. *J. Phys. Chem.*, 98:11623, 1994.

[209] S. F. Sousa, P. A. Fernandes, and M. J. Ramos. *J. Phys. Chem. A*, 111:10439, 2007.

[210] J. Tomasi. *Chem. Rev.*, 94:2027, 1994.

[211] V. Barone and M. Cossi. *J. Phys. Chem. A*, 102:1995, 1998.

[212] M. Cossi, N. Rega, G. Scalmani, and V. Barone. *J. Comput. Chem.*, 24:669, 2003.

[213] R. Car and M. Parrinello. *Phys. Rev. Lett.*, 55:2471, 1985.

[214] A. Laio and M. Parrinello. *Proc. Natl. Acad. Sci. U.S.A.*, 99:12562, 2002.

[215] M. Iannuzzi, A. Laio, and M. Parrinello. *Phys. Rev. Lett.*, 90:23802, 2003.

[216] B. Ensing, A. Laio, M. Parrinello, and M. L. Klein. *J. Phys. Chem. B*, 109:6676, 2005.

[217] A. Laio, A. Rodríguez-Fortea, F. Luigi Gervasio, M. Ceccarelli, and M. Parrinello. *J. Phys. Chem. B*, 109:6714, 2005.

[218] C. P. Casey, J. B. Johnson, S. W. Singer, and Q. Cui. *J. Am. Chem. Soc.*, 127:3100, 2005.

[219] C. P. Casey, T. B. Clark, and I. A. Guzei. *J. Am. Chem. Soc.*, 129:11821, 2007.

[220] C. P. Casey, S. W. Singer, and D. R. Powell. *Can. J. Chem.*, 79:1002, 2001.

[221] L. F. Veiros. *Organometallics*, 19:5549, 2000.

[222] A. Habib, R. S. Tanke, E. M. Holt, and R. H. Crabtree. *Organometallics*, 8:225, 1989.

[223] H. J. Fan and M. B. Hall. *Organometallics*, 20:5724, 2001.

[224] C. P. Casey and J. B. Johnson. *Can. J. Chem.*, 83:1339, 2005.

[225] D. J. Gorin, B. D. Sherry, and F. D. Toste. *Chem. Rev.*, 108:3351, 2008.

[226] A. S. K. Hashmi and M. Rudolph. *Chem. Soc. Rev.*, 37:1766, 2008.

[227] Z. Li, C. Brouwer, and C. He. *Chem. Rev.*, 108:3239, 2008.

[228] A. Arcadi. *Chem. Rev.*, 108:3266, 2008.

[229] E. Jimenez-Nuñez and A. M. Echavarren. *Chem. Rev.*, 108:3326, 2008.

[230] J. Zhang, C. G. Yang, and C. He. *J. Am. Chem. Soc.*, 128:1798, 2006.

[231] M. R. Fructos, T. L. Beldarrain, P. de Fremont, N. M. Scott, S. P. Nolan, M. M. Diaz-Requejo, and P. J. Pérez. *Angew. Chem. Int. Ed.*, 44:5284, 2005.

[232] C. González-Arellano, A Corma, M. Iglesias, and F. Sánchez. *J. Catal.*, 238:497, 2006.

[233] C. González-Arellano, A Corma, M. Iglesias, and F. Sánchez. *Chem. Commun.*, 3451, 2005.

[234] X. Giner and C. Nájera. *Org. Lett.*, 10:2919, 2008.

[235] S. Antoniotti, E. Genin, V. Michelet, and J. P. Genêt. *J. Am. Chem. Soc.*, 127:9976, 2005.

[236] P. Pykkö. *Angew. Chem. Int. Ed.*, 43:4412, 2004.

[237] P. Pykkö. *Inorg. Chim. Acta*, 358:4113, 2005.

[238] D. J. Gorin and D. Toste. *Nature*, 446:395, 2007.

[239] A. Fürstner and P. W. Davies. *Angew. Chem. Int. Ed.*, 46:3410, 2007.

[240] G. Kóvacs, G. Ujaque, and A. Lledós. *J. Am. Chem. Soc.*, 130:853, 2008.

[241] C. Nieto-Oberhuber, S. López, M. P. Muñoz, D. J. Cárdenas, E. Buñuel, C. Nevado, and A. M. Echavarren. *Angew. Chem. Int. Ed.*, 44:6146, 2005.

[242] O. N. Faza, C. S. López, R. Álvarez, and A. R. de Lera. *J. Am. Chem. Soc.*, 128:2434, 2006.

[243] B. Trillo, F. López, S. Montserrat, G. Ujaque, L. Castedo, A. Lledós, and J. L. Mascareñas. *Chem. Eur. J.*, 15:3336, 2009.

[244] V. Gandon, G. Lemière, A. Hours, L. Fensterbank, and M. Malacria. *Angew. Chem. Int. Ed.*, 47:7534, 2008.

[245] A. Correa, N. Marion, L. Fensterbank, M. Malacria, S. P. Nolan, and L. Cavallo. *Angew. Chem. Int. Ed.*, 47:718, 2008.

[246] G. Lemière, V. Gandon, N. Agenet, J. P. Goddard, A. de Kozak, C. Aubert, L. Fensterbank, and M. Malacria. *Angew. Chem. Int. Ed.*, 45:7596, 2006.

[247] J. H. Groen, A. D. Zwart, M. J. M. Vlaar, J. M. Ernsting, P. W. N. van Leeuwen, K. Vrieze, H. Kooijman, W. J. J. Smeets, A. L. Spek, P. H. M. Budselaar, Q. Xiang, and R. P. Thummel. *Eur. J. Inorg. Chem.*, 1129, 1998.

[248] P. Pelagatti, A. Venturini, A. Leporati, M. Carcelli, M. Costa, A. Bacchi, G. Pelizzi, and C. J. Pelizzi. *Chem. Soc. Dalton Trans.*, 16:2715, 1998.

[249] G. Henrici-Olivé and S. Olivé. *Angew. Chem. Int. Ed.*, 13:549, 1974.

[250] G. Henrici-Olivé and S. Olivé. *J. Mol. Catal.*, 1:121, 1975/6.

[251] D. R. Armstrong, O. Novaro, M. E. Ruiz-Vizcaya, and R. Linarte. *J. Catal.*, 48:8, 1977.

[252] D. G. Musaev, R. D. J. Froese, M. Svensson, and K. Morokuma. *J. Am. Chem. Soc.*, 119:367, 1997.

[253] I. Demachy, M. A. Esteruelas, Y. Jean, A. Lledós, F. Maseras, L. A. Oro, C. Valero, and F. Volatron. *J. Am. Chem. Soc.*, 118:8388, 1996.

[254] D. J. Thorn and R. Hoffmann. *J. Am. Chem. Soc.*, 100:2079, 1978.

[255] P. M. Reis, C. C. Romão, and B. Royo. *Dalton Trans.*, 1842, 2006.

[256] M. Abrantes, A. Santos, J. Mink, F. Kühn, and C. C. Romão. *Organometallics*, 22:2112, 2003.

[257] J. Zhao, A. M. Santos, E. Herdtweck, and F. E. Kühn. *J. Mol. Catal. A*, 222:265, 2004.

[258] A. M. Martins, C. C. Romão, M. Abrantes, M. C. Azevedo, Cui. J., A. R. Dias, M. T. Duarte, M. A. Lemos, T. Lourenço, and R. Poli. *Organometallics*, 24:2582, 2005.

[259] J. Zhao, E. Herdtweck, and F. E. Kühn. *J. Organomet. Chem.*, 691:2199, 2006.

[260] R. Poli. *Chem. Eur. J.*, 10:332, 2004.

[261] E. Collange, J. Garcia, and R. Poli. *New J. Chem.*, 26:1249, 2002.

[262] F. E. Kühn, M. Groarke, E. Bencze, E. Herdtweck, A. Prazeres, A. M. Santos, M. J. Calhorda, C. C. Romão, I. S. Gonçalves, A. D. Lopes, and M. Pillinger. *Chem. Eur. J.*, 8:2370, 2002.

[263] M. B. Trost and R. G. Bergman. *Organometallics*, 10:1172, 1991.

[264] L. F. Veiros, A. Prazeres, P. J. Costa, C. C. Romão, F. E. Kühn, and M. J. Calhorda. *Dalton Trans.*, 1383, 2006.

[265] A. Lledós and J. Beltrán. *Tetrahedron Lett.*, 22, 1981.

[266] O. N. Ventura, A. Lledós, R. Bonaccorsi, J. Beltrán, and J. Tomasi. *Theor. Chim. Acta*, 72:175, 1987.

[267] M. C. P. Lima, K. Coutinho, S. Canuto, and W. R. Rochta. *J. Phys. Chem.*, 110:7253, 2006.

[268] J. R. Sambrano, J. Andres, L. Gracia, V. S. Safont, and A. Beltrán. *Chem. Phys. Lett.*, 384:56, 2004.

[269] H. P. Hratchian, J. L. Sonnenberg, P. J. Hay, R. L. Martin, B. E. Bursten, and H. B. Schlegel. *J. Phys. Chem. A*, 109:8579, 2005.

[270] C. Bergquist, B. M. Bridgewater, C. J. Harlan, J. R. Norton, R. A. Friesner, and G. Parkin. *J. Am. Chem. Soc.*, 122:10581, 2000.

[271] R. Prabhakar, M. R. A. Blomberg, and P. E. M. Siegbahn. *Theor. Chem. Acc.*, 104:461, 2000.

[272] I. Tuñón, E. Silla, and J. Beltrán. *J. Phys. Chem.*, 97:5547, 1993.

[273] D. Wei and D. R. Salahub. *J. Chem. Phys.*, 101:7633, 1994.

[274] D. Marx, M. E. Tuckerman, J. Hutter, and M. Parrinello. *Nature*, 397:601, 1999.

[275] U. W. Schmitt and G. A. Voth. *J. Chem. Phys.*, 111:9361, 1999.

[276] B. Lane and K. Burgess. *Chem. Rev.*, 103:2457, 2003.

[277] D. V. Deubel, J. Sundermeyer, and G. Frenking. *J. Am. Chem. Soc.*, 122:10101, 2000.

[278] D. V. Deubel, J. Sundermeyer, and G. Frenking. *Inorg. Chem.*, 39:2314, 2000.

[279] D. V. Deubel. *J. Phys. Chem. A*, 105:4765, 2001.

[280] P. Gisdakis, I. V. Yudanov, and N. Rösch. *Inorg. Chem.*, 40:3755, 2001.

[281] O. Hamed, P. M. Henry, and C. Thompson. *J. Org. Chem.*, 64:7745, 1999.

[282] J. W. Francis and P. M. Henry. *Organometallics*, 11:2832, 1992.

[283] J. A. Keith, R. J. Nielsen, J. Oxgaard, W. A. Goddard, and P. M. Henry. *Organometallics*, 28:1618, 2009.

Part V

Publicacions

Capítol 9

Article I

Article

Hydrogen Transfer to Ketones Catalyzed by Shvo's Ruthenium Hydride Complex: A Mechanistic Insight

Aleix Comas-Vives, Gregori Ujaque, and Agust Lledós

Organometallics, **2007**, 26 (17), 4135-4144 • DOI: 10.1021/om7004832 • Publication Date (Web): 12 July 2007

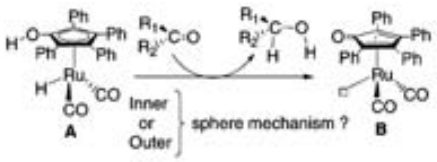

Organometallics **2007,** *26,* 4135−4144

Hydrogen Transfer to Ketones Catalyzed by Shvo's Ruthenium Hydride Complex: A Mechanistic Insight

Aleix Comas-Vives, Gregori Ujaque,* and Agusti Lledós*

Unitat de Química Física, Departament de Química, Edifici Cn, Universitat Autònoma de Barcelona, 08193 Bellaterra, Catalonia, Spain

Received May 15, 2007

The Shvo catalyst is one of the most prominent examples of a hydrogen-transfer catalyst successfully applied in a broad scope of hydrogen-transfer processes. The reaction takes place by transferring a hydride (bonded to the metal center) and a proton (bonded to a ligand) to a double bond. The reaction mechanism for the hydrogen-transfer process, however, is a matter of controversy. Experimental studies by means of primary deuterium isotope effects on the hydrogenation of ketones via the active reducing form of the Shvo catalyst by the Casey and Bäckvall groups concluded that carbonyl hydrogenation is concerted. Nevertheless, it is not clear whether the reaction goes through an outer-sphere mechanism (without substrate coordination) or through an inner-sphere mechanism (with substrate coordination). In the present work several inner- and outer-sphere mechanisms are explored by means of theoretical methods. Energy reaction profiles clearly support the outer-sphere mechanism. Theoretically combined KIEs also suggests the concerted outer-sphere mechanism for this reaction. Some interesting features on the behavior of the Ru complex were found during the mechanistic investigations.

Introduction

The homogeneous hydrogenation of polar double bonds is one of the most useful reactions in organic synthesis.[1] Among the methodologies developed, hydrogen-transfer reactions have gained a prominent position in recent years.[2] They offer a viable alternative to the conventional hydrogenation using hydrogen gas due to its simplicity and the favorable properties of the reductant (generally alcohols) as environmentally friendly and also easy to handle.

The hydrogen transfer to ketones (or aldehydes) reactions are generally described by three general pathways. The "direct hydrogen transfer" is thought to work for main group elements, with no implication of a metal hydride intermediate. The "hydridic route", however, works for most transition metal catalysts, involving the participation of a metal hydride intermediate in the hydrogen-transfer process. The metal−ligand bifunctional catalysts, a concept developed to describe a type of hydrogenation catalysts where the metal has a hydridic hydrogen and a ligand an acidic hydrogen, operate through the hydridic route.[3] Recently, the so-called "ionic mechanism" has been also proposed for some transition-metal-catalyzed hydrogenations.[4]

Hydrogen transfer to ketones following the "hydridic route", and more specifically for catalysts that are monohydride complexes, has been suggested to go through two different pathways, "inner-sphere" and "outer-sphere" hydrogen-transfer mechanisms.[2b,e] In both mechanisms the hydride migrates to the carbonylic carbon atom. Nevertheless, whereas in the inner-sphere mechanism it is supposed that a metal alkoxide intermediate is formed (therefore, the substrate must become coordinated to the catalyst), in the outer-sphere mechanism the hydrogen transfer may proceed in a concerted manner (without the coordination of the substrate to the catalyst).

One of the most prominent examples of a hydrogen-transfer catalysts corresponds to the Shvo catalyst, $\{[Ph_4(\eta^4\text{-}C_4CO)]_2H\}\text{-}Ru_2(CO)_4H$ (**1**).[5] It has been applied successfully in a broad scope of hydrogen-transfer processes[5,6] such as hydrogenation of alkynes,[7] carbonyls,[8] and imines,[9] oxidation of alcohols[10] and amines,[11] and dynamic kinetic resolution of secondary alcohols[12] and primary amines[13] in combination with lipases. The Shvo

* Corresponding authors. E-mail: gregori@klingon.uab.es; agusti@klingon.uab.es.

(1) Clarke, M. L.; Roff, G. J. In *Handbook of Homogeneous Hydrogenation*; de Vries, J. G., Elsevier, C. J., Eds.; Wiley-VCH: Weinheim, 2007; Vol. 1, p 413.

(2) For reviews see: (a) Gladiali, S.; Alberico, E. *Chem. Soc. Rev.* **2006**, *35*, 226−236. (b) Samec, J. S. M.; Bäckvall, J.-E.; Andersson, P. G.; Brant, P. *Chem. Soc. Rev.* **2006**, *35*, 237−248. (c) Clapham, S. E.; Hadzovic, A.; Morris, R. H. *Coord. Chem. Rev.* **2004**, *248*, 2201−2237. (d) Bäckvall, J.-E. *J. Organomet. Chem.* **2002**, *652*, 105−111. (e) Noyori, R.; Hashiguchi, R. *Acc. Chem. Res.* **1997**, *30*, 97−102. (f) Zassinovich, G.; Mestroni, G.; Gladiali, S. *Chem. Rev.* **1992**, *92*, 1051−1069.

(3) (a) Noyori, R.; Ohkuma, T. *Angew. Chem.* **2001**, *113*, 40−75; *Angew. Chem., Int. Ed.* **2001**, *40*, 40−73. (b) Sandoval, C. A.; Ohkuma, T.; Muñiz, K.; Noyori, R. *J. Am. Chem. Soc.* **2003**, *125*, 13490−13503. (c) Fujii, A.; Hashiguchi, S.; Uematsu, N.; Ikariya, T.; Noyori, R. *J. Am. Chem. Soc.* **1996**, *118*, 2521−2522. (d) Uematsu, N.; Fujii, A.; Hashiguchi, S.; Ikariya, T.; Noyori, R. *J. Am. Chem. Soc.* **1996**, *118*, 4916−4917.

(4) (a) Bullock, R. M. *Chem.−Eur. J.* **2004**, *10*, 2366−2374. (b) Guan, H.; Iimura, M.; Magee, M. P.; Norton, J. R.; Zhu, G. *J. Am. Chem. Soc.* **2005**, *127*, 7805−7814.

(5) (a) Blum, Y.; Czarkie, D.; Rahamim, Y.; Shvo, Y. *Organometallics* **1985**, *4*, 1459−1461. (b) Shvo, Y.; Czarkie, D.; Rahamim, Y. *J. Am. Chem. Soc.* **1986**, *108*, 7400−7402.

(6) Karvembu, R.; Prabhakaran, R.; Natarajan, K. *Coord. Chem. Rev.* **2005**, *249*, 911−918.

(7) Shvo, Y.; Goldberg, I.; Czerkie, D.; Reshef, D.; Stein, Z. *Organometallics* **1997**, *16*, 133−138.

(8) Menashe, N.; Salant, E.; Shvo, Y. *J. Organomet. Chem.* **1996**, *514*, 97−102.

(9) Samec, J. S. M.; Bäckvall, J.-E. *Chem.−Eur. J.* **2002**, *8*, 2955−2961.

(10) Csjernyk, G.; Éll, A. H.; Fadini, L.; Pugin, B.; Bäckvall, J.-E. *J. Org. Chem.* **2002**, *67*, 1657−1662.

(11) (a) Samec, J. S. M.; Éll, A. H.; Bäckvall, J.-E. *Chem.−Eur. J.* **2005**, *11*, 2327−2334. (b) Éll, A. H.; Samec, J. S. M.; Brasse, C.; Bäckvall, J.-E. *Chem. Commun.* **2002**, 1144−1145.

(12) (a) Larsson, A. L. E.; Persson, B. A.; Bäckvall, J.-E. *Angew. Chem.* **1997**, *109*, 1256−1258; *Angew. Chem., Int. Ed.* **1997**, *36*, 1211−1212. (b) Persson, B. A.; Larsson, A. L. E.; Ray, M. L.; Bäckvall, J.-E. *J. Am. Chem. Soc.* **1999**, *121*, 1645−1650.

10.1021/om7004832 CCC: $37.00
Publication on Web 07/12/2007

Scheme 1. Equilibrium between Precursor and Active Species of the Shvo Catalyst

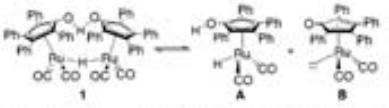

Scheme 2. Proposed Mechanisms for the Carbonyl Hydrogenation by Means of the Shvo Catalyst

catalyst, synthesized two decades ago, is probably the first developed catalyst belonging to the so-called metal−ligand bifunctional catalysts. Since then, a number of metal−ligand bifunctional catalysts have been prepared based on Ru,[1,2,14] such as those by Noyori, Ru(diamine)(BINAP) and the Ru(η^6-arene)-TsDPEN,[3] and on other metal centers such as Rh, Ir, and Os.[15]

The Shvo catalyst under heating produces two active species, **A** and **B** (Scheme 1), which are able to hydrogenate unsaturated substrates or dehydrogenate saturated substrates, respectively. This equilibrium is what made the Shvo catalyst so versatile in hydrogen-transfer processes. In addition, the hydrogenation process starting from **A** generates **B**, and this one can be hydrogenated by alcohols or by H_2. In this last process, the explicit participation of a polar protic solvent molecule (EtOH) is playing a critical role in activating the hydrogen molecule.[16] This effect has also been reported in other systems.[3b,14b,17−19]

The reaction mechanism for the hydrogen-transfer process, however, is a matter of controversy. Studies by Casey by means of primary deuterium isotope effects on the hydrogenation of PhCHO via the active reducing form (**A**) of the Shvo tolyl analogue catalyst, [2,5-Ph_2-3,4-Tol_2(η^5-C_4COH)]Ru(CO)$_2$H, concluded that carbonyl hydrogenation is concerted without substrate coordination (outer-sphere mechanism, Scheme 2);[20] this conclusion was also supported by DFT calculations performed by the same authors.[21] Bäckvall, using a similar methodology, also reported a concerted mechanism for alcohol dehydrogenation using species **B**.[22] Nevertheless, although there is agreement in that catalytic reaction using the Shvo catalyst is concerted, Bäckvall suggested that the substrate coordinates the metal via a $\eta^5 \rightarrow \eta^3$ ring slippage[22,23] of the aromatic ligand, followed by a simultaneous β-hydride addition and a proton transfer to the unsatured organic substrate (inner-sphere mechanism, Scheme 2).

In imine hydrogenation there is also a similar mechanistic debate,[24−26] and although trapping experiments have provided additional information, they again have led to opposite conclusions concerning the mechanism.[21,26] In ketone hydrogenation this approach is not possible because of the high lability of alcohol complexes.[27] In related systems such as the Ru(η^6-arene)TsDPEN and the Ru(η^6-arene)(amino alcohol) catalysts, Noyori, Casey, and Andersson have provided evidence, both experimentally and theoretically, that carbonyl hydrogenation takes place by an outer-sphere mechanism via a six-membered transition state.[28]

In the present work we performed an extensive theoretical analysis on both the inner- and outer-sphere mechanisms, trying to clarify the mechanism of this useful reaction. For the inner-sphere mechanism, in addition to the concerted pathway two additional pathways involving the substrate coordination were also evaluated. For the outer-sphere mechanism, a concerted reaction without substrate coordination was examined in detail.

Computational Details

An extensive mechanistic analysis was performed on a model reaction system. Formaldehyde was selected as a substrate, whereas the Shvo catalyst was modeled by [(η^5-C_4H_4COH)Ru(CO)$_2$H]; the phenyl substituents of the aromatic ligand, hereafter named CpOH, were replaced by hydrogens. These four H's were calculated using the 6-31G basis set, and the other main group elements (C, O, the rest of H) were calculated using the 6-31G(d,p) basis set. The effective core potential LANL2DZ[29] along with its associated basis set was employed for Ru.

Calculations for the model system were carried out using the program package Gaussian03[30] at density functional theory (DFT) level by means of the hybrid B3LYP functional.[31] All the calculations were done without any geometrical constraints. Ad-

(13) Paetzold, J.; Bäckvall, J.-E. *J. Am. Chem. Soc.* **2005**, *127*, 17620−17621.

(14) (a) Gómez, M.; Jansat, S.; Muller, G.; Aullón, G.; Maestro, M. A. *Eur. J. Inorg. Chem.* **2005**, 4341−4351. (b) Ito, M.; Hirakawa, M.; Murata, K.; Ikariya, T. *Organometallics* **2001**, *20*, 379−381. (c) Abdur-Rashid, K.; Clapham, S. E.; Hadzovic, A.; Harvey, J. N.; Lough, A. J.; Morris, R. H. *J. Am. Chem. Soc.* **2002**, *124*, 15104−15118.

(15) (a) Wu, X.; Vinci, D.; Ikariya, T.; Xiao, J. *Chem. Commun.* **2005**, 4447−4449. (b) Clapham, S. E.; Morris, R. H. *Organometallics*, **2005**, *24*, 479−481. (c) Mao, J.; Baker, D. C. *Org. Lett.* **1999**, *1*, 841−843. (d) Martin, M.; Sola, E.; Tejero, S.; Andres, J. L.; Oro, L. A *Chem.−Eur. J.* **2006**, *12*, 4043−4056.

(16) Casey, C. P.; Johnson, J. B.; Singer, S. W.; Cui, Q. *J. Am. Chem. Soc.* **2005**, *127*, 3100−3109.

(17) Rautenstrauch, V.; Hoang-Cong, X.; Churland, R.; Abdur-Rashid, K.; Morris, R. H. *Chem.−Eur. J.* **2003**, *9*, 4954−4967.

(18) Hedberg, C.; Källström, K.; Arvidsson, P. I.; Brandt, P.; Andersson, P. G. *J. Am. Chem. Soc.* **2005**, *127*, 15083−15090.

(19) Comas-Vives, A.; González-Arellano, C.; Corma, A.; Iglesias, M.; Sánchez, F.; Ujaque, G. *J. Am. Chem. Soc.* **2006**, *128*, 4756−4765.

(20) Casey, C. P.; Singer, S. W.; Powell, D. R.; Hayashi, R. K.; Kavana, M. *J. Am. Chem. Soc.* **2001**, *123*, 1090−1100.

(21) Casey, C. P.; Bikzhanova, G. A.; Cui, Q.; Guzei, I. A. *J. Am. Chem. Soc.* **2005**, *127*, 14062−14071 (see also Supporting Information therein).

(22) Johnson, J. B.; Bäckvall, J.-E. *J. Org. Chem.* **2003**, *68*, 7681−7684.

(23) (a) Csjernyik, G.; Éll, A. H.; Fadini, L.; Pugin, B.; Bäckvall, J.-E. *J. Org. Chem.* **2002**, *67*, 1657−1662. (b) In ref 7 Shvo proposed the same ring slippage for alkyne hydrogenation.

(24) (a) Casey, C. P.; Bikzhanova, G. A.; Guzei, I. A. *J. Am. Chem. Soc.* **2006**, *128*, 2286−2293. (b) Casey, C. P.; Johnson, J. B. *J. Am. Chem. Soc.* **2005**, *127*, 1883−1894.

(25) (a) Samec, J. S. M.; Éll, A. H.; Bäckvall, J.-E. *Chem. Commun.* **2004**, 2748−2749. (b) Éll, A. H.; Johnson, J. B.; Bäckvall, J.-E. *Chem. Commun.* **2003**, 1652−1653.

(26) Samec, J. S. M.; Éll, A. H.; Åberg, J. B.; Privalov, T.; Eriksson, L.; Bäckvall, J.-E. *J. Am. Chem. Soc.* **2006**, *128*, 14293−14305.

(27) Casey, C. P.; Bikzhanova, G. A.; Bäckvall, J.-E.; Johansson, L.; Park, J.; Kim, Y. H. *Organometallics* **2002**, *21*, 1955−1959.

(28) (a) Yamakawa, M.; Ito, H.; Noyori, R. *J. Am. Chem. Soc.* **2000**, *122*, 1466−1478. (b) Casey, C. P.; Johnson, J. B. *J. Org. Chem.* **2003**, *68*, 1998−2001. (c) Alonso, D. A.; Brandt, P.; Nordin, S. J. M.; Andersson, P. G. *J. Am. Chem. Soc.* **1999**, *121*, 9580−9588.

(29) Hay, P. J.; Wadt, W. R. *J. Chem. Phys.* **1985**, *82*, 270−283.

(30) Frisch, M. J.; et al. *Gaussian03*; Gaussian, Inc.: Wallingford, CT, 2004.

(31) (a) Becke, A. D. *J. Chem. Phys.* **1993**, *98*, 5648−5652. (b) Lee, C.; Yang, W.; Parr, R. G. *Phys. Rev. B* **1988**, *37*, 785−789. (c) Stephens, P. J.; Devlin, F. J.; Chabalowski, C. F.; Frisch, M. J. *J. Phys. Chem.* **1994**, *98*, 11623−11627.

ditional MP2[32] and CCSD(T)[33] single-point energy calculations were also performed (see Supporting Information).

The most energetically favorable inner- and outer-sphere mechanisms were evaluated using a complete Shvo catalyst (including the [$Ph_4(\eta^5$-$C_4COH)$] ligand) by means of the Jaguar program suite.[34] The 6-31G(d,p) basis set was used for all the atoms except for Ru. For the latter, the Los Alamos relativistic ECP was used, together with a Jaguar-developed triple-ζ modification of the standard Los Alamos basis set to describe the outermost core and valence 4s, 4p, 4d, and 5s electrons (LACV3P basis).

For the saddle points the existence of only one imaginary frequency was checked by means of analytical frequency calculations. Polarization functions were added to hydrogens of the phenyl rings: 6-31G(d,p). Solvent effects (THF) were included using the CPCM[35] model performing single-point calculations on gas-phase optimized geometries. KIEs were also evaluated as shown in eqs 1 and 2 using the calculated free energies at 298.15 K. The concerted pathway for the complete system was optimized with Gaussian, along with the frequency analysis.

$$\Delta G_X = G_{TS} - G_R \qquad X = H, D \tag{1}$$

$$KIE = k_H/k_D = \exp[(\Delta G_D - \Delta G_H)/RT] \tag{2}$$

Results and Discussion

This section is divided in two subsections. In the first one, three different inner-sphere mechanisms are discussed. Two of them start with an initial coordination of the substrate (formaldehyde) to the catalyst, whereas in the last one the coordination is simultaneous to the hydrogen transfer. In the second subsection a concerted pathway for the outer-sphere mechanism is discussed.

Inner-Sphere Mechanisms. In this section three inner-sphere mechanisms are analyzed. Two of them involve the replacement of one of the occupied coordination sites of the metal center by the substrate. The first one involves the replacement of one CO, whereas the second one consists on the ring slippage of the aromatic ring to accommodate the substrate. In the third one, the incorporation of the substrate to the coordination sphere is simultaneous to the hydrogen transfer.

Substrate Coordination by Replacing the CO Ligand. The initial reactants and final products shown in Figure 1 are the same for all the studied mechanisms. Two rotamers have been localized for the active reducing species of the Shvo catalyst, **a1** and **a2**. These two conformers differ energetically only by 0.2 kcal/mol, indicating that the different rotamers are equally accessible. Once the hydrogenation occurs, the dehydrogenated form of the catalyst (**b**) and the hydrogenated product, methanol, are produced. Reactants and products are isoenergetic in the gas phase, and when solvent effects are taken into account, the reaction energy is −3.5 kcal/mol.

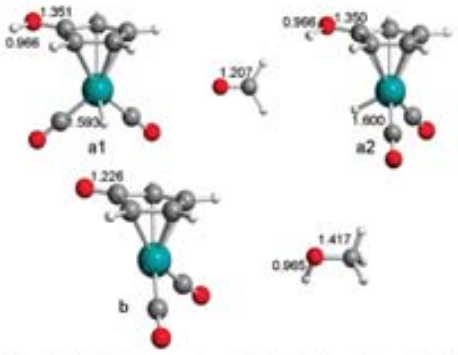

Figure 1. Optimized structures for the initial reactants and final products of the hydrogenation reaction. Distances in Å.

Scheme 3. Reaction Steps of the CO Leaving Mechanism

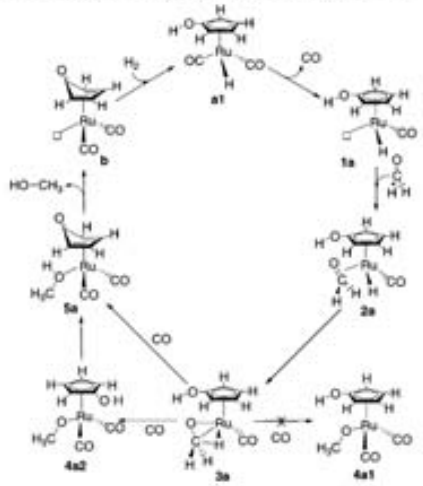

In the Scheme 3 are shown the steps found for this mechanism. It is initiated with the generation of a vacant site by a CO bond-breaking process and the subsequent coordination of formaldehyde.[36] After that, a hydride transfer to the carbonylic carbon takes place followed by the proton transfer to the carbonylic oxygen atom, giving raise to the final product, methanol.

The CO departure step was found to be endothermic by 51.2 kcal/mol (**1a**). This highly endothermic process is in agreement with experimental results where Casey and co-workers found that the exchange of a CO by a ^{13}CO molecule was very slow

(32) (a) Møller, C.; Plesset, M. S. *Phys. Rev.* **1934**, *46*, 618−622. (b) Head-Gordon, M.; Pople, J. A.; Frisch, M. J. *Chem. Phys. Lett.* **1988**, *153*, 503−506. (c) Frisch, M. J.; Head-Gordon, M.; Pople, J. A. *Chem. Phys. Lett.* **1990**, *166*, 275−280. (d) Frisch, M. J.; Head-Gordon, M.; Pople, J. A. *Chem. Phys. Lett.* **1990**, *166*, 281−289. (e) Head-Gordon, M.; Head-Gordon, T. *Chem. Phys. Lett.* **1994**, *220*, 122−128. (f) Saebo, S.; Almlöf, J. *Chem. Phys. Lett.* **1989**, *154*, 83−89.

(33) (a) Cizek, J. *Adv. Chem. Phys.* **1969**, *14*, 35−89. (b) Purvis G. D., III; Bartlett, R. J. *J. Chem. Phys.* **1982**, *76*, 1910−1918. (c) Scuseria, G. E.; Janssen, C. L.; Schaefer, H. F., III. *J. Chem. Phys.* **1988**, *89*, 7382−7387. (d) Scuseria, G. E.; Schaefer, H. F., III. *J. Chem. Phys.* **1989**, *90*, 3700−3703. (e) Pople, J. A.; Head-Gordon, M.; Raghavachari, K. *J. Chem. Phys.* **1987**, *87*, 5968−5975.

(34) *Jaguar 5.5*; Schrödinger, L.L.C.: Portland, OR, 1991−2003.

(35) (a) Barone, V.; Cossi, M. *J. Phys. Chem. A* **1998**, *102*, 1995−2001. (b) Cossi, M.; Rega, N.; Scalmani, G.; Barone, V. *J. Comput. Chem.* **2003**, *24*, 669−681.

(36) For aldehyde or ketone coordination, either η^1 or η^2, see for instance: (a) Bergamo, M.; Beringhelli, T.; D'Alfonso, G.; Maggioni, D.; Mercandelli, P.; Sironi, A. *Inorg. Chim. Acta* **2003**, *350*, 475−485. (b) Méndez, N. Q.; Arif, A. M.; Gladysz, J. A. *Angew. Chem., Int. Ed.* **1990**, *29*, 1473−1474. (c) Méndez, N. Q.; Mayne, C. L.; Gladysz, J. A. *Angew. Chem., Int. Ed.* **1990**, *29*, 1475−1476. (d) Méndez, N. Q.; Seyler, J. W.; Gladysz, J. A. *J. Am. Chem. Soc.* **1993**, *115*, 2323−2334. (e) Boone, B. J.; Klein, D. P.; Seyler, J. W.; Méndez, N. Q.; Arif, A. M.; Gladysz, J. A. *J. Am. Chem. Soc.* **1996**, *118*, 2411−2421.

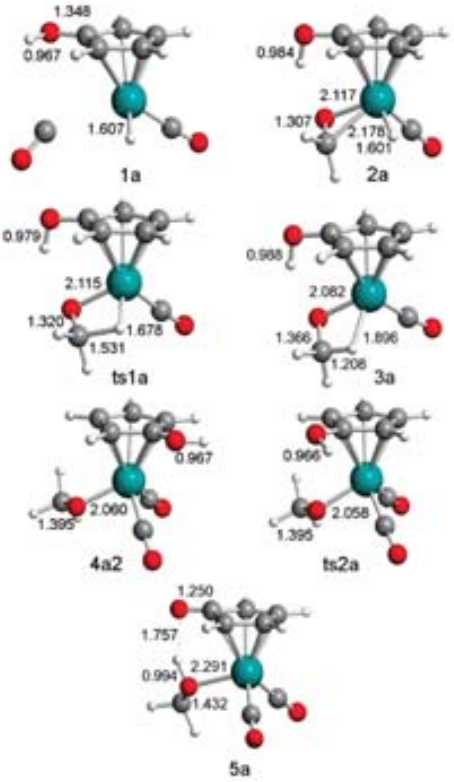

Figure 2. Located stationary points for the CO leaving mechanism. Distances in Å.

unless the reaction took place under fluorescent light.[20] Although this process should be entropically favored, the calculated free energy difference is still too large: 38.7 kcal/mol.

The CO leaving generates a vacant site that can be occupied by the substrate, forming intermediate **2a**. In this intermediate the formaldehyde is η^2-coordinated with Ru−C and Ru−O distances of 2.178 and 2.117 Å, respectively. The energy of this intermediate, **2a**, is 23.8 kcal/mol with respect to the initial reactants. Figure 2 shows the intermediates and transition states involved in this reaction mechanism.

Once the formaldehyde is coordinated to the catalyst, the hydrogen-transfer process may proceed following two sequences: the initial transfer of the CpOH proton to the carbonylic oxygen atom or the initial hydride transfer to the carbonylic carbon atom. The hydride transfer to the carbonylic carbon has a barrier of 7.9 kcal/mol, giving rise to intermediate **3a**. The transition state for this step, **ts1a**, is characterized by a forming C−H bond distance of 1.531 Å, whereas the Ru−H breaking distance is 1.678 Å. This step is endothermic by 5.7 kcal/mol, with the product **3a** having an agostic interaction with the metal via the newly formed C−H bond. The C−H bond distance is 1.208 Å, whereas the Ru···H distance is 1.896 Å. As far as the C═O distance is concerned, it is elongated from 1.307 Å to 1.320 Å and to 1.366 Å in the reactant, **2a**, transition state, **ts1a**, and product, **3a**, respectively.

The coordination site occupied by the agostic interaction can be subsequently replaced by a CO molecule. Depending on the relative position of the CpOH ligand, the proton-transfer step can be barrierless or show a very low barrier. When the position of the proton is near the alkoxide ligand, an intermediate (**4a1** in Scheme 3) could not be located because the proton transfer takes place spontaneously. An alkoxide intermediate, **4a2**, could be located only when the proton of the CpOH ring was in the opposite site of the alkoxide ligand. The energy barrier for the proton transfer from intermediate **4a2** is 3.3 kcal/mol, mainly corresponding to the CpOH ring rotation. This step is exothermic by 19.7 kcal/mol, and the final product, methanol, remains bonded to the catalyst through an agostic interaction. The energy profile for this reaction is presented in Figure 3.

We also evaluated a pathway that once the formaldehyde is coordinated, intermediate **2a**, the mechanism goes through the inverse hydrogen-transfer order, starting with the proton transfer followed by the migration of the hydride. Results are quite similar to the previous mechanism with the opposite transfer order (vide supra). The proton and hydride migrations barriers are 9.7 and 10.5 kcal/mol, respectively, slightly higher than those found in the preceding mechanism.

The inclusion of solvent effects (THF) by means of the CPCM method does not significantly change the energy profile. The CO leaving step is the most affected one, by decreasing the energy 5.5 kcal/mol; the overall reaction becomes slightly exothermic by 3.5 kcal/mol (Figure 3). Thus, the high reported endothermicity for the CO leaving process brought us to reject this mechanism as a feasible mechanism for this process, in agreement with the experimental results.[20]

Substrate Coordination with CpOH Ring Slippage. A different pathway to coordinate the unsaturated substrate to the Ru center involves a ring slippage. This process creates a vacant site that can be occupied by the formaldehyde. In Scheme 4 is presented the general pathway found for this mechanism.

The initial structure found for this reaction mechanism presents a hydrogen bond between the formaldehyde and the acidic hydrogen of the CpOH ligand; the O···H distance is 1.793 Å (see Figure 4). The next step should correspond to the coordination of the formaldehyde to the catalyst. The transition state for this step, **ts1b**, shows that the substrate coordination and the ring slippage take place simultaneously. The Ru−O distance in **ts1b** is 2.502 Å. The ring slippage is observed by the Ru−C distances: two carbon atoms of the CpOH ring remain close to the metal with Ru−C bond distances of 2.311 and 2.358 Å, respectively, whereas the other Ru−C distances are elongated to 2.823, 3.154, and 2.886 Å, respectively. These distances in transition state **ts1b** indicate that the CpOH ring becomes η^2-coordinated to the metal center. Two additional transition states are expected to be formed by simple rotation of the CpOH ligand. Their geometries and energies, however, are expected to be very similar. We calculated the isomers of the formed intermediate **2b**; if the OH group is on the symmetrical position of **2b** (with the OH at one bond distance of the coordinated double bond), forming the **2b2** intermediate, the energy is very similar, 16.3 kcal/mol. Nevertheless, we did not find the isomer where the OH group is on the opposite side of the coordinated double bond, the geometry optimizations led to losing the ketone, generating the η^2-CpOH ring coordination.

In the formed intermediate, **2b**, the Ru−O bond distance is 2.206 Å. The ring coordination in **2b** can also be described by a η^2-coordination mode (as in the transition state). The Ru−C

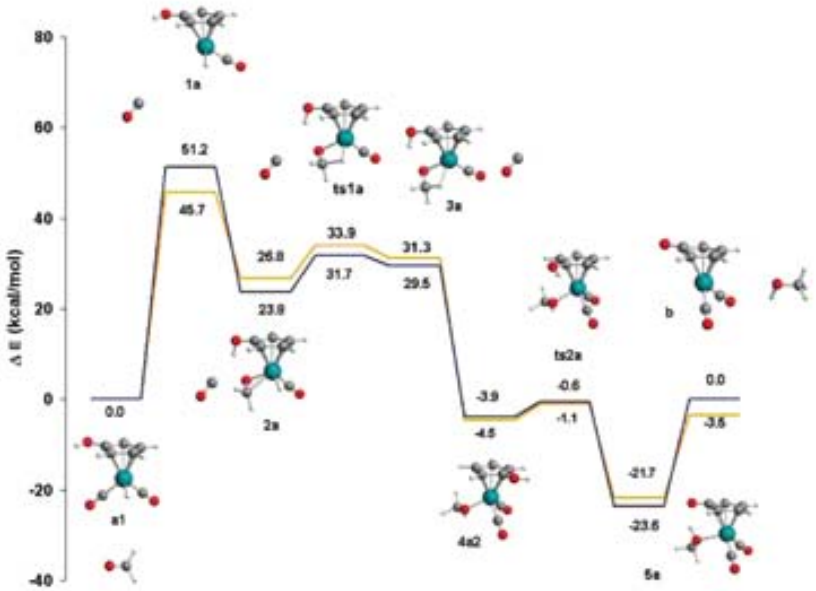

Figure 3. Energy profile for the CO leaving mechanism at the B3LYP level in the gas phase (blue) and solution (orange).

Scheme 4. Reaction Steps of the Stepwise $\eta^5 \rightarrow \eta^2$ Ring Slippage Mechanism

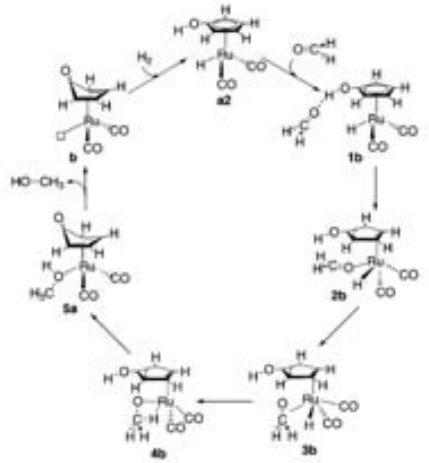

distances for the coordinating carbon atoms are 2.312 and 2.479 Å. For the noncoordinated carbons the Ru−C distances are 3.103, 3.559, and 3.216 Å, respectively. The addition of formaldehyde to the complex shortens the metal−ligand distances. Thus, the Ru−H distance is 1.575 Å in **2b** and 1.606 Å in **1b**, thus, the Ru−H distance has been considerably affected by the change in the geometry from structure **1b** to **2b**.

Both the transition state, **ts1b**, and the intermediate, **2b**, present a η^2-coordination mode of the aromatic ring. These results are different from those initially proposed where the ring slippage was changing the coordination mode from η^5 to η^3. Nevertheless, recent theoretical studies on the ring slippage of the Cp ring by the addition of a new ligand on related transition metal complexes showed that the most stable coordination mode of the Cp is η^2 once the ligand is coordinated[37] and also in some transition states of the ligand coordination step.[38]

The next step in the catalytic cycle corresponds to the change of the coordination mode of the substrate from η^1 to η^2 coordination going from intermediates **2b** to **3b**. Furthermore, the carbonylic carbon atom should be oriented toward the hydride in order to allow the hydride migration. The step involving these two changes is thermodynamically endothermic by 4.2 kcal/mol. Intermediate **3b** has Ru−O and Ru−C distances of 2.296 and 2.424 Å, respectively. At this point the hydrogen-transfer process starts by a pathway quite similar to that described in the previous section. The carbonyl group is inserted into the Ru−H bond, giving rise to intermediate **4b**. The transition state, **ts2b**, is located only 1.5 kcal/mol above the intermediate **3b**. This step is exothermic by 4.4 kcal/mol. The **ts2b** structure is characterized by a C−H bond forming distance of 1.689 Å. The atoms involved in the insertion have a Ru−O−C−H torsion angle of −14.1°. The C=O distance of the formaldehyde is gradually enlarged from 1.253 Å in **3b**, to 1.276 Å in **ts2b**, and to 1.371 Å in **4b**, therefore becoming a single C−O bond. As far as the intermediate **4b** is concerned, it contains an agostic interaction between the recently formed C−H bond and the Ru atom, as shown by the large C−H distance, 1.169 Å. The Ru−O distance of the alkoxide ligand

(37) Veiros, L. F. *Organometallics* **2000**, *19*, 5549−5558.
(38) Fan, H.-J.; Hall, M. B. *Organometallics* **2001**, *20*, 5724−5730.

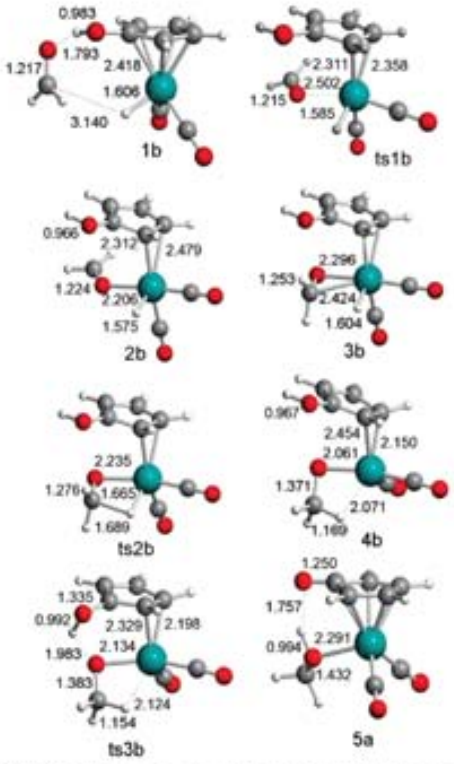

Figure 4. Located stationary points for the stepwise $\eta^5 \rightarrow \eta^2$ ring slippage mechanism. Distances in Å.

is 2.061 Å, being shortened almost 0.3 Å with respect to intermediate **3b**.

The last step, the proton transfer to the alkoxy oxygen, gives rise to the final product, ethanol. This step is exothermic by 41.6 kcal/mol. The corresponding transition state, **ts3b**, has a relatively low energy barrier, 4.2 kcal/mol. Although the proton transfer does not involve the CpOH ring rotation, the **ts3b** structure is also unique. The O−H bond-breaking distance is not very enlarged, 0.992 Å, compared to that in intermediate **4b**, 0.967 Å, the length of the newly forming O−H bond is 1.983 Å. The change in the C−C−O−H dihedral angle on going from intermediate **4b** to **ts3b** is quite large (from −1.8° to −111.5°), indicating that the OH group from the CpOH ligand must be located in the proper alignment for the proton transfer to take place.

The energy profile for this mechanism is presented in Figure 5. The highest relative energy barrier concerns the simultaneous aldehyde coordination with the $\eta^5 \rightarrow \eta^2$ ring slippage. Nevertheless, the highest point within the energy profile is the **ts2b** structure, where the hydride migration is taking place. The energy difference between the lowest energy intermediate and the highest energy transition state is 34.3 kcal/mol. Other possibilities could be considered from structure **4b** to reach final products, because the hydride migration leaves a vacant site that could be occupied by the ring changing its hapticity. In any case, this mechanism must go through **ts2b**, and therefore, the energy barrier to overcome is higher than 30 kcal/mol.

Concerning the calculations in solution, there are no significant changes. The major differences are for **1b** and products (**b** + CH_3OH) with energy changes of 3.3 and 3.5 kcal/mol, repectively. The energy difference between the minima **1b** and the transition state **ts2b** including solvent effects is 33.0 kcal/mol. These results indicate that the stepwise $\eta^5 \rightarrow \eta^2$ mechanism is more favorable than the stepwise mechanism involving the CO leaving, 45.7 versus 33.0 kcal/mol (in solution), although the energy barrier is still too high.

Concerted Pathway with Simultaneous Substrate Coordination and Ring Slippage. The third inner-sphere mechanism analyzed corresponds to the concerted hydrogen transfer having the substrate in the coordination sphere of the catalyst. Figure 6 shows the structures of the species involved in this reaction pathway.

The initial structure corresponds to an intermediate with the formaldehyde hydrogen bonded to the catalyst, **1b**, the same structure presented in the previous section. The concerted hydrogen transfer produces intermediate **2c**, where the ethanol product is weakly coordinated to the metal center through an agostic interaction. The Ru−H distance is 1.959 Å, whereas the newly formed C−H bond distance is 1.155 Å, clearly showing the agostic interaction. During this process, the CpOH ligand loses a proton, breaking the ring aromaticity, becoming bonded to the Ru by a η^4-coordination. The dihedral angle of the four coordinated carbon atoms is −0.2°, the dihedral angles of the carbonylic carbon atom within the ring are 8.3° and −7.9°, showing that this carbon atom is actually out of the plane of the four coordinated atoms.

The Ru−C distances for the four coordinated carbon atoms are 2.288, 2.224, 2.223, and 2.282 Å, respectively. The Ru−C distance for the carbon atom that is out of the plane in **2c** is 2.508 Å. In this step there is also a change of the nature of the C−O bond of the ring, changing from a single bond (1.338 Å) to a double bond (1.241 Å). The hydrogen bond distance between the OH of the formed methanol and the oxygen atom from the formed ketone is 1.773 Å.

In the transition state for this step, **ts1c**, the newly forming C−H and O−H bonds follow a different trend. The C−H forming bond is quite advanced with a distance of 1.233 Å, whereas the O−H forming bond distance is 1.884 Å, indicating a rather small interaction; the O−H bond distance of the CpOH ring is practically unchanged, going from 0.983 Å in **1b** to 0.988 Å in **ts1c**. In order to corroborate that **ts1c** actually connects the **1b** and **2c** intermediates, we performed an IRC calculation.[39] Starting from structure **ts1c** we obtained **1b** and **2c**, the initial reactant and the final product, respectively, and no other intermediates were found on this pathway.

Concerning the CpOH ligand in the **ts1c**, it is η^3-coordinated to the Ru atom. The Ru−C distances for the coordinated carbons atoms are 2.372, 2.296, and 2.463 Å, whereas the Ru−C distances for the other carbon atoms are 2.767 and 2.868 Å, respectively. It is remarkable that η^3 coordination was observed only in structure **ts1c**. This hapticity has already been observed in other transition metal complexes during a ligand substitution process.[38] In fact, the $\eta^5 \rightarrow \eta^3$ ring slippage allows the η^2 coordination of the unsaturated substrate to the metal; the Ru−O and Ru−C distances are 2.300 and 2.475 Å, respectively. The

(39) (a) Fukui, K. *Acc. Chem. Res.* **1981**, *14*, 363−368. (b) Gonzalez, C.; Schlegel, H. B. *J. Chem. Phys.* **1989**, *90*, 2154−2161. (c) Gonzalez, C.; Schlegel, H. B. *J. Phys. Chem.* **1990**, *94*, 5523−5527.

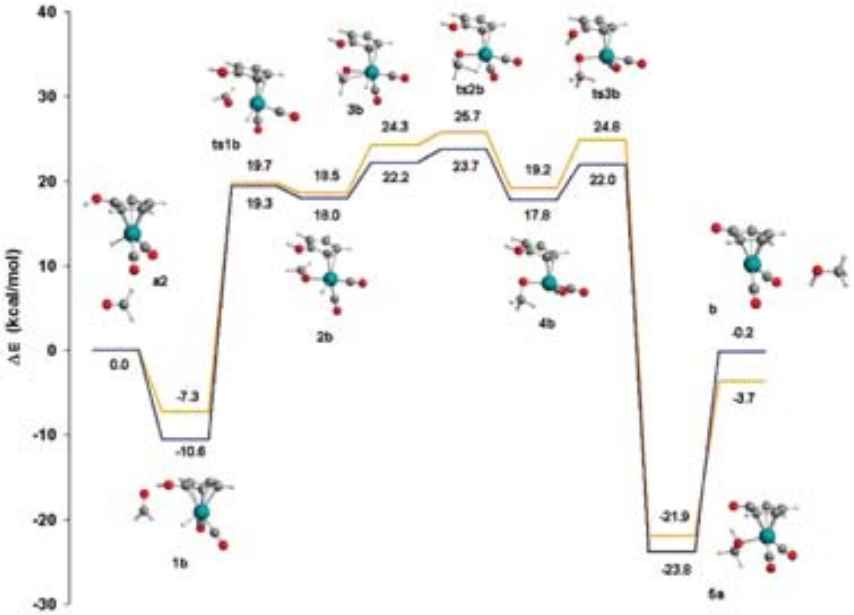

Figure 5. Energy profile for the stepwise $\eta^5 \rightarrow \eta^3$ ring slippage mechanism at the B3LYP level in the gas phase (blue) and in solution (orange).

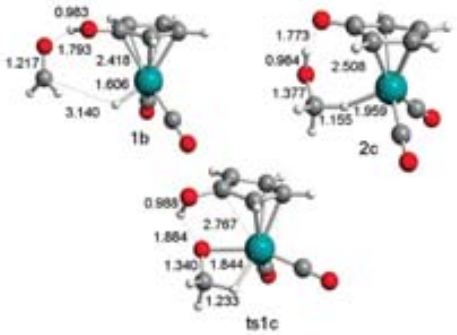

Figure 6. Optimized structures of the transition state **ts1c** and minima structures that connect **1b** and **2c**. Distances in Å.

C=O bond distance of the formaldehyde is 1.340 Å, so it has been enlarged by 0.123 Å in the transition state compared to the reactant **1b**, where the distance is 1.217 Å.

The barrier height for this pathway is 36.0 kcal/mol, with an associated reaction energy of −2.3 kcal/mol. The solvent effects do not significantly modify the energetics of the reaction: the energy barrier is 34.6 kcal/mol, whereas the reaction energy is −4.5 kcal/mol.

Outer-Sphere Mechanism. Concerted Hydrogen-Transfer Mechanism. In this mechanism, the hydrogen transfer takes place without coordination of the substrate on the catalyst. The proton and hydride transfers occur simultaneously in a single step. The initial intermediate **1b** and the final product **2c** are the same as those obtained in the previous concerted pathway. Nevertheless, the major difference between these two pathways relies on the nature of the transition state.

In the transition state for this step, **ts1d**, the newly forming C−H and O−H bond distances are 1.432 and 1.325 Å, respectively (Figure 7). The C−O distance for the substrate is 1.278 Å, slightly shorter than in structure **ts1c** (1.340 Å). Surprisingly, this transition state links exactly the same intermediates, **1b** and **2c**, as that found in the concerted $\eta^5 \rightarrow \eta^3$ ring slippage pathway, respectively. As far as the energies are concerned, the relative energy barrier found in this process is 9.1 kcal/mol in the gas phase and 7.7 kcal/mol in solution, in good agreement with experiment and previous computational work.[21] Casey and co-workers reported a value of $\Delta H^{\ddagger} = 12.0 \pm 1.5$ kcal/mol for the reduction of PhCHO in THF-d_8 with 0.1 mol/L of H_2O or D_2O using the Shvo tolyl analogue.[20] More recently, they reported the barrier for the analogous process in dry THF-d_8, $\Delta H^{\ddagger} = 11.2 \pm 0.9$ kcal/mol.[40] In their computational study of the concerted mechanism Casey, Cui, and co-workers reported a barrier height of 13.8 kcal/mol, in agreement with the results presented here. Figure 8 shows the energy profile for both concerted pathways in solution and gas phase.

After the analysis of several inner- and outer-sphere mechanisms on a model system, computational results strongly support the outer-sphere mechanism with no coordination of the substrate in the catalyst. The reported barrier of 9.1 kcal/mol in the gas phase (7.7 kcal/mol in solution) is in agreement with previously determined experimental energy barriers; $\Delta H^{\ddagger}$

(40) Casey, C. P.; Johnson, J. B. *Can. J. Chem.* **2005**, *83*, 1339.

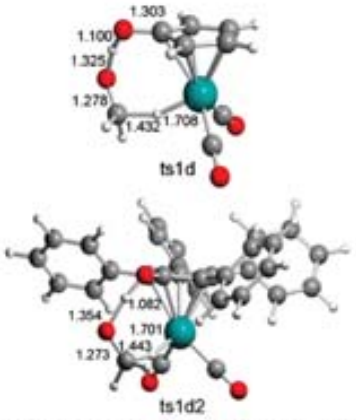

Figure 7. Transition state for the outer-sphere mechanism: model system (**ts1d**) and complete system (**ts1d2**). Distances in Å.

= 12.0 ± 1.5 kcal/mol for the reduction of PhCHO in THF-d_8 in the presence of 0.1 mol/L of H_2O or D_2O[39] and $\Delta H^{\ddagger}$ = 11.2 ± 0.9 for the same process in dry THF-d_8.[40] Moreover, this mechanism is the most feasible one of all the analyzed pathways.

Model System versus Complete System. The concerted outer-sphere mechanism as well as the most favorable inner-sphere mechanism were analyzed taking for the calculations a complete Shvo catalyst, including four phenyl groups in the CpOH ring, [Ph$_4$(η^5-C$_4$COH)]. For the outer-sphere mechanism the analogous transition state **ts1d** was localized, with an energy of 1.9 kcal/mol in the gas phase. This value is quite similar to the one obtained for the model system (−1.5 kcal/mol), showing that the inclusion of the phenyl rings does not change significantly the results for the outer-sphere pathway. The energy barrier calculated is 8.8 kcal/mol, quite close to that of the model system, 9.1 kcal/mol.

For the most favorable inner-sphere mechanism (stepwise $\eta^5 \rightarrow \eta^3$ ring slippage) all the minima along the pathway were localized. The gas-phase energies for the model system intermediates **1b**, **2b**, **3b**, **4b**, and **5a** and final products (**b** + CH_3OH) were −10.6, 18.0, 22.2, 17.8, −23.8, and −0.2 kcal/mol, respectively, related to separated reactants (see Figure 5). Exploring the potential energy surface for the complete system drove us to the localization of all the analogous intermediates found for the model system. Their relative energy values related to separated reactants are −6.9, 24.7, 27.6, 20.7, −22.4, and −0.9 kcal/mol for **1b'**, **2b'**, **3b'**, **4b'**, **5a'**, and final products (**b'** + CH_3OH), respectively. The highest and lowest energetic intermediates are the same for the model and the complete system, **3b**, **3b'**, and **4b**, **4b'**, respectively. The energy profile for the outer-sphere mechanism on the complete system is clearly energetically more favorable than that for the inner-sphere mechanism. The energy barrier for the outer-sphere mechanism is 8.8 kcal/mol, whereas the most stable intermediate for the inner-sphere mechanism (before formation of coordinated ethanol, **5a'**), **4b'**, has an energy of 20.7 kcal/mol. Therefore, calculations on the complete system give similar trends to those on the model system.

In the concerted transition state for the complete system,[41] **ts1d2** (see Figure 7), the O−H and Ru−H distances are 1.082 and 1.701 Å, respectively, whereas for the model catalyst these distances are slightly enlarged by 0.018 and 0.007 Å, for O−H and Ru−H distances, respectively. The length of the C−O bond of the formaldehyde in **ts1d2** is 1.273 Å, whereas that in **ts1d** (model system) was 1.278 Å. Hence, the inclusion of the phenyl substituents on the aromatic ring ligand has no significant effects on the transition state geometry.

The **1b2** and **2c2** geometries are the analogues of **1b** and **2c** for the model system. In **1b2** the distance of the hydrogen bond between the CpOH and the aldehyde oxygen is 1.807 Å. In **2c2**, there is also an agostic interaction through the newly formed C−H, revealed by the C−H distance of 1.146 Å. The recently formed OH bond has a distance of 0.981 Å. Like in **2c**, the hapticity of the ring is η^4, with the ring bonded to the metal through two double bonds formed in the ring after the hydrogen transfer. The four coordination carbons of the ring have distances with the ruthenium atom of 2.295, 2.252, 2.265, and 2.310 Å, respectively. The last carbon atom of the ring in **2c2** is out of the ring plane, as in **2c**, having a Ru−C distance of 2.468 Å, slightly shortened with respect to the model system, 2.507 Å. The distance of the C−O bond of the ring ligand in **2c2** is 1.381 Å. The OH group of the formed methanol is interacting through a hydrogen bond with the recently formed C=O group of the ring, characterized by a distance of 1.803 Å.

Calculation of Kinetic Isotope Effects. Casey and co-workers reported individual kinetic isotope effects in benzaldehyde hydrogenation using an analogue of the Shvo catalyst (where two Ph groups were substituted by two Tol groups) for the Ru−D and O−D bonds with values of 1.5 ± 0.2 and 2.2 ± 0.1, respectively, in THF in the presence of a small amount of water. On the basis of the agreement between the product of both individual isotope effects (1.5 × 2.2 = 3.3) and the measured one for RuD−OD species (3.6 ± 0.3), they concluded that the hydrogenation takes place through a concerted proton and hydride transfer.[20] In a recent study, they showed that the addition of water to THF led to a decrease of the Ru−D kinetic isotope effect with a concomitant increase of the O−D kinetic isotope effect.[40] The combined isotope effect also was found to increase. In dry THF (at 22 °C) the individual isotope effects were 2.60 ± 0.09 for Ru−D and 1.30 ± 0.02 for O−D, whereas the combined isotope effect was 3.38 ± 0.19. Conversely, addition of water (0.120 mol/L) led to values of 1.32 ± 0.11 for Ru−D and 2.99 ± 0.35 for O−D, with a value of 4.25 ± 0.62 for the combined isotope effect. The authors also analyzed the KIEs in other solvents such as toluene and CH_2Cl_2, the reported kinetic isotope effects in these solvents are quite similar to the reported ones in dry THF (see Table 1).

In a parallel study by the group of Bäckvall on the dehydrogenation of 1-(4-fluorophenyl)ethanol by the Shvo catalyst, they reported KIEs of 1.87 ± 0.17 and 2.57 ± 0.26 for the rupture of O−H and C−H bonds of the alcohol, respectively, and the combined isotope effect of 4.61 ± 0.37, also supporting a concerted transfer.[22]

We have performed kinetic isotope effect calculations (KIEs) for both concerted mechanisms previously described. The free energy barriers used for KIE calculations are those between the initial reactants and the corresponding transition states. The obtained results are gathered in Table 1. For the outer-sphere

(41) The transition state **ts1d2** (for the complete system) was recalculated with Gaussian03. The geometries and energies obtained are very similar. The energy barriers found here were 8.3 and 8.0 kcal/mol in the gas phase and in solution, respectively.

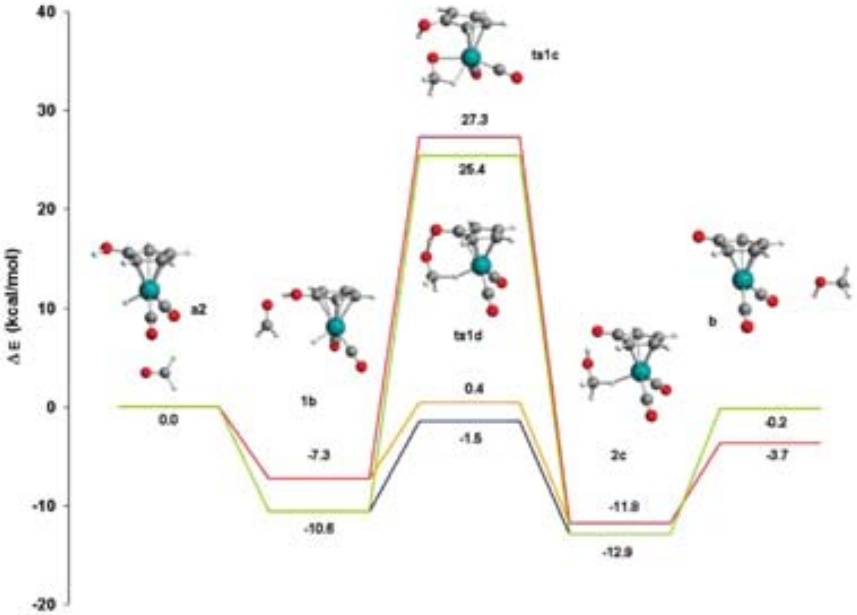

Figure 8. Energy profiles for both concerted pathways at the B3LYP level. Inner-sphere mechanism: green (gas phase) and red (solution), respectively. Outer-sphere mechanism: blue (gas phase) and orange (solution) respectively.

Table 1. Calculated Kinetic Isotope Effects for the Concerted Mechanisms Including the Experimental Values

mechanism	Ru−D bond	O−D bond	dideuterated species
concerted inner sphere	0.7	1.1	0.8
concerted outer sphere (model system)	1.3	3.1	3.8
concerted outer sphere (complete system)	1.3	2.8	3.5
THF (no water)[a]	2.60 ± 0.09	1.30 ± 0.02	3.38 ± 0.19
THF (0.120 mol/L water)[a]	1.32 ± 0.11	2.99 ± 0.35	4.25 ± 0.62
CH_2Cl_2[a]	2.51 ± 0.28	1.33 ± 0.13	3.36 ± 0.56
toluene[a]	2.65 ± 0.18	1.38 ± 0.08	3.63 ± 0.25
THF[b]	1.5 ± 0.2	2.2 ± 0.1	3.6 ± 0.3

[a] From ref 40. [b] From ref 20.

mechanism we calculated the KIEs for the model and the complete systems. The obtained values are similar in both cases, showing that the model system is good enough to study the system. Notice that all calculations were performed using formaldehyde as substrate, whereas the experimental values used benzaldehyde as substrate.

Our results, based on gas-phase calculations, are expected to be closer to the KIEs reported in toluene than the other solvents since it presents the lowest dielectric constant ($\epsilon = 2.4$). For the complete system in the outer-sphere mechanism, the value for the combined isotope effect is very close to the experimental one: 3.5 (calculated) versus 3.63 ± 0.25 (toluene). The individual isotope effects present a different trend. For Ru−D, we obtained a KIE value of 1.3 compared to the experimental value of 2.65 ± 0.18 (toluene). For the O−D bond the calculated value is 2.8 compared to the experimental value of 1.38 ± 0.08 (toluene). Surprisingly, theoretical values are closer to the individual kinetic isotope effects reported in THF with a small amount of water (see Table 1) than those in dry THF or toluene.

The value for the combined isotope effect for the concerted inner-sphere mechanism is quite different from the experimental value in toluene: 0.8 versus 3.63 ± 0.25. Concerning the individual isotope effects, the O−D bond agrees fairly well with the experimental value in toluene, whereas the Ru−D bond does not. The fact that the combined isotope effect is quite far from the experimental result does not support the concerted inner-sphere mechanism.

In conclusion, the calculated combined isotope effect for the outer-sphere mechanism is in better agreement with the experimentally reported values than that obtained for the concerted inner-sphere mechanism. Therefore, in accordance with the previous analysis of the energy reaction profiles, these results also suggest a concerted outer-sphere mechanism for the hydrogen-transfer process.

Conclusions

The hydrogen-transfer process to ketones catalyzed by the Shvo catalyst was extensively analyzed by means of DFT theoretical calculations. Several inner-sphere mechanisms (that imply the coordination of the substrate on the coordination sphere of the metal catalyst) and the outer-sphere mechanism (without substrate coordination) were considered. The energy profiles in the gas phase and including solvation effects for all the proposed mechanisms were calculated, and the KIEs for the most favorable concerted mechanisms were also evaluated.

According to our results, the most viable mechanism (that with the lowest energy barrier) is the outer-sphere mechanism where the hydrogen transfer takes place without coordination

of the substrate to the metal center; the proton and the hydride are transferred simultaneously to the C=O double bond. The energy barrier for the model system is 9.1 kcal/mol in the gas phase and 7.7 kcal/mol in solution (THF). For the complete system (where the entire Shvo catalyst was included in the calculations) these barriers adopted values of 8.3 and 8.0 kcal/mol in the gas phase and solution, respectively. The calculated KIEs for this mechanism are also in good agreement with the experimental reported ones.

Within the inner-sphere mechanisms, that involving the initial CO leaving is highly endothermic in the initial dissociative process. The energy barrier for this step is 51.2 kcal/mol in the gas phase and 45.7 kcal/mol in solution; the free energy barrier associated with this process in the gas phase is 38.7 kcal/mol. As expected, inclusion of entropic effects clearly diminishes the energy barrier for a dissociative process, although the barrier is still too high to be a feasible mechanism.

The inner-sphere mechanism involving the substrate coordination along with the ring slippage has an energy barrier in the gas phase of 34.3 kcal/mol, too high to be a feasible mechanism. A noticeable feature about this mechanism is that it involves a $\eta^5 \rightarrow \eta^2$ ring slippage instead of the initially proposed $\eta^5 \rightarrow \eta^3$ ring slippage. Our results are in agreement with previous studies on the ring slippage process on related transition metal complexes.

Concerning the concerted inner-sphere mechanism where the hydrogen transfer takes place simultaneously with the $\eta^5 \rightarrow \eta^3$ ring slippage, it has a barrier of 36.0 kcal/mol in the gas phase and 34.6 kcal/mol in solution. Despite being a concerted pathway, the energy barrier is too high compared with the outer-sphere mechanism. Moreover, the calculated combined kinetic isotope effect for this mechanism is clearly different from the experimentally reported value.

In summary, the feasibility of the outer-sphere mechanism (a concerted hydrogen transfer without carbonyl coordination) is supported by presenting the lowest energy barrier among all the studied processes and calculated KIEs closest to those obtained experimentally. These results are in agreement with other hydrogen-transfer processes based on metal−ligand bifunctional catalysts, even though this catalyst has the proton donor moiety quite far from the metal center. All reported studies to date suggest that metal−ligand bifunctional catalysts work through an outer-sphere mechanism. These conclusions may be applicable to the hydrogenation of other polar double bonds, and an analysis is in progress in our lab.

Acknowledgment. We are grateful to the Spanish MEC (Project CTQ2005-09000-C02-01, "Ramón y Cajal" contract to G.U. and FPU fellowships to A.C.-V.), as well as to the Generalitat de Catalunya (2005/SGR/00896).

Supporting Information Available: Complete ref 30, absolute energies, and Cartesian coordinates. This material is available free of charge via the Internet at http://pubs.acs.org.

OM7004832

Capítol 10

Article II

Article

Theoretical Analysis of the Hydrogen-Transfer Reaction to C#N, C#C, and C#C Bonds Catalyzed by Shvo's Ruthenium Complex

Aleix Comas-Vives, Gregori Ujaque, and Agustí Lledós

Organometallics, **2008**, 27 (19), 4854-4863 • DOI: 10.1021/om700975k • Publication Date (Web): 13 September 2008

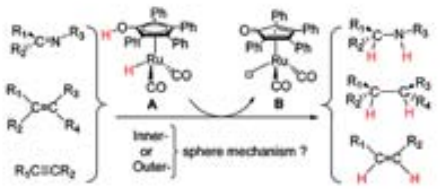

4854 *Organometallics* **2008,** *27,* 4854–4863

Theoretical Analysis of the Hydrogen-Transfer Reaction to C=N, C=C, and C≡C Bonds Catalyzed by Shvo's Ruthenium Complex

Aleix Comas-Vives, Gregori Ujaque,* and Agustí Lledós*

Unitat de Química Física, Departament de Química, Universitat Autònoma de Barcelona, 08193 Bellaterra, Catalonia, Spain

Received October 5, 2007

The Shvo catalyst $[[Ph_4(\eta^5\text{-}C_4CO)]_2H]Ru_2(CO)_4H$ belongs to the so-called bifunctional catalysts, containing one hydride (bonded to Ru) and one proton (bonded to a ligand), which are easily transferred. The mechanism of hydrogenation of polar double bonds by Shvo's catalyst has been extensively studied; however, imine hydrogenation is still a controversial topic. The outer-sphere mechanism (without substrate coordination) and the inner-sphere mechanism (with substrate coordination) are the two main proposals. Several experimental observations account for each proposed mechanism, besides a theoretical analysis of their respective suggested mechanism. In the present work inner- and outer-sphere mechanisms for hydrogenation of C=N, C=C, and C≡C bonds are analyzed and compared by means of theoretical calculations, complementing our previous work in C=O hydrogenation. The obtained energy profiles support an outer-sphere mechanism in all the cases.

Introduction

The homogeneous hydrogenation of polar double bonds is a widely employed reaction in synthetic chemistry.[1] Industrially, it offers an alternative over classical reducing agents such as $NaBH_4$ and $LiAlH_4$ for its better atom economy, cleaner synthesis, and easier workup procedures, also providing milder conditions and better functional tolerance and chemoselectivity over heterogeneous catalysis. In addition, H_2 is not the only source to perform hydrogenation, and other molecules such as alcohols are also used as hydrogen source.[1,2]

Concerning the hydrogen-transfer mechanism, most transition-metal catalysts operate through the "hydridic route" via a metal-hydride intermediate.[3] The "direct transfer" (without participation of a metal-hydride intermediate) is thought to operate for main group elements. In some transition-metal-catalyzed hydrogenations, the so-called "ionic mechanism" has been proposed for systems involving the addition of H_2 in the form of formally H^+ and H^- species.[4] In this sense, the metal−ligand bifunctional hydrogenation catalysts are those containing two hydrogens with hydridic and acidic character, respectively.[5] The hydridic hydrogen is attached to the metal, whereas the acidic hydrogen is provided by one ligand. One of the most paradigmatic examples of this type of catalysts is the Shvo catalyst[6,7] $[[Ph_4(\eta^5\text{-}C_4CO)]_2H]Ru_2(CO)_4H$ (**1**), which has been very versatile and used for a great variety of processes involving hydrogen transfer.[8−15] The bimetallic dimer **1** decomposes upon heating, producing the species **A** and **B**, which are able to perform hydrogenation and dehydrogenation processes, respectively (Scheme 1). A modification of the Shvo tolyl analogue with the exchange of one CO by one PPh_3, $[2,5\text{-}Ph\text{-}3,4\text{-}Tol_2(\eta^5\text{-}C_4COH)]Ru(CO)(PPh_3)H$, has recently appeared.[16,17]

Scheme 1. Equilibrium of the Shvo Catalyst

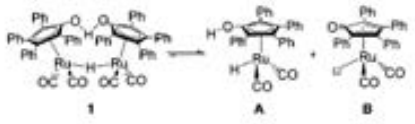

1 **A** **B**

* Corresponding authors. E-mail: gregori@klingon.uab.es; agusti@klingon.uab.es.

(1) *Handbook of Homogeneous Hydrogenation*; de Vries, J. G., Elsevier, C. J., Eds.; Wiley-VCH: Weinheim, 2007.

(2) *Homogeneous Hydrogenation*; Chaloner, P. A., Esteruelas, M. A., Joó, F., Oro, L. A., Eds.; Kluwer Academic Publishers: Dordrecht, 1994.

(3) (a) Gladiali, S.; Alberico, E. *Chem. Soc. Rev.* **2006**, *35*, 226–236. (b) Samec, J. S. M.; Bäckvall, J.-E.; Andersson, P. G.; Brant, P. *Chem. Soc. Rev.* **2006**, *35*, 237–248.

(4) (a) Bullock, R. M. In *Handbook of Homogeneous Hydrogenation*; de Vries, J. G., Elsevier, C. J., Eds.; Wiley-VCH: Weinheim, 2007; Vol. 1, p 153. (b) Bullock, R. M. *Chem.−Eur. J.* **2004**, *10*, 2366–2374. (c) Guan, H.; Iimura, M.; Magee, M. P.; Norton, J. R.; Zhu, G. *J. Am. Chem. Soc.* **2005**, *127*, 7805–7814.

(5) (a) Noyori, R.; Ohkuma, T. *Angew. Chem.* **2001**, *113*, 40–75. *Angew. Chem. Int. Ed.* **2001**, *40*, 40−73. (b) Sandoval, C. A.; Ohkuma, T.; Muñiz, K.; Noyori, R. *J. Am. Chem. Soc.* **2003**, *125*, 13490–13503. (c) Fujii, A.; Hashiguchi, S.; Uematsu, N.; Ikariya, T.; Noyori, R. *J. Am. Chem. Soc.* **1996**, *118*, 2521–2522. (d) Uematsu, N.; Fujii, A.; Hashiguchi, S.; Ikariya, T.; Noyori, R. *J. Am. Chem. Soc.* **1996**, *118*, 4916–4917.

(6) (a) Blum, Y.; Czarkie, D.; Rahamim, Y.; Shvo, Y. *Organometallics* **1985**, *4*, 1459–1461. (b) Shvo, Y.; Czarkie, D.; Rahamim, Y. *J. Am. Chem. Soc.* **1986**, *108*, 7400–7402.

(7) Bullock, R. M. In *Handbook of Homogeneous Hydrogenation*; de Vries, J. G., Elsevier, C. J., Eds.; Wiley-VCH: Weinheim, 2007; Vol. 1, pp 186−193.

(8) Karvembu, R.; Prabhakaran, R.; Natarajan, K. *Coord. Chem. Rev.* **2005**, *249*, 911–918.

(9) Shvo, Y.; Goldberg, I.; Czerkie, D.; Reshef, D.; Stein, Z. *Organometallics* **1997**, *16*, 133–138.

(10) Menashe, N.; Salant, E.; Shvo, Y. *J. Organomet. Chem.* **1996**, *514*, 97–102.

(11) Samec, J. S. M.; Bäckvall, J.-E. *Chem.−Eur. J.* **2002**, *8*, 2955–2961.

(12) Csjernyk, G.; Éll, A. H.; Fadini, L.; Pugin, B.; Bäckvall, J.-E. *J. Org. Chem.* **2002**, *67*, 1657–1662.

(13) (a) Samec, J. S. M.; Éll, A. H.; Bäckvall, J.-E. *Chem.−Eur. J.* **2005**, *11*, 2327–2334. (b) Éll, A. H.; Samec, J. S. M.; Brasse, C.; Bäckvall, J.-E. *Chem. Commun.* **2002**, 1144–1145.

(14) (a) Larsson, A. L. E.; Persson, B. A.; Bäckvall, J.-E. *Angew. Chem.* **1997**, *109*, 1256–1258; *Angew. Chem., Int. Ed.* **1997**, *36*, 1211−1212. (b) Persson, B. A.; Larsson, A. L. E.; Ray, M. L.; Bäckvall, J.-E. *J. Am. Chem. Soc.* **1999**, *121*, 1645–1650.

(15) Paetzold, J.; Bäckvall, J.-E. *J. Am. Chem. Soc.* **2005**, *127*, 17620–17621.

10.1021/om700975k CCC: $40.75
Publication on Web 09/13/2008

Scheme 2. Proposed Catalytic Cycle for Alkyne Hydrogenation (left); Formation of Species D Poisons the Catalyst (right)

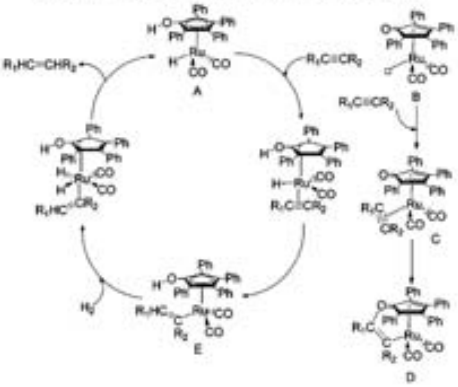

The Shvo catalyst is able to hydrogenate polar (C═O, C═N) and nonpolar double and triple bonds (C═C, C≡C), though it is more efficient for the former. The reaction mechanism for these processes, however, is a matter of controversy. For alkyne hydrogenation Shvo proposed a catalytic cycle involving CpOH ring slippage (see Scheme 2).[9] The formation of a very stable species (labeled as **D** in Scheme 2) poisoned the catalyst. In the same work Shvo suggested that an analogous catalytic cycle may be considered for alkene hydrogenation. Moreover, for alkene hydrogenation, Casey suggested a different mechanism with initial loss of one CO molecule, followed by alkene coordination and hydride transfer, and finally one H_2 molecule performs the cleavage of the Ru-alkyl intermediate, producing alkane.[18]

For the case of C═O hydrogenation mainly two different mechanisms were proposed, where the hydride and proton transfers took place concertedly: (i) outer-sphere mechanism and (ii) inner-sphere mechanism; the latter mechanism involves coordination of the substrate along with the CpOH ring slippage. In this case, however, theoretical calculations clearly support the outer-sphere mechanism.[19a,20]

Concerning imine hydrogenation analogous inner- and outer-sphere mechanisms have been also proposed (Scheme 3). Casey and co-workers suggest a change in the rate-limiting step of imine hydrogenation depending on the substituents on nitrogen.[21] For electron-withdrawing substituents the high reported kinetic isotope effect brings them to conclude that the concerted hydrogen transfer is the rate-limiting step. In contrast, for electron-donating alkyl substituents they observed inverse kinetic isotope effects, deuterium scrambling, and isomerization, concluding that in this case the rate-limiting process was amine coordination on the Ru atom and that hydrogenation was reversible. Since proton and hydride transfer occurred prior to amine coordination, it was not possible to discern using mechanistic information if those processes occurred via a concerted or a stepwise process. Nevertheless, the combination of successful intramolecular trapping besides the failure of the intermolecular one was given as proof against the ring-slippage mechanism (inner-sphere mechanism).[19] They assumed that nitrogen coordination of the newly generated amine was faster than breaking the hydrogen bond between the products, diffusion from the solvent cage, or inversion of the nitrogen lone pair. The same group reported different stereochemistry for the hydrogen transfer depending on the nature of the imine. For N-aryl imines the process was shown to be trans stereoespecific.[22] The N-alkyl imine hydrogenation however was a stereorandom process attributed to a reversible dehydrogenation faster than amine coordination to the metal. Amine escape from the solvent cage and inversion of the nitrogen were considered to be slower than dehydrogenation and amine coordination to the ruthenium.

Scheme 3. Proposed Mechanisms for Polar Double-Bond Hydrogenation

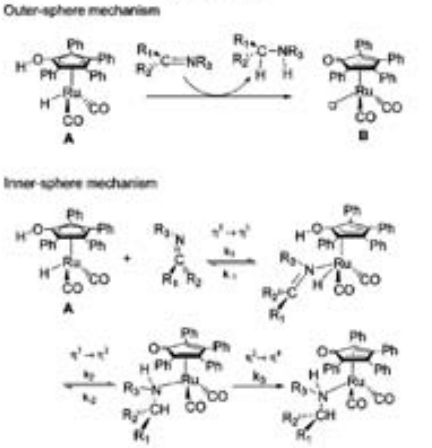

The inner-sphere mechanism proposed by Bäckvall (Scheme 3) starts with the imine-promoted $\eta^3 \rightarrow \eta^1$ CpOH ring slippage allowing imine coordination. The following steps are hydrogenation and the $\eta^2 \rightarrow \eta^4$ rearrangement giving the corresponding amine complex.[23] For the catalytic transfer dehydrogenation of *N*-phenyl-*N*-(1-phenylethylamine) the large reported kinetic isotope effect for the C−H cleavage (3.24) besides the fact that the combined isotope effect (C−H and N−H cleavages) is practically the same (3.26) brought the authors to the conclusion that transfer dehydrogenation of an amine is stepwise, the hydride transfer being the rate-limiting step.[24] In the stochiometric reduction of *N*-phenyl-[1-(4-methoxyphenyl)ethylidene]-amine they suggested that the hydrogen-transfer process was

(16) Casey, C. P.; Strotman, N. A.; Beetner, S. E.; Johnson, J. B.; Priebe, D. C.; Vos, T. E.; Khodavandi, B.; Guzei, I. A. *Organometallics* **2006**, *25*, 1230–1235.
(17) Casey, C. P.; Strotman, N. A.; Beetner, S. E.; Johnson, J. B.; Priebe, D. C.; Guzei, I. A. *Organometallics* **2006**, *25*, 1236–1244.
(18) Casey, C. P.; Singer, S. W.; Powell, D. R. *Can. J. Chem.* **2001**, *79*, 1002–1011.
(19) (a) Casey, C. P.; Bikzhanova, G. A.; Cui, Q.; Guzei, I. A. *J. Am. Chem. Soc.* **2005**, *127*, 14062–14071. See also Supporting Information therein. (b) Casey, C. P.; Clark, T. B.; Guzei, I. A. *J. Am. Chem. Soc.* **2007**, *129*, 11821–11827.
(20) Comas-Vives, A.; Ujaque, G.; Lledós, A. *Organometallics* **2007**, *26*, 4135–4144.
(21) Casey, C. P.; Johnson, J. B. *J. Am. Chem. Soc.* **2005**, *127*, 1883–1894.
(22) Casey, C. P.; Bikzhanova, G. A.; Guzei, I. A. *J. Am. Chem. Soc.* **2006**, *128*, 2286–2293.
(23) Samec, J. S. M.; Ell, A. H.; Åberg, J. B.; Privalov, T.; Eriksson, L.; Bäckvall, J.-E. *J. Am. Chem. Soc.* **2006**, *128*, 14293–14305.
(24) Ell, A. H.; Johnson, J. B.; Bäckvall, J.-E. *Chem. Commun.* **2003**, 1652–1653.

not the rate-limiting step on the basis on the low reported combined isotope effect (1.05).[25] The same group also performed trapping experiments, which support the inner-sphere mechanistic proposal because using an internal amine trap gave only the Ru complex with the newly formed amine from the imine at low temperatures.[23,26]

Different theoretical studies have addressed a mechanistic analysis.[19a,23,27] Casey and co-workers focused on the concerted outer-sphere mechanism for a model imine (H_2C=N-CH_3) and a model catalyst. This mechanism was reported to be feasible with an energy barrier of 4.8 kcal/mol including solvent effects (THF) by means of single-point IEF-PCM calculations.[19a] Privalov, Samec, and Bäckvall analyzed the inner-sphere mechanism. Calculations were performed taking an electron-donating imine ($(CH_3)_2$C=N-CH_3) and the complete catalyst including solvent effects by PCM and explicit solvent molecules. The reported energy barrier was 15 kcal/mol, corresponding to imine coordination coupled with ring slippage. The following steps, hydride transfer and $\eta^2 \rightarrow \eta^4$ ring slippage, were found to be similar but lower in energy. They suggested that any of these steps may become rate-limiting depending on the electronic nature of the imine.[27]

Given all these different and contraposed mechanistic considerations and following our previous mechanistic studies on the hydrogenation using Shvo's catalyst[20] we decided to perform an extensive analysis of the reaction mechanism for imines, alkenes, and alkynes by means of theoretical calculations. Our aim is to perform an unbiased comparative theoretical study of both inner- and outer-sphere mechanisms for these substrates in order to cast light on new evidence trying to discern between these pathways.

Computational Details

Calculations were carried out using the program package Gaussian03[28] at density functional theory (DFT) level by means of the hybrid B3LYP functional.[29]

Mechanistic analysis was performed extensively by using a model reaction system. We used as substrates the simplest species containing C=N, C=C, and C≡C groups, methanimine, ethylene, and acetylene, respectively. The Shvo catalyst was modeled by [(η^5-C_4H_4COH)Ru(CO)$_2$H]; the phenyl substituents of the aromatic ligand, hereafter named CpOH, were replaced by hydrogens. These four H's were calculated using the 6-31G basis set and the other main group elements (C, N, the rest of H) were calculated using the 6-31G(d,p) basis set. For the case of imine hydrogenation, a model taking the complete catalyst [(η^5-C_4Ph_4COH)Ru(CO)$_2$H] along with an example of electron-donating imine [H_2C-N=C(CH_3)$_2$] was also evaluated; the 6-31G(d,p) basis set was used for all the atoms except the Ru, which was described by the LANL2DZ effective core potential[30] and its associated basis set for the outermost electrons. To check the basis set dependence, single-point calculations using a larger basis set were performed:

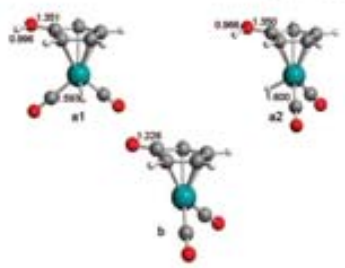

Figure 1. Optimized structures for the initial and final catalyst. The two rotamers for the initial catalyst, **a1** and **a2**, are depicted. Distances are in Å.

the 6-311++G(d,p) basis set was used for C, N, O, and H and f polarization functions were added to the Ru atom using the lanl2dz pseudopotential. No significant changes were observed when increasing the basis set (see Supporting Information).

For the saddle points the existence of only one imaginary frequency was checked by means of frequency calculations. The IRC approach was used to corroborate the minima linked by every transition state.[31] Solvent effects (THF, ε = 7.58) were included using CPCM[32] single-point calculations. For the hydrogens directly involved in the reaction the SPHEREONH option was used in order to place individual cavities on them. Some steps for imine hydrogenation mechanisms (indicated in the text) were evaluated reoptimizing the structures including the solvent effects by means of the CPCM method.

Results and Discussion

This section is divided into two subsections, which analyze imine and both alkene and alkyne hydrogenation mechanisms, respectively. In all of them both inner- and outer-sphere mechanisms are evaluated. The inner-sphere mechanisms require the coordination of the substrate to the catalyst, whereas in the outer-sphere mechanism the hydrogenation occurs by simultaneous hydride and proton transfer to the substrate without coordination to the metal.

In our previous study[20] two rotamers were also localized for the active reducing species of the Shvo catalyst, **a1** and **a2**. These structures besides the final dehydrogenated catalyst **b** are depicted in Figure 1. These two conformers differ energetically only by 0.2 kcal/mol, indicating that the different rotamers are equally accessible. Only the **a2** rotamer is considered in this study.

Once the hydrogenation takes place, the dehydrogenated form of the catalyst (**b**) and the hydrogenated product, methylamine, ethane, and ethene are produced. The reaction energies for the imine, alkene, and alkyne hydrogenation are −6.4, −15.4, and −27.3 kcal/mol in the gas phase, respectively. In solution these energies do not change significantly: −9.0, −17.7, and −28.9 kcal/mol. For formaldehyde hydrogenation we reported values of −0.2 and −3.7 kcal/mol in the gas phase and solution, respectively.[20]

Imine Hydrogenation. Inner-Sphere Mechanisms. These mechanisms require the creation of a vacant site in order to

(25) Samec, J. S. M.; Éll, A. H.; Bäckvall, J.-E. *Chem. Commun.* **2004**, 2748–2749.
(26) Bäckvall considers that hydrogen transfer to electron-deficient imines should be faster than to electron-rich ones, whereas the newly formed amine coordination should be slower in case the outer-sphere mechanism was the operative one.
(27) Privalov, T.; Samec, J. S. M.; Bäckvall, J.-E. *Organometallics* **2007**, *26*, 2840–2848.
(28) Frisch, M. J.; et al. *Gaussian03*; Gaussian, Inc.: Wallingford, CT, 2004.
(29) (a) Becke, A. D. *J. Chem. Phys.* **1993**, *98*, 5648–5652. (b) Lee, C.; Yang, W.; Parr, R. G. *Phys. Rev. B* **1988**, *37*, 785–789. (c) Stephens, P. J.; Devlin, F. J.; Chabalowski, C. F.; Frisch, M. J. *J. Phys. Chem.* **1994**, *98*, 11623–11627.
(30) Hay, P. J.; Wadt, W. R. *J. Chem. Phys.* **1985**, *82*, 270–283.
(31) (a) Fukui, K. *Acc. Chem. Res.* **1981**, *14*, 363–368. (b) Gonzalez, C.; Schlegel, H. B. *J. Chem. Phys.* **1989**, *90*, 2154–2161. (c) Gonzalez, C.; Schlegel, H. B. *J. Phys. Chem.* **1990**, *94*, 5523–5527.
(32) (a) Barone, V.; Cossi, M. *J. Phys. Chem. A* **1998**, *102*, 1995–2001. (b) Cossi, M.; Rega, N.; Scalmani, G.; Barone, V. *J. Comput. Chem.* **2003**, *24*, 669–681.

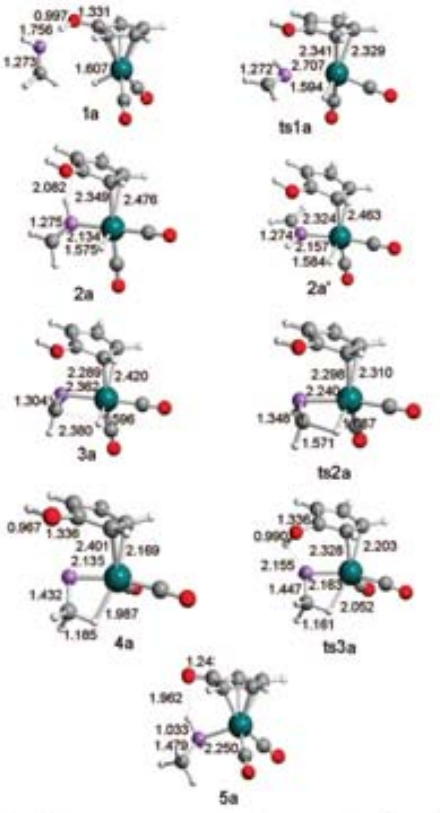

Figure 2. Located stationary points for the stepwise $\eta^5 \rightarrow \eta^2$ ring-slippage mechanism of $H_2C{=}NH$ hydrogenation. Distances are in Å.

coordinate the substrate species. For the creation of a vacant site by a CO leaving we reported an initial energy cost of 45.7 kcal/mol in CPCM with THF as solvent and 38.7 kcal/mol for the free energy difference in the gas phase.[20] Thus, we did not further consider this mechanism. In this line, Casey and co-workers found noticeable CO exchange only under fluorescent light.[33]

$\eta^5 \rightarrow \eta^2$ Stepwise Mechanism. In this stepwise mechanism we considered as a first step the $\eta^5 \rightarrow \eta^2$ ring slippage of the CpOH ring, allowing the imine coordination. In Figure 2 are shown all the located stationary points of this pathway for the model catalyst and the simplest imine.

In the intermediate **2a** the imine group is η^1 coordinated to the metal through the N atom of the imine ligand with a Ru−N distance of 2.134 Å. Two carbons of the CpOH group remains attached to the Ru atom, having Ru−C distances of 2.349 and 2.476 Å. A recent theoretical study showed that the η^2 coordination mode of the Cp was the most stable upon ligand addition on related transition-metal complexes.[34] This coordination mode was also found in some ligand addition transition states.[35]

The first transition state involves the $\eta^5 \rightarrow \eta^2$ CpOH ring slippage (**ts1a**) along with the η^1-imine coordination producing intermediate **2a**. The relative barrier height is considerably high, 27.4 kcal/mol with respect to the hydrogen-bonded adduct of the reactants (**1a**). This transition state is characterized by a Ru−N distance of 2.707 Å and Ru−C distances for the incoming coordinated carbons of the CpOH ring of 2.341 and 2.329 Å. In the Figure 3 are shown the energy profiles for this pathway both in the the gas phase and solution.

From **2a** to **2a'** there is a rotation of the imine ligand that facilitates the subsequent steps.[36] Once the intermediate **2a'** is formed, there are two ways to proceed from this intermediate: first proton transfer followed by hydride transfer or first hydride transfer followed by proton transfer. We calculated the direct proton transfer, reporting a transition state located at 33.1 kcal/mol with respect to our origin of energies (this is 46.7 kcal/mol with respect to the **1a** structure). This result leads us to discard this option, in favor of the hydride transfer followed by the proton transfer (vide infra).

For the hydride migration to the carbon of the imine, the coordination mode of the imine changes to a η^2 coordination mode (**3a**), with Ru−C and Ru−N distances of 2.510 and 2.362 Å, respectively. This change is thermodynamically noticeable in the imine case, 13.8 kcal/mol, confirming the known preference of imines for a η^1 mode of coordination over the η^2 one. The relative barrier height for the hydride migration (**ts2a**) is only 3.9 kcal/mol, producing species **4a**, located at 21.8 kcal/mol on the potential energy surface. The intermediate **4a** is characterized by an agostic interaction with C−H and Ru−H distances of 1.185 and 1.987 Å, respectively. Finally, the proton transfer from the CpOH group to the iminic N atom has a relative barrier of 3.2 kcal/mol, giving the final product **5a**. This step is highly exothermic (60.6 kcal/mol) with a relative energy in the complete energy profile (Figure 3) of −38.8 kcal/mol.

As shown in Figure 3 the highest energy points in the complete gas-phase pathway are hydride and proton-transfer processes, having similar energies of 25.2 and 25.0 kcal/mol, respectively. Thus, the overall energy barrier is 38.8 kcal/mol (40.4 kcal/mol in solution). The energy profile is not significantly affected by considering solvent effects (THF); the differences are not higher than 5 kcal/mol. Both hydride and proton transfer show similar energy barriers in the gas phase and solution.

For the model system studied the relative energy values obtained by single-point CPCM calculations for **1a**, **2a'**, **4a**, and **5a** are −10.8, 8.7, 24.9, and −37.9 kcal/mol, respectively. In order to check the molecular model employed, the previous points were reoptimized in solution including the phenyl rings of the catalyst (complete catalyst), obtaining values of −8.6, 9.5, 25.5, and −37.2 kcal/mol, respectively. Thus, the full geometry reoptimization performed in solvent and taking the complete catalyst does not significantly change the results for this $\eta^5 \rightarrow \eta^2$ mechanism.

(33) Casey, C. P.; Singer, S. W.; Powell, D. R.; Hayashi, R. K.; Kavana, M. *J. Am. Chem. Soc.* **2001**, *123*, 1090–1100.

(34) Veiros, L. F. *Organometallics* **2000**, *19*, 5549–5558.

(35) Fan, H.-J.; Hall, M. B. *Organometallics* **2001**, *20*, 5724–5730.

(36) The reaction profile starting from structure **2a** was also analyzed. A new transition state, **ts2an**, analogous to **ts2a** was characterized. Nevertheless, this transition state is higher in energy compared to **ts2a** (27.5 vs 25.2 kcal/mol). A structure analogous to **3a** (labeled as **3an**) was also found for this pathway with a relative energy of 18.2 kcal/mol.

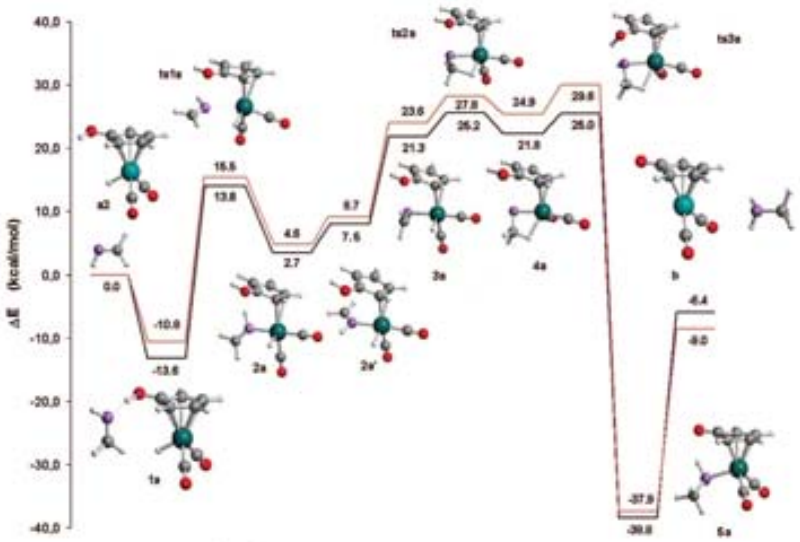

Figure 3. Energy profile for the stepwise $\eta^5 \rightarrow \eta^2$ ring-slippage mechanism of $H_2C{=}NH$ hydrogenation in the gas phase (blue) and solution (orange).

$\eta^6 \rightarrow \eta^5$ Concerted Mechanism. In the case of carbonyl hydrogenation and using an analogous model system, we reported a transition state structure for a concerted hydride and proton transfer with an η^3-CpOH coordination to the metal.[20] In the present case, however, we were unable to localize an analogous transition state for imine hydrogenation. This fact may suggest that for the model system, if existing, this mechanism would be too energy demanding to be a reasonable pathway, as we actually found in carbonyl hydrogenation, with a relative barrier height in the gas phase of 36.0 kcal/mol.[20]

This particular reaction mechanism, a concerted $\eta^5 \rightarrow \eta^3$ mechanism, has been already theoretically analyzed in detail by Privalov, Samec, and Bäckvall utilizing an imine with electron-donating groups and a complete catalyst model.[27] In their analysis, where solvent effects were included by a combination of explicit solvent molecules (CH_2Cl_2) and a polarized continuum method, they found that the highest energy barrier for this mechanism corresponds to the first step: the σ-bond imine coordination concomitantly to the $\eta^5 \rightarrow \eta^3$ CpOH ring slippage. Subsequently, they proposed a fast proton transfer followed by a slower hydride transfer. Finally, the $\eta^2 \rightarrow \eta^4$ ring slippage takes place. All the steps presented lower but quite similar activation barriers than the initial imine coordination. The authors showed that the inclusion of solvent effects stabilizes the low-hapticity complexes, and in fact, the lowest energy reaction barrier (15 kcal/mol) was obtained when explicit solvent molecules (along with the continuum model) were included in the calculations. According to their results, this could be a reasonable pathway for the reaction.

Outer-Sphere Mechanism. In the outer-sphere mechanism the hydrogenation takes place concertedly outside the coordination sphere of the metal. Figures 4 and 5 present the localized stationary points and the reaction energy profile, respectively.

The initial structure **1a** is 13.6 kcal/mol lower in energy compared to separated reactants, mainly due to a hydrogen-bond interaction. The concerted hydride and proton transfer (**ts1b**) has a relative barrier height of 11.0 kcal/mol (9.6 kcal/mol in solution). In the product (**2b**) the recently formed C−H bond is interacting with the Ru atom, whereas the aminic N−H bond is interacting with the recently formed C=O bond of the CpO ring.

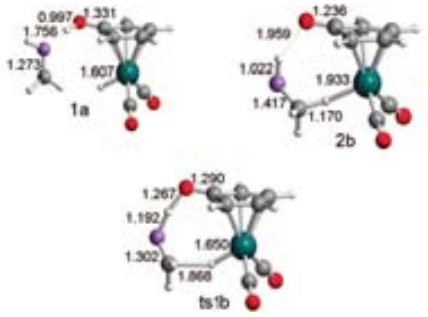

Figure 4. Optimized structures for the concerted outer-sphere mechanism of $H_2C{=}NH$ hydrogenation. Distances are in Å.

For the model imine the concerted hydrogen-transfer pathway is by far more favorable (11.0 kcal/mol) than the $\eta^6 \rightarrow \eta^2$ stepwise mechanism (38.8 kcal/mol).

Given the fact that the presence of the Ph groups on the aromatic ligands of the catalyst has been suggested to help the ring-slippage mechanism[27] and that this mechanism was already studied using a complete catalyst, we decided to investigate the concerted pathway employing also the complete catalyst.

When including phenyl rings in the catalyst, a concerted transition state was also found with a barrier height of 9.3 kcal/

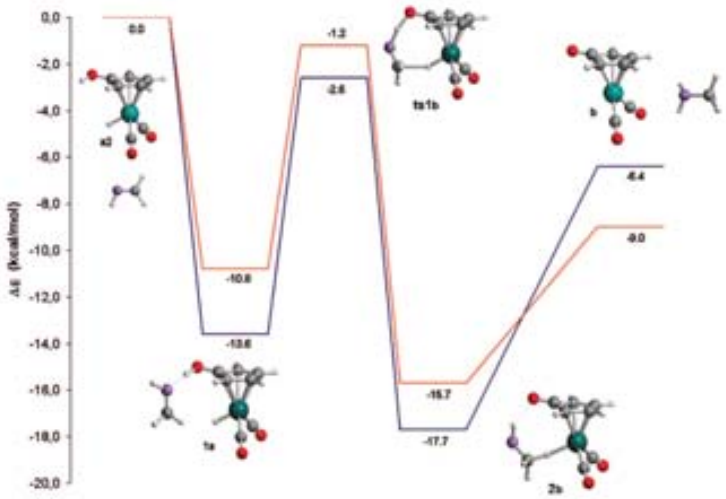

Figure 5. Energy profile for the concerted outer-sphere mechanism of $H_2C{=}NH$ hydrogenation in the gas phase (blue) and solution (orange).

mol in the gas phase. In this transition state, the proton is slightly more transferred to the substrate compared to the model system, having O−H (CpOH group) and N−H distances of 1.299 and 1.178 Å, respectively, whereas the hydride is slightly less transferred, with respective C−H and Ru−H distances of 1.898 and 1.646 Å, respectively. These results are analogous to those found in carbonyl hydrogenation, where the inclusion of the phenyl rings did not change significantly the energy profile of the concerted outer-sphere mechanism.[20] When single-point CPCM calculations are performed the energy barrier diminishes, taking a final value of 7.1 kcal/mol. In addition, in order to check whether performing the geometry optimization in solution changes the results, we reoptimized the complete catalyst within the CPCM methodology in THF. The energy barrier obtained (6.8 kcal/mol) does not change significantly with respect to the single-point solvent calculations. When comparing the transition-state geometry optimized in solution with respect to the gas phase one (values presented in parentheses), the geometrical trend is even more pronounced than that observed when including the phenyl rings in the model system. The proton is again in a more advanced stage (more transferred to the iminic nitrogen), whereas the hydride transfer is in an earlier stage (less transferred to the iminic carbon). The N−H bond and the O−H bond distances of the CpOH group are 1.084 (1.178) and 1.505 Å (1.299 Å), whereas the C−H and Ru−H bonds distances are 2.077 (1.898) and 1.642 Å (1.646 Å); values in parentheses are those of the model system in the gas phase. Thus, although the energy profile does not significantly change the geometry of the transition state, it does change when including the phenyl rings and optimizing in solution, resulting in a concerted but significantly asynchronic transition state. This geometrical trend observed when improving both the model and the methodology opens the door to a stepwise mechanism with an initial proton transfer followed by a hydride transfer for some particular systems.

In any case, according to all these results, the hydrogen transfer to imines will be through an outer-sphere mechanism. In order to check whether this conclusion is also valid for electron-donating imines, we calculated the energy profile for $(CH_3)_2C{=}N\text{-}CH_3$, taking the complete catalyst (including phenyl rings) and optimizing the structures in solvent (THF). On the basis of our results the outer-sphere mechanism is also the most favorable mechanism for this electron-rich imine, with energy barriers of 6.1 and 4.0 kcal/mol, in the gas phase and solution (optimizing geometries in both cases), respectively.

This result is consistent with that obtained by Casey and co-workers on a model system using $H_2C{=}N\text{-}CH_3$ as imine. They obtained a barrier height of 4.8 kcal/mol by performing single-point MP2 calculations over B3LYP-optimized geometries including solvent effects by means of the PCM method.[19a] The energy barrier for the outer-sphere mechanism is more than 10 kcal/mol lower in energy than the lowest barrier reported for the inner-sphere mechanism,[27] using a similar computational methodology (15.0 kcal/mol).

The presence of electron-donating groups increases the basicity of the imine. This could explain the advanced stage of the proton transfer to the nitrogen in the transition-state structure (**ts1c**). Concerning the hydride transfer, it is more transferred to the iminic carbon (see Figure 6). Thus, a mechanism involving stepwise proton transfer followed by hydride transfer would be also conceivable for the hydrogenation of electron-donating imines. The general conclusion from all these results is that for the hydrogen transfer to imines a concerted but asynchronic outer-sphere pathway is clearly favored over the inner-sphere mechanisms.

Alkyne and Alkene Hydrogenation. The Shvo catalyst is also active for hydrogenation of alkenes and alkynes. For alkene and ketone hydrogenation (at mainly 145 °C and 500 psi of H_2) Shvo reported turnover numbers of almost 2000 in most cases.[6a] Conversely, for alkyne hydrogenation the turnover numbers were only a few hundreds. The difference of reactivity between nonpolar and polar double bonds was also evaluated by Casey. The cyclohexene reduction by the tolyl analogue **A** (see Scheme 2) took place by heating to 80 °C under 1 atm of

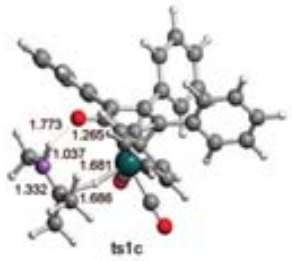

Figure 6. Transition state for the concerted outer-sphere mechanism of $(CH_3)_2C{=}N\text{-}CH_3$ optimized in solution (THF). Distances are in Å.

H_2, reaching only 5 turnovers in 24 h. Nevertheless, the hydrogenation of polar double bonds occurred below room temperature.[33]

Shvo found that alkene hydrogenation was not occurring by using HCO_2H as reducing agent.[10] In another study, Casey and co-workers found that a hydroxycyclopentadienyl ruthenium formate intermediate was not able to perform hydrogenation of benzaldehyde. Only after decarboxylation of the ruthenium formate intermediate was the tolyl analogue **A** formed, which is the active species of hydrogenation. On the basis of their observations, Casey and co-workers suggested that alkene hydrogenation may proceed involving initial loss of CO from the tolyl analogue **A**. Alkene insertion into the Ru−H bond and final cleavage of the H_2 molecule by the Ru-alkyl intermediate to produce the alkane were suggested as subsequent steps.[19]

Concerning alkyne hydrogenations, Shvo isolated by reaction of **1** with the alkyne $C_2(4\text{-Cl-Ph})_2$ an analogous species to the one depicted as **D** in Scheme 3.[9] Isostructural species with several alkynes were obtained and characterized using IR, NMR, and elementary analysis, obtaining also the X-ray crystallographic data for $C_2(4\text{-Cl-Ph})_2$. This species was found to be stable during hydrogenation conditions, its formation being irreversible.

The route that leads to this undesired product (**B** to **D** of Scheme 2) is computationally analyzed using the model catalyst and acetylene as alkyne. The energies in this case are referred to the dehydrogenated form of the catalyst (**b**) and acetylene. The coordination of the alkyne is exothermic by 17.2 kcal/mol and leads to intermediate **c**. The transition step that leads to **d** has a barrier height of 22.8 kcal/mol (23.4 kcal/mol in solution), and the formation of the species **d** is thermodynamically favored by 39.9 kcal/mol (34.8 kcal/mol in solution). We can compare the optimized **d** species with the X-ray diffraction geometry obtained by Shvo and co-workers. The alkyne is σ-bonded through both carbon atoms to the Ru and to the O of the CpO ring, respectively. The experimental Ru−C and C−O distances are 2.114(11) and 1.409(11) Å, respectively,[9] whereas the calculated ones are 2.083 and 1.396 Å, respectively. The X-ray C−C distance is 1.351(17) Å, whereas the calculated one is 1.338 Å, showing an excellent agreement.

The reaction of **1** with the dimethyl acetylenedicarboxylate $(C_2(CO_2Me)_2)$ alkyne gave the analogous complex to that depicted as **E** in Scheme 2.[9] This complex was identified within the catalytic cycle. This species is very stable thermodynamically; at 140 °C for 10 h in toluene it does not eliminate the alkene. Nevertheless, with 15 atm of hydrogen pressure at 110 °C in THF it gives back the initial complex **1** and dimethyl succinate (alkane). From these observations, Shvo and co-workers proposed the catalytic cycle shown in Scheme 2. Thus, the oxidative addition of the incoming H_2 molecule followed by a reductive elimination giving the final product and regenerating the catalyst was postulated for closing the catalytic cycle. For the case of alkenes, a similar mechanism was supposed to be operative. Thus, the mechanism for alkyne and alkene hydrogenation was computationally evaluated.

Scheme 4. Reaction Steps of the $\eta^5 \rightarrow \eta^2$ Stepwise Mechanism for Alkynes[a]

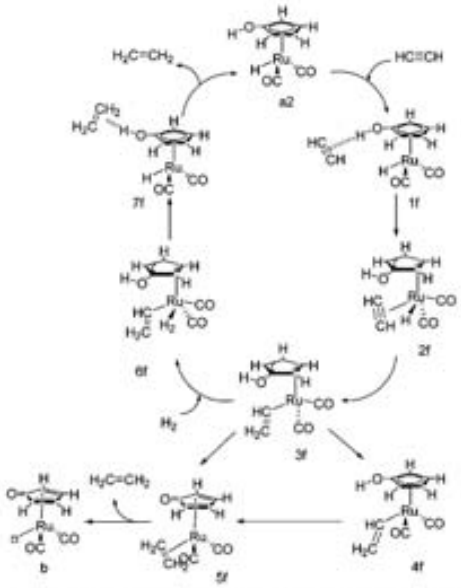

[a] A completely analogous mechanism is found for alkenes. In this case, the initial intermediate is **7f**.

Due to the small reported differences when including the phenyl groups and optimizing in solvent in imine hydrogenation, we studied alkene and alkyne hydrogenation with the simplified catalyst (without phenyl groups) and introducing solvent effects by means of single-point CPCM calculations.

$\eta^5 \rightarrow \eta^2$ Stepwise Mechanism for Alkyne and Alkene and Hydrogenation. The evaluation of this mechanism for both alkynes and alkenes shows that the minima and transition states are analogous to those found in the imine hydrogenation parent mechanism up to the first hydride migration. In the first step ($\eta^5 \rightarrow \eta^2$ ring slippage), however, both substrates become directly η^2-coordinated to the metal. The schematic representation of this mechanism for alkynes is depicted in Scheme 4. A completely analogous mechanism is found for alkenes.

The geometries of the transition states for $\eta^5 \rightarrow \eta^2$ CpOH ring slippage with substrate coordination and the subsequent hydride transfer are shown in Figure 7 for both alkyne (**ts1f**, **ts2f**) and alkene (**ts1g**, **ts2g**) hydrogenations. The relative energies for these mechanisms are shown in Table 1 for alkynes and in Table 2 for alkenes.

The $\eta^5 \rightarrow \eta^2$ ring slippage coupled with the corresponding substrate coordination is characterized by Ru−C distances of 2.839 and 2.757 Å in the case of acetylene. Concerning the

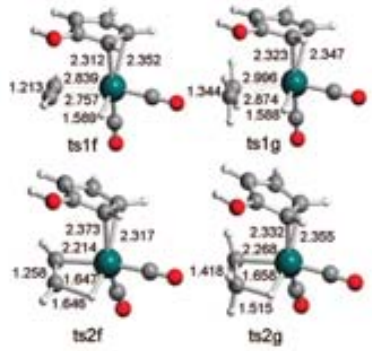

Figure 7. Transition states for the $\eta^5 \rightarrow \eta^2$ CpOH ring slippage and the hydride-transfer steps in alkyne (**ts1f** and **ts2f**, respectively) and alkene (**ts1g** and **ts2g**, respectively) hydrogenations. Distances are in Å.

Table 1. Computed Energies (in kcal/mol) of the $\eta^5 \rightarrow \eta^2$ CpOH Ring-Slippage Mechanism for Alkynes in the Gas Phase ($E_{\mathrm{GAS/VP}}$) and Solution (E_{THF})

	structure	$E_{\mathrm{GAS/VP}}$	E_{THF}
reactants	**a2** + **HC≡CH**	0.0	0.0
	1f	−6.0	−2.9
$\eta^5 \rightarrow \eta^2$ CpOH ring slippage	**ts1f**	21.8	23.4
	2f	19.7	21.2
hydride transfer	**ts2f**	27.6	29.4
η^2-CpOH alkenyl	**3f**	4.2	6.7
η^5-CpOH alkenyl	**4f**	−37.7	−35.2
proton transfer from the η^5-CpOH	**ts3f**	−3.4	−2.2
product of the proton transfer	**5f**	−49.8	−50.2
products 1	**b** + $H_2C{=}CH_2$	−27.3	−28.9
hydrogen complex	**6f**	−1.4	−0.5
H_2 σ-bond metathesis	**ts4f**	5.6	6.9
product of the H_2 σ-bond metathesis	**7f**	−58.6	−55.4
products 2	**a2** + $H_2C{=}CH_2$	−53.7	−53.8

Table 2. Computed Energies (in kcal/mol) of the $\eta^5 \rightarrow \eta^2$ CpOH Ring-Slippage Mechanism for Alkenes in the Gas Phase ($E_{\mathrm{GAS/VP}}$) and Solution (E_{THF})

	structure	$E_{\mathrm{GAS/VP}}$	E_{THF}
reactants	**a2** + $H_2C{=}CH_2$	0.0	0.0
	7f	−4.9	−1.6
$\eta^5 \rightarrow \eta^2$ CpOH ring slippage	**ts1g**	22.0	22.7
	2g	18.4	19.0
hydride transfer	**ts2g**	27.2	28.0
η^2-CpOH alkyl	**3g**	19.9	21.3
η^5-CpOH alkyl	**4g**	−18.0	−18.1
proton transfer from the η^5-CpOH	**ts3g**	25.0	25.0
proton transfer from the η^2-CpOH	**ts3g2**	52.9	54.9
product of the proton transfer	**5g**	−19.7	−18.5
products 1	**b** + $H_3C{-}CH_3$	−15.4	−17.7
hydrogen complex	**6g**	18.1	17.5
H_2 σ-bond metathesis	**ts4g**	24.7	24.5
product of the H_2 σ-bond metathesis	**7g**	−43.2	−41.3
products 2	**a2** + $H_3C{-}CH_3$	−41.8	−42.6

analogous step for ethene coordination the Ru−C distances present values of 2.996 and 2.874 Å. The transition states for the next step, the insertion into the Ru−H bond, are characterized by C−H distances of 1.646 and 1.515 Å in the case of alkynes (**ts2f**) and alkenes (**ts2g**), respectively.

The relative barrier height in the gas phase for the $\eta^5 \rightarrow \eta^2$ ring slippage coupled with the corresponding substrate coordination is 27.8 (**ts1f**) and 26.9 (**ts1g**) kcal/mol for acetylene and ethene, respectively. Concerning the hydride migration, there are no remarkable changes in the energetics between acetylene and ethene hydrogenations, presenting relatives barrier heights of 7.9 (**ts2f**) and 8.8 (**ts2g**) kcal/mol, respectively. The first remarkable difference comes from the energetics of **3f** and **3g** intermediates (4.2 and 19.9 kcal/mol, respectively), which are the intermediates after the hydride migration for alkynes and alkenes, respectively. In these intermediates, however, the coordinated species are quite different, an alquilidene in **3f** and an ethyl group in **3g**, respectively.

From this point, two different alternatives were found. According to the Shvo mechanism, next step corresponds to the addition of H_2. On the basis of the fact that the experimental analogue of **4f** (that corresponds to **E** in Scheme 2) produces **1** and the corresponding alkane under 15 atm of H_2 at 110 °C in THF, Shvo proposed one intermediate of Ru(IV) after the oxidative addition of one H_2 molecule. The transfer of one hydride was required to fully hydrogenate the substrate. The dihydride species with a formal Ru(IV) species could not be located in the potential surface energy; all the optimizations lead to a dihydrogen complex. Nevertheless, a different pathway involving a σ-bond metathesis of the H_2 molecule was found. We calculated this transition state, and it leads to the final product and regenerates the initial catalyst **a2**. This step is affordable with a relative barrier of 7.0 kcal/mol (**ts4f**) and 6.6 kcal/mol (**ts4g**) from the **6f** and **6g** intermediates for alkynes and alkenes, respectively. The σ-bond metathesis step gives rise to the final product and the regeneration of the initial catalyst (**a2**), a process greatly exothermic: 57.2 and 61.3 kcal/mol for alkynes and alkenes, respectively.

The other alternative consists in the proton transfer from the CpOH group to form the final product. This step can occur with or without previous change in the hapticity of the CpOH ring, changing from an η^2 to an η^5 coordination to the Ru atom. In the case of alkynes the change of hapticity is exothermic by 41.9 kcal/mol and the intermediate obtained (**4f**) is located at −37.7 kcal/mol in the energy profile. The analogous minimum in alkene hydrogenation (**4g**) is located at −18.0 kcal/mol in the energy profile, the change of hapticity being exothermic by 37.9 kcal/mol. The proton-transfer transition state from the η^5-coordinated CpOH ring intermediate (**ts3f**) is located at −3.4 kcal/mol in the energy profile, and it presents a relative barrier height of 34.3 kcal/mol. In the case of alkenes the related transition state is located at 25.0 kcal/mol (**ts3g**) with a relative barrier height of 43.0 kcal/mol. For alkynes this step is exothermic by 12.1 kcal/mol (**5f**), whereas for alkenes the process is almost isoenergetic (**5g**), being exothermic by only 1.7 kcal/mol. In contrast to polar double-bond hydrogenation, in carbon−carbon multiple bonds proton-transfer processes become highly energy demanding steps. This is reasonable taking into account the higher basicity of carbonyl and imine groups than that of the nonpolar double and triple bonds.

In acetylene hydrogenation only the proton transfer of the CpOH group from the **4f** intermediate was localized, where the CpOH ring is η^5 coordinated to the Ru. Conversely, in ethene hydrogenation the proton-transfer processes from both the η^2 and η^5 hapticities of the CpOH ring were analyzed.

Concerning alkene hydrogenation, the absolute energies of the transition states involving the η^5-CpOH proton transfer and the σ-bond metathesis of the H_2 molecule are quite similar (25.0 vs 24.7 kcal/mol). However, the relative barrier heights show that the σ-bond metathesis of the H_2 molecule is favored over the η^5-CpOH proton transfer (6.6 vs 43.0 kcal/mol). In Figure 8 are shown the transition-state geometries for the second hydrogenation step of alkenes and alkynes. These are the proton-

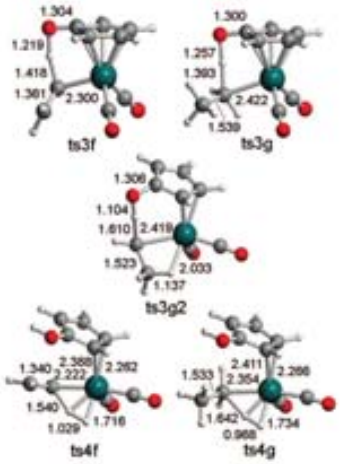

Figure 8. Transition states for the proton transfers from the CpOH ring for alkynes (**ts3f**, only η^5-CpOH ring) and alkenes (**ts3g**, **ts3g2**) and for the σ-bond metathesis of one incoming H_2 molecule for alkynes and alkenes, **ts4f** and **ts4g**, respectively. Distances are in Å.

transfer processes from the CpOH ring for alkynes (**ts3f**) and alkenes (**ts3g** and **ts3g2**) and the σ-bond metathesis of one incoming H_2 molecule (**ts4f** and **ts4g**).

This mechanism is related to that proposed by Shvo; the σ-bond metathesis makes sense within the $\eta^5 \rightarrow \eta^3$ stepwise mechanism because of the lower relative barrier height. Nevertheless, from the **4f** analogue the barrier is higher than for the η^5-CpOH proton transfer (by 9.0 kcal/mol in the gas phase). According to experimental results the analogue of **4f** is stable at 140 °C in toluene; this is supported by theoretical calculations because this species is very stable (−37.7 kcal/mol with respect to initial reactants), representing a clear well in the potential energy surface. Under H_2 pressure the substrate was completely reduced. These last observations are more according to the σ-bond metathesis mechanism than the η^5-CpOH proton transfer from the **4f** substrate.

The overall stepwise $\eta^5 \rightarrow \eta^7$ mechanism for alkyne hydrogenation presents a barrier height of 33.6 kcal/mol (32.3 kcal/mol in solution) corresponding to the steps from **1f** to **ts2f**. The highest point in the potential energy surface corresponds to the hydride transfer (**ts2f**). If the second hydrogenation process is the σ-bond metathesis of the H_2 molecule, the energy profile of the catalytic cycle is smoother than through the η^5-CpOH proton-transfer pathway, because in the last case the relative barrier height for the proton transfer is significantly higher (7.0 vs 34.3 kcal/mol in the gas phase), although lower than the hydride-transfer transition state (**ts2f**).

The stepwise $\eta^5 \rightarrow \eta^7$ mechanism in alkene hydrogenation presents a barrier height for the overall process of 30.1 kcal/mol (29.6 kcal/mol in solution), corresponding to the processes from **7f** to **ts2g** (hydride-transfer step).

Table 3. Relative Energies (in kcal/mol) in the Gas Phase (E_{RELVP}) and Solution (E_{THF}) for the Concerted Outer-Sphere Mechanisms of Alkyne and Alkene Hydrogenation

	structure	E_{RELVP}	E_{THF}
reactants	**a2** + HC≡CH	0.0	0.0
	1f	−6.0	−2.9
concerted transfer	**ts1d**	13.3	15.6
	2d	−31.2	−29.2
products	**b** + H_2C=CH_2	−27.3	−28.9
reactants	**a2** + H_2C=CH_2	0.0	0.0
	7f	−4.9	−1.6
concerted transfer	**ts1e**	14.5	16.3
	2e	−19.8	−18.6
products	**b** + H_2C−CH_3	−15.4	−17.7

The other possibility suggested by Casey for alkene hydrogenation,[18] which is initiated with the loss of one CO molecule, was not considered due to the highly reported energy value for the CO dissociation process.[21,37]

Outer-Sphere Mechanism for Alkyne and Alkene Hydrogenation. An analogous concerted outer-sphere mechanism localized for carbonyls and imines was also evaluated for alkynes and alkenes. The relative energies in both the gas phase and solution for the different intermediates of the concerted outer-sphere mechanism for alkyne and alkene hydrogenation are summarized in Table 3. For the alkynes, the barrier is significantly high, 19.3 kcal/mol (18.5 kcal/mol in solution), compared to polar double bonds, although it is the most feasible mechanism among those evaluated for the nonpolar multiple bonds. The related transition state (**ts1d**) is characterized by Ru−H and O−H distances of 1.672 and 1.041 Å, respectively, whereas the incoming C−H bonds are characterized by distances of 1.527 and 1.637 Å, respectively. These distances show a small variation of the catalyst structure when reaching the transition state; therefore, the proton of the CpOH group is less transferred than in polar double-bond hydrogenation. In Figure 9 are shown the transition states for the concerted outer-sphere mechanisms of alkyne (**ts1d**) and alkene (**ts1e**) hydrogenation.

Concerning the outer-sphere mechanism in alkene hydrogenation, the energy barrier is very similar to that of the alkynes, 19.4 kcal/mol (17.9 kcal/mol in solution). The related transition state (**ts1e**) is characterized by O−H and Ru−H distances of 1.101 and 1.727 Å, respectively, whereas the respective C−H distances are 1.514 and 1.401 Å.

These results show that the concerted outer-sphere mechanisms for alkynes and alkenes are around 10 kcal/mol higher in energy than the analogous ones in carbonyl and imine hydrogenations. This explains why polar double bonds react faster than multiple carbon−carbon bonds.

From all the results obtained for alkyne and alkene hydrogenation it can be concluded that the concerted outer-sphere mechanism is the most favorable pathway in both cases. Their relative barrier heights in the gas phase are 19.3 kcal/mol (18.5 kcal/mol in solution) and 19.4 kcal/mol (17.9 kcal/mol in solution), respectively. In alkyne hydrogenation, the formation

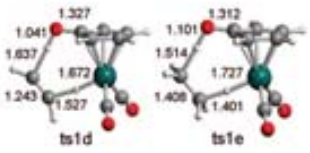

Figure 9. Transition states for the concerted outer-sphere mechanisms for HC≡CH (**ts1d**) and H_2C=CH_2 (**ts1e**) hydrogenations. Distances are in Å.

of **d** species proposed by Shvo can compete with the hydrogenation reaction, because of its relatively affordable energy barrier height of 22.8 kcal/mol (27.4 kcal/mol in solution) and the exothermicity of the process (−39.9 kcal/mol in the gas phase; −38.4 kcal/mol in solution).

Conclusions

The reaction mechanisms for the hydrogen tranfer to C=N, C=C, and C≡C bonds catalyzed by the Shvo catalyst have been extensively analyzed, complementing our previous theoretical study on the C=O hydrogenation.[20] Both suggested mechanisms, inner- and outer-sphere mechanisms, along with some variations have been computationally evaluated.

Our results show that the most favorable pathway for imine hydrogenation is the outer-sphere mechanism, which presents the lowest energy barrier of all the studied mechanisms. Similar results were previously found for the hydrogenation of carbonyls.[20] This conclusion is consistent independently of the selected system used for the calculations. Thus, calculations on a model catalyst and model imine in the gas phase show that the outer-sphere mechanism is the most feasible one with a barrier of 11.0 kcal/mol. The use of the complete catalyst (including the phenyl rings on the CpOH ligand) lead to the same conclusion (energy barrier of 9.3 kcal/mol). The effect of solvent, by means of both single-point calculations and geometry optimizations, is proven to be unremarkable (energy barriers of 7.1 and 6.8 kcal/mol, respectively). It should be noted, however, that the inclusion of solvent effects and phenyl rings (the latter to a minor extent) causes asynchronicity in the transition state, with the proton more transferred than the hydride. The same conclusions are found for the case of an imine with electron-donating groups: the energy profile obtained by geometry optimizations including solvent effects on the complete catalyst gives an energy barrier of 4.0 kcal/mol with an asynchronic transition state for the concerted outer-sphere mechanism. Thus, the energy barrier for the outer-sphere mechanism is lower than for the inner-sphere mechanisms in all the studied cases.

For multiple carbon−carbon bonds the most favorable hydrogenation mechanisms using the Shvo catalyst are also the outer-sphere mechanisms. Hydrogenation of nonpolar multiple bonds presents energy barriers approximately 10 kcal/mol higher than polar double bonds, having values of 18.5 and 17.9 kcal/mol for ethyne and ethene hydrogenations in solution, respectively. The difference between the outer-sphere mechanism and the most favorable inner-sphere mechanism is reduced in alkyne and alkene hydrogenation compared to those for polar double-bond hydrogenation. For the case of alkyne hydrogenation, the route proposed by Shvo that leads to catalyst deactivation has been calculated. On the basis of the relative energy barriers and the exothermicity of the process, this secondary reaction can compete with the hydrogenation reaction.

The energy differences for the outer-sphere mechanisms between polar double bonds and multiple carbon−carbon bonds agree with the observed chemoselectivity for polar double-bond hydrogenation over multiple carbon−carbon bond hydrogenation. According to these results, hydrogenation reactions of polar and nonpolar multiple bonds take place through an outer-sphere mechanism where the former substrates hydrogenate more easily, in agreement with experiment.

Acknowledgment. We are grateful to the Spanish MEC (Projects CTQ2005-09000-C02-01 and Consolider Ingenio 2010 CSD2007-00006, "Ramón y Cajal" contract to G.U. and FPU fellowship to A.C.-V.), as well as to the Generalitat de Catalunya (2005/SGR/00896).

Supporting Information Available: Complete ref 28, absolute energies, and Cartesian coordinates. This material is available free of charge via the Internet at http://pubs.acs.org.

OM700975K

(37) At high temperatures, this mechanism cannot be discarded.

Capítol 11

Article III

ARTICLE IN PRESS

Journal of Molecular Structure: THEOCHEM xxx (2009) xxx–xxx

Contents lists available at ScienceDirect

Journal of Molecular Structure: THEOCHEM

journal homepage: www.elsevier.com/locate/theochem

Mechanistic evaluation of metal-catalyzed hydrogen-transfer processes: The Shvo catalyst as an example of computational unravelling

Aleix Comas-Vives *, Gregori Ujaque, Agustí Lledós *

Unitat de Química Física, Departament de Química, Edifici Cn, Universitat Autònoma de Barcelona, 08193 Bellaterra, Catalonia, Spain

ARTICLE INFO

Article history:
Received 4 August 2008
Accepted 10 November 2008
Available online xxxx

Keywords:
Hydrogen-transfer processes
Mechanistic analysis
Theoretical calculations
Transition-metal complexes
Shvo catalyst

ABSTRACT

Hydrogen-transfer processes allow hydrogenation under mild conditions reaching high selectivity. They use readily available solvents such as 2-propanol instead of molecular H_2. The mechanism of these processes can be classified into: (a) Direct hydrogen-transfer or Meerwein–Ponndorf–Verley (MPV) reduction and (b) Hydridic route, with the formation of a metal-hydride species. The latter can be divided into both dihydride and hydridic routes depending on the catalytic species involved, a dihydride or a monohydride, respectively. Within the monohydridic route the reaction can go through an inner-sphere mechanism (with substrate coordination) or through an outer-sphere mechanism (without coordination to the metal substrate).

The proposed mechanisms for the hydrogen-transfer processes catalyzed by several metal complexes within the literature are reviewed, paying special attention to its computational analysis concerning the factors affecting the mechanism such as ligand lability and alkoxide stability. Afterwards, we focus on one of the most paradigmatic hydrogen-transfer processes catalyzed by the Shvo complex. It presents great versatility applied in a broad range of hydrogen-transfer processes to polar (ketones, imines) and non-polar (alkene, alkynes) bonds, and even successfully heterogenized by a sol–gel process.

© 2009 Elsevier B.V. All rights reserved.

1. Introduction

Hydrogen-transfer reactions are a prominent option of homogeneous hydrogenation mainly of polar double bonds (Scheme 1) [1–7]. They offer a green-chemistry alternative to the classical reduction methods ($NaBH_4$ and $LiAlH_4$). Moreover, there are other advantages over conventional hydrogenations, such as allowing mild reaction conditions reaching high selectivity or the use of hydrogen-donors different to hydrogen gas (usually alcohols) allowing a high concentration of the reductant avoiding mass transfer limitations.

Hydrogen-transfer processes are generally applied to polar double bonds (ketones and imines); the reduction of non-polar double and triple bonds using H_2 is generally performed using H_2 instead of transfer-hydrogenation processes, although some cases have been also reported for the latter [8–12]. Due to its reversibility, hydrogen-transfer processes have additional applications such as dynamic kinetic resolution [13–15].

Concerning hydrogen-transfer mechanisms, they are commonly classified in two groups: (a) direct hydride transfer from the donor to the acceptor species, (b) an indirect mechanism in which the hydride is transferred from the donor to the acceptor through a metal-hydride species. The first route (a) is the so-called Meerwein–Ponndorf–Verley (MPV) reduction [16–18]. The reverse process: dehydrogenative oxidation of alcohols with acetone is known as the Oppenauer oxidation (Scheme 2) [19]. This process is thought to occur through a six-membered transition-state via Lewis acid centers as depicted in the Scheme 2. Thus, Lewis acid centers are needed, typically aluminum 2-propoxides [20], for the MPV reduction in combination with 2-propanol as hydride-donor. Later, lanthanide salts were also found to catalyze the reaction [21,22].

The so-called hydridic route is the preferred one for metal complexes, where affinity for the hydride species is needed, though the MPV reduction has been also observed in some metal complexes [23,24]. In the hydridic route a hydride intermediate is formed prior to the final transfer to the acceptor group. Within the so-called hydridic route exists an additional classification depending on the metal intermediate formed within the catalytic cycle: a dihydride or a monohydride species (Scheme 3).

The dihydride route involves a formal oxidative addition of the metal center followed by a favourable reductive elimination. Conversely, the monohydride route is going through a heterolytic route [25–27], generating a monohydride intermediate. Afterwards, a hydride and a proton are transferred to the acceptor group from the monohydride intermediate and a proton-donor (HX),

* Corresponding authors.
E-mail addresses: alexis@klingon.uab.cat (A. Comas-Vives), agusti@klingon.uab.es (A. Lledós).

0166-1280/$ - see front matter © 2009 Elsevier B.V. All rights reserved.
doi:10.1016/j.theochem.2008.11.043

Please cite this article in press as: A. Comas-Vives et al., J. Mol. Struct. (THEOCHEM) (2009), doi:10.1016/j.theochem.2008.11.043

Scheme 1. Hydrogen-transfer process.

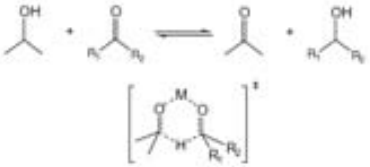

Scheme 2. Metal-catalyzed hydrogen-transfer between ketones and 2-propanol through the Meerwein–Ponndorf–Verley (MPV) reduction.

respectively. If the proton comes from a metal ligand, then the bifunctional catalyst term is used [6]. In Scheme 4, there are some examples of metal-ligand bifunctional catalysts [6,28–35].

The ionic hydrogenation term has been also used for the systems where a proton and a hydride are transferred [36,37]. The proton can come from a metal-cationic dihydride followed by the hydride transfer from the neutral hydride complex and final regeneration of the dihydride through the oxidative addition of molecular H_2. The proposed mechanism for catalytic ionic hydrogenation of ketones is shown in Scheme 5. Although in ionic hydrogenation molecular H_2 is the hydrogen source, the so-called bifunctional catalysts (where a ligand acts as proton-donor) have been also referred as ionic hydrogenation: because H_2 is considered as the sum of H^+ and H^- [36,37].

The monohydridic route has been suggested to go through two different pathways: an inner-sphere pathway where the substrate is coordinating to the metal followed by hydride-transfer, or an outer-sphere pathway where the mechanism is concerted without coordination of the substrate to the metal. For the inner-sphere mechanism a vacant site is needed within the coordination sphere of the metal center to allow substrate coordination, that it is not a requirement for the outer-sphere mechanism (see Scheme 6).

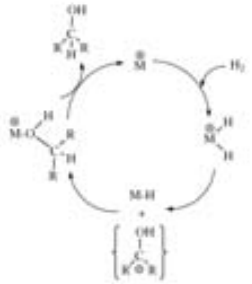

Scheme 5. Proposed mechanism for catalytic ionic hydrogenation of ketones.

Scheme 6. (a) Inner-sphere and (b) outer-sphere mechanisms for ketone hydrogenation within the hydridic route.

The aim of this paper is to review the proposed mechanisms for the hydrogen-transfer process catalyzed by several metal complexes and their theoretical analysis and characterization. We then focus on the Shvo catalyst, one of the most paradigmatic catalysts due to its great versatility. There has been an enormous controversy about the mechanism and here it is shown how computational analysis can help unravelling the mechanism.

2. Meerwein–Ponndorf–Verley (MPV) reduction

This mechanism consists in the direct hydrogen-transfer between the donor and the acceptor (Scheme 2). This mechanism

Scheme 3. (a) Dihydridic route and (b) monohydridic route. Metal complex (M), donor group (DH_2), acceptor group (A), proton donor (HX).

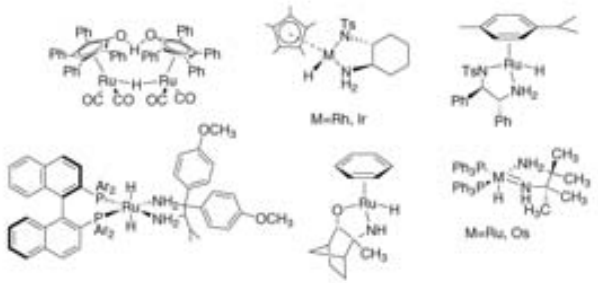

Scheme 4. Examples of metal-ligand bifunctional catalysts.

Please cite this article in press as: A. Comas-Vives et al., J. Mol. Struct. (THEOCHEM) (2009), doi:10.1016/j.theochem.2008.11.043

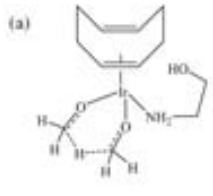

Scheme 7. Direct hydrogen-transfer transition-states for the (a) Ir(COD)(amino alcohol) and (b) Ir(COD)(amino sulfide) complexes.

has been mainly proposed for systems with aluminum and lanthanides and for some particular transition-metal systems.

For the case of the hydrogen-transfer to ketones using Ir(COD)(aminoalcohol) and Ir(COD)(aminosulfide) complexes Handgraaf and co-workers proposed that the mechanism occurs through the direct hydrogen-transfer mechanism based on BLYP calculations [23]. Formaldehyde coordinates to the Ir methoxide complex and subsequently a methyl hydride is exchanged between the methoxide and the formaldehyde species. For both Ir complexes the formaldehyde coordination is endothermic by 1–3 kcal/mol whereas the subsequent hydride exchange proceeds via an energy barrier of 24 and 19 kcal/mol for the Ir aminoalcohol and aminosulfide complexes, respectively (see Scheme 7).

The MPV mechanism for Ru(arene)(aminoalcohol) complex was also analyzed through DFT calculations [38], obtaining an energy barrier of 36.6 kcal/mol. This transition-state presented an η^2-coordination of the arene ring in order to allow the coordination of both donor and acceptor groups. Due to this high reported barrier this mechanism was unlikely for this complex. Finally, the complex was found to go through the monohydridic route (vide infra).

The MPV mechanism was also evaluated for the carbonyl reduction through the $RhH(C_2H_4)_2[N(CH_3)_3]_2$ system in order to explain the absence of enantioselectivity when tertiary amine ligands are within the coordination sphere in comparison with primary and secondary ones. The MPV reduction energy barrier was found to be 22 kcal/mol by theoretical methods, involving an inner-sphere mechanism [39]; this proposal could explain the experimental absence of enantioselectivity for tertiary amines [24].

3. Monohydridic and dihydridic routes

One of the most famous hydrogen-transfer systems which proceed through a hydridic route is the Wilkinson catalyst [40–42]. Although this catalyst is typically used for C=C hydrogenation, it can also be used in C=O bond hydrogenation, such other Rh systems [43]. The Wilkinson catalyst has the particularity that its pathway depends on the hydrogen source; proceeding through a dihydridic pathway when using molecular H_2 [44] and a monohydridic pathway when using 2-propanol (for the latter see Scheme 8) [45].

After generation of the monohydridic active catalytic species $(PPh_3)_3RhH$, the carbonyl species is coordinated forming an alkoxide by the insertion of the C=O bond into the Rh–H bond (or hydride migration). A β-elimination regenerating the initial catalyst closes the catalytic cycle. Catalysts operating through this mechanism are quite common containing different metal centers such as Rh, Mo, Ir and Ru. For instance: $(bipy)_2Rh_2Cl_2$, the precursor of the previous $(PPh_3)_3RhH$, $(PPh_3)_3RhCl$, $Mo_2(OH)_2Cp_4$, $[Ir(COD)(bipy)]BF_4$, $Ir_2Cl_2(dppp)_2$, $Ir(COD)(bipy)]BF_4$ and $[Ir(COD)(dppp)]BF_4$ [45–47].

An example of the dihydride mechanism is the $RuCl_2(PPh_3)_3$ catalyst. The proposed active catalytic species $RuH_2(PPh_3)_3$ is generated by the addition of a base (Scheme 9) [48]. The catalytic cycle starts by ketone coordination with the subsequent alkoxide

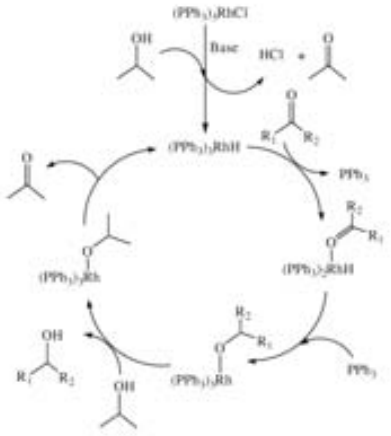

Scheme 8. Monohydridic route proposed for the carbonyl hydrogenation using the Wilkinson catalyst $(RhCl(PPh_3)_3)$.

formation, alcohol exchange and final β-elimination, regenerating the dihydride species. In this case, the monohydridic species $RuHCl(PPh_3)_2$ was found to be inactive. Theoretical calculations showed that the thermodynamics of the hydride migration step was more favoured for the dihydridic complex than for the monohydridic one, being exothermic for the former (1.3 kcal/mol) and endothermic for the latter (5.3 kcal/mol) [48]. Another complex that has been proposed to operate through the dihydridic route is the $Ru(diamino)Cl_2(PPh_3)_2$ complex [45].

Bäckvall and co-workers developed an ingenious experiment in order to distinguish between the dihydridic and the monohydridic routes. This is to racemize an optically active α-deuterated alcohol. If the dihydridic route is occurring the deuterium will be scrambled between carbon and oxygen atoms whereas if the monohydridic route is taking place the deuterium will end up in the α position of the racemized alcohol [3,45].

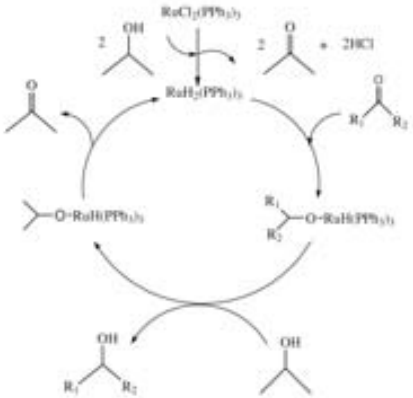

Scheme 9. Proposed catalytic cycle for the hydrogenation of ketones by $RuCl_2(PPh_3)_3$ complex.

Please cite this article in press as: A. Comas-Vives et al., J. Mol. Struct. (THEOCHEM) (2009), doi:10.1016/j.theochem.2008.11.043

4. Monohydridic routes: inner-sphere vs. outer-sphere mechanisms

4.1. Inner-sphere mechanism

The inner-sphere mechanism requires the coordination of the substrate to the metal center. In the pioneering work by Noyori the $[RuCl_2(\eta^6\text{-benzene})]_2$ complex, *N*-tosylethylenediamine or ethanolamine, and KOH was developed as a catalyst for the hydrogen transfer between alcohols and carbonyl compounds [6,49,50]. The use of chiral amine auxiliaries promotes asymmetric transformation. The computational study on the insertion mechanism for the Ru(η^6-benzene)($NHCH_2CH_2Y$) (Y=O, NH) family of complexes also involving ring slippage allowing substrate coordination (inner-sphere mechanism). Surprisingly, B3LYP calculations tend to give η^2-coordinated intermediates, whereas MP2 results favour η^4-coordinated geometries. The highest relative energy barrier was of 19.2 kcal/mol at MP4 level, corresponding to the final proton-transfer to the alkoxide intermediate. This high barrier is due to the great stability of the alkoxide intermediate. Conversely, at the B3LYP level, the highest energy barrier was substrate coordination, presenting an activation energy of 20.9 kcal/mol [51]. Similar conclusions for analogous systems were raised by other authors [38].

Handgraaf and co-workers analyzed the inner-sphere mechanism for the Ir(COD)amino alcohol, Ir(COD)amino sulfide and Ru(arene)amino alcohol complexes in the transfer hydrogenation among alcohols and ketones. In the case of the ruthenium complex the insertion mechanism (as well as the direct hydride transfer) required $\eta^6 \rightarrow \eta^2$ partial decoordination of the strongly bounded benzene ring. In contrast, for the iridium complexes the alcohol/sulfide part of the hemilabile amino alcohol/amino sulfide ligand decoordinates relatively easily allowing the coordination of the carbonyl species. The energies were referred to the metal-alkoxide intermediates, being the most stable species within the catalytic cycle. For the ruthenium complex the highest energy barrier found is 30 kcal/mol whereas for both Ir(COD)(amino alcohol), Ir(COD)(amino sulfide) complexes the energy barriers are 26 and 30 kcal/mol, respectively.

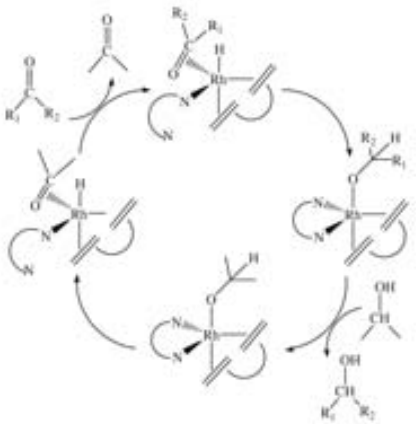

Scheme 10. Proposed catalytic cycle for ketone hydrogenation with Rh(COD)(diamine)hydride complexes.

In a recent computational study of the reaction mechanism of Ir-catalyzed alkylation of primary amines with primary alcohols the initial and final steps were alcohol dehydrogenation to aldehyde and imine hydrogenation to amine. For the dehydrogenation of the alcohol and the reduction of the imines an inner-sphere mechanism through coordination of the metal center for both substrates (the alcohol and the imine) was proposed [52].

Concerning Rh(COD)(diamine)hydride complexes, the inner-sphere mechanism was analyzed. The substrate coordination takes place by the previous decoordination of an amine ligand (Scheme 10). The subsequent hydride migration has a relative energy barrier of 6–9 kcal/mol depending on the substrate. Next steps involving amine recoordination, alcohol exchange and amine decoordination to leave a vacant site were found to take place easily. The β-elimination step was forming the final carbonyl species regenerating the hydride, being the rate-limiting one with a relative energy barrier of 23.6 kcal/mol due to the high stability of the previous alkoxide intermediate [53].

In a subsequent paper [39] the same authors analyzed a mechanism proposed by Gladiali et al. [54] where the hydride-transfer occurs concomitantly with ketone coordination. The second step is an exchange with 2-propanol, followed by the reverse reaction of the first step, leading to the regeneration of the hydride complex. This mechanism, on the basis of the obtained reaction barriers was found to be unrealistic.

The $[RuH(i\text{-}PrOH)(CH_3\text{–}CONH)(CO)(PCy_3)_2]$ catalyst is able to perform ketone and imine hydrogenations. For this catalyst, initial PCy_3 dissociation was proposed due to the observed competitive rate-inhibition by added PCy_3 and the hydrogen-transfer could proceed after coordination of the substrate to the metal through fast stepwise proton and hydride-transfer on the basis the observation of inverse kinetic isotope effects (KIEs) [55].

4.2. Outer-sphere mechanism

In an outer-sphere mechanism the hydrogen-transfer takes place concertedly without the ligand coordination to the metal center. For the case of Ru(η^6-benzene)($NHCH_2CH_2Y$) (Y=O, NH) family of complexes according to the obtained energy profiles the balance for the outer-sphere mechanism was significantly more favourable than for the inner-sphere one. The reported energy barrier for the outer-sphere mechanism was of 15.8 kcal/mol for the H_2C=O substrate [51]. In their work Noyori and co-workers also analyzed the concerted outer-sphere mechanism in the hydrogenation of unsaturated species such as C=N and C=C bonds by analyzing CH_2=NH and CH_2=CH_2 as model substrates. The relative activation energies were 26.9 and 26.7 kcal/mol, respectively. This observed chemoselectivity [56] agreed with the experimental observations in transfer-hydrogenation with this catalyst [57,58]. Based on the concerted outer-sphere mechanism in a subsequent study the origin of enantioselectivity was assigned not only to the chiral ligand but to CH/π interaction [59]. Andersson and co-workers found similar conclusions about the concerted outer-sphere mechanism in carbonyl hydrogenation catalyzed by an analogous system; this mechanism was the most favourable one, with an activation energy of 12.9 kcal/mol by means of the B3PW91 functional [38]. The work by Andersson among others [60] allowed the rationalization of the enantioselectivity through the concerted outer-sphere mechanism. Casey and co-workers also proposed that carbonyl hydrogenation with the Ru(η^6-arene)TsDPEN complex was going through a concerted outer-sphere mechanism, where the hydride and the proton were transferred concertedly going through a six-membered transition-state based on KIEs (Scheme 11) [61]. Ru(η^6-arene)H($NH_2CHPhCHPhNHTs$) was also proposed to hydrogenate imines by the metal-ligand bifunctional outer-sphere mechanism [62]. The concerted outer-

Please cite this article in press as: A. Comas-Vives et al., J. Mol. Struct. (THEOCHEM) (2009), doi:10.1016/j.theochem.2008.11.043

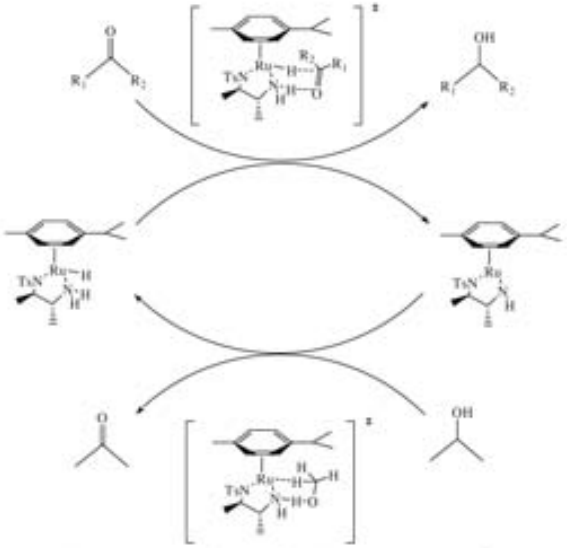

Scheme 11. Concerted outer-sphere mechanism for the transfer-hydrogenation using the Ru(η⁶-arene)TsDPEN complex.

sphere mechanism has been also proposed for Ru(diphosphine)(diamine) complexes reporting very favourable energy profiles for the hydrogen-transfer ketone/alcohol reaction [6]. A systematic study with a different set of density functionals has been also performed raising energy barrier heights relatively small (4 kcal/mol at the most) [63]. The origin of the enantioselectivity was also rationalized through this reaction mechanism [64–66].

For Rh(COD)(diamine)hydride complexes, a concerted transfer of both the hydride and a proton present on the amine ligand (Noyori-like) was very probable (3.9–5 kcal/mol) in the hydrogenation process and the subsequent and reverse process in order to complete the hydrogen-transfer process was the rate-limiting step with an energy barrier height of 18.7 kcal/mol. Thus, it was the preferred one for primary and secondary amines. Moreover, it could explain the observed enantioselectivity [24].

For the successive hydrogenation of the CN triple bond and then the CN double bond of the intermediate imine (benzonitrile to benzylamine) by proton and hydride transfer from a trans dihydride ruthenium complex P–NH–NH–P tetradentate ligands catalyst the concerted outer-sphere mechanism was also proposed on the basis of both experimentally and theoretically results [67].

Finally, the catalyst $IrH_3[(iPr_2PC_2H_4)_2NH]$ developed by Abdur-Rashid and Morris [68] was modeled as $IrH_3[(Me_2PC_2H_4)_2NH]$ [69] in order to study the hydrogen-transfer process with 3-pentanone and 2-propanol as hydrogen-acceptor and donor, respectively. A feasible mechanism was again obtained for the concerted outer-sphere mechanism.

4.3. The Shvo catalyst

The Shvo catalyst is one of the most paradigmatic hydrogen-transfer catalysts due to its great versatility. It is able to hydrogenate polar (ketones, imines) and non-polar bonds (alkenes, alkynes) and can use H_2 or alcohol (usually isopropanol) as hydrogen source [28,29,70]. Its versatility comes from the equilibrium

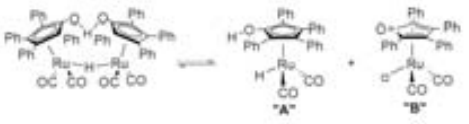

Scheme 12. Equilibrium of the Shvo catalyst.

shown in Scheme 12 generating two structures able to perform hydrogenation and oxidation, "A" and "B" in the same Scheme, respectively. The applications in hydrogen-transfer processes are broad: hydrogenation of carbonyls [71], imines [72], alkynes [73], oxidation of alcohols [74] and amines [75,76] dynamic kinetic resolution of secondary alcohols [13,14] and primary amines [15] in combination with lipases, etc. Moreover, it has been synthesized a heterogeneous version of the Shvo complex by a sol–gel process, being recoverable and reusable catalyst for the efficient dehydrogenation of alcohols [77].

The mechanism of the Shvo's catalyst has been one of the most controversial regarding the nature of the hydrogen-transfer. The inner- and outer-sphere dichotomy in polar double bond hydrogenation of C=O [78–80] and C=N functional group is commonly found in the recent literature [81–88]. In addition to experimental work, theoretical calculations were fundamental in studying the process, including also some controversy. In the next subsections are presented the mechanistic studies for the hydrogenation of ketones, imines and alkenes alkynes, respectively.

4.4. Hydrogenation of ketones

The experimental work done by Casey's group analyzing the primary deuterium isotope effects on the hydrogenation of PhCHO using the tolyl analogue of the Shvo catalyst $[2,5\text{-}Ph_2\text{-}3,4\text{-}Tol_2(\eta^5\text{-}C_4OH)][Ru(CO)_2H$ concluded that carbonyl hydrogenation was

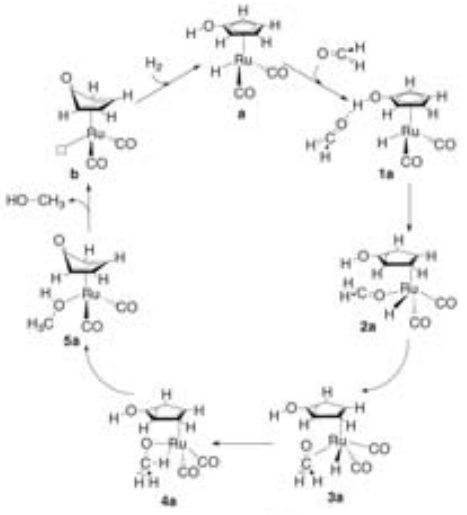

Scheme 13. Reaction steps of the stepwise $\eta^5 \rightarrow \eta^2$ ring slippage mechanism for the hydrogenation of ketones.

going through a concerted outer-sphere mechanism [78]. The work by Bäckvall's group also supported a concerted mechanism, though taking place via an inner-sphere mechanism involving $\eta^5 \rightarrow \eta^3$ ring slippage [79].

The inner-sphere and outer-sphere mechanisms were compared for the Shvo catalyst by means of the B3LYP functional both in the gas phase and solution (CPCM calculations) [80]. In that work, several reaction mechanisms were analyzed. The first one involves the CO ligand leaving from the Ru coordination sphere. The high energy reported for this process; 51.2 kcal/mol in the gas phase and 45.7 kcal/mol in solution (THF) led the authors to discard this mechanism. Concerning the energy of the substitution of one CO ligand by formaldehyde, it was found to be 26.8 kcal/mol in the gas phase and 23.8 kcal/mol in THF. This was in agreement with the Casey and co-workers observance that the exchange of a CO by one ^{13}CO molecule was very slow unless the reaction took place under fluorescent light [78].

Another mechanism investigated by Comas-Vives et al. [80] involves the ring slippage of the CpOH ligand thus generating a vacant site to coordinate the substrate. In this sense, Crabtree found that ligand exchange took place through ring slippage of the substituted Cp ring in related $(C_5H_4Ph)IrHL_2$ complexes [89]. The computational analysis of the ligand exchange on other metal complexes showed the η^2 was the most favourable coordination mode [90]. For the Shvo catalyst previous proposals suggested the η^3 ring slippage was taking place [73,74,79]. Computational analysis, however, could only find the related η^2 intermediate. The same was observed for transition-states of the ligand coordination step [91]. In Scheme 13 it is shown the $\eta^5 \rightarrow \eta^2$ CpOH ring slippage mechanism. This mechanism starts with the $\eta^5 \rightarrow \eta^3$ CpOH ring slippage concomitantly with η^1 ketone coordination (**2a** intermediate). Changing the coordination mode of the ketone from η^1 to η^2 facilitates the hydride and proton transfers, releasing the final product, methanol.

The resulting energy profile both in the gas phase and solution it is shown in Fig. 1, with an overall barrier height of 33.0 kcal/mol in solution corresponding to the ring slippage (from **1a** to **ts2a**). The highest transition-state in energy corresponds to the hydride-transfer step.

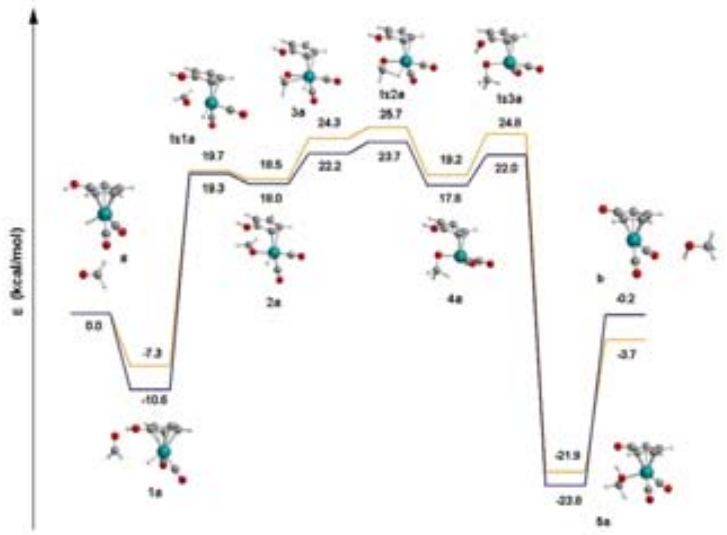

Fig. 1. Energy profile for the stepwise $\eta^5 \rightarrow \eta^3$ ring slippage mechanism at B3LYP level in gas phase (blue) and solution (orange) for the hydrogenation of ketones. (For interpretation of the references to colour in this figure legend, the reader is referred to the web version of this article.)

Please cite this article in press as: A. Comas-Vives et al., J. Mol. Struct. (THEOCHEM) (2009), doi:10.1016/j.theochem.2008.11.043

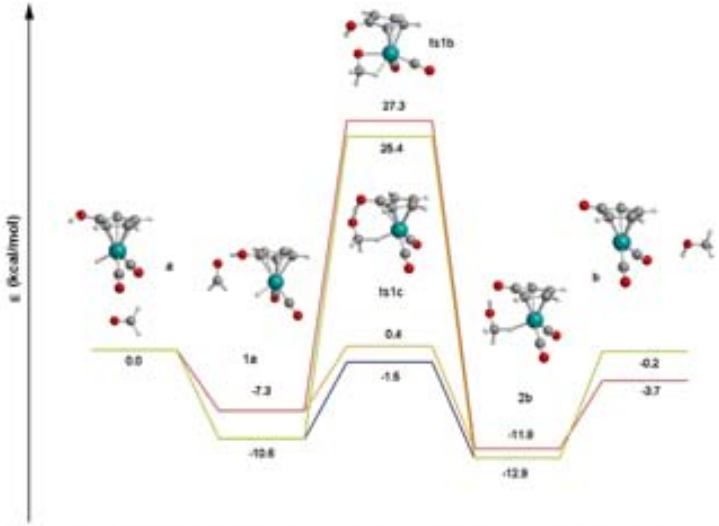

Fig. 2. Energy profiles for both concerted pathways at B3LYP level for the hydrogenation of ketones. Inner-sphere mechanism: green (gas phase) and red (solution), respectively. Outer-sphere mechanism: blue (gas phase) and orange (solution) respectively. (For interpretation of the references to colour in this figure legend, the reader is referred to the web version of this article.)

On top of the two previous mechanisms, the same authors were able to find another inner-sphere mechanism. In this case, the $\eta^5 \rightarrow \eta^3$ ring slippage takes place concertedly to the hydride and proton transfers. This was the only case when a $\eta^5 \rightarrow \eta^3$ pathway could be theoretically characterized for C=O reduction. The energy barrier for this pathway in solution is 34.6 kcal/mol (Fig. 2).

The outer-sphere mechanism with the concerted H^+ and H^- transfer was also investigated (Scheme 14). The energy barrier in solution is 7.7 kcal/mol, therefore presenting by far the most favourable energy pathway among those theoretically evaluated (Fig. 2). In a previous theoretical work Casey and Cui reported an energy barrier of 13.8 kcal/mol for a very similar theoretical model and computational level [81]. The energy values obtained agreed well with the experimental values for the reduction of PhCHO in THF-d_8: $\Delta H^{\ddagger} = 12.0 \pm 0.5$ kcal/mol using the Shvo tolyl analogue [78] and $\Delta H^{\ddagger} = 11.2 \pm 0.9$ kcal/mol for the analogous process in dry THF-d_8 [92].

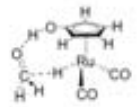

Scheme 14. Concerted outer-sphere mechanism for carbonyl hydrogenation by using the Shvo's catalyst.

The influence of the phenyl groups was also theoretically considered by performing calculations including these substituents in the CpOH ring of the catalyst. No significant differences were observed neither in the $\eta^5 \rightarrow \eta^2$ CpOH ring slippage mechanism nor in the concerted outer-sphere one. The energy barrier height for the concerted outer-sphere mechanism with the complete catalyst (including the phenyl rings) was 8.0 kcal/mol in solution. The related transition-states for both the model and the complete catalyst for the outer-sphere mechanism are depicted in Fig. 3.

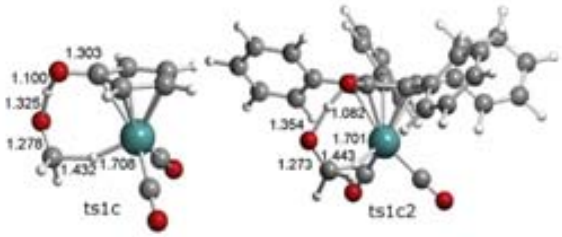

Fig. 3. Related transition-states for the concerted outer-sphere mechanisms both in the model (**ts1c**) and complete (**ts1c2**) Shvo catalysts for the hydrogenation of ketones. Distances in Å.

Please cite this article in press as: A. Comas-Vives et al., J. Mol. Struct. (THEOCHEM) (2009), doi:10.1016/j.theochem.2008.11.043

Theoretical calculations of KIEs for the concerted outer-sphere mechanisms were also in agreement with experimental values. Casey reported combined KIEs by deuterating the Ru–D and C–D bonds of the Shvo tolyl analogue (where two phenyl groups were substituted by two tolyl groups). In a first work they obtained a KIE of 3.6 ± 0.3 in the presence of a small amount of water [78] whereas they obtained a KIE of 3.38 ± 0.19 in dry THF [92] among other values in different solvents. In both cases the combined KIE was very similar to the product of the individual KIEs of the Ru–D and O–D bonds. Bäckvall reported the KIEs on the reverse process (dehydrogenation) of 1-4(fluorophenyl)ethanol by the Shvo catalyst with a combined isotope effect of 4.61 ± 0.37 and individual KIEs of 1.87 ± 0.17 and 2.57 ± 0.26 for the rupture of O–H and C–H bonds of the alcohol, respectively [79]. KIEs were also theoretically evaluated by free energy calculations from initial reactants and the corresponding transition states for the evaluated reaction mechanisms. The one which was more resembling to the experimental value was the concerted outer-sphere one with a KIE value of 3.8. The calculated KIE for the concerted inner-sphere mechanism was 0.8 [80].

In summary, the feasibility of the concerted outer-sphere mechanism is supported by presenting the lowest energy barrier among all the studied mechanisms and the closest calculated KIEs to those obtained experimentally.

4.5. Hydrogenation of Imines

For the hydrogenation of imines by the Shvo catalyst, the analogous inner- [86,87] and outer-sphere mechanisms have been also theoretically investigated [88].

The inner-sphere mechanism involving the $\eta^5 \rightarrow \eta^2$ CpOH ring slippage presents an energy profile like that shown in the Fig. 4. This mechanism is analogous to the one analyzed for ketones with an initial $\eta^5 \rightarrow \eta^2$ CpOH ring slippage of an energy barrier height of 26.3 kcal/mol in THF. The resulting minimum presents a η^1 coordination of the imine to the Ru atom with a relative energy of 4.6 kcal/mol in solution. Next step involves a change in the coordination mode of the imine from η^1 to η^2 facilitating the subsequent hydride and proton-transfer steps to the iminic carbon and nitrogen, respectively. Both steps have the highest transition-state energy values at 27.8 and 29.6 kcal/mol in solution, respectively.

The inclusion of the phenyl rings of the CpOH ligand in the model and reoptimizing the structures in solution for the $\eta^5 \rightarrow \eta^2$ mechanism did not modify the energies for some selected intermediates of the energy profile. These new values for **1d'**, **2d''**, **4d'**, **5d'** are −8.6, 9.5, 25.5 and −37.2 kcal/mol, respectively. These results are analogous to those obtained by single point CPCM calculations on the model system, with energy values of −10.8, 4.6, 24.9 and −37.9 kcal/mol, respectively.

The $\eta^5 \rightarrow \eta^3$ concerted inner-sphere mechanism was computationally analyzed by Bäckvall and Privalov for an electron-donating imine and using the complete catalyst (including the phenyl rings) for theoretical calculations [86,87]. In their study the solvent was taken into account by including explicit CH_2Cl_2 molecules and a polarized continuum method. The authors proposed a $\eta^5 \rightarrow \eta^3$ CpOH ring slippage coupled with an η^1 imine coordination, a fast proton-transfer followed by hydride-transfer and a final $\eta^2 \rightarrow \eta^4$ ring slippage. All the steps presented similar energy barriers with an overall energy barrier of 15 kcal/mol [87].

The concerted outer-sphere mechanism was evaluated by Comas-Vives et al. [88] obtaining an energy barrier height of 9.6 kcal/mol in solution for the model system (**ts1e** of the Fig. 5). The inclusion of the phenyl rings on the chemical model along with the optimization in solution slightly decreased the energy barrier height to 6.8 kcal/mol (**ts1e2** of the Fig. 5). Thus, on the basis of these results, the concerted outer-sphere mechanism is more favourable than any of the inner-sphere evaluated mechanisms. The transition-state for the outer-sphere mechanism shows certain degree of asynchronicity: the proton was relatively more transferred to the iminic nitrogen atom than the hydride to the iminic carbon atom.

In order to check if the concerted outer-sphere mechanism is also the operating one for electron-donating imines ($(CH_3)_2C{=}N{-}CH_3$),

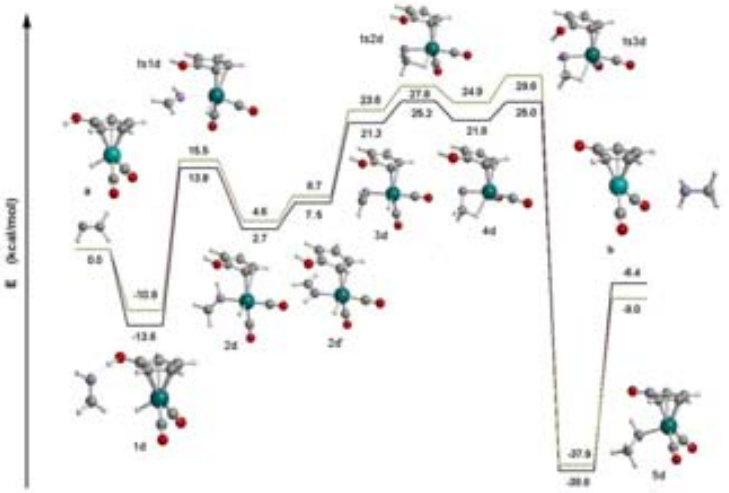

Fig. 4. Energy profile for the stepwise $\eta^5 \rightarrow \eta^3$ ring slippage mechanism of imine hydrogenation at B3LYP level in gas phase (blue) and solution (orange). (For interpretation of the references to colour in this figure legend, the reader is referred to the web version of this article.)

Please cite this article in press as: A. Comas-Vives et al., J. Mol. Struct. (THEOCHEM) (2009), doi:10.1016/j.theochem.2008.11.043

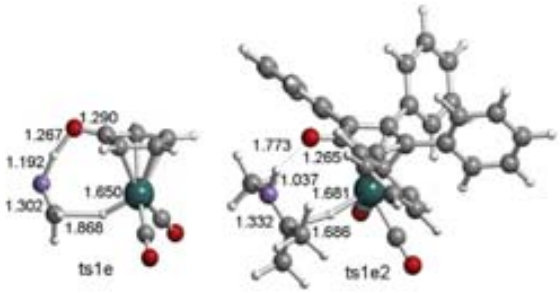

Fig. 5. Related transition-states for the concerted outer-sphere mechanisms both in the model and the complete Shvo catalysts; the former is for $H_2C{=}NH$ hydrogenation (**ts1e**) whereas the latter is for $(CH_3)_2C{=}N{-}CH_3$ hydrogenation optimized in solution (THF) (**ts1e2**). Distances in Å.

the same authors evaluated imine hydrogenation including the phenyl rings and optimizing in solvent. The geometry of this transition-state is depicted in Fig. 5. Concerning the energy barrier it was quite similar (4.0 kcal/mol) to that of the model imine (6.8 kcal/mol). These results agree with those reported by Casey and Cui on the same mechanism through single point calculations at MP2 level over structures optimized at the B3LYP level including solvent effects by means of the PCM method; 4.8 kcal/mol [81]. As expected, due to the increased basicity of a more electron-donating imine, the asynchronicity was higher than for the model imine.

In summary, from the overall theoretical analysis it can be concluded that the concerted outer-sphere mechanism is near to 10 kcal/mol lower in energy than the lowest energy barrier reported for the inner-sphere mechanism. Therefore, theoretical analysis supports the concerted outer-sphere mechanism for the imine hydrogenation using the Shvo's catalyst.

4.6. Hydrogenation of alkenes and alkynes

Concerning the hydrogenation of non-polar multiple bonds (alkenes and alkynes) both inner- and outer-sphere mechanisms were also evaluated [88]. For alkyne hydrogenation the $\eta^5 \rightarrow \eta^3$ inner-sphere mechanism presents an overall barrier height of 32.3 kcal/mol in solution (hydride-transfer step) in contrast with the concerted outer-sphere one, which presents a more favourable value of 18.5 kcal/mol in solution. For alkene hydrogenation similar values are found; the $\eta^5 \rightarrow \eta^3$ inner-sphere mechanism presents an overall barrier height of 29.6 kcal/mol in solution (hydride-transfer step) whereas the concerted outer-sphere mechanism has a barrier height of 17.9 kcal/mol in solution. Thus, in both cases the most feasible pathway is again the concerted outer-sphere mechanism. Theoretical calculations [88] were also able to explain two experimental evidences [73] in alkyne hydrogenation: a route proposed by Shvo leading to catalyst deactivation and the location of a very stable metal-alkenyl intermediate (−35.2 kcal/mol respects to the initial reactants) even stable at 140 °C for 10 h in toluene.

When comparing the hydrogenation barriers between polar and nonpolar bonds, the latter presents energy barriers height approximately 10 kcal/mol higher in energy. This observation agreed with the observed chemoselectivity for polar double bond hydrogenation over multiple carbon–carbon bond hydrogenation.

5. Conclusions

The hydrogen-transfer mechanisms for several metal-based catalysts along with their theoretical interpretations have been reviewed and described. There are several pathways: the direct hydrogen-transfer or MPV reduction and both the dihydridic and monohydridic routes. Within the monohydridic route the inner-sphere (with coordination of the substrate) and the outer-sphere (without substrate coordination) mechanisms have been tackled. For most of the described catalysts there is a clear preference for the concerted outer-sphere mechanism, which is also able to rationalize the origin of the enantioselectivity in case of the asymmetric version of the reaction. Regarding the nature of the metal center it has been observed that ruthenium-based catalysts are usually operating through an outer-sphere mechanism whereas this is not the case for iridium and rhodium-based catalysts (they use to operate through a different hydrogen-transfer mechanism). Regardless the metal center a common trend observed within the inner-sphere routes is the great stability of the metal-alkoxide intermediate when no vacant sites remind within the coordination sphere of the metal, limiting the subsequent reaction step. Moreover, for the direct hydride-transfer and for the inner-sphere mechanism a high lability of one of the ligands is needed in order to be competitive with the concerted outer-sphere mechanism. All these conclusions are supported by theoretical analysis.

For the case of the Shvo catalyst both inner- and outer-sphere mechanisms have been computationally analysed for a sort of unsaturated bonds such as C=O, C=N, C=C and C≡C. According to theoretical results, in all the cases the most feasible hydrogenation mechanism is the concerted outer-sphere mechanism. The results also accounted for the observed chemoselectivity for polar double bonds hydrogenation over non-polar multiple bonds being more favoured by approximately 10 kcal/mol. The studies here presented are a clear example of how computational analysis can help in unravelling hydrogen-transfer reaction mechanisms.

Acknowledgments

We are grateful to the Spanish MEC (Projects CTQ2005-0900-C02-01 and Consolider Ingenio 2010 CSD2007-00006, FPU fellowship to A.C.-V.), as well as to the Generalitat de Catalunya (2005/SGR/00896).

References

[1] D. Klomp, U. Hanefeld, J.A. Peeters, in: J.G. de Vries, C.J. Elsevier (Eds.), Handbook of Homogeneous Hydrogenation, Wiley-VCH, Weinheim, 2007.
[2] S. Gladiali, E. Alberico, Chem. Soc. Rev. 35 (2006) 226.
[3] J.S.M. Samec, J.-E. Bäckvall, P.G. Andersson, P. Brandt, Chem. Soc. Rev. 35 (2006) 237.
[4] S.E. Clapham, A. Hadzovic, R.H. Morris, Coord. Chem. Rev. 248 (2004) 2201.
[5] J.-E. Bäckvall, J. Organomet. Chem. 652 (2002) 105.
[6] R. Noyori, S. Hashiguchi, Acc. Chem. Res. 30 (1997) 97.

[7] G. Zassinovich, G. Mestroni, S. Gladiali, Chem. Rev. 92 (1992) 1051.
[8] P. Hauwert, G. Maestri, J.W. Sprengers, M. Catellani, C.J. Elsevier, Angew. Chem. Int. Ed. 47 (2008) 3223.
[9] A.G. Campanya, R.E. Estévez, N. Fuentes, R. Robles, J.M. Cuerva, E. Bufuel, D. Cárdenas, J.E. Oltra, Org. Lett. 9 (2007) 2195.
[10] D. Gnanamgari, A. Moores, E. Rajaseelan, R.H. Crabtree, Organometallics 26 (2007) 1226.
[11] K. Tani, A. Iski, T. Yamagata, Chem. Commun. (1999) 1821.
[12] K. Tani, N. Ono, S. Okamoto, F. Sato, J. Chem. Soc., Chem. Commun. (1993) 386.
[13] A.L.E. Larsson, B.A. Persson, J.-E. Bäckvall, Angew. Chem. Int. Ed. 36 (1997) 1211.
[14] B.A. Persson, A.L.E. Larsson, M.L. Ray, J.-E. Bäckvall, J. Am. Chem. Soc. 121 (1999) 1645.
[15] J. Paetzold, J.E. Bäckvall, J. Am. Chem. Soc. 127 (2005) 17620.
[16] H. Meerwein, R. Schmidt, Justus Liebigs Ann. Chem. 444 (1925) 221.
[17] A. Verley, Bull. Soc. Chim. Fr. 37 (1925) 537.
[18] W. Ponndorf, Angew. Chem. 29 (1926) 138.
[19] R.V. Oppenauer, Recl. Trav. Chim. Pays-B. 56 (1937) 137.
[20] A.L. Wilds, Org. React. 2 (1944) 178.
[21] J.L. Namy, J. Souppe, J. Collin, H.B. Kagan, J. Org. Chem. 49 (1984) 2045.
[22] D.A. Evans, S.G. Nelson, M.R. Gagné, A.R. Muci, J. Am. Chem. Soc. 115 (1993) 9800.
[23] J.-W. Handgraaf, J.N.H. Reek, E.-V. Meijer, Organometallics 22 (2003) 3150.
[24] P. Gamez, F. Fache, M. Lemaire, Tetrahedron: Asymmetry 6 (1995) 705.
[25] C. Hedberg, K. Källström, P.I. Arvidsson, P. Brandt, P.G. Andersson, J. Am. Chem. Soc. 127 (2005) 15083 (and references therein).
[26] A. Comas-Vives, C. González-Arellano, A. Corma, M. Iglesias, F. Sánchez, G. Ujaque, J. Am. Chem. Soc. 128 (2006) 4756 (and references therein).
[27] A. Comas-Vives, C. González-Arellano, M. Boronat, A. Corma, M. Iglesias, F. Sánchez, G. Ujaque, J. Catal. 254 (2008) 226.
[28] Y. Blum, D. Czarkie, Y. Rahamim, Y. Shvo, Organometallics 4 (1985) 1459.
[29] Y. Shvo, D. Czarkie, Y. Rahamim, J. Am. Chem. Soc. 108 (1986) 7400.
[30] R. Noyori, T. Ohkuma, Angew. Chem. Int. Ed. 40 (2001) 40.
[31] C.A. Sandoval, T. Ohkuma, K. Muñiz, R. Noyori, J. Am. Chem. Soc. 125 (2003) 13490.
[32] A. Fujii, S. Hashiguchi, N. Uematsu, T. Ikariya, R. Noyori, J. Am. Chem. Soc. 118 (1996) 2521.
[33] N. Uematsu, A. Fujii, S. Hashiguchi, T. Ikariya, R. Noyori, J. Am. Chem. Soc. 118 (1996) 4916.
[34] X. Wu, D. Vinci, T. Ikariya, J. Xiao, Chem. Commun. (2005) 4447.
[35] S.E. Clapham, R.H. Morris, Organometallics 24 (2005) 479.
[36] R.M. Bullock, Chem. Eur. J. 10 (2004) 2366.
[37] H. Guan, M. Iimura, M.P. Magee, J.R. Norton, G. Zhu, J. Am. Chem. Soc. 127 (2005) 7805.
[38] D.A. Alonso, P. Brandt, S.J.M. Nordin, P.G. Andersson, J. Am. Chem. Soc. 121 (1999) 9580.
[39] V. Guiral, F. Delbecq, P. Sautet, Organometallics 20 (2001) 2207.
[40] J.A. Osborn, F.H. Jardine, J.F. Young, G. Wilkinson, J. Chem. Soc. A (1966) 1711.
[41] R.S. Coffey, British Patent No.1121642 (18 February 1965).
[42] F.H. Jardine, Prog. Inorg. Chem. 28 (1981) 63.
[43] R.R. Schrock, J.A. Osborn, J. Chem. Soc., Chem. Commun. (1970) 567.
[44] P.A. Chaloner, M.A. Esteruelas, F. Joó, L.A. Oro (Eds.), Homogeneous Hydrogenation, Kluwer Academic Publishers, Dordrecht, 1998.
[45] O. Pàmies, J.-E. Bäckvall, Chem. Eur. J. 7 (2001) 5052.
[46] L.Y. Kuo, D.M. Finigan, N.N. Tadros, Organometallics 22 (2003) 2422.
[47] G. Mestroni, G. Zassinovich, A. Camus, F. Martinelli, J. Organomet. Chem. 198 (1980) 87.
[48] A. Aranyos, G. Csjernyik, K.J. Szabó, J.-E. Bäckvall, Chem. Commun. (1999) 351.
[49] J. Takehara, S. Hashiguchi, A. Fujii, S. Inoue, T. Ikariya, R. Noyori, Chem. Commun. (1996) 233.
[50] S. Hashiguchi, A. Fujii, J. Takehara, T. Ikariya, R. Noyori, J. Am. Chem. Soc. 117 (1995) 7562.
[51] M. Yamakawa, H. Ito, R. Noyori, J. Am. Chem. 122 (2000) 1466.
[52] D. Balcells, A. Nova, E. Clot, D. Gnanamgari, R.H. Crabtree, O. Eisenstein, Organometallics 27 (2008) 2529.
[53] V. Guiral, F. Delbecq, P. Sautet, Organometallics 19 (2000) 1589.
[54] S. Gladiali, L. Pinna, G. Delogu, S. De Martin, G. Zassinovich, G. Mestroni, Tetrahedron: Asymmetry 1 (1990) 635.
[55] C.S. Yi, Z. He, I.A. Guzei, Organometallics 20 (2001) 3641.
[56] (a) G. Kovács, G. Ujaque, A. Lledós, F. Joó For theoretical works addressing C=O vs. C=C chemoselectivity see, Organometallics 25 (2006) 862;
(b) A. Rossin, G. Kovács, G. Ujaque, A. Lledós, F. Joó, Organometallics 25 (2006) 5010.
[57] U. Uematsu, A. Fujii, S. Hashiguchi, T. Ikariya, R. Noyori, J. Am. Chem. Soc. 118 (1996) 4916.
[58] S. Hashiguchi, A. Fujii, K.-J. Haack, K. Matsumura, T. Ikariya, R. Noyori, Angew. Chem. Int. Ed. Engl. 36 (1997) 288.
[59] M. Yamakawa, I. Yamada, R. Noyori, Angew. Chem. Int. Ed. 40 (2001) 2818.
[60] D.G.I. Petra, J.N.H. Reek, J.-W. Handgraaf, E.J. Meijer, P. Dierkes, P.C.J. Kamer, J. Brusse, H.E. Schoemaker, P.W.N.M. van Leeuwen, Chem. Eur. J. 6 (2000) 2818.
[61] C.P. Casey, J.B. Johnson, J. Org. Chem. 68 (2003) 1998.
[62] K. Abdur-Rashid, S.E. Clapham, A. Hadzovic, J.N. Harvey, A.J. Lough, R.H. Morris, J. Am. Chem. Soc. 124 (2002) 15104.
[63] D. Di Tommaso, S.A. French, C.R.A. Catlow, J. Mol. Struct. 812 (2007) 39.
[64] S.A. French, D. Di Tommaso, A. Zanotti-Gerosa, F. Hancock, C.R.A. Catlow, Chem. Commun. (2007) 2381.
[65] D. Di Tommaso, S.A. French, A. Zanotti-Gerosa, F. Hancock, E.J. Palin, C.R.A. Catlow, Inorg. Chem. 47 (2008) 2674.
[66] T. Leyssens, D. Peeters, J.N. Harvey, Organometallics 27 (2008) 1514.
[67] T. Li, I. Bergner, F.-N. Haque, M.-Z.-D. Iuliis, D. Song, R.H. Morris, Organometallics 26 (2007) 5940.
[68] Z.E. Clarke, P.T. Maragh, T.P. Dasgupta, D.G. Gusev, A.J. Lough, K. Abdur-Rashid, Organometallics 25 (2006) 4113.
[69] S. Bi, Q. Xie, X. Zhao, Y. Zhao, X. Kong, J. Organomet. Chem. 693 (2008) 633.
[70] R. Karvembu, R. Prabhakaran, K. Natarajan, Coord. Chem. Rev. 249 (2005) 911.
[71] N. Menashe, E. Salant, Y. Shvo, J. Organomet. Chem. 514 (1996) 97.
[72] J.S.M. Samec, J.E. Bäckvall, Chem. Eur. J. 8 (2002) 2955.
[73] Y. Shvo, I. Goldberg, D. Czierke, D. Reshef, Z. Stein, Organometallics 16 (1997) 133.
[74] G. Csjernyk, A.H. Éll, L. Fadini, B. Pugin, J.-E. Bäckvall, J. Org. Chem. 67 (2002) 1657.
[75] J.S.M. Samec, A.H. Éll, J.-E. Bäckvall, Chem. Eur. J. 11 (2005) 2327.
[76] A.H. Éll, J.S.M. Samec, C. Brasse, J.-E. Bäckvall, Chem. Commun. (2002) 1144.
[77] J.H. Choi, N. Kim, Y.J. Shin, J.H. Park, J. Park, Tetrahedron Lett. 45 (2004) 4607.
[78] C.P. Casey, S.W. Singer, D.R. Powell, R.K. Hayashi, M. Kavana, J. Am. Chem. Soc. 123 (2001) 1090.
[79] J.B. Johnson, J.-E. Bäckvall, J. Org. Chem. 68 (2003) 7681.
[80] A. Comas-Vives, G. Ujaque, A. Lledós, Organometallics 26 (2007) 4135.
[81] C.P. Casey, G.A. Bikzhanova, Q. Cui, I.A. Guzei, J. Am. Chem. Soc. 127 (2005) 14062 (and supporting information therein).
[82] C.P. Casey, G.A. Bikzhanova, I.A. Guzei, J. Am. Chem. Soc. 128 (2006) 2286.
[83] C.P. Casey, J.B. Johnson, J. Am. Chem. Soc. 127 (2005) 1883.
[84] J.S.M. Samec, A.H. Éll, J.-E. Bäckvall, Chem. Commun. (2004) 2748.
[85] A.H. Éll, J.B. Johnson, J.-E. Bäckvall, Chem. Commun. (2003) 1652.
[86] J.S.M. Samec, A.H. Éll, J.B. Åberg, T. Privalov, L. Eriksson, J.-E. Bäckvall, J. Am. Chem. Soc. 128 (2006) 14293.
[87] T. Privalov, J.S.M. Samec, J.-E. Bäckvall, Organometallics 26 (2007) 2840.
[88] A. Comas-Vives, G. Ujaque, A. Lledós, Organometallics 27 (2008) 4854.
[89] A. Habib, R.S. Tanke, E.M. Holt, R.H. Crabtree, Organometallics 8 (1989) 225.
[90] L.F. Veiros, Organometallics 19 (2000) 5549.
[91] H.-J. Fan, M.B. Hall, Organometallics 20 (2001) 5724.
[92] C.P. Casey, J.B. Johnson, Can. J. Chem. 83 (2005) 1339.

Please cite this article in press as: A. Comas-Vives et al., J. Mol. Struct. (THEOCHEM) (2009), doi:10.1016/j.theochem.2008.11.043

Apèndix A

Annex 1. Publicacions que per motius legals no formen part d'aquesta tesi

A.1 Article IV

Article

Single-Site Homogeneous and Heterogeneized Gold(III) Hydrogenation Catalysts: Mechanistic Implications

Aleix Comas-Vives, C. Gonzlez-Arellano, A. Corma, M. Iglesias, F. Snchez, and Gregori Ujaque

J. Am. Chem. Soc., **2006**, 128 (14), 4756-4765 • DOI: 10.1021/ja057998o • Publication Date (Web): 17 March 2006

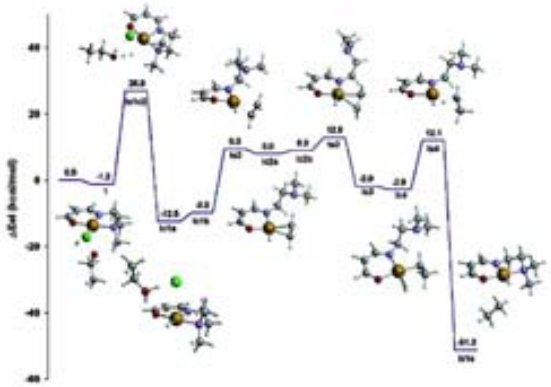

J|A|C|S
ARTICLES
Published on Web 03/17/2006

Single-Site Homogeneous and Heterogeneized Gold(III) Hydrogenation Catalysts: Mechanistic Implications

Aleix Comas-Vives,[⊥] C. Gonzalez-Arellano,[†,§] A. Corma,[*,†] M. Iglesias,[‖] F. Sánchez,[†] and Gregori Ujaque[*,⊥]

Contribution from the Instituto de Química Orgánica General, CSIC, C/ Juan de la Cierva 3, 28006 Madrid, Spain, Instituto de Tecnología Química, UPV-CSIC, Universidad Politécnica de Valencia, Avenida de los Naranjos s/n, 46022 Valencia, Spain, Instituto de Ciencia de Materiales de Madrid, CSIC, C/Sor Juana Inés de la Cruz s/n, Cantoblanco, 28049 Madrid, Spain, and Unitat de Química Física, Departament de Química, Universitat Autònoma de Barcelona, 08193 Bellaterra, Barcelona, Catalonia, Spain

Received November 24, 2005; E-mail: acorma@itq.upv.es; Gregori.Ujaque@uab.es

Abstract: Au(III)−Schiff base complexes are active hydrogenation catalysts, giving turnover frequencies similar to those of the corresponding complexes of Pd(II), which has the same d^8 electronic structure as Au(III). The mechanism of the reaction has been studied in detail by a combination of kinetic experiments and theoretical calculations. It is predicted and tested that the nature of the solvent plays a critical role for the heterolytic cleavage of H_2 (controlling step). Taking this into account, and by properly selecting the nature of solid supports (polarity and proton-donating ability), it was possible to strongly increase the activity of the homogeneous Au(III) and Pd(II) catalysts by grafting them onto the surface.

Introduction

Gold catalysis in homogeneous and heterogeneous systems is a matter of increasing interest, owing to the unique properties of this metal for a continuously increasing number of reactions. Following the work of Bond and Sermon,[1] Hutchings,[2] and Haruta et al.,[3] gold has appeared as an interesting catalyst when in the form of salts, gold complexes, and gold supported on different carriers.[4−13] In this way, gold has been successfully used in catalyzing reactions such as CO oxidation at low temperature,[8−10,13] the water−gas shift reaction,[14] decomposition of NO_x with hydrocarbons,[15] selective hydrogenations,[16] carbon−carbon bond formation,[17−20] selective oxidations,[21−25] enantioselective asymmetric aldol condensation,[26] and enantioselective hydrogenation of olefins and imines[27] among others.[28] In the case of heterogeneous catalysis, different hypotheses have been put forward to explain the nature of the gold active sites involved, especially in the case of CO oxidation. In some cases the high activity of gold is associated with negatively charged gold,[29] while in other cases it is claimed that the activity of gold nanoparticles is rather related to atoms bearing a positive density of charge.[9−11,30] Catalysis by gold transition metal complexes can help to elucidate the nature of the active sites for a particular reaction since these can be perfectly characterized and analogies with solid catalysts can be established. We believe that Au(I) and Au(III) species are stabilized on supported gold nanoparticles and they can act as active species.[18] Furthermore, Pd(II) and Au(III) have the same d^8 electronic structure, and therefore they may behave similarly, at least for some reactions.

Here we present our findings that Au(III) complexes are able to hydrogenate olefinic molecules with high turnover frequencies

† Instituto de Química Orgánica General, CSIC.
‡ Universidad Politécnica de Valencia.
§ Instituto de Ciencia de Materiales de Madrid, CSIC.
⊥ Universitat Autònoma de Barcelona.

(1) Bond, G. C.; Sermon, P. A. *Gold Bull.* **1973**, *6*, 102.
(2) Hutchings, G. J. *Gold Bull.* **1996**, *29*, 123.
(3) Haruta, M.; Tsubota, S.; Kobayashi, T.; Iijima, S. *J. Catal.* **1989**, *115*, 301.
(4) Dyker, G. *Angew. Chem., Int. Ed.* **2000**, *39*, 4237 and references therein.
(5) Corma, A.; García, H. *Chem. Rev.* **2003**, *103*, 4307.
(6) Yao, X.; Li, Ch.-J. *J. Am. Chem. Soc.* **2004**, *126*, 6884.
(7) Wei, Ch.; Li, Ch.-J. *J. Am. Chem. Soc.* **2003**, *125*, 9584.
(8) Haruta, M. *Catal. Today* **1997**, *36*, 153.
(9) Guzman, J.; Gates, B. C. *J. Phys. Chem. B* **2002**, *106*, 7659; *J. Am. Chem. Soc.* **2004**, *126*, 2672.
(10) Valden, M.; Lai, X.; Goodman, D. W. *Science* **1998**, *281*, 1647.
(11) Carrettin, S.; Concepción, P.; Corma, A.; López-Nieto, J. M.; Puntes, V. F. *Angew. Chem., Int. Ed.* **2004**, *43*, 2538.
(12) Hutchings, G. J. *Gold Bull.* **2004**, *37*, 3.
(13) Guzman, J.; Carrettin, S.; Corma, A. *J. Am. Chem. Soc.* **2005**, *127*, 3286.
(14) Fu, Q.; Saltsburg, H.; Flytzani-Stephanopoulos, M. *Science* **2003**, *301*, 935.
(15) Bamwenda, G. R.; Obuchi, A.; Ogata, A.; Oi, J.; Kushiyama, S.; Mizuno, K. *J. Mol. Catal. A* **1997**, *126*, 151.
(16) Milone, C.; Ingoglia, R.; Pistone, A.; Neri, G.; Frusteri, F.; Galvano, S. *J. Catal.* **2004**, *222*, 348.
(17) Hoffman-Röder, A.; Krause, N. *Org. Biomol. Chem.* **2005**, *3*, 387.
(18) Carrettin, S.; Guzman, J.; Corma, A. *Angew. Chem., Int. Ed.* **2005**, *44*, 2242.
(19) González-Arellano, C.; Corma, A.; Iglesias, M.; Sánchez, F. *Chem. Commun.* **2005**, 1990.
(20) Hashmi, A. S. K. *Gold Bull.* **2004**, *37*, 51.
(21) Biella, S.; Rossi, M. *Chem. Commun.* **2003**, 378.
(22) Prati, L.; Rossi, M. *J. Catal.* **1998**, *176*, 552.
(23) Carretin, S.; McMorn, P.; Johnston, P.; Griffin, K.; Hutchings, G. J. *Chem. Commun.* **2002**, 696.
(24) Abad, A.; Concepción, P.; Corma, A.; García, H. *Angew. Chem., Int. Ed.* **2005**, *44*, 4066.
(25) Corma, A.; Domine, M. *Chem. Commun.* **2005**, 4042.
(26) Ito, Y.; Sawamura, M.; Hayashi, T. *J. Am. Chem. Soc.* **1986**, *108*, 6405.
(27) González-Arellano, C.; Corma, A.; Iglesias, M.; Sánchez, F. *Chem. Commun.* **2005**, 3451.
(28) Hashmi, A. S. K. *Angew. Chem., Int. Ed.* **2005**, *44*, 6990.
(29) (a) Chen, M.; Kumar, D.; Yi, C.; Goodman, D. W. *Science* **2005**, *310*, 291. (b) Hakkinen, H.; Abbet, S.; Sánchez, A.; Heiz, U.; Landman, U. *Angew. Chem., Int. Ed.* **2003**, *42*, 1297.
(30) Lemire, C.; Meyer, R.; Shaikhutdinov, S.; Freund, H. J. *Angew. Chem., Int. Ed.* **2004**, *43*, 118.
(31) Pyykkö, P. *Angew. Chem., Int. Ed.* **2004**, *43*, 4412.

10.1021/ja057996b CCC: $33.50

Scheme 1. Synthesis of Soluble Ligands and Homogeneous Complexes

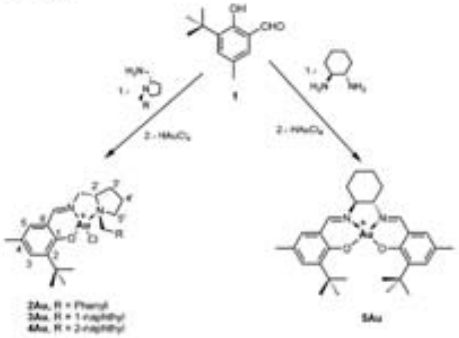

(TOFs), and by a combination of experimental and theoretical calculations[31-33] a feasible mechanism is proposed. The reaction mechanism has been studied in detail, and the energetics of each elementary step have been calculated. Theoretical calculations show the effect of the solvent on the reaction mechanism and predict that the use of polar supports should favor the activity of the homogeneous catalysts when supported on solid carriers, this being confirmed by experimental results. The presence of surface protons on the carrier increases further the activity of the catalyst, showing that the Au(III) can be as active as the corresponding Pd(II) complexes.

Experimental Section

Homogeneous Catalysts. The synthesis of soluble ligands is based on the condensation of (*S*)-(*N*-benzyl-2-pyrrolidinyl)methylamine, (*S*)-[1-(1-naphthylmethyl)-2-pyrrolidinyl]methylamine, (*S*)-[1-(2-naphthylmethyl)-2-pyrrolidinyl]methylamine, and (1*S*,2*S*)-1,2-diaminecyclohexane with 3-*tert*-butyl-5-methylsalicylaldehyde in the presence of 3 Å molecular sieves.[34] Their respective Au complexes were prepared by addition of tetrachloroauric acid to an ethanolic solution of ligand; one chloride anion was displaced by the phenolic anion while the amine and imine nitrogens were coordinated with the metal in a square planar arrangement (Scheme 1). The complexes precipitated in EtOH were obtained as microcrystalline stable solids, soluble in organic solvents, with high purity and yields. The structure of all the complexes was confirmed by elemental analysis (C, H, N, and Au), by IR, ^{1}H, and ^{13}C NMR spectroscopies, and by electrospray mass spectrometry.

Heterogenized Catalysts. Au(III) complexes were prepared on all-silica and silica−alumina MCM-41,[32] as well as on pure silica ITQ-2 supports.[35] All solids were functionalized in the same manner according to the procedure showed in Scheme 2.

Supported precursors **1**−**(support)** were obtained by refluxing in toluene for 16 h a mixture of 3-*tert*-butyl-5-methylsalicylaldehyde and the respective support. These anchored aldehydes reacted with an equimolecular amount of the respective amine to afford the supported Schiff base ligands, **2**−**5**−**(support)**, as fine powdered solids. These materials were characterized by microanalysis, FTIR, and ^{13}C NMR. The heterogenized ligands were reacted with tetrachloroauric acid to give the corresponding anchored gold complexes.

Catalytic Experiments. In a typical experiment the reaction was carried out in a 100 mL autoclave at 40 ºC, 4 bar of H_2, and 1/1000 metal-to-substrate molar ratio with ethanol as solvent. The evolution of the hydrogenated products with time was monitored by GC with a glass capillary column (methylsilicone (OV-1701)) and methylsilicone−heptakis[2,3-dipentyl-6-(*tert*-butyldimethylsilyl)]-β-cyclodextrin.

Computational Details. Calculations were carried out using the program package Gaussian03[36] at the density functional theory (DFT) level by means of the hybrid B3LYP functional.[37] The basic set is double-ζ for all the atoms; for the Au, the LANL2DZ[38] pseudopotential and its associated basis set for the valence electrons were used. The O and N atoms were described by the 6-31g(d) basis set; for the Cl atom additional diffuse functions were added, 6-31+g(d). For the C and H atoms directly involved in the reaction, the 6-31g(d) and 6-31g(d,p) basis sets were employed, respectively, whereas the 6-31g basis set was used for the remaining C and H atoms. For the saddle points, the existence of only one imaginary frequency was checked by means of analytical frequency calculations.

To corroborate which are the correspondent minima linked by the considered TS, normal coordinate analyses were performed on these TS structures by intrinsic reaction coordinate (IRC) routes[39] in both reactant and product directions. Additional geometry optimizations starting from the last IRC structures were carried out when the IRC calculations did not converge themselves. The reaction pathway is assumed to be the minimum energy pathway within the potential energy surface.

Scheme 2. Synthesis of Heterogenized Ligands and Complexes

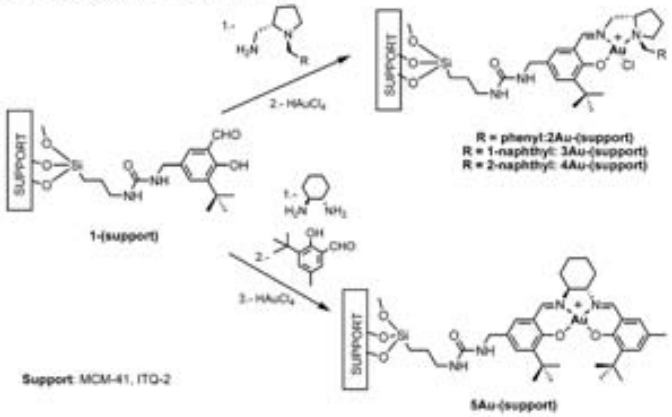

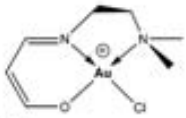

Figure 1. Model complex.

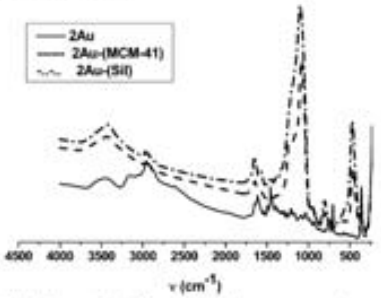

Figure 2. FTIR spectra for **2Au** complexes (homogeneous and supported).

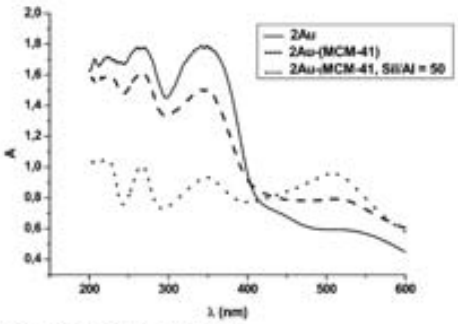

Figure 3. DFTR for **2Au** complexes.

Solvent effects were included by means of the polarized continuum model[40] (PCM). The olefin selected for the theoretical calculations is ethene since it is the simplest alkene. Concerning the catalyst, calculations were performed on a complex that serves as a model for catalysts **2**, **3**, and **4**, as labeled in Scheme 1. The model complex is depicted in Figure 1.

Results and Discussion

The nature of the complexes was verified by various spectroscopic techniques. Thus, FTIR spectra of the Au(III) complexes (see Figure 2) are characteristic of the binding of imine nitrogen. The 1600 cm^{-1} band can be assigned to C=C and azomethine C=N vibrations, shifted to lower wavenumbers (relative to the free ligands due to the N-coordination of the imine). New bands in the 500−600 cm^{-1} region are ascribed to ν(M−O).

The DFTR spectra for all complexes (Figure 3) were obtained in the 200−800 nm range. The complexes show several bands as intraligand $\pi \rightarrow \pi^*$, $n \rightarrow \pi^*$ transitions in the aromatic ring,

Table 1. Turnover Frequencies (TOF, h^{-1})[a] for the Catalytic Hydrogenation of Diethyl Itaconate in EtOH[b]

ligand	TOF
2	3 430
3	9 560
4	11 240
5	3 690

[a] TOF = mol substrate/mol catalyst·h. [b] 4 bar H_2, 40 °C and substrate/catalyst ratio 1000:1.

Table 2. Turnover Frequencies (TOF, h^{-1})[a] for the Catalytic Hydrogenation of Diethyl Itaconate in EtOH[b]

ligand	Au(III)	Pd(II)
5	3 690	3 730
5−(MCM-41)	10 520	9 730
5−(ITQ-2)	8 980	9 870
2	3 430	3 360
2−(MCM-41)	4 920	4 980
2−(MCM-41, Si/Al = 50)	6 730	6 000

[a] TOF = mol substrate/mol catalyst·h. [b] 4 bar H_2, 40 °C and substrate/catalyst ratio 1000:1.

azomethine group, and charge-transfer transition. The bands in the 400−450 nm region correspond to d−d transitions expected for planar complexes and metal-to-ligand charge-transfer bands. The diffuse reflectance spectra of M(ligand) complexes are almost identical before and after the heterogenization process, indicating that the complexes maintain their geometry and their electronic surrounding after heterogenization without significant distortion.

The diamagnetic gold complexes have been characterized by ^{13}C NMR spectroscopy (see Figure 4 for an example). In all cases, the spectra show the simultaneous occurrence of two sets of signals which are attributable on one hand to the substituted benzaldimine entity and on the other hand to the aliphatic part of the ligand. The ^{13}C NMR spectra showed the signals assigned to the C=N carbon high-field shifted and C_1 at δ ~160 downfield shifted, confirming that metalation has occurred.

Catalytic Activity of Gold Complexes. Soluble complexes **2Au**−**5Au** and their corresponding heterogenized ones have been tested in hydrogenation reactions of diethyl ethylidenesuccinates (diethyl itaconate, diethyl citraconate, and diethyl benzylidenesuccinate) under mild conditions (20−70 °C and 2−6 bar H_2). The results on the hydrogenation of diethyl itaconate (40 °C/4 bar H_2) are given in Tables 1 and 2. It can be seen that the homogeneous gold catalysts not only are active but also give the same activity as the corresponding Pd complexes. In the case of the supported catalysts, the TOFs increase with respect to the homogeneous complex, indicating that both silica mesostructured molecular sieves (MCM-41) and

(32) Krenge, C. T.; Leonowicz, W. J.; Roth, W. J.; Vartuli, J. C.; Beck, J. S. *Nature* **1992**, *359*, 710.

(33) (a) *Computational Modelling of Homogeneous Catalysis*; Lledós, A., Maseras, F., Eds.; Kluwer: Dordrecht, 2002. (b) Braga, A. A. C.; Morgon, N. H.; Ujaque, G.; Maseras, F. *J. Am. Chem. Soc.* **2005**, *127*, 9298. (c) Balcells, D.; Maseras, F.; Ujaque, G. *J. Am. Chem. Soc.* **2005**, *127*, 3624.
(34) González-Arellano, C.; Gutierrez-Puebla, E.; Iglesias, M.; Sánchez, F. *Eur. J. Inorg. Chem.* **2004**, 1955.
(35) Corma, A.; Fornés, V.; Pergher, S. B.; Maesen, Th.; Buglass, J. *Nature* **1998**, *396*, 353.
(36) Frisch, M. J.; et al. *Gaussian03*; Gaussian, Inc.: Wallingford, CT, 2004.
(37) (a) Becke, A. D. *J. Chem. Phys.* **1993**, *98*, 5648. (b) Stephens, P. J.; Devlin, J. F.; Chabalowski, C. F.; Frisch, M. J. *J. Phys. Chem.* **1994**, *98*, 11623.
(38) Hay, P. J.; Wadt, W. R. *J. Chem. Phys.* **1985**, *82*, 270.
(39) Fukui, K. *Acc. Chem. Res.* **1981**, *14*, 363.
(40) (a) Cances, M. T.; Mennucci, B.; Tomasi, J. *J. Chem. Phys.* **1997**, *107*, 3032. (b) Cossi, M.; Barone, V.; Mennucci, B.; Tomasi, J. *J. Chem. Phys. Lett.* **1998**, *286*, 253. (c) Mennucci, B.; Tomasi, J. *J. Chem. Phys.* **1997**, *106*, 5151.

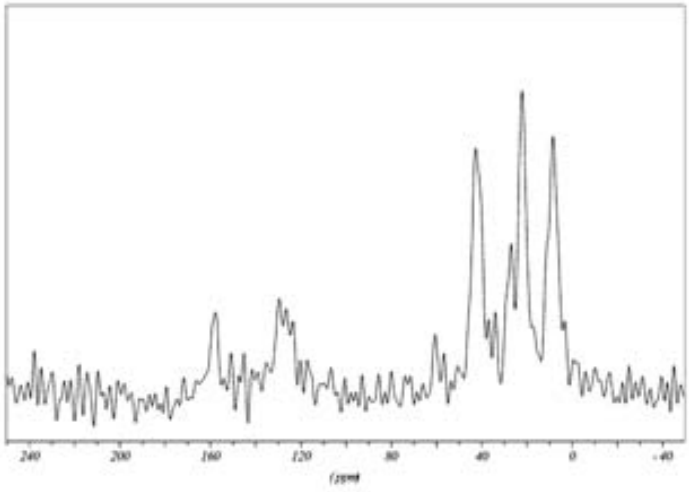

Figure 4. ^{13}C NMR spectra of the **5Au**−**(MCM-41)**.

delaminated zeolites (ITQ-2) are suitable supports for heterogenizing metal complex homogeneous catalysts.

It has been shown that the introduction of acetic acid increases the rate of hydrogenation of imines by rhodium xyliphos complexes, due to the stabilization of the negatively charged transition state by the protons.[41] In our case, the introduction of surface protons in the MCM-41 support has been achieved by isomorphic substitution of Al by Si (MCM-41, Si/Al = 50). The resultant gold or Pd catalysts have a higher activity than the homogeneous or the heterogenized catalysts on the pure silica neutral supports (Table 2). These results suggest that, during the hydrogenation of imines on Au and Pd complexes, the hydrogen is activated via a heterolytic cleavage to give a hydride intermediate, which involves charge separation without any oxidative addition of hydrogen to the metal. In this case, an increase of the polarity and acidity of the support should increase the reaction rate, as has been experimentally observed (Table 2). Heterogenized catalysts are stable with time, since storage of the catalysts at room temperature for 6 months has no effect on their catalytic performance. They are also stable under reaction conditions and can be recycled at least six times without any appreciable loss in activity.

Reaction Mechanism. (i) Activation of H_2. The hydrogenation of the double bond requires the activation of molecular hydrogen by the gold complex. Two routes are known for this activation: the homolytic activation and the heterolytic cleavage of molecular hydrogen. The homolytic activation is highly improbable for the reaction system studied here due to the difficulty of the metal center to reach the oxidation number Au(V). Nevertheless, we have carried out the theoretical calculations, and the product of the oxidative addition lies ~50 kcal/mol above reactants (in the gas phase). The barrier for this reaction will be therefore no lower than 50 kcal/mol, and consequently homolytic cleavage was rejected as a possible pathway. Thus, in the detailed reaction mechanistic study, we have considered as the first step the heterolytic cleavage of H_2.

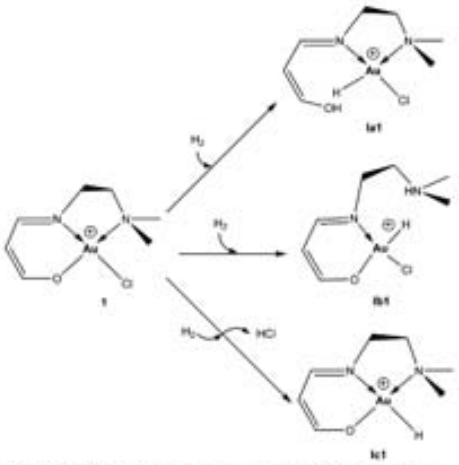

Figure 5. Possible heterolytic cleavages of the dihydrogen molecule.

The H_2 heterolytic cleavage is more common in early transition metals, even though some cases have recently been reported for late transition metals.[42−48] For this particular system, the catalyst possesses several ligands that are potential candidates to undergo [2 + 2] σ bond metathesis of the dihydrogen molecule: the oxygen and nitrogen of the ligand and the chlorine atom. These pathways are depicted in Figure 5.

The potential energy barriers for the direct heterolytic cleavage for each of the pathways are 47.4, 53.4, and 37.8 kcal/mol with respect to the corresponding separated reactants for the O (**tsa1**), N(amine) (**tsb1**), and Cl (**tsc1**) ligands, respec-

(41) Pugin, B.; Landert, H.; Spindler, F.; Blaser, H. U. *Adv. Synth. Catal.* **2002**, *344*, 974.

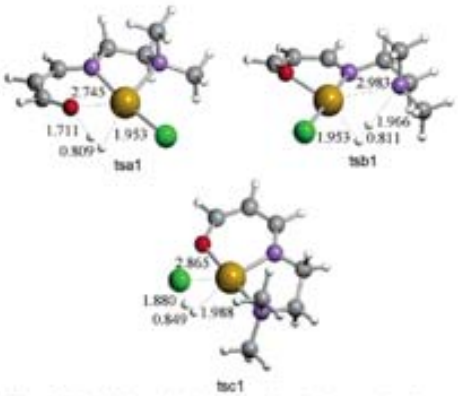

Figure 6. TS of the heterolytic cleavages of the dihydrogen molecule over O (**tsa1**), N (**tsb1**), and Cl (**tsc1**). Atom colors: C, gray; H, white; Cl, green; N, purple; O, red; and Au, golden.

tively. In these pathways, the hydrogen molecule is heterolytically activated by the catalyst, and the proton goes to the ligand whereas the hydride remains bonded to the metal center. The oxidation state of the Au remains unchanged. These three transition states are similar geometrically, all of them involving a four-centered transition state with the incoming broken hydrogen molecule, the metal, and the respective ligand atom as shown in Figure 6.

The distances of the broken hydrogen are 0.809 and 0.811 Å for O (**tsa1**) and N (**tsb1**) ligands respectively, whereas in the splitting over Cl atom (**tsc1**) is slightly larger (0.849 Å). Concerning the hydride−metal bond, it follows a similar trend, with distances of 1.953 Å for **tsa1** and **tsb1** and a distance of 1.988 Å for **tsc1**. The proton−ligand distances are 1.711, 1.966, and 1.880 Å for **tsa1**, **tsb1**, and **tsc1**, whereas the heteroatom−metal distances are 2.745, 2.983, and 2.865 Å for O, N, and Cl ligands, respectively.

The barriers obtained for these processes are too high for a hydrogenation catalytic process, and we directed our efforts to search alternative pathways with lower energy barriers. It has been reported[49] that, for the heterolytic splitting of H_2 with related organometallic complexes, the solvent may play an active role in the reaction mechanism. By taking this into account, our attempts were focused on a six-membered-ring transition state where the heterolytic cleavage was mediated by a hydrogen-bonded ethanol molecule, since this was the solvent used experimentally (Tables 1 and 2).

(42) Dedieu, A.; Humbel, S.; Cornelis, J. E.; Grauffel, C. *Theor. Chem. Acc.* **2004**, *112*, 305.
(43) Niu, S.; Hall, M. B. *Chem. Rev.* **2000**, *100*, 353.
(44) Hutschka, F.; Dedieu, A.; Leitner, W. *Angew. Chem., Int. Ed.* **1995**, *34*, 1742.
(45) Hutschka, F.; Dedieu, A.; Eichberger, M.; Fornika, R.; Leitner, W. *J. Am. Chem. Soc.* **1997**, *119*, 4432.
(46) Milet, A.; Dedieu, A.; Kapteijn, G.; van Koten, G. *Inorg. Chem.* **1997**, *36*, 3223.
(47) Musaev, D. G.; Froese, R. D. J.; Morokuma, K.; Strömberg, S.; Zetterberg, K.; Siegbahn, P. E. M. *Organometallics* **1997**, *16*, 1933.
(48) Musaev, D. G.; Froese, R. D. J.; Morokuma, K. *Organometallics* **1998**, *17*, 1850.
(49) (a) Sandoval, C. A.; Ohkuma, T.; Muñiz, K.; Noyori, R. *J. Am. Chem. Soc.* **2003**, *125*, 13490. (b) Casey, C. P.; Johnson, J. B.; Singer, S. W.; Cui, Q. *J. Am. Chem. Soc.* **2005**, *127*, 3100.

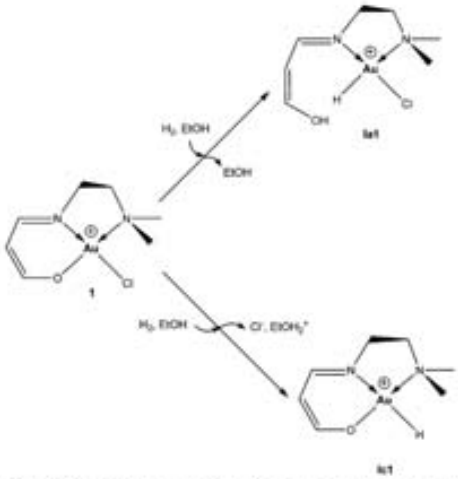

Figure 7. Heterolytic cleavages of the H_2 assisted by a solvent molecule (EtOH) over O and Cl atoms.

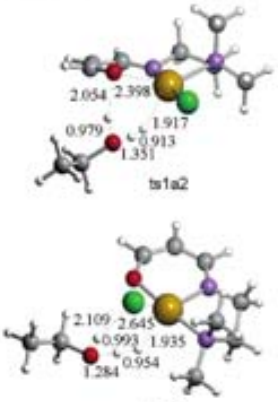

Figure 8. Solvent-assisted dihydrogen heterolytic cleavage over O (**ts1a2**) and Cl atom (**ts1c2**), respectively. Atom colors: C, gray; H, white; Cl, green; N, purple; O, red; and Au, golden.

In Figure 7 are presented the two alternative pathways studied: the H_2 heterolytic cleavages over O and Cl ligands with ethanol assistance. The third alternative, in which the activation takes place by means of the N(amine) ligand was not considered, since the barrier for the nonassisted mechanism was the highest one and, in addition, this ligand can easily be replaced by the olefin within the catalytic cycle (vide infra).

The structures of the transition states, involving a solvent molecule, **ts1a2**, and **ts1c2**, are shown in Figure 8. The geometry of these transition states can be associated with a trigonal bipyramid structure, where the leaving ligand and the forming hydride are both at the equatorial plane. With the inclusion of the solvent molecule, the distance of the breaking H−H bond

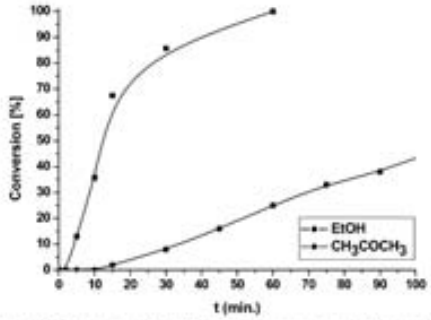

Figure 9. Hydrogenation of diethyl benzylidenesuccinate under the reaction conditions given in Table 1, using two different solvents.

has been enlarged from 0.849 to 0.954 Å in the cleavage over the chlorine atom (**ts1c2**), and from 0.809 to 0.913 Å in the splitting over the oxygen atom (**ts1a2**). The metal−hydride distance, however, has decreased in both cases, from 1.988 to 1.935 Å in **ts1c2** and from 1.953 to 1.917 Å in **ts1a2**. Compared to the unassisted mechanism, the metal−ligand distances have decreased by 0.347 Å (2.398 Å) and by 0.220 Å (2.645 Å) for the O and Cl atom ligands.

The energies of the transition states with respect to the initial reactants are 31.5 and 26.8 kcal/mol over O and Cl, respectively, these values being much more consistent with the experimental results than those obtained for the direct heterolytic activation. The results indicate that the heterolytic cleavage of H_2 mediated by ethanol significantly lowers the activation barriers, decreasing those by almost 16 and 11 kcal/mol, respectively, indicating that the solvent can play a critical role in the reaction mechanism. To prove this experimentally, the hydrogenation of diethyl benzylidenesuccinate with **3Au(III)** has been carried out under the same reaction conditions but using two solvents with different proton donor ability, i.e., ethanol and acetone. The results given in Figure 9 show that, in agreement with the prediction, the initial rate of the reaction increases (the extension of the induction period decreases) when the solvent is changed from acetone to ethanol. In a more general way, these results, together with others,[45] suggest that protic polar solvents can play a determinant role in the activation of the molecular hydrogen.

The intermediate species formed after the heterolytic cleavage of H_2 over the O and Cl are not analogous. In the first case, the gold hydride and the EtOH molecule are formed, while the proton goes to the alkoxy ligand to form the corresponding alcohol. In the second case, besides the metal hydride, the proton goes to the alcohol molecule, forming $EtOH_2^+$ and Cl^- species.

In summary, the initial activation of the dihydrogen molecule with the assistance of an ethanol molecule, forming the hydride complex, chloride, and $EtOH_2^+$ species (intermediate **Ic1a**), is the most feasible pathway to initiate the catalytic cycle.

(ii) Coordination of the Olefin to the Catalyst. The next step in the catalytic cycle should involve the alkene molecule. Hence, two alternative ways to coordinate the ethene molecule to the gold complex have been studied. One consists of replacing the amine of the salen ligand, giving rise to intermediate **Ic2a**, whereas the other consists of forming a five-coordinated intermediate, **Ic2bis**, with the alkene occupying the fifth coordination site. These two pathways are schematically presented in Figure 10.

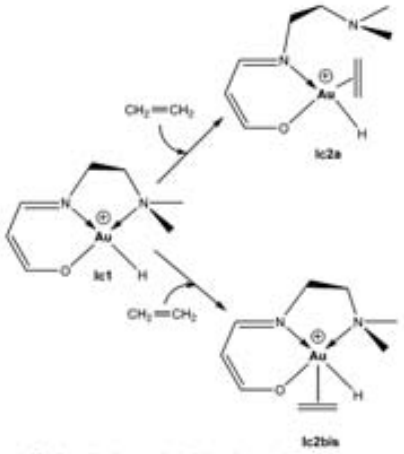

Figure 10. Coordination modes of the ethene molecule.

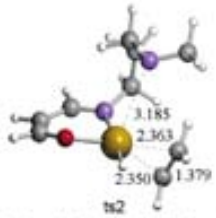

Figure 11. TS for the ligand substitution of the salen amine ligand by the incoming ethene. Atom colors: C, gray; H, white; Cl, green; N, purple; O, red; and Au, golden.

For the case where the alkene replaces the N(amine) of the salen ligand, the metallic complex remains with a square planar structure. The transition state, **ts2**, is quite product-like, with distances between the carbon atoms of the ethene and the gold atom of 2.350 and 2.363 Å, respectively (Figure 11). The Au−N bond is practically broken, with a distance of 3.185 Å. The energy of the transition state, **ts2**, for this ligand replacement is 9.3 kcal/mol, whereas the intermediate, **Ic2a**, lies 8.0 kcal/mol above the separate initial reactants.

In a related study by Vrieze, van Leeuwen, and co-workers on the insertion reaction of CO into a Pd−C bond on complexes containing terdentate nitrogen ligands, it was analogously proposed that one of the terminal N's of the chelate ligand is substituted by the incoming CO within the reaction mechanism.[50]

Comparing thermodynamically the trigonal bipyramid, **Ic2bis**, and the square planar **Ic2a**, the relative energies for these two isomers are 6.7 and 8.0 kcal/mol, respectively. Nevertheless, the energy of the transition state to obtain the pentacoordinated structure is 22.2 kcal/mol, above the energy of the separate

(50) Groen, J. H.; Zwart, A. D.; Vlaar, M. J. M.; Ernsting, J. M.; van Leeuwen, P. W. N. W.; Vrieze, K.; Kooijman, H.; Smeets, W. J. J.; Spek, A. L.; Budzelaar, P. H. M.; Xiang, Q.; Thummel, R. P. *Eur. J. Inorg. Chem.* **1998**, 1129.

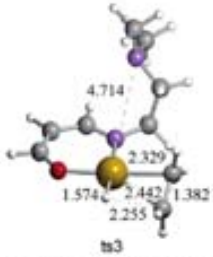

Figure 12. TS of the insertion process of the ethene molecule into the Au−H bond. Atom colors: C, gray; H, white; Cl, green; N, purple; O, red; and Au, golden.

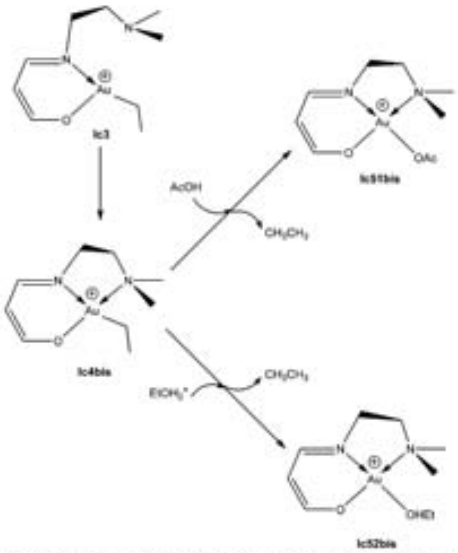

Figure 13. Different protonation processes depending on the protonating agent.

reactants. Thus, the energy of the transition state within the potential energy surface is much lower than that obtained for the formation of the pentacoordinated structure (9.3 vs 22.2 kcal/mol). Hence, according to these results, the pathway going through a trigonal bipyramidal structure is less energetically favorable by 12.9 kcal/mol than that involving a square planar structure where the aminic N is not coordinated to the metal.[30]

The difference between **Ic2a** and the next intermediate, **Ic2b**, is a rotation of the lateral chain of the aminic N ligand (0.9 kcal/mol), the coordination of the olefin in both cases being perpendicular to the plane containing the metal center and the other ligands.

Once the olefin is in the coordination sphere of the catalyst, the following step corresponds to the insertion of the alkene into the Au−H bond. The energy of the formed intermediate, **Ic3**, is −2.0 kcal/mol. The **ts3** structure (see Figure 12) involves the rotation of the olefin concomitantly to the insertion process

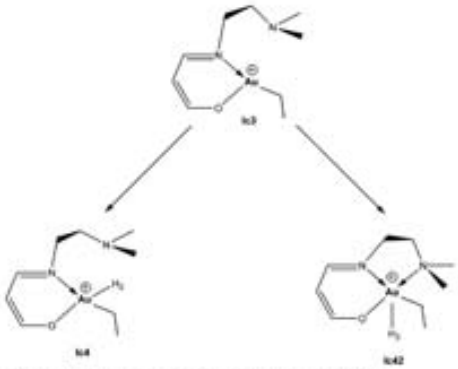

Figure 14. Coordination modes of the dihydrogen molecule.

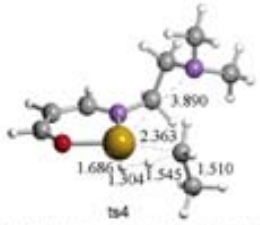

Figure 15. TS of H_2 hydrogenolysis to close the catalytic cycle. Atom colors: C, gray; H, white; Cl, green; N, purple; O, red; and Au, golden.

itself. The forming C−H bond is 2.255 Å, and the associated barrier is around 4 kcal/mol.

(iii) Closing the Catalytic Cycle. The next step in the reaction mechanism corresponds to the second hydrogenation process. At this point, several hydrogen sources have been considered: a proton donor present in solution, like an acid (AcOH), a protonated solvent molecule ($EtOH_2^+$, generated in the heterolytic activation of H_2), and the dihydrogen molecule (H_2).

Figure 13 shows the possible pathways when the hydrogen source is a proton donor present in solution. In this case, we considered that the N(amine) of the salen ligand coordinates to the vacant site to form the **Ic4bis** intermediate. This process is exothermic by 37.2 kcal/mol. The reaction between **Ic4bis** and AcOH gives rise to the **Ic51bis** intermediate and the ethane products. The energy barrier for this process is 57.5 kcal/mol, which is too high for the reaction to proceed through this mechanism. In a similar way, using ethanol (the solvent itself) as a proton donor, the barrier will be even higher due to the lower acidity of ethanol.

We have also considered a protonated solvent molecule ($EtOH_2^+$), which is the strongest acid species in an ethanol solution, as a proton donor. This species may be generated in the initiation step after the heterolytic cleavage of a H_2 molecule, or from the addition of acetic acid to the reaction media. The energy barrier for this process, which generates the intermediate **Ic52bis**, is 37.5 kcal/mol. Though lower than in the previous case, this is still too high to be acceptable within the reaction mechanism.

Given the fact that these two species explored as proton donors give very high energy barriers, we have considered an

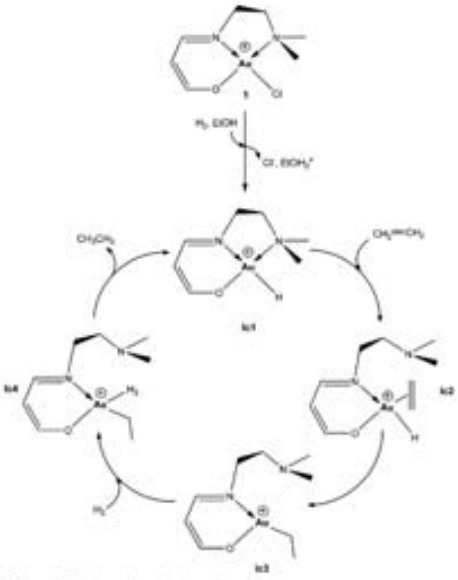

Figure 16. Proposed catalytic cycle.

alternative pathway where the proton source is the dihydrogen molecule. For the coordination of the H_2 into the intermediate **Ic3**, there are two alternatives: a process where the dihydrogen molecule coordinates into the vacant site of intermediate **Ic3** to form intermediate **Ic4**, or a process where the N(amine) of the salen ligand coordinates to the vacant site (**Ic4bis**), and after that the H_2 molecule coordinates to the complex, forming a pentacoordinated complex, **Ic42** (see Figure 14).

Extensive investigation of the energy potential surface around the coordination mode for **Ic42** intermediate was performed with no success, suggesting that if this intermediate exists, it will be very high in energy.

The analysis of the other alternative pathway, in which the H_2 molecule coordinates to the vacant site, shows that the energy of the **Ic4** intermediate is −2.9 kcal/mol. Once H_2 is coordinated, the next step should correspond to hydrogenolysis, giving both the regenerated hydride−metal catalyst and the final product, ethane (**Ic1c**). The H_2 activation proceeds via a four-centered metathesis-like transition state (**ts4**, see Figure 15), which is characterized by a highly dissociated H−H bond (1.304 Å). The Au−H bond-forming distance is 1.686 Å, whereas the C−H bond-forming distance is 1.545 Å. Although the Au−N distance is quite long (3.890 Å), the aminic N atom ends up coordinating to the metal center, and therefore regenerating the catalyst.

The barrier for this step, 15.0 kcal/mol, is not very energetically demanding and provides an elegant and easy way of closing the catalytic cycle. An analogous hydrogenolysis step has also been proposed by Morokuma, Musaev, and co-workers in diimine−nickel-catalyzed ethylene polymerization.[51]

The Global Reaction Mechanism. The complete catalytic cycle, simplifying the steps which involve conformational rearrangements, is shown in Figure 16. The corresponding energy profile for the complete catalytic cycle is shown in Figure 17.

In the proposed catalytic mechanism, the highest energy barrier corresponds to the heterolytic activation of the H_2 molecule, giving rise to the substitution of the chlorine by H. This should result in an induction period in the kinetic curve, which is found experimentally to be more significant at low temperature (Figure 18a) and when the steric impediment for the olefin increases (diethyl itaconate < diethyl citraconate <

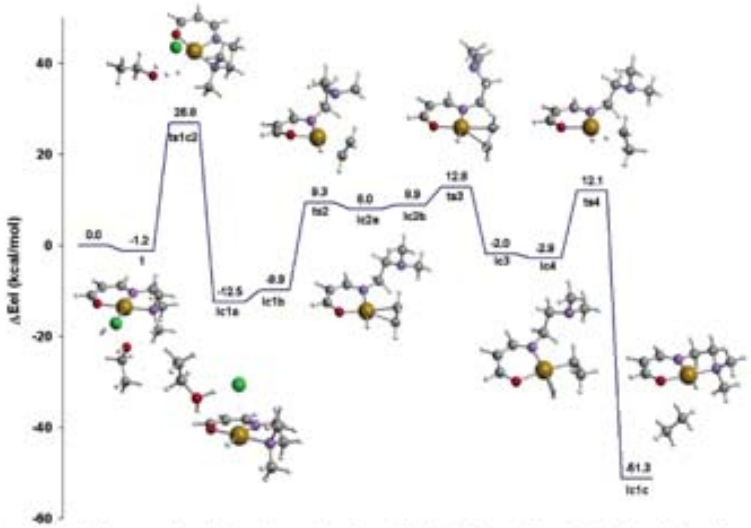

Figure 17. Energy profile for the proposed mechanism. Atom colors: C, gray; H, white; Cl, green; N, purple; O, red; and Au, golden.

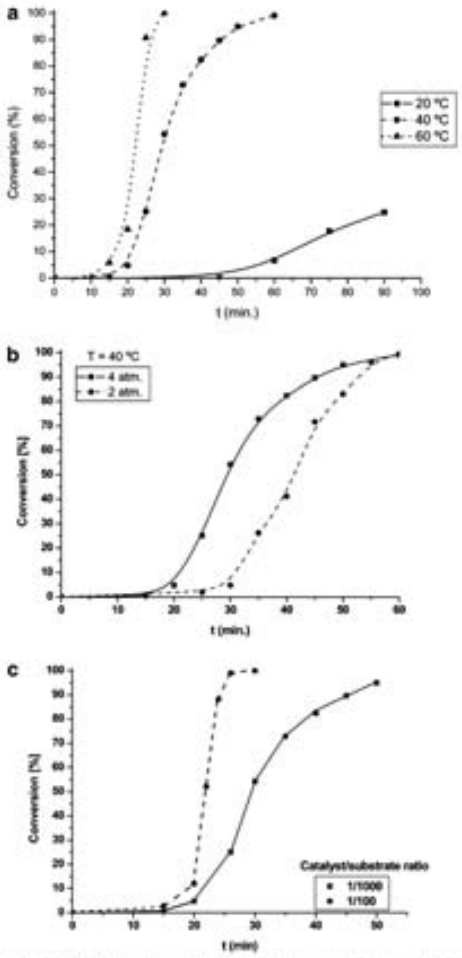

Figure 18. Hydrogenation of diethyl benzylidenesuccinate using catalyst **2Au(III)** and ethanol as solvent: (a) influence of the reaction temperature, (b) influence of the H_2 pressure, and (c) influence of the substrate concentration.

diethyl benzylidenesuccinate). Also in agreement with this, we have seen that the induction period diminishes when the partial pressure of H_2 is increased from 2 to 4 bar (Figure 18b). In this step, the solvent is playing a critical role by lowering the activation barrier, as is observed experimentally (Figure 9). Also, Figure 18c shows the influence of the substrate concentration on the kinetic profile.

The hydrogen molecule only has to be initially activated by means of solvent-assisted heterolytic cleavage. After this initiation step, the activation of the H_2 molecule takes place in a different way within the catalytic cycle. The H_2 molecule coordinates to a vacant site to undergo a hydrogenolysis process.

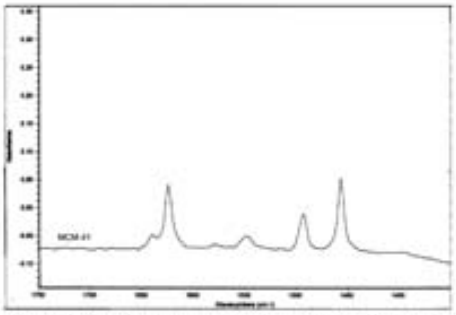

Figure 19. IR spectrum of pyridine adsorbed on MCM-41, Si/Al = 50.

In such a way, the catalytic cycle proceeds much more easily. After the induction period that corresponds to the formation of species **Ie1a** (see Figures 7 and 17), the highest energy barrier step within the catalytic cycle corresponds to the inclusion of the olefin (**ts2**). In good agreement with this, we observe that, after the induction period, the rate of the reaction increases with increasing olefin concentration up to a value in which saturation of active sites occurs and the pseudo-order of the reaction becomes zero with respect to the olefin.

The activation energy for the olefin insertion step calculated theoretically is in the order of 19 kcal/mol. If we calculate to a first approximation the apparent activation energy from the reaction rate corresponding to the conversion data at different temperatures given in Figure 18a for the hydrogenation of diethyl benzylidenesuccinate, a value of ~10 kcal/mol is obtained, which is in the range of values found very often for alkene hydrogenation.

Enhancing Catalytic Activity by Supporting the Homogeneous Catalysts: Lessons from the Theoretical Study. From the theoretical study on the reaction mechanism for hydrogenation of olefins with the gold catalyst, it was concluded that the solvent plays an important role. Furthermore, the presence of proton donor species can also be positive for the reaction to occur. Then, if this is the case, it may very well be that, by supporting the homogeneous gold complex on a polar support, its activity can increase instead of decreasing as generally occurs when supporting metal complexes on solid carriers. Furthermore, if protons are generated on the surface of the support, this can have a further positive catalytic effect, as explained in previous sections. To test these hypotheses, we have supported Au(III) complexes **2** and **5** on pure silica MCM-41 and ITQ-2, whose surfaces have many silanol groups (very polar supports), as well as on MCM-41 in the form of aluminosilicate that presents surface Brönsted acid sites.[52] All solids were functionalized in the same manner according to the procedure showed in Scheme 2. The heterogenized complexes were also characterized by spectroscopic and analytical methods, and they remain unaltered after the heterogenization process, as can be seen in Figures 2 and 3.

The catalytic results presented in Table 2 clearly show an increase in TOF when Au(III) complexes **2** and **5** are supported on the two high surface polarity carriers. In the case of ligand

(51) Munaev, D. G.; Froese, R. D. J.; Svensson, M.; Morokuma, K. *J. Am. Chem. Soc.* **1997**, *119*, 367.
(52) Corma, A. *Chem. Rev.* **1997**, *97*, 2373.

2, this has also been supported on the corresponding aluminosilicate (ratio Si/Al = 50) of the MCM-41 that presents Brönsted acidity, as demonstrated by pyridine adsorption. Indeed, the IR spectrum of pyridine adsorbed on the MCM-41 (Si/Al = 50) shows, after desorption at 150 °C in a vacuum to remove the physisorbed pyridine (Figure 19), a band at ~1545 cm^{-1} that corresponds to the pyridinium ion formed by protonation of pyridine by surface Brönsted acid sites. The results in Table 2 indicate that the presence of surface acidity further increases the activity of the catalyst owing to the stabilization of the charged transition state.

It is worth mentioning that the gold complexes have an activity similar to those of Pd (see Table 2), the effects of the support being very similar. This can be an indication that the hydrogenation proceeds through a similar mechanism on both types of complexes.

Conclusions

It has been found that Au(III)−Schiff base complexes are active catalysts for hydrogenation of olefins, their activity being similar to that of the corresponding Pd complexes.

The mechanism of the reaction involves as the first step the heterolytic cleavage of H_2, this being the controlling step of the reaction, as demonstrated by the presence of an induction period in the kinetic curve.

In this step, the selection of the solvent plays a critical role for lowering the activation barrier. After the induction period, which corresponds to the formation of the active catalytic species, has occurred, the controlling step of the reaction is the insertion of the olefin.

It is found that, by supporting the Au(III) complexes on a high surface polarity support, the catalytic activity does not, as usual, decrease but rather increases. This increase is even larger when the surface of the carrier contains Brönsted acid sites.

Salen complexes of Au(III) give the same TOF as the corresponding complexes of Pd(II), Au(III) having the same d^8 electronic structure as Pd(II). The same positive effect of the support is also observed with the Pd(II) complex, suggesting that a similar mechanism of reaction should apply to the salen−Pd(II) complexes.

Acknowledgment. The authors thank Ministerio de Educación y Ciencia (Project MAT2003-07945-C02-01 and -02, Project CTQ2005-09000-C02-01, Ramón y Cajal contract to G.U., and FPU fellowships to A.C.-V.), the Auricat EU Network (HPRN-CT-2002-00174), and Generalitat de Catalunya (2005/SGR/00896) for financial support.

Supporting Information Available: Complete ref 36 and absolute energies and Cartesian coordinates. This material is available free of charge via the Internet at http://pubs.acs.org.

JA057998O

A.2 Article V

Inorg. Chem. 2007, 46, 4103–4113

Nature of $Cp^*MoO_2^+$ in Water and Intramolecular Proton-Transfer Mechanism by Stopped-Flow Kinetics and Density Functional Theory Calculations

Joo-Eun Jee,[†] Aleix Comas-Vives,[‡] Chiara Dinoi,[§] Gregori Ujaque,[‡] Rudi van Eldik,*[†] Agustí Lledós,*[‡] and Rinaldo Poli*[§]

Institute for Inorganic Chemistry, University of Erlangen-Nürnberg, Egerlandstrasse 1, 91058 Erlangen, Germany, Unitat de Química Física, Departament de Química, Edifici Cn, Universitat Autònoma de Barcelona, 08193 Bellaterra, Catalonia, Spain, and Laboratoire de Chimie de Coordination, UPR CNRS 8241 liée par convention à l'Université Paul Sabatier et à l'Institut National Polytechnique de Toulouse, 205 Route de Narbonne, 31077 Toulouse Cedex, France

Received December 15, 2006

A stopped-flow study of the $Cp^*MoO_3^-$ protonation at low pH (down to zero) in a mixed H_2O–MeOH (80:20) solvent at 25 °C allows the simultaneous determination of the first acid dissociation constant of the oxo–dihydroxo complex, $[Cp^*MoO(OH)_2]^+$ ($pK_{a1} = -0.56$), and the rate constant of its isomerization to the more stable dioxo–aqua complex, $[Cp^*MoO_2(H_2O)]^+$ ($k_{-2} = 28\ s^{-1}$). Variable-temperature (5–25 °C) and variable-pressure (10–130 MPa) kinetics studies have yielded the activation parameters for the combined protonation/isomerization process (k_{-2}/K_{a1}) from $Cp^*MoO_2(OH)$ to $[Cp^*MoO_2(H_2O)]^+$, viz., $\Delta H^{\ddagger} = 5.1 \pm 0.1$ kcal mol^{-1}, $\Delta S^{\ddagger} = -37 \pm 1$ cal mol^{-1} K^{-1}, and $\Delta V^{\ddagger} = -9.1 \pm 0.2$ cm^3 mol^{-1}. Computational analysis of the two isomers, as well as the $[Cp^*MoO_2]^+$ complex resulting from the dissociation of water, reveals a crucial solvent effect on both the isomerization and the water dissociation energetics. Introducing a solvent model by the conductor-like polarizable continuum model and especially by explicitly inclusion of up to three water molecules in the calculations led to the stabilization of the dioxo–aqua species relative to the oxo–dihydroxo isomer and to the substantial decrease of the energy cost for the water dissociation process. The presence of a water dissociation equilibrium is invoked to account for the unusually low effective acidity ($pK_{a1}' = 4.19$) of the $[Cp^*MoO_2(H_2O)]^+$ ion. In addition, the computational study reveals the positive role of external water molecules as simultaneous proton donors and acceptors, having the effect of dramatically lowering the isomerization energy barrier.

Introduction

The precise structure of aqua complexes and ions in a water solution is rarely known. For instance, molybdic acid (H_2MoO_4) is commonly represented as $Mo(OH)_6$, $MoO_2(OH)_2(H_2O)_2$, and $MoO_3(H_2O)_3$,[1–6] while its first protonation product has been described as $Mo(OH)_5(H_2O)^+$ or $MoO_2(OH)(H_2O)_3^+$,[1,4,5] although the isomeric formulation $MoO(OH)_3(H_2O)_2^+$ could also be envisaged. To the best of our knowledge, the factors regulating the relative energy of a transition-metal–dihydroxo complex and its isomeric aqua–oxo form (Chart 1) are not well understood. In terms of the rate and mechanism of water-exchange reactions, the correct assignment of such species is of utmost importance because

* To whom correspondence should be addressed. Tel: +33-561333173. Fax: +33-561553003. E-mail: vaneldik@chemie.uni-erlangen.de (R.v.E.), agusti@klingon.uab.es (A.L.), poli@lcc-toulouse.fr (R.P.).
† University of Erlangen-Nürnberg.
‡ Universitat Autònoma de Barcelona.
§ UPR CNRS 8241 liée par convention à l'Université Paul Sabatier et à l'Institut National Polytechnique de Toulouse.

(1) Cruywagen, J. J.; Heyns, J. B. B.; Rohwer, E. F. C. H. *J. Inorg. Nucl. Chem.* **1976**, *38*, 2033–2036.
(2) Cruywagen, J. J.; Draaijer, A. G.; Rypstra, T. *S. Afr. J. Chem.* **1988**, *41*, 89–96.
(3) Castro-Garcia, S.; Pecquenard, B.; Bender, A.; Livage, J.; Julien, C. *Ionics* **1997**, *3*, 104–109.
(4) Cruywagen, J. J.; Draaijer, A. G.; Heyns, J. B. B.; Rohwer, E. A. *Inorg. Chim. Acta* **2002**, *331*, 322–329.
(5) Paffett, M. T.; Anson, F. C. *Inorg. Chem.* **1981**, *20*, 3967–3972.
(6) Cruywagen, J. J. *Adv. Inorg. Chem.* **2000**, *49*, 127–182.

10.1021/ic062409g CCC: $37.00
Published on Web 04/10/2007

Chart 1

it is well-known that water-exchange reactions follow the reactivity order $M-OH_2 \gg M-OH \gg M=O$.[7]

In the organometallic area, the complex $Cp^*_2Zr(OH)_2$ is a stable compound,[8] whereas Cp^*_2ZrO is a reactive intermediate.[9] On the other hand, Cp^*_2WO and $Cp^*_2Ta(O)H$ are stable compounds that exchange water through $Cp^*_2W(OH)_2$ and $Cp^*_2Ta(OH)_2H$ intermediates.[10] Finally, the closely related oxo and dihydroxo complexes $[CpMoO(PMe_3)_2]^+$ and $[(\eta^5\text{-}C_5Et_5)Mo(OH)_2(dppe)]^+$ have been isolated and structurally characterized.[11,12] In these systems, Cp, Cp*, and related chelates are expected to have a drastic influence on the rate and mechanism of the water-exchange process on the basis of data reported in the literature for water exchange on $[Cp^*Rh(H_2O)_3]^{2+}$ and $[Cp^*Ir(H_2O)_3]^{2+}$, which is 14 orders of magnitude faster than that for the corresponding hexaaqua complexes and proceeds according to a more dissociative substitution mode.[13,14]

Some of us have initiated an investigation of the aqueous chemistry of high-oxidation-state organometallic compounds, focusing initially on Cp*Mo derivatives in a variety of oxidation states (VI, V, IV, and mixed-valence clusters).[15] High-oxidation-state oxomolybdenum compounds are employed in a variety of catalytic reactions, such as olefin epoxidation, the selective oxidation of alcohols to aldehydes, the dehydrogenation and isomerization of alkenes, and even reductive processes such as the hydrosilylation of carbonyl compounds.[16] Organometallic versions of these systems have shown high activities, notably in olefin epoxidation.[17−20] It would therefore be of interest to adapt these catalytic processes to an aqueous environment. To this end, knowledge of the nature of the Cp^*Mo^{VI} aqua ion under different pH conditions is very useful.

A previous investigation of the aqueous speciation of Cp^*Mo^{VI} has given the results summarized in Figure 1.[21] In

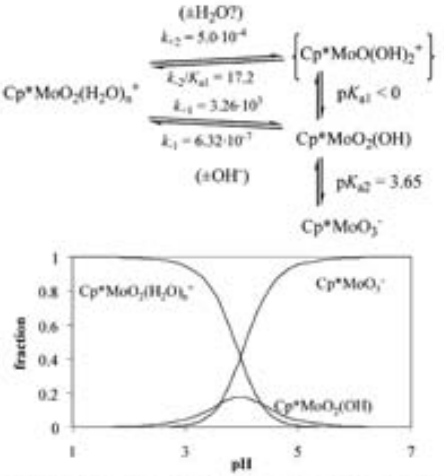

Figure 1. Thermodynamic and kinetic parameters related to the Cp^*Mo^{VI} system in a $H_2O-MeOH$ (80:20) solution.[21]

particular, the rate of conversion of compound $Cp^*MoO_2(OH)$ (generated quantitatively by the rapid protonation of $Cp^*MoO_3^-$ at pH $\leq$ 2) to the final cationic product was found to be first order in $[H^+]$. The interpretation of this result leaves two possibilities, as detailed in Scheme 1, both involving a proton addition pre-equilibrium to yield an intermediate cationic dihydroxo complex. The first possibility (path a) involves a rapid equilibrium rearrangement to an aqua−oxo isomer, followed by a rate-determining loss of a water ligand, whereas the second one (path b) involves the intramolecular isomerization process as a rate-determining step. The $[Cp^*MoO(OH)_2]^+$ ion is likely a strong acid in water ($pK_{a1} < 0$) because most multiprotic inorganic oxo acids (e.g., H_2CO_3, H_2SO_3, H_3PO_4, ...) are characterized by a ΔpK_a of ca. 4−5 and the pK_{a2} [acid dissociation of $Cp^*MoO_2(OH)$] is 3.65. Thus, the aquation state of the final cationic product is uncertain, $[Cp^*MoO_2(H_2O)_n]^+$ with either $n = 0$ or 1. The two possibilities cannot be distinguished on the basis of the kinetics experiment or by use of ^1H NMR spectroscopy because only the large solvent resonance was observed under all pH conditions, providing only negative evidence for water coordination (either the resonance of the coordinated water molecule could be overshadowed by the much stronger solvent resonance or the ligand exchange is in the fast regime, leading to a single averaged resonance). IR spectroscopy is also useless for such dilute solutions in a strongly absorbing medium.

Subsequent attempts to crystallize a salt of the $[Cp^*MoO_2(H_2O)_n]^+$ ion and to determine its aquation state by X-ray crystallography have not been successful, always yielding

(7) Richens, D. T. *Chem. Rev.* **2005**, *105*, 1961−2002.
(8) Bertolin, R.; Patel, V.; Munday, I.; Taulor, N. J.; Carty, A. J. *J. Chem Soc., Chem. Commun.* **1985**, 456−458.
(9) Carney, M. J.; Walsh, P. J.; Bergman, R. G. *J. Am. Chem. Soc.* **1990**, *112*, 6426−6428.
(10) Parkin, G.; Bercaw, J. E. *Polyhedron* **1988**, *7*, 2053−2082.
(11) Fettinger, J. C.; Kraatz, H.-B.; Poli, R.; Quadrelli, E. A. *J. Chem Soc., Dalton Trans.* **1999**, 497−508.
(12) Morales, D.; Pleune, B.; Poli, R.; Richard, P. *J. Organomet. Chem.* **2000**, *596*, 64−69.
(13) Dadci, L.; Elias, H.; Frey, U.; Hoernig, A.; Koelle, U.; Merbach, A. E.; Paulus, H.; Schneider, J. S. *Inorg. Chem.* **1995**, *34*, 306−315.
(14) Helm, L.; Merbach, A. E. *Chem. Rev.* **2005**, *105*, 1923−1959.
(15) Poli, R. *Chem.−Eur. J.* **2004**, *10*, 332−341.
(16) Reis, P. M.; Romão, C. C.; Royo, B. *J. Chem. Soc., Dalton Trans.* **2006**, 1842−1846.
(17) Abrantes, M.; Santos, A.; Mink, J.; Kühn, F.; Romão, C. *Organometallics* **2003**, *22*, 2112−2118.
(18) Zhao, J.; Santos, A. M.; Herdtweck, E.; Kühn, F. E. *J. Mol. Catal. A* **2004**, *222*, 265−271.
(19) Martins, A. M.; Romão, C. C.; Abrantes, M.; Azevedo, M. C.; Cui, J.; Dias, A. R.; Duarte, M. T.; Lemos, M. A.; Lourenço, T.; Poli, R. *Organometallics* **2005**, *24*, 2582−2589.
(20) Zhao, J.; Herdtweck, E.; Kühn, F. E. *J. Organomet. Chem.* **2006**, *691*, 2199−2206.
(21) Collange, E.; Garcia, J.; Poli, R. *New J. Chem.* **2002**, *26*, 1249−1256.

Scheme 1

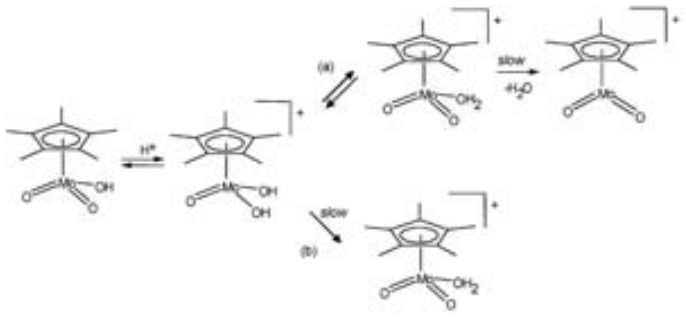

instead the neutral dinuclear compound $Cp^*_2Mo_2O_5$.[22] In fact, the low-solubility product of this compound drives its precipitation by combination with the thermodynamically unfavorable (at low pH; see Figure 1) anionic hydrolysis product, $Cp^*MoO_3^-$. Another point that has remained unexplained from the previous study[23] concerns the greater thermodynamic stability of the dioxo cation, $Cp^*MoO_2^+$ (or its water adduct), relative to the oxo−dihydroxo isomer, $Cp^*MoO(OH)_2^+$.

In this contribution, we present a more detailed stopped-flow kinetics investigation of the generation of the $[Cp^*MoO_2(H_2O)_n]^+$ ion in the low-pH regime, including variable-temperature and variable-pressure experiments, as well as a density functional theory (DFT) computational study aimed at establishing (i) the aquation state of this ion and (ii) the mechanism of the slow process that leads to its generation. The results of this theoretical investigation are potentially of more general interest because they illustrate the effect of the medium on the relative stability of oxo− and dihydroxo−transition-metal species.

Results and Discussion

(a) Aquation State of $[Cp^*MoO_2(H_2O)_n]^+$. The reaction shown in eq 1 was studied computationally by DFT methods on the full systems (i.e., no ligand simplification was adopted). Both complexes were optimized in the gas phase. These two minima are shown in Figure 2. The unsolvated species give rise to a bent geometry, with the Mo−Cp* ring centroid axis forming an angle of 136.9° from the MoO_2 plane, which is only slightly smaller than the same angle in the water adduct (141.9°). Relative to the ideal planar structure (optimized independently under constrained C_s symmetry), this configuration is more stable by only 2.9 kcal mol^{-1}.

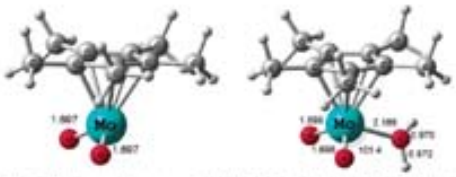

Figure 2. Optimized structures of the $[Cp^*MoO_2]^+$ and $[Cp^*MoO_2(H_2O)]^+$ (**2a**) complexes.

$$[Cp^*MoO_2]^+ + H_2O \rightleftarrows [Cp^*MoO_2(H_2O)]^+ \quad (1)$$
2a

The electronic structure of two-legged piano-stool complexes has been analyzed before,[21−25] including the effect of the coordination environment[26,27] and spin state[28,29] on the relative stability of planar and bent geometries. All previous studies, however, are restricted to electronically unsaturated (16-electron) d^0 systems, typically containing π-acidic (e.g., CO), neutral (e.g., H), or weakly donating (e.g., Cl) ligands. On the other hand, complex $[Cp^*MoO_2]^+$ features two strong double-sided π donors on a d^0 metal center. Because the Cp^{*-} ligand is electronically isolobal with the O^{2-} ligand (both are potentially 6-electron, $\sigma + 2\pi$ donors), the compound can also be considered as isolobally related to MoO_3, which is a d^0 MX_3 system with strong double-sided π-donor ligands. The geometric preference for d^0 MX_3 systems has been recently analyzed by Eisenstein et al.[30] for M = group 3, group 4, and lanthanide elements and X = alkyl, halide, and amido groups. It was found that the pyramidal structure is always preferred because of the d orbital participation in M−X σ bonding, whereas the ionic component should favor the planar structure. The contribution from π donation provides a driving force toward flattening of the structure. Therefore, it seems that the Mo−Cp* and

(22) Collange, E.; Meneau, L.; Richard, P.; Poli, R. *Polyhedron* **2004**, *23*, 2605−2610.
(23) Hofmann, P. *Angew. Chem., Int. Ed. Engl.* **1977**, *16*, 536−537.
(24) Schilling, B. E. R.; Hoffmann, R.; Lichtenberger, D. L. *J. Am. Chem. Soc.* **1979**, *101*, 585−591.
(25) Schilling, B. E. R.; Hoffmann, R.; Faller, J. W. *J. Am. Chem. Soc.* **1979**, *101*, 592−598.
(26) Johnson, T. J.; Folting, K.; Streib, W. E.; Martin, J. D.; Huffman, J. C.; Jackson, S. A.; Eisenstein, O.; Caulton, K. G. *Inorg. Chem.* **1995**, *34*, 488−499.
(27) Ward, T. R.; Schafer, O.; Daul, C.; Hofmann, P. *Organometallics* **1997**, *16*, 3207−3215.
(28) Smith, K. M.; Poli, R.; Legzdins, P. *Chem. Commun.* **1998**, 1903−1904.
(29) Smith, K. M.; Poli, R.; Legzdins, P. *Chem.−Eur. J.* **1999**, *5*, 1598−1608.
(30) Perrin, L.; Maron, L.; Eisenstein, O. *Faraday Discuss.* **2003**, *124*, 25−39.

Mo−O σ interactions dominate the geometric preference for the $[Cp^*MoO_2]^+$ ion. We have also calculated the isolobal MoO_3 system and found that the pyramidal structure (O−Mo−O = 109.7°) is again favored, in this case by 9.5 kcal mol^{-1} with respect to the D_{3h} structure. The Mo−ligand interactions, nevertheless, have a significant contribution from ionicity. This is suggested by the values of the Mulliken charges; for instance, the charges in the $[Cp^*MoO_2]^+$ ion are +1.38 for Mo and −0.52 (average) for the two O atoms, whereas in the MoO_3 molecule, they are +1.88 and −0.63, respectively, showing that the metal is electron-richer in $[Cp^*MoO_2]^+$ than in MoO_3.

As expected, the addition of a water molecule results in an energetic stabilization of the $[Cp^*MoO_2]^+$ complex, corresponding to a potential energy gain of 39.7 kcal mol^{-1} in the gas phase. In addition to providing additional covalent bonding stabilization, this process is also favorable from an electrostatic point of view because a positively charged Mo atom (Mulliken charge 1.37) is directly linked to the O atom of a water molecule, which has a marked anionic character (Mulliken charge −0.71). Although this addition process is entropically disfavored, the free-energy difference of the reaction is still exergonic by 28.1 kcal mol^{-1}. The inclusion of solvent effects by means of the conductor-like polarizable continuum model (CPCM) method significantly changes the results. The energetic difference remains in favor of the water adduct, but the gain is reduced to 10.1 kcal mol^{-1}. Having the $Cp^*MoO_2^+$ ion and the water molecules separated in the gas phase is a very energy-costing process because a strong cation−dipole interaction is broken. Adding solvent effects stabilizes the separated reactants by interacting with the dielectric continuum of the polar medium, leading to a considerable decrease in the energy difference between the isolated species and the aqua complex. The conclusion of this investigation is to establish the nature of the acidic form of Cp^*Mo^{VI} in water as the aqua complex $[Cp^*MoO_2(H_2O)]^+$, although the dissociation of the water ligand to afford the $[Cp^*MoO_2]^+$ intermediate may be a facile process. As mentioned in the Introduction, from a kinetics point of view, the Cp* ligand is known to exert a strong trans effect on ligand dissociation processes. The introduction of the Cp* ligand on the very inert hexaaqua complexes of iridium(III) and rhodium(III), i.e., on going from the $[M(H_2O)_6]^{3+}$ complexes to the $[Cp^*M(H_2O)_3]^{2+}$ complexes (M = Rh and Ir), increases the water-exchange rate by 12−14 orders of magnitude.[13] A ^{17}O NMR investigation of the water-exchange process for the $Cp^*Mo^{VI}_{aq}$ system as a function of pH is currently ongoing in our laboratories and will be reported in detail in a separate contribution, but we are already able to state that this appears to be an extremely fast process. Therefore, the mechanism of the low-pH transformation leading from $Cp^*MoO_2(OH)$ to $[Cp^*MoO_2(H_2O)]^+$ may be formulated as path b in Scheme 1, with the slow step being the intramolecular proton-transfer process, leading from the intermediate dihydroxo complex $[Cp^*MoO(OH)_2]^+$ to the final product.

(b) Protonation Kinetics in the Low-pH Regime. In an effort to determine the first acid dissociation constant of $[Cp^*MoO(OH)_2]^+$ (pK_{a1}), the acidification kinetics of $[Cp^*MoO_3]^-$ was studied at low pH (down to zero), where the complex is present in the $[Cp^*MoO_2(OH)]$ form (pK_{a2} = 3.65; see Figure 1). Consistent with the previous study,[21] acidification kinetics showed a linear $[H^+]$ dependence up to 0.35 M (pH = 0.45), but a slight saturation effect was visible at concentrations up to 1 M (pH down to 0) as shown in Figure 3. This behavior is fully consistent with the previously established scheme (Figure 1) because the rate law for the acidification reaction can be expressed as in eq 2 (the equilibrium K_{a1} is rapidly maintained on the time scale of k_{-1} and k_{-2}).[21] At low $[H^+]$ ($K_{a1}^{-1}[H^+] \ll 1$), the rate law further simplifies to eq 3, which accounts for the linear dependence observed under such conditions. The small intercept could be ascribed to a minor contribution of the parallel k_{-1} path. It is useful to remind the reader here that at low pH the k_{-1} pathway, corresponding to direct loss of OH^- from $Cp^*MoO_2(OH)$, should be negligible ($k_{-1} = 6.32 \times 10^{-7}$ s^{-1}) compared to the k_{-2} pathway, corresponding to protonation and isomerization of the $[Cp^*MoO(OH)_2]^+$ intermediate, e.g., $k_{-2}K_{a1}^{-1}[H^+] = 1.73$ s^{-1} at pH = 1. Alternatively, the intercept can also be due to a contribution of the back reaction, i.e., the k_2 path.

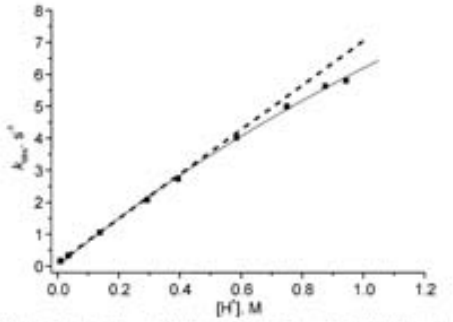

Figure 3. Plot of k_{obs} vs $[H^+]$ for the acidification of $[Cp^*MoO_3]^-$ with HNO_3 in the range 0.01−0.95 M. Experimental conditions: $[Cp^*_2Mo_2O_5]$ = 4 × 10^{-4} M, λ_{det} = 390 nm, 20% MeOH−H_2O, temp = 25 °C, μ_{tot} = 1 M (adjusted with $NaNO_3$).

$$k_{obs} = \{k_{-1} + k_{-2}K_{a1}^{-1}[H^+]\}/\{1 + K_{a1}^{-1}[H^+]\} \quad (2)$$

$$k_{obs} \sim k_{-1} + k_{-2}K_{a1}^{-1}[H^+] \quad (\text{if } [H^+] \text{ is small}) \quad (3)$$

The fit of the data in Figure 3 with the expression of eq 4, for which the small contribution of the intercept was ignored, resulted in $k_{-2} = 28 \pm 1$ s^{-1} (log $k_{-2} = 1.44$) and $K_{a1} = 3.6 \pm 0.6$ M, from which $pK_{a1} = -0.56$. It follows that k_{-2} is almost 8 orders of magnitude larger than k_{-1} and that ΔpK_a (i.e., $pK_{a2} - pK_{a1}$) = 4.1. These values are consistent with expectations because as mentioned above the ΔpK_a of a typical inorganic diprotic oxo acid is ≥4. Thus, the new results described here fully confirm the validity of the previously proposed kinetic scheme (Figure 1), where a rapid pre-equilibrium protonation precedes a slow step, which is now known to be the intramolecular proton transfer; see

Scheme 2

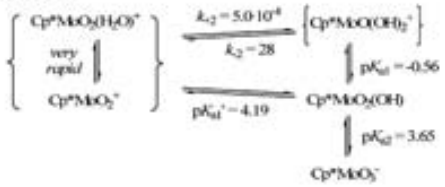

the next sections. It is worth mentioning that the proton transfer to the oxo ligands in compound Re(O)I(2,7-nonadiyne) by CF_3SO_3H in MeCN was shown to be relatively slow (11.9 M^{-1} s^{-1} at −40 °C).[31]

$$k_{obs} \sim k_{-2}K_{a1}^{-1}[H^+]/\{1 + K_{a1}^{-1}[H^+]\} \quad \text{(if } k_{-1} \text{ is negligible)} \quad (4)$$

It should be noted that the individual values of K_{a1} and k_{-2} obtained by the above analysis give rise to a ratio $k_{-2}/K_{a1} = 7.8$, in relatively good agreement with the previously determined value (17.2).[21] The discrepancy may be attributed to the difference in the ionic strength used in these studies. However, one point remains to be discussed on the thermodynamics of the system before we can turn to the kinetics. The combination of the individual rate constants for the tautomerization of the cationic system in both directions (k_2 and k_{-2}, as shown in Scheme 2) yields the tautomerization equilibrium constant, $K_T = k_2/k_{-2} = 1.8 \times 10^{-5}$, which corresponds to a free-energy difference of 6.5 kcal mol^{-1} in favor of the oxo−aqua isomer. The combination of this value with the experimentally determined pK_{a1} value (−0.56) according to the thermodynamic cycle shown in Scheme 2 (the deprotonation of the two isomeric cations affords the same neutral hydroxo complex) yields the thermodynamic proton dissociation constant of the dioxo−aqua species, $K_{a1}' = 6.5 \times 10^{-5}$ M ($pK_{a1}' = 4.19$). This compares well with the value calculated from k_{-2}/K_{a1} determined in the previous study ($K_{a1}' = 2.9 \times 10^{-5}$ M; $pK_{a1}' = 4.54$). Note that this value is also given by the expression $(k_{+1}/k_{-1})K_a$, from the thermodynamic cycle in Figure 1. At first sight, it may appear unreasonable that the first acid dissociation constant of this aqua complex is weaker than the second one. However, this observation can be rationalized if the water ligand is extensively dissociated as a result of the labilization caused by the Cp* chelate as referred to above. In this case, the calculated pK_{a1}' value must be treated as an apparent pK_a value because it includes the equilibrium constant for the dissociation of water, which is expected to be large in order to offset the observed pK_a value. Thus, the effective thermodynamic acidity of the cationic complex is a weighted average of the coordinated water molecule acidity, which is expected to be intrinsically very high, and the acidity of the free water molecule ($pK_a = 15.6$). The hypothesis of an extensive water dissociation from the cationic complex is not inconsistent with the computational study because the water adduct is calculated as only 10.1 kcal mol^{-1} more stable than the dissociated species according to the CPCM, but this calculation does not consider explicit interactions of the adduct and the separate fragments with additional water molecules. For instance, the stabilization of a water molecule by hydrogen bonding to additional water molecules is expected to contribute significantly to the equilibrium energetics (the solvation free energy of a water molecule in water has recently been estimated at −6.3 kcal mol^{-1}).[32] It is also interesting to recall that an electrospray mass spectrometric investigation of a H_2O−MeOH solution of Cp^*Mo^{VI} at low pH (ca. 4 and 1) revealed the presence of both $Cp^*MoO_2^+$ and $Cp^*MoO_2(H_2O)^+$ species, as well as the related $Cp^*MoO_2(MeOH)^+$ adduct.[33,34] Whether the rapid equilibrium highlighted at the left-hand side of Scheme 2 involves only species $Cp^*MoO_2^+$ and $Cp^*MoO_2(H_2O)^+$ or whether a MeOH solvate is also present does not affect the measured values of all rate and equilibrium constants or their significance.

In general, it is expected that ground-state labilization caused by metal−carbon bonds in the trans position to coordinated water molecules will not only drastically accelerate the water-exchange process but will also significantly increase the pK_a value of the coordinated water, as found in the present case. Bond weakening of the $M-OH_2$ bond will cause a decrease in the acidity of the coordinated water molecule.[7,14] In addition, the bond strength will follow the order M=O ≫ M−OH ≫ $M-OH_2$ as mentioned before. Thus, the combination of bond labilization and pH will control the lability of the coordinated water and lead to apparent pK_a values that seem to be "abnormal".

It is also interesting to analyze the Cp^*Mo^{VI} system in terms of the isolobal analogy between the O^{2-} and Cp^{*-} ligands. Thus, the $Cp^*MoO_2^+$ system is isolobally related to MoO_3, $Cp^*MoO_2(OH)$ to $HMoO_4^-$, and $Cp^*MoO_3^-$ to MoO_4^{2-}. Interestingly, while MoO_4^{2-} and $HMoO_4^-$ are always described as tetrahedral ions, aqueous MoO_3 is described as having coordination number 6 [as either $MoO_2(H_2O)_3$ or $MoO_2(OH)_2(H_2O)_2$] possibly because an octahedral environment is found for MoO_3,[35] as well as for its water adduct $MoO_3 \cdot 2H_2O$,[36] in the solid state. However, equilibria with 5- or 4-coordinate species may, in fact, exist. A comparison between the pK_a of $HMoO_4^-$ (3.48)[4] and $Cp^*MoO_2(OH)$ (3.65) suggests that the Cp^{*-} ligand is a marginally better electron donor than the isolobal O^{2-} ligand for this system in an aqueous solvent. This means that the Mo center is electron-richer in $Cp^*MoO_2^+$ than in MoO_3, as supported by the Mulliken charges in the Mo atom (+1.38 vs +1.88). In combination with the greater steric bulk of the Cp* ligand versus the oxo ligand, this may lead to a weaker interaction between $[Cp^*MoO_2]^+$ and water.

(31) Han, Y.; Harlan, C. J.; Stoessel, P.; Frost, B. J.; Norton, J. R.; Miller, S.; Bridgewater, B.; Xu, Q. *Inorg. Chem.* **2001**, *40*, 2942−2952.
(32) Kelly, C. P.; Cramer, C. J.; Truhlar, D. G. *J. Phys. Chem. B* **2006**, *110*, 16066−16081.
(33) Gun, J.; Modestov, A.; Lev, O.; Saurenz, D.; Vorotyntsev, M. A.; Poli, R. *Eur. J. Inorg. Chem.* **2003**, 482−492.
(34) Gun, J.; Modestov, A.; Lev, O.; Poli, R. *Eur. J. Inorg. Chem.* **2003**, 2264−2272.
(35) Wooster, N. *Nature (London, U.K.)* **1931**, *127*, 93.
(36) Krebs, B. *Acta Crystallogr., Sect. C: Struct. Crystallogr. Cryst. Chem.* **1972**, *28*, 2222−2231.

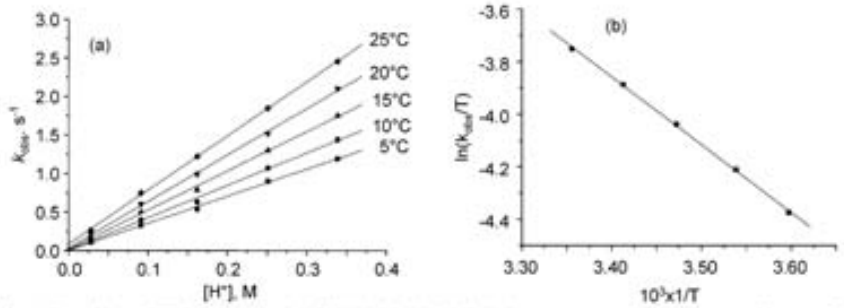

Figure 4. (a) Plots of k_{obs} vs [H$^+$] for the acidification of [Cp*MoO$_3$]$^-$ with HNO_3 in the temperature range 5−25 °C measured by stopped flow. (b) Corresponding Eyring plot for the slope in part a. Experimental conditions: [Cp*$_2$Mo$_2$O$_3$] = 4 × 10^{-4} M, λ_{det} = 390 nm, 20% MeOH−H$_2$O, μ_{tot} = 1 M (adjusted with $NaNO_3$).

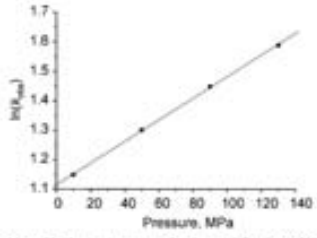

Figure 5. Plot of ln(k_{obs}) vs pressure for the acidification of [Cp*MoO$_3$]$^-$ with HNO_3 in the range 10−130 MPa. Experimental conditions: [Cp*$_2$Mo$_2$O$_3$] = 4 × 10^{-4} M, [H$^+$] = 0.4 M, λ_{det} = 390 nm, 20% MeOH−H$_2$O, temp = 25 °C, μ_{tot} = 1 M (adjusted with $NaNO_3$).

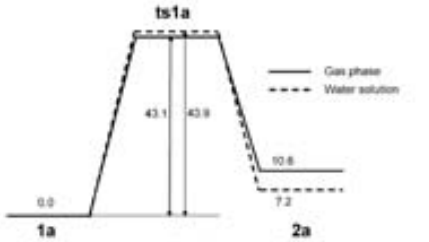

Figure 6. Relative energy profile (in kcal mol^{-1}) in the gas phase and a water solution for the starting complex (**1a**), transition state (**ts1a**), and product (**2a**) of eq 5.

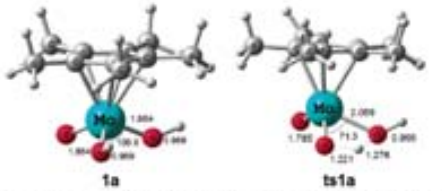

Figure 7. Optimized structures of the dihydroxo complex (**1a**) and the proton-transfer transition state (**ts1a**) of eq 5 (distances in angstroms, angles in degrees).

(c) Activation Parameters for the Low-pH Transformation. The temperature and pressure dependence of the acidification process for the protonation reaction in the low-acidity range have also been investigated. The data were collected only in the pH range where the rate depends linearly on [H$^+$]; see Figure 4. The obtained activation parameters are $\Delta H^{\ddagger}_{slope}$ = 5.1 ± 0.1 kcal mol^{-1} and $\Delta S^{\ddagger}_{slope}$ = −37 ± 1 cal mol^{-1} K^{-1}. The double-logarithmic plots (log k vs pH) are linear with slopes very close to unity, demonstrating that the intercept plays a minor role in the fitting of the data.

The pressure dependence of the reaction was studied at 0.4 M acid, for which the data are shown in Figure 5. The obtained activation parameter $\Delta V^{\ddagger}_{slope}$ is −9.1 ± 0.2 cm^3 mol^{-1}. The activation parameters for the slope of the plots in Figures 4 and 5 represent those for k_{-2}/K_{a1}. Because nothing is presently known about the temperature dependence of K_{a1}, it is difficult to speculate about the meaning of the reported activation parameters. It is reasonable to speculate that K_{a1} should not show a significant pressure dependence because it involves no changes in electrostriction and at most can be slightly positive. The overall significantly negative activation entropy and volume values favor a process in which significant bond formation or charge creation occurs. According to the slow reaction for path b of Scheme 1, formation of the aqua complex involves bond formation between OH and H, as well as shortening of the Mo−O bond during conversion of Mo−OH to Mo═O. These processes are suggested to account for the observed volume collapse and decrease in entropy on going to the transition state.

(d) Computational Study of the Intramolecular Proton-Transfer Process. In order to validate the intramolecular proton-transfer mechanism and find the possible origin of the negative activation parameters (entropy and volumes), we carried out calculations on the initial (**1a**) and end (**2a**) products of eq 5, as well as on the transition state (**ts1a**), in the absence and in the presence of additional water molecules. The gas-phase and water-solution energy profiles obtained in the absence of additional water molecules are shown in Figure 6, whereas the optimized **1a** and **ts1a** species are shown in Figure 7. The barrier height is quite high, having a value of 43.1 kcal mol^{-1} in the gas phase, whereas the reaction is endoergic by 10.6 kcal mol^{-1}. Both results disagree with the experimental evidence because the isomer-

ization process is rather facile and the oxo−aqua complex is the thermodynamically more stable product. When the nonspecific solvent effects are accounted for by use of the CPCM method, the barrier is nearly the same (43.9 kcal mol^{-1}), whereas the reaction is endoergic by 7.2 kcal mol^{-1}, so the energetic difference has decreased by 3.4 kcal mol^{-1} by inclusion of the solvent dielectric effects. Concerning the Gibbs free-energy values (in the gas phase), they are very similar to the potential energy ones; for example, the difference between **1a** and **2a** is 10.6 kcal mol^{-1} in potential energy, whereas the free-energy difference is 9.9 kcal mol^{-1}. The high activation barrier is probably related to the distortion of the OMoO fragment as reflected in the large decrease in the O−Mo−O angle on going from **1a** (106.8°) to the transition-state structure **ts1a** (71.3°). The transition state is also characterized by distances of 1.221 and 1.276 Å for the O−H bonds being broken and formed, respectively, when going from **1a** to **2a**. Thus, the old O−H bond is already almost fully broken, whereas the new one has not yet formed to a significant extent, and the two Mo−O bond distances have intermediate values between those of the corresponding distances in the starting and final compounds. In conclusion, the intramolecular proton transfer implies a remarkable change in the geometry, and this is associated with a high energetic cost.

$$\underset{\mathbf{1a}}{[Cp^*MoO(OH)_2]^+} \rightarrow \underset{\mathbf{2a}}{[Cp^*MoO_2(H_2O)]^+} \qquad (5)$$

In order to further probe the mechanistic details of this reaction, we considered that the explicit inclusion of water molecules could afford an easier proton-transfer pathway because the system contains both donor and acceptor sites for the establishment of hydrogen bonds with water molecules. Many theoretical works have already reported the active participation of water chains in tautomerization[37−39] and proton-exchange processes.[40,41] The mechanism is described as a water-assisted reaction in which one or more water molecules act as a bifunctional catalyst. Recent theoretical studies of the tautomerization process between the hydrated oxide, $[MO(H_2O)]^+$, and the dihydroxide, $[M(OH)_2]^+$, cations (M = V, Nb, and Ta) also point out that the participation of water acting as proton donor and acceptor can effectively lower the barrier height for the isomerization process.[42] The same water catalysis has been found for the isomerization of $UO_2(OH)_2$.[43] The resulting energy profiles with one additional water molecule are shown in Figure 8. In Figure 9, the main geometric characteristics of the

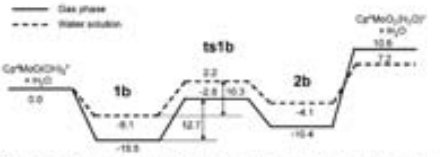

Figure 8. Relative energy profiles (in kcal mol^{-1}) in the gas phase and a water solution for the starting complex (**1b**), transition state (**ts1b**), and product (**2b**) of eq 6.

optimized structures are depicted. First of all, the interaction of the additional water molecule with systems **1a** and **2a** gives rise to a significant energetic stabilization (15.5 and 8.1 kcal mol^{-1} in the gas phase and in a water solution, respectively, for the dihydroxo complex **1b**; 21.0 and 11.3 kcal mol^{-1} under the same conditions for the oxo−aqua complex **2b**). The stabilization of **2b** is slightly greater than that of **1b**, which renders the isomerization process less endothermic relative to the situation of the isolated system (ΔE = +5.1 and +4.0 kcal mol^{-1} in the gas phase and in a water solution, respectively). The corresponding free-energy difference in the gas phase is +3.4 kcal mol^{-1}. This change seems related to the stronger hydrogen bonding of water with the proton of the aqua ligand in **2b**, relative to the proton of one of the two hydroxo ligands in **1b** (as measured by the greater O−H bond elongation, 1.025 vs 0.997 Å, and by the shorter O···H distance, 1.511 vs 1.655 Å). The most dramatic effect relative to the water free system, however, is observed at the relative barrier height, which is now only 12.7 kcal mol^{-1} (vs 43.1 without water) in the gas phase and only 10.3 kcal mol^{-1} (vs 43.9 without water) in solution above the **1b** species. This effect is related to the ability of the additional water molecule to act, at the same time, as a proton acceptor for the donating O−H ligand and as a proton donor for the receiving O−H ligand, thereby mediating the proton transfer. Both hydrogen-bonding interactions are established at the level of the transition state (**ts1b**), giving a six-membered transition state, as shown in Figure 9. The most likely cause of such a dramatic decrease in the activation barrier is the smaller distortion of the OMoO fragment in the transition states, as evidenced by the wider O−Mo−O angle in **ts1b** (92.5°) in comparison with the 71.3° value optimized for the **ts1a** structure. The optimized O−Mo−O angles in **1b** and **2b**, on the other hand, are essentially unchanged relative to those of **1a** and **2a**. Thus, the structural rearrangement in **ts1b** is not as marked as that in **ts1a**, with respect to the relative reactants. It is worth mentioning that a very slow rate of intramolecular proton transfer was reported for complex $Re(O)(^{18}OH)(MeC{\equiv}CMe)_2$ in a benzene solution.[44] Although the rate of transformation was shown not to strongly depend on the presence or absence of stoichiometric amounts of ethanol, trace amounts of CF_3SO_3H strongly accelerate the reaction. It is possible that the transformation could also be accelerated by excess water. Another slow intramolecular proton-transfer process was reported for *trans*-

(37) Lledós, A.; Bertrán, J. *Tetrahedron Lett.* **1981**, *22*, 775−778.
(38) Ventura, O. N.; Lledos, A.; Bonaccorsi, R.; Bertran, J.; Tomasi, J. *Theor. Chim. Acta* **1987**, *72*, 175−195.
(39) Lima, M. C. P.; Coutinho, K.; Canuto, S.; Rocha, W. R. *J. Phys. Chem. A* **2006**, *110*, 7253−7261.
(40) Bergquist, C.; Bridgewater, B. M.; Harlan, C. J.; Norton, J. R.; Friesner, R. A.; Parkin, G. *J. Am. Chem. Soc.* **2000**, *122*, 10581−10590.
(41) Prabhakar, R.; Blomberg, M. R. A.; Siegbahn, P. E. M. *Theor. Chim. Acc.* **2000**, *104*, 463−470.
(42) Sambrano, J. R.; Andres, J.; Gracia, L.; Safont, V. S.; Beltran, A. *Chem. Phys. Lett.* **2004**, *384*, 56−62.
(43) Hratchian, H. P.; Sonnenberg, J. L.; Hay, P. J.; Martin, R. L.; Bursten, B. E.; Schlegel, H. B. *J. Phys. Chem. A* **2005**, *109*, 8579−8586.
(44) Erikson, T. K. G.; Mayer, J. M. *Angew. Chem., Int. Ed. Engl.* **1988**, *27*, 1527−1529.

Figure 9. Optimized structures of the starting complex (**1b**), transition state (**ts1b**), and product (**2b**) of eq 6 (distances in angstroms; angles in degrees).

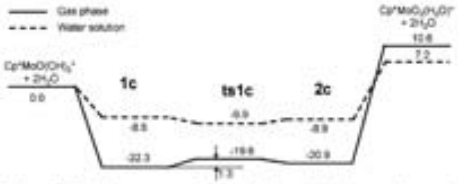

Figure 10. Relative energy profiles (in kcal mol^{-1}) in the gas phase and a water solution for the starting complex (**1c**), transition state (**ts1c**), and product (**2c**) of eq 7.

$[Ru^{IV}(tpy)(O)(O{=}P(Ph)_2CH_2CH_2PPh_2)(H_2O)]^{2+}$ in a MeCN solution.[45]

Another noteworthy characteristic of **ts1b** is that the proton originating from the donating O−H group has already migrated onto the water molecule (1.088 Å), whereas the proton that eventually ends up in the aqua ligand is still bonded to the added water molecule (1.026 Å). These distances suggest that the transition state involves the interaction between a hydronium ion (H_3O^+) and the neutral $Cp^*MoO_2(OH)$ molecule, through the establishment of two hydrogen bonds (1.382 Å to the oxo ligand and 1.591 Å to the hydroxo ligand). We have reported a similar transition state in hydrogenation performed by gold catalysts for the heterolytic cleavage of H_2 assisted by a solvent molecule (ethanol).[46] In conclusion, the explicit consideration of a water molecule confirms the feasibility of the rearrangement of **1b** to **2b** by solvent-assisted intramolecular proton transfer.

$$\underset{\mathbf{1b}}{[Cp^*MoO(OH)_2]^+ \cdot H_2O} \rightarrow \underset{\mathbf{2b}}{[Cp^*MoO_2(H_2O)]^+ \cdot H_2O} \quad (6)$$

On the basis of the above results, we have imagined that the addition of a second water molecule could further lower the energy of the transition state. An eight-membered transition state (**ts1c**) having two water molecules acting as proton and donor acceptors concurrently between the two complexes **1c** and **2c** (eq 7) may further reduce the necessary geometric reorganization to reach the transition state. The resulting energy profiles in the gas phase and a water solution on this system are shown in Figure 10, and the optimized structures for the related species are drawn in Figure 11. As was already seen on going from the water-free adduct to the water adduct, going from the mono- to bis(water) adduct further stabilizes the oxo−aqua isomer relative to the dihydroxo isomer. The oxo−aqua complex is now only 1.4 kcal mol^{-1} less stable than the dihydro isomer in the gas phase [cf. 5.1 and 10.6 kcal mol^{-1} for the mono(water) and water-free system, respectively] and actually *more stable* by a small margin (0.4 kcal mol^{-1}) in a water solution. The gas-phase free energy is still in favor of the dihydroxo isomer, but only by 2.4 kcal mol^{-1}. Undoubtedly, the correct relative energy can be obtained at this level of theory, provided the effect of the water solvation is considered by the explicit inclusion of a sufficient number of water molecules in the calculation. Although the relative free energy computed by including two water molecules is still a bit far from the experimental value of 6.5 kcal mol^{-1} in favor of the oxo−aqua isomer, the explicit inclusion of water molecules in the calculations moves the energetic balance in the right direction. In conclusion, our calculations indicate an intrinsic preference of the system for the dihydroxide form (gas phase). The nonspecific interactions (continuum calculations) are not sufficient to reverse this stability order, whereas a reversal, in agreement with the experiment, is observed upon inclusion of the specific interactions (hydrogen bonds) with the water solvent.

$$\underset{\mathbf{1c}}{[Cp^*MoO(OH)_2]^+ \cdot 2H_2O} \rightarrow \underset{\mathbf{2c}}{[Cp^*MoO_2(H_2O)]^+ \cdot 2H_2O} \quad (7)$$

Concerning the energetic profile, the proton-transfer barrier is now reduced to a very low value (1.3 and 3.5 kcal mol^{-1} in potential and free energy, respectively). In CPCM single-point calculations, the energy of the transition state is even lower than the corresponding reactant energy. We consider that this difference is within the error of the CPCM method. Compared to **ts1b** and **ts1a**, the structure of **ts1c** is characterized by an even wider O−Mo−O angle (102.0°). Now the Mo−O bonds barely have to bend in order to reach the suitable configuration for the proton transfer. The explicit inclusion of the two water molecules also has the effect of further weakening the O−H bonds for the hydroxo ligands (1.049 Å in **1c** vs 0.997 Å in **1b**) and the aqua ligand (1.132 Å in **2c** vs 1.025 Å in **2b**). Thus, the proton becomes effectively more transferred to the medium. As was the case for **ts1b**, the structure of **ts1c** may also be viewed as resulting from the hydrogen-bonding interaction of a hydronium ion (in this case $H_5O_2^+$) with neutral $Cp^*MoO_2(OH)$, according to the observed pattern of O−H and O···H distances.

(45) Dovletoglou, A.; Meyer, T. *J. J. Am. Chem. Soc.* **1994**, *116*, 215−223.
(46) Comas-Vives, A.; Gonzalez-Arellano, C.; Corma, A.; Iglesias, M.; Sanchez, F.; Ujaque, G. *J. Am. Chem. Soc.* **2006**, *128*, 4756−4765.

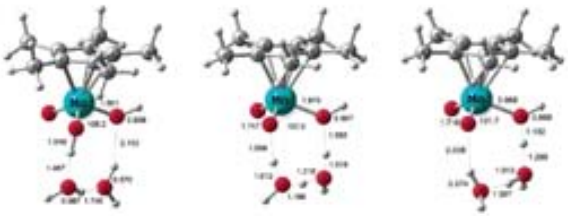

1c ts1c 2c

Figure 11. Optimized structures of the starting complex (**1c**), transition state (**ts1c**), and product (**2c**) of eq 7 (distances in angstroms, angles in degrees).

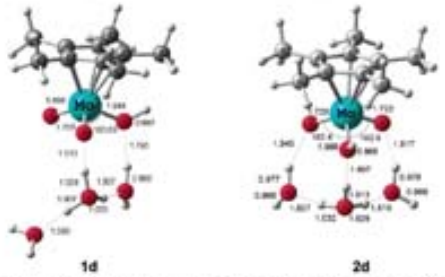

1d 2d

Figure 12. Optimized structures of **1d** and **2d**, featuring the $Cp^*MoO_2(OH)$ molecule interacting with the $[(H_2O)(H_2O)_2]^+$ cluster (distances in angstroms; angles in degrees).

For the sake of completion, we have pursued the study by adding a third water molecule to the system. In this case, however, the optimization of both hydroxo and oxo−aqua isomers **1d** and **2d** resulted in an optimized structure where the water proton is completely transferred to the water cluster, which thereby becomes a $H_7O_3^+$ hydronium ion and interacts via hydrogen bonding with the neutral $Cp^*MoO_2(OH)$ complex; see Figure 12. These results confirm the trend reported in **2b** and **2c**, where the O−H bond became more elongated as more water molecules were added in the system. This trend reflects the acidity of the cationic species; thus, a more water-rich environment favors the proton transfer to the medium. The two structures **1d** and **2d** are isomers in terms of the arrangement of the hydrogen-bonded water molecules. Structure **2d** is more stable than **1d** by 1.8 kcal mol^{-1} in a water solution. It is interesting to note that the protonated water molecule (H_3O^+) interacts with the O−H group in structure **2d**, whereas it prefers an oxo ligand in structure **1d**. Although this difference is fairly small and the final point depends on the starting point in the optimization, it may be attributed to the fact that in **2d** there is an additional hydrogen bond. Moreover, the O(OH) interacting with H_3O^+ in **2d** presents a more negative Mulliken charge than the O interacting with H_3O^+ in **1d**: −1.11 vs −0.89.

A comparison of all isomeric pairs shows that the aqua O−H bond in the oxo−aqua isomer systematically experiences a greater lengthening effect than the hydroxo O−H bond in the dihydroxo isomer (1.025 Å in **2b** vs 0.997 Å in **1b**, 1.132 Å in **2c** vs 1.049 Å in **1c**; these distances are essentially identical in **1a** and **2a**). This suggests that $[Cp^*MoO_2(H_2O)]^+$ is intrinsically more acidic than its dihydroxo isomer, which may seem in contradiction with the experimental evidence (oxo−aqua isomer, $pK_a = 4.19$; dihydroxo isomer, $pK_a = -0.56$). However, as argued above, the high effective pK_a value of $[Cp^*MoO_2(H_2O)]^+$ is proposed to result from an equilibrium with $[Cp^*MoO_2]^+$ and free water. Thus, these computational results indirectly validate the water dissociation hypothesis.

The calculations agree with the experimental evidence that the cationic systems, $[Cp^*MoO(OH)_2]^+$ and $[Cp^*MoO_2(H_2O)]^+$, can be deprotonated in a slightly acidic medium. However, the predominant species in very acidic media is a cationic complex. As a very simple way of modeling the effect of lowering the pH, we have added an extra proton to the system, i.e., using the $[H_3O(H_2O)_2]^+$ cluster as a model of the medium. The resulting system is dipositive. This is a rough simulation of a low-pH aqueous solution but can give some insight of what occurs when increasing the acidity of the medium. Several theoretical studies have addressed the question of the nature of the hydronium species in solution and its solvation shell.[47−50] The $[H_3O(H_2O)_2]^+$ cluster has been used as a model of the hydronium species in solution in other reactions involving transition-metal complexes.[51,52] Different structures were optimized, exploring several starting points, and the various optimized species are shown in Figure 13. For species **1e** and **2e**, the hydronium ion (H_3O^+) is located in the second-coordination sphere, whereas species **1e2**, **1e3**, and **2e2** feature this ion in the first-coordination sphere, directly interacting with the molybdenum complex. Obviously, these are not necessarily all of the possible minima but probably the most favored ones.

In no case was the proton of the cationic complex ($[Cp^*MoO_2(H_2O)]^+$ or $[Cp^*MoO(OH)_2]^+$) transferred to the medium, in contrast to what occurred for the monopositive system with three water molecules. This is not a surprising result, with the medium (modeled here as $[H_3O(H_2O)_2]^+$) being too acidic in the gas phase to accept an additional proton because it has an excess of positive charge. Neverthe-

(47) Tunon, I.; Silla, E.; Bertran, J. *J. Phys. Chem.* **1993**, *97*, 5547−5552.
(48) Wei, D.; Salahub, D. R. *J. Chem. Phys.* **1994**, *101*, 7633−7642.
(49) Marx, D.; Tuckerman, M. E.; Hutter, J.; Parrinello, M. *Nature (London, U.K.)* **1999**, *397*, 601−604.
(50) Schmitt, U. W.; Voth, G. A. *J. Chem. Phys.* **1999**, *111*, 9361−9381.
(51) Kovács, G.; Ujaque, G.; Lledós, A.; Joó, F. *Organometallics* **2006**, *25*, 862−872.
(52) Kovács, G.; Schubert, G.; Joó, F.; Papai, I. *Organometallics* **2005**, *24*, 3059−3065.

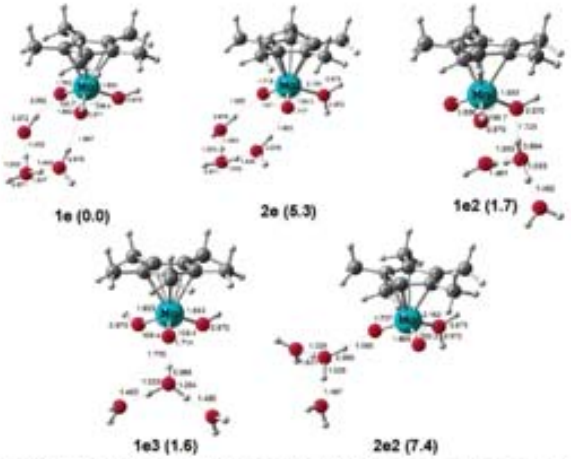

Figure 13. Optimized structures of the $[Cp^*MoO(OH)_2]^+$ and $[Cp^*MoO_2(H_2O)]^+$ complexes interacting with the $[(H_2O)(H_2O)_2]^+$ cluster (relative energies in kcal mol^{-1} in parentheses).

less, this approach gives a nice representation of what occurs when lowering the pH value because the cationic species now become favorable and can be obtained as real minima in the potential energy surface for both isomers.

Concerning the relative energies, placing the hydronium ion in the first-coordination sphere carries an energy cost of ca. 2 kcal mol^{-1}, relative to having it in the second sphere (e.g., going from **1e** to **1e2** and **1e3** for the dihydroxo complex and from **2e** to **2e2** for the oxo−aqua complex). On the other hand, the dihydroxo isomer is more stable than the oxo−aqua species by 5.3 kcal mol^{-1} (**1e** vs **2e** structure). As discussed before, we believe that a larger number of water molecules (at least the complete first solvation sphere) should be included in order to reproduce the experimental relative stability.

The experimental data also show that the dominant species at pH > 5 is the anionic complex $[Cp^*MoO_2]^-$.[21] We suggest that when the hydroxide concentration is increased, the proton of the $[Cp^*MoO_2(OH)]$ complex can be easily transferred to hydroxide in solution, analogous to what occurs to one proton of the aqua complex when water molecules are added to the system. Nevertheless, although theoretical calculations reported here provide some relevant energy trends, geometries, and activation barriers, a complete theoretical analysis of the species present in solution as a function of the pH is beyond the scope of this study, mainly because of the intrinsic difficulty of simulating an aqueous solution at a given pH. More information could be extracted from dynamics simulations.

Conclusions

A combination of kinetics and computational investigations on the Cp^*Mo^{VI} system in an acidic aqueous medium has greatly improved our understanding of what factors regulate the properties of the oxo−dihydroxo ($[Cp^*MoO(OH)_2]^+$) and dioxo−aqua ($[Cp^*MoO_2(H_2O)]^+$) isomers in solution. The computational study shows that the dihydroxo isomer is favored for the isolated system in the gas phase, but the subsequent introduction of the solvent model (by CPCM) and especially the explicit introduction of water molecules in the calculations attenuate and even reverse this stability trend. The study further suggests that the medium strongly affects the water dissociation energy cost from the dioxo−aqua isomer (10.1 kcal mol^{-1} in a water solution vs 39.7 kcal mol^{-1} in the gas phase). A generalization of these trends suggests that the dihydroxo species for any given system have a better chance to be stable in apolar organic solvents, whereas a rearrangement to oxo complexes accompanied by water dissociation may be favored in stronger dielectric solvents.

The above trend also rationalizes the unusually low acidities that are sometimes found for high-oxidation-state cationic complexes. While the water ligand in the oxo−aqua isomer, $[Cp^*MoO_2(H_2O)]^+$, is an intrinsically stronger proton donor than the hydroxo ligand in the dihydroxo isomer, $[Cp^*MoO(OH)_2]^+$, the much lower observed acidity for the former ($pK_a = +4.19$ vs -0.56 for the latter) is related to a water dissociation equilibrium. In turn, this is related to the coordination sphere and particularly to how the ligands are able to satisfy the electron deficiency at the metal center upon loss of the water lone-pair donation. In the present system, the extremely high lability of the coordinated water molecule can be ascribed to the trans labilization effect of the Cp* chelate, which, in turn, favors the formation of the dioxo complex and is responsible for the apparent high pK_a value of the oxo−aqua isomer. We are not aware of any other analogous study in the literature.

Concerning the isomerization mechanism leading from the dihydroxo species to the oxo−aqua species, the direct

intramolecular proton transfer from the dihydroxo complex to the aqua complex can be ruled out because of the high calculated barrier for the direct proton transfer, viz., 43.9 kcal mol^{-1} including solvent effects. The assistance of either one or two water molecules renders proton transfer feasible by dramatically lowering the barrier height. The mechanism involving assistance by two water molecules even yields a lower energy for the transition state than for the reactant and product when including the CPCM, suggesting that this is indeed a very facile process. The assistance by amphiphilic external molecules, such as water, is increasingly found to be crucial to lower activation barriers of intramolecular proton-transfer rearrangements.

Experimental Section

Solution Preparation and Measurements. All chemicals used in this study were of analytical grade. The solution pH was controlled by using HNO_3. The total ionic strength (μ) was kept constant at 1 M with $NaNO_3$. pH measurements were carried out on a Metrohm 623 pH meter equipped with a Sigma glass electrode. UV−vis spectra were recorded in gastight cuvettes on a Shimadzu UV-2100 spectrophotometer equipped with a thermostated cell compartment CDS-260.

Stopped-flow kinetics measurements on the acidification of $[Cp^*MoO_3]^-$ with HNO_3 in the pH range from 0.025 to 0.35 were carried out using an Applied Photophysics SX-18MV stopped-flow spectrophotometer. 20% MeOH−H_2O solutions of $[Cp^*MoO_3]^-$ were rapidly mixed with varying pH solutions in a gastight syringe. The kinetics of the reaction was monitored at 390 nm, where the change in the absorbance is a maximum for the acidified molybdenum product. The rate constant for acidification was determined from the slope of linear plots of k_{obs} vs $[H^+]$, as described in more detail under the Results and Discussion section. All kinetics experiments were performed under pseudo-first-order conditions, i.e., with at least 10-fold excess of $[H^+]$ over the $Cp^*_2Mo_2O_5$ complex. Reported rate constants are the mean values of at least five kinetic runs, and the quoted uncertainties are based on the standard deviation. High-pressure stopped-flow studies were performed on a custom-built instrument (from 10 to 130 MPa).[53] Kinetic traces were recorded on an IBM-compatible computer and analyzed with the use of the OLIS KINFIT (Bogart, GA) set of programs.

(53) Van Eldik, R.; Gaede, W.; Wieland, S.; Kraft, J.; Spitzer, M.; Palmer, D. A. *Rev. Sci. Instrum.* **1993**, *64*, 1355−1357.

Computational Details. Calculations were carried out using the *Gaussian 03* package[54] at the DFT level by means of the B3LYP functional.[55−57] For the Mo atom, the LANL2DZ pseudopotential[58] was used with the addition of f polarization functions.[59] The 6-31G(d) basis set was used for C atoms while for O atoms additional diffuse functions were added because of their anionic character [6-31+G(d)]. For the H atoms, the 6-31G(d,p) basis set was employed. IRC calculations were made in order to get the two minima linked by every transition state.[60−62]

Solvent effects were included by means of CPCM single-point calculations.[63,64] Additional spheres were included for all of the H atoms except for the Cp* H atoms by means of the SPHEREONH option. Frequency calculations were made in order to get the Gibbs free energy. The temperature used was 298.15 K.

Acknowledgment. We gratefully acknowledge the European Commission for funding this work through the AQUACHEM Research Training Network (Contract MRTN-CT-2003-503864). Financial support from the Spanish MEC through Project CTQ2005-09000-C02-01 and from Generalitat de Catalunya through Grant 2005SGR00896 is gratefully acknowledged. A.C.-V. acknowledges the Spanish MEC for a FPU fellowship.

Supporting Information Available: Complete refs 19, 51, and 56 and absolute energies and Cartesian coordinates of the optimized structures. This material is available free of charge via the Internet at http://pubs.acs.org.

IC062409G

(54) Frisch, M. J.; et al. *Gaussian 03*, revision C.02; Gaussian, Inc.: Wallingford, CT, 2004.
(55) Becke, A. D. *J. Chem. Phys.* **1993**, *98*, 5648−5652.
(56) Lee, C. T.; Yang, W. T.; Parr, R. G. *Phys. Rev. B* **1988**, *37*, 785−789.
(57) Stephens, P.; Devlin, F.; Chabalowski, C.; Frisch, M. *J. Phys. Chem.* **1994**, *98*, 11623−11627.
(58) Hay, P. J.; Wadt, W. R. *J. Chem. Phys.* **1985**, *82*, 270−283.
(59) Ehlers, A. W.; et al. *Chem. Phys. Lett.* **1993**, *208*, 111−114.
(60) Fukui, K. *Acc. Chem. Res.* **1981**, *14*, 363−368.
(61) Gonzalez, C.; Schlegel, H. B. *J. Chem. Phys.* **1989**, *90*, 2154−2161.
(62) Gonzalez, C.; Schlegel, H. B. *J. Phys. Chem.* **1990**, *94*, 5523−5527.
(63) Barone, V.; Cossi, M. *J. Phys. Chem. A* **1998**, *102*, 1995−2001.
(64) Cossi, M.; Rega, N.; Scalmani, G.; Barone, V. *J. Comput. Chem.* **2003**, *24*, 669−681.

A.3 Article VI

Available online at www.sciencedirect.com
ScienceDirect
Journal of Catalysis 254 (2008) 226–237
JOURNAL OF CATALYSIS
www.elsevier.com/locate/jcat

Mechanistic analogies and differences between gold- and palladium-supported Schiff base complexes as hydrogenation catalysts: A combined kinetic and DFT study

Aleix Comas-Vives [a], Camino González-Arellano [b,c], Mercè Boronat [d], Avelino Corma [d,*], Marta Iglesias [c], Félix Sánchez [b], Gregori Ujaque [a,*]

[a] Unitat de Química Física, Departament de Química, Edifici C.n., Universitat Autònoma de Barcelona, 08193 Bellaterra, Catalonia, Spain
[b] Instituto de Química Orgánica General, CSIC, C/Juan de la Cierva 3, 28006 Madrid, Spain
[c] Instituto de Ciencia de Materiales de Madrid, CSIC, C/Sor Juana Inés de la Cruz 3, Cantoblanco, 28049 Madrid, Spain
[d] Instituto de Tecnología Química, UPV-CSIC, Universidad Politécnica de Valencia, Av. de los Naranjos, s/n, 46022 Valencia, Spain

Received 17 July 2007; revised 13 November 2007; accepted 24 December 2007

Abstract

The mechanism of olefin hydrogenation catalyzed by Pd^{II} and Au^{III} Schiff base complexes, both with an analog d^8 electronic structure, is analyzed by means of kinetic and computational methods. The computational study is able to explain the differences experimentally observed in relation to the influence of the solvent (polarity and proton donor ability) and of the hydrogen pressure on the Au^{III}- and Pd^{II}-catalyzed reaction mechanisms. These considerations can guide the proper selection of solid supports for heterogenization of catalysts to significantly increase their activity.

Keywords: Density functional calculations; Mechanism; Catalysis; Hydrogenation

1. Introduction

Whereas platinum, palladium, and rhodium have been used for decades as catalysts in various homogeneous and heterogeneous reactions [1–6], gold was long believed to be chemically inert. Only in recent years have gold complexes and gold supported on different carriers attracted much interest as catalysts [7–9]. Small-crystal size gold supported on inorganic oxides or carbon (particle size $\leqslant 5$ nm) are highly active and selective for such reactions as CO oxidation at low temperature [10–13], water–gas shift [14], alcohol oxidation [15,16], carbon–carbon bond formation reactions [17], and chemoselective reduction of substituted nitroarenes [18]. Homogeneous gold complexes have been applied in cross-coupling and homocoupling reactions, as well as in hydrogenation of alkenes and imines [19]. Because Au^{III} and Pd^{II} have the same d^8 electronic structure, similar behavior could be expected for Au^{III} and Pd^{II} complexes, at least for some reactions. Consequently, to gain insight into the similarities and differences in reactivity between species that have similar electronic compositions at the outer shell but other differences that can affect their reactivity, we compared the mechanism of olefin hydrogenation catalyzed by two well-defined single-site molecular catalysts formed by Au^{III} and Pd^{II} organic complexes. We carried out kinetic experiments to evaluate the catalytic performance of different heterogenized Schiff base complexes of Au^{III} and Pd^{II} for the hydrogenation of diethyl ethylidensuccinates, and studied the effect of reaction variables on the kinetics of the reaction. The experimental results suggest that a slightly different mechanism should operate in the 2 catalysts. Consequently, we carried out a detailed computational study of the mechanism of olefin hydrogenation catalyzed by a Pd^{II} complex using density functional theory methods and compared the results with those obtained previously for Au^{III} catalysis [20]. The computational

* Corresponding authors. Faxes: +34 96 3877809, +34 93 5812920.
E-mail addresses: acorma@itq.upv.es (A. Corma), Gregori.Ujaque@uab.es (G. Ujaque).

0021-9517/$ – see front matter
doi:10.1016/j.jcat.2007.12.015

study was able to explain the differences observed experimentally between the 2 catalytic systems.

2. Experimental

The synthesis and characterization of homogeneous and heterogenized ligands and metal-complexes is fully described in the Supplementary material [21,22].

2.1. Catalytic experiments

We studied the catalytic properties of the Pd and Au complexes in hydrogenation reactions in a 100-mL batch reactor (Autoclave Engineers) at 40 °C, 4 atm dihydrogen pressure, and a metal/substrate molar ratio of 1/1000. The evolution of the reaction of hydrogenated product was monitored by gas chromatography analysis using a Hewlett–Packard 5890 II with a flame ionization detector in a cross-linked methylsilicone column.

2.2. Catalyst recovery and recycling

At the end of the hydrogenation process, the mixture of reaction was filtered. The residue of the mesoporous support was washed to completely remove the remains of products and/or reactants and then reused.

2.3. Computational details

Calculations were carried out using the program package Gaussian03 [23] at a density functional theory (DFT) level using the hybrid B3LYP functional [24]. The basis set for N and O was 6-31g(d), that for Cl was 6-31 + g(d), that for C and H directly involved in the reaction was 6-31g(d,p), and that for the rest of the C and H atoms was 6-31g. The Pd was described by means of the LANL2DZ [25] pseudopotential and its associated basis set for the valence electrons. Solvent effects were included by means of the polarized continuum model (PCM) [26].

For the transition states, analytical frequencies were calculated to ensure that only 1 imaginary value was obtained. Normal coordinate analyses were performed on these saddlepoints by intrinsic reaction coordinate (IRC) routes [27] in both directions to the corresponding minima. When the IRC calculations did not converge, additional geometry optimizations starting from the IRC structures were carried out to identify the reactants and products linked by the specific TS considered.

3. Results and discussion

3.1. Synthesis and characterization of ligands and complexes

In recent years, we have developed a modular system combining functionalized ligands with different supports and linkers, to allow systematic access to various immobilized chiral catalysts [28]. Here we applied this methodology to immobilize the Schiff base ligand **2** (see Scheme S3 in Supplementary material) on a mesoporous silica support such as MCM-41.

Table 1
Turnover frequencies (TOF, h^{-1}),[a] for the catalytic hydrogenation of diethyl itaconate in EtOH[b]

Ligand	Au^{III}	Pd^{II}
2	3430	3360
2-(MCM-41)	4920	4980
2-(MCM-41, Si/Al = 50)	6730	6000

[a] TOF = $mmol_{subs.}/mmol_{cat.}$ h.
[b] 4 bar H_2, 40 °C and substrate/catalyst ratio 1000.

MCM-41 is a short-range amorphous material containing a large number of silanol groups available for grafting, but has long-range ordering with hexagonal symmetry with regular monodirectional channels 3,5 nm in diameter.

All solids were functionalized in the same manner according to the procedure described in the Supplementary Material. Supported precursors, ligands, and heterogenized ligands were characterized by microanalysis, FT IR, and ^{13}C NMR. The heterogenized ligands reacted with palladium(II) acetate or tetrachloroauric acid to furnish the corresponding anchored Pd^{II} and Au^{III} complexes used for catalytic reactions. The catalysts prepared on this way presented metal loading of 0,10–0.30 $mmol_{metal}/g_{support}$ as determined by atomic absorption analysis and were characterized by various spectroscopic techniques (see Supplementary material).

3.2. Catalytic hydrogenation activity

The hydrogenation of diethyl ethylidensuccinates (i.e., diethyl itaconate, diethyl citraconate, and diethyl benzylidensuccinate) with these structurally well-defined Pd^{II} and Au^{III} complexes was carried out under mild conditions (EtOH as the solvent, 4 atm. hydrogen pressure, 40 °C). The hydrogenation was carried out to explore the possibilities of recovering the catalysts, the influence of the nature of the support, and the comparison of the activity and stability of supported catalysts with their homogeneous counterpart. The results for the hydrogenation of diethyl itaconate catalyzed by Pd^{II} and Au^{III} complexes are given in Table 1.

It can be seen that the activity of the homogeneous Au^{III} and Pd^{II} complexes is similar and, for both metals, the TOFs in the case of the supported catalysts increase with respect to the homogeneous systems. This indicates that silica mesostructured molecular sieves (MCM-41) are suitable supports for heterogenizing metal-complex homogeneous catalysts. Storage of the heterogenized catalysts at room temperature for 6 months had no effect on their catalytic performance, indicating that they are stable over time. They also were stable under reaction conditions and could be recycled at least 6 times with no appreciable loss in activity (Fig. 1).

It has been shown [20] that in the case of Au^{III}-catalyzed alkene hydrogenation, the hydrogen is activated through heterolytic cleavage to give a hydride intermediate. This process involves charge separation with no oxidative addition of hydrogen to the metal; thus, increasing polarity and acidity of the support should increase the reaction rate. To test this hypothesis, we supported complexes **2Au** and **2Pd** on pure silica

MCM-41 (a very polar support due to its numerous surface silanol groups) and on MCM-41 in the form of aluminosilicate (Si/Al = 15), which presents surface Brönsted acid sites. In both cases, the catalytic activity of the supported complexes increased with respect to the homogeneous systems, suggesting that the activation of H_2 by Pd^{II} is similar to that previously obtained for Au^{III} [22].

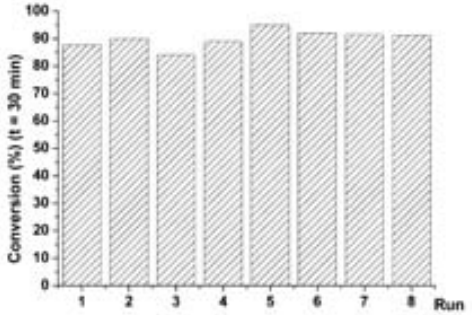

Fig. 1. Catalytic hydrogenation of diethyl itaconate with 2Pd-MCM-41.

We evaluated the influence of reaction temperature and H_2 pressure on the activity of the **2Pd** complex for hydrogenation of diethyl benzylidensuccinate; the results are shown in Fig. 2. As in the case of gold, the kinetic curves show an induction period that is more significant at low temperature; however, when the partial pressure of H_2 is varied from 2 to 4 bar, the induction period diminished for the **2Au** catalyst but did not change for the **2Pd** catalyst (Fig. 2b). With respect to the influence of the solvent used (depicted in Fig. 3), it is considerably greater in the case of gold. We discuss these effects and their causes throughout the article.

3.3. Reaction mechanism

According to the literature [29,30], the proposed mechanism of alkene hydrogenation catalyzed by Pd^{II} complexes comprises 3 main steps, which we describe in this section: (i) initial activation of the dihydrogen molecule, (ii) incorporation of the alkene into the coordination sphere of the catalyst and inser-

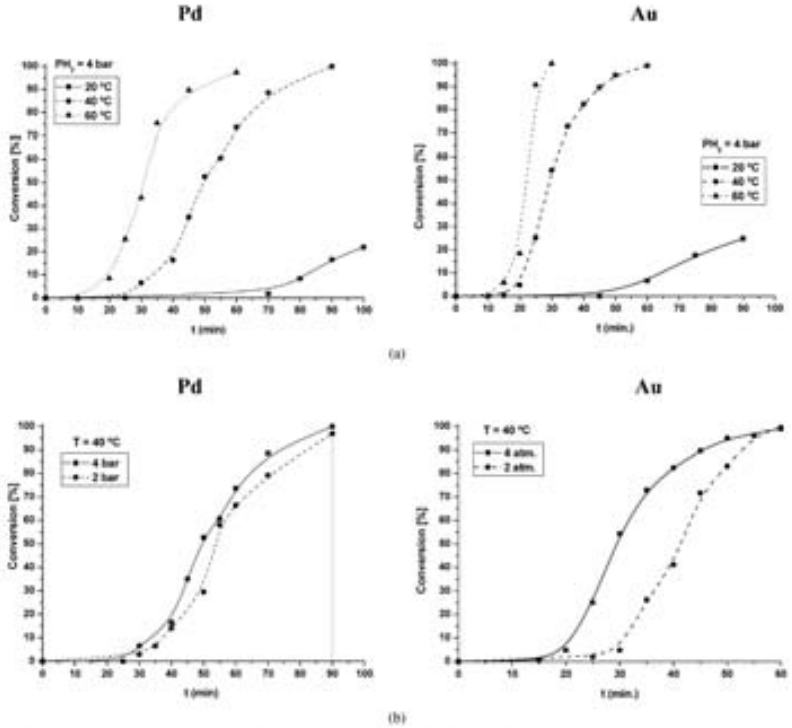

Fig. 2. Hydrogenation of diethyl benzylidensuccinate using **2Pd** (left) and **2Au** (right) catalysts and ethanol as solvent. Influence of (a) reaction temperature and (b) H_2 pressure.

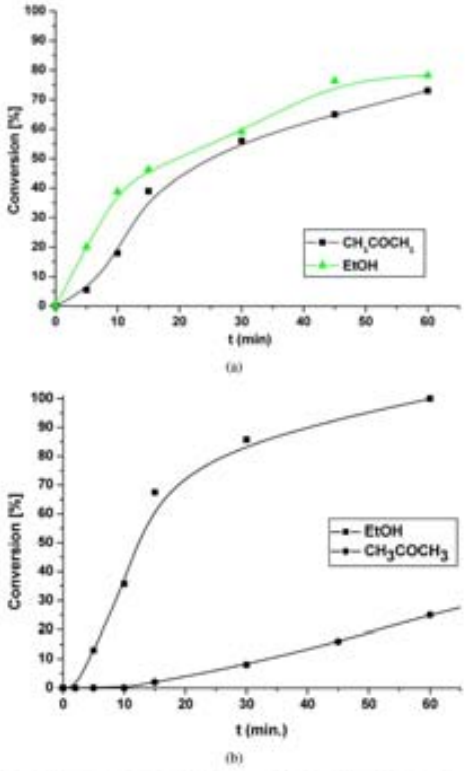

Fig. 3. Influence of solvent on the hydrogenation of diethyl benzylidenesuccinate using (a) **2Pd** and (b) **2Au** catalysts.

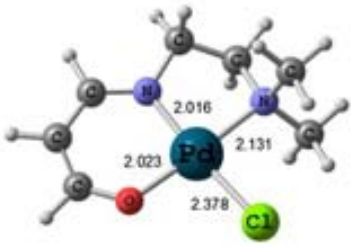

Fig. 4. Model complex for the catalyst. Distances in Å.

tion into the Pd–H bond, and (iii) a second hydrogen transfer closing the catalytic cycle. The mechanism of the reaction catalyzed by **2Pd**, as shown in Scheme S3 in the Supplementary material, was calculated using the complex depicted in Fig. 4 as a model for the catalyst and ethylene as the simplest alkene. We next discuss the results obtained for these 3 main steps.

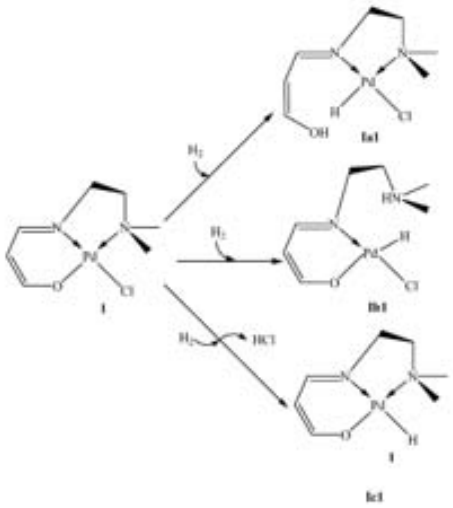

Fig. 5. Possible heterolytic cleavage pathways for the dihydrogen molecule.

3.3.1. Activation of the H_2 molecule

Because the hydrogen source in the present reaction was molecular hydrogen, the H_2 molecule had to be activated by the metallic complex to perform alkene hydrogenation. Two known routes are available for activating the dihydrogen molecule: homolytic cleavage and heterolytic cleavage. As discussed previously, the influence of the support on the activity of Pd^{II} complexes (similar to that of Au^{III}), along with the difficulty that the metal center has in reaching the oxidation number Pd^{IV}, make homolytic activation of the dihydrogen molecule highly improbable for this complex. This is commonly accepted for Pd(II) hydrogenation catalysts [29–31]. This was indeed confirmed by theoretical calculations; the product of the oxidative addition was found to lay 37.9 kcal/mol above that of the reactants, indicating that the barrier for this reaction will be at least 37.9 kcal/mol. Thus, we discounted homolytic cleavage as a possible pathway for H_2 activation.

H_2 heterolytic cleavage is more common in early-transition metals, even though several cases have recently been reported for late-transition metals [32–39]. For this particular system, the catalyst had several ligands that were able to undergo $[2+2]$ σ bond metathesis of the dihydrogen molecule: the oxygen and nitrogen of the Schiff base ligand and the chlorine ligand. In all of these pathways (depicted in Fig. 5), the hydrogen molecule is heterolytically activated by the catalyst; a proton goes to the ligand, whereas a hydride is bonded to the metal, keeping the oxidation state of Pd unchanged. The participation of hydride palladium species in hydrogenation reactions has been proposed previously [40,41].

A previous computational study of alkene hydrogenation catalyzed by Au^{III} complexes [20] found the highest barrier in the pathway in which activation occurs by means of the

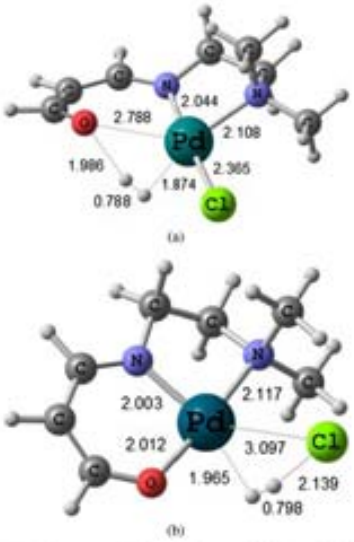

Fig. 6. Optimised geometry of the transition states for the heterolytic cleavage of H_2: (a) over the O ligand (**ts1a**) and (b) over the Cl ligand (**ts1c**). Distances in Å.

N(amine) ligand. In addition, the N(amine) ligand can be easily replaced by the olefin within the catalytic cycle (vide infra). Thus, in the case of the Pd catalyst, we did not consider this possibility for hydrogen activation, and performed calculations for the heterolytic cleavage only over O and Cl ligands.

Heterolytic cleavage over the O atom presented a barrier of 32.0 kcal/mol in the gas phase. Including solvent effects, the barrier remained practically unchanged, with a value of 32.7 kcal/mol. Referring to the possibility of dihydrogen splitting over the chlorine atom in the gas phase, the barrier was 28.1 kcal/mol with respect to the corresponding reactants, in which the hydrogen molecule is weakly interacting with the catalyst. In this case, however, the barrier height decreased significantly when solvent effects were included through a continuum model, adopting a value of 19.2 kcal/mol. The transition states for the heterolytic cleavage of H_2 over O and Cl are shown in Fig. 6, and the variation in the Mulliken charges on selected atoms in relation to separated reactants is given in Table 2. In the case of H_2 splitting over O (**ts1a**), the Pd center decreased its positive charge considerably, whereas the O atom did not significantly change its negative charge, because the oxygen atom can delocalize the charge over the adjacent π system. In contrast, in the case of H_2 cleavage over Cl (**ts1c**), there was a considerable increase in the negative charge on the chlorine atom, indicating that the polarity of the solvent (ethanol) played a significant role in this case, decreasing the activation barrier by about 9 kcal/mol.

In the case of the analogous Au^{III} catalyst [20], as well as in other samples reported by other authors using different catalysts [39], it was shown that the participation of species with proton donor-acceptor capabilities could significantly modify the reaction energy profiles. Therefore, we focused our efforts on searching for a reaction step in which a solvent molecule (ethanol) is directly implicated in the heterolytic activation of H_2. The optimized structures of the solvent-assisted transition states obtained over both the oxygen and the chlorine ligand atoms are depicted in Fig. 7.

Table 2
Variation in the Mulliken calculated atomic charges on selected atoms in relation to separated reactants in the gas phase (g) and with the solvent included by means of the PCM method (PCM)

	ts1a (g)	ts1a (PCM)	ts1c (g)	ts1c (PCM)
Pd	−0.214	−0.227	0.089	0.073
Cl	0.067	0.089	−0.321	−0.314
O	0.015	0.007	−0.004	0.002

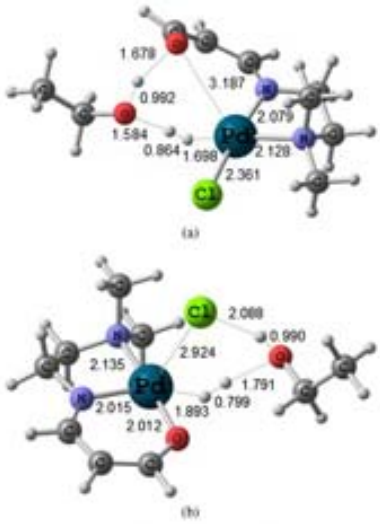

Fig. 7. Optimised geometry of the transition states for the solvent-assisted heterolytic cleavage of H_2: (a) over the O ligand (**ts1a2**) and (b) over the Cl (**ts1c2**). Distances in Å.

The geometry of these transition states can be associated with a trigonal bipyramid structure in which the leaving ligand and the forming hydride both lay at the equatorial plane. The barrier heights of these steps are 32.8 for O and 18.6 kcal/mol for Cl, practically equivalent to those calculated for the non-solvent-assisted process. These results indicate that, as in the Au^{III} complex, the heterolytic activation of H_2 was far more favorable over the chlorine atom than over the oxygen atom. Nevertheless, in contrast to the Au^{III} complexes, the direct assistance of a solvent molecule did not significantly decrease the activation barrier for the H_2 heterolytic splitting. Fig. 3 compares the influence of the solvent on the activity of Au^{III} and Pd^{II} complexes as determined experimentally. For Pd^{II}, the ac-

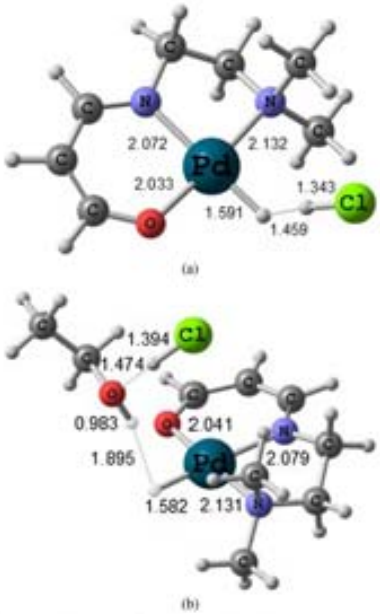

Fig. 8. Products of the heterolytic splitting of the dihydrogen molecule over the Cl ligand: (a) product for the non-assisted pathway (**Ic1–HCl**), (b) product of the assisted pathway (**Ic1–EtOH**). Distances in Å.

tivity was slightly improved when ethanol was used instead of acetone; this may be related to the slightly higher polarity of ethanol (dielectric constant $\varepsilon = 24.55$) with respect to acetone ($\varepsilon = 20.70$) [42]. For Au^{III}, however, the effect of the solvent was much more pronounced, because the activity in ethanol was considerably higher than that in acetone. This effect cannot be explained only in terms of solvent polarity, but rather is related to the active role of the ethanol molecule in the heterolytic activation of H_2. According to the mechanism calculated for Au^{III} complexes, a solvent with proton-donating ability, such as ethanol, is required for the reaction to proceed.

Fig. 8 shows the optimized geometry of the products of the nonassisted and the solvent-assisted pathways for the **2Pd** catalyzed reaction. It can be seen that in the product of the heterolytic cleavage without solvent assistance, a dihydrogen bond exists between the hydride of the Pd–H bond and the proton of the recently formed HCl molecule characterized by a distance of 1.459 Å (**Ic1–HCl**). This product is located at 18.8 kcal/mol with respect to the catalyst and the hydrogen molecule. The solvent-assisted heterolytic cleavage of the dihydrogen molecule produced an intermediate in which the proton of the HCl molecule was hydrogen-bonded with the oxygen atom of the ethanol molecule (**Ic1–EtOH**). This hydrogen bond is strong, with a distance of 1.474 Å. In this product, the proton of the ethanol molecule forms a dihydrogen bond with the hydride

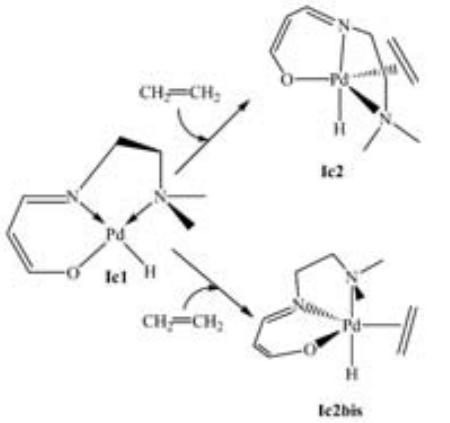

Fig. 9. Trigonal bipyramid structures after ethylene coordination.

ligand [43], with a H–H distance of 1.895 Å. This product is located 12.5 kcal/mol above the respective reactants: H_2, ethanol, and the catalyst interacting. It should be noted that in the analogous process in gold catalysis this step was exothermic by more than 10 kcal/mol [20]. This difference is likely due to the fact that the Au^{III} catalyst was positively charged, and the products in that case were $EtOH_2^+$ and Cl^- forming an ionic pair.

Based on the foregoing results, we can conclude that when Pd^{II} complexes are used as catalysts, the dihydrogen heterolytic cleavage is more favorable over chlorine than over the oxo group. Our calculations also indicate, in agreement with experimental evidence, that although solvent effects are important in lowering the activation barrier, the direct assistance of a solvent molecule is not needed for the reaction to occur, in contrast with the results obtained for the Au^{III} catalysts.

3.3.2. Coordination and insertion of the olefin to the catalyst

The next step in the catalytic cycle involves the alkene molecule. Exploring the potential energy surface for a pentacoordinated structure including the alkene in the coordination sphere of the catalyst identified two isomers, **Ic2** and **Ic2bis**. These isomers exhibited geometry close to that of a trigonal bipyramid structure. The relative energies of **Ic2** and **Ic2bis** intermediates with respect to ethylene and **Ic1** were 14.6 and 14.9 kcal/mol, respectively. These two structures are schematically represented in Fig. 9, and their optimized geometries are depicted in Fig. 10.

In principle, the reaction could evolve from any of these isomers. Therefore, we examined a reaction pathway starting from each of these intermediates. The two pathways found for olefin insertion into the Pd–H bond are schematically depicted in Fig. 11. From the **Ic2** intermediate, the reaction may evolve through ligand coordination breaking to regenerate a square planar structure, with the alkene occupying the position previously occupied by the N(amine) ligand. The optimized geometry of the transition state for this step (**ts2**) is depicted in Fig. 12.

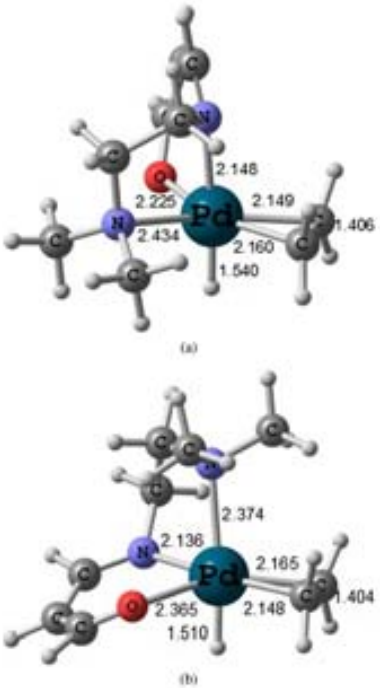

Fig. 10. Optimised geometry of the trigonal bipyramid isomers: (a) **Ic2** and (b) **Ic2bis**. Distances in Å.

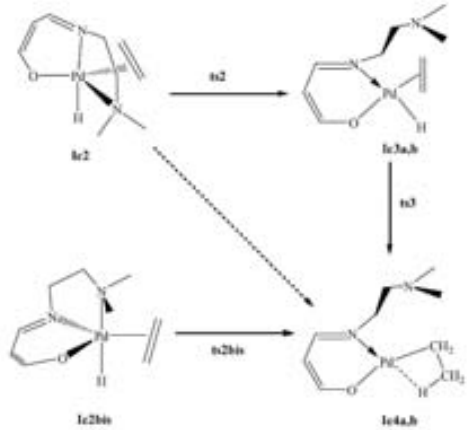

Fig. 11. Different pathways to obtain the alkyl intermediate (**Ic4a,b**) from **Ic2** and **Ic2bis**.

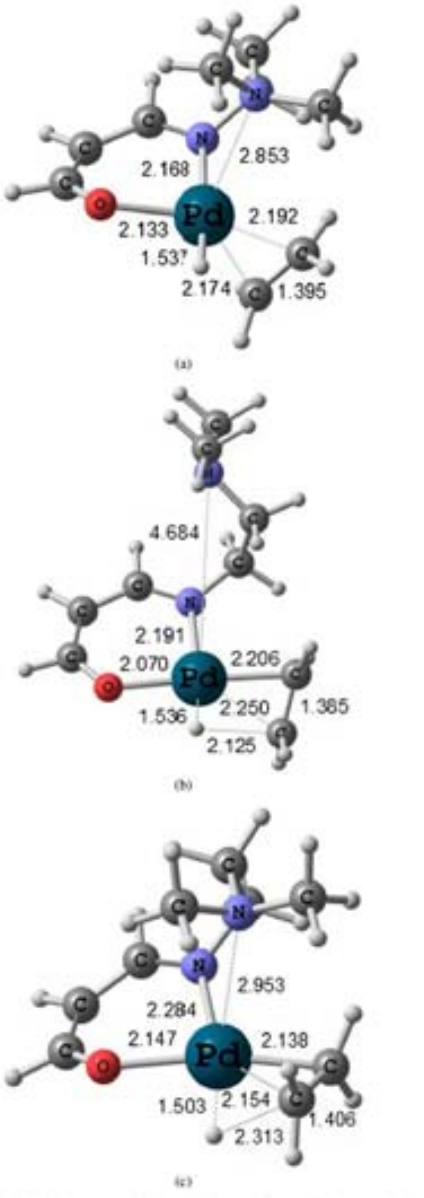

Fig. 12. Optimised geometry of the transition states for (a) ethylene coordination with N(aminic) leaving (**ts2**), (b) ethylene insertion into the Pd–H bond after N(aminic) leaving (**ts3**) and (c) N(aminic) leaving and ethylene insertion into the Pd–H bond occurring concomitantly (**ts2bis**). Distances in Å.

The energy cost for N(amine) removal and ethylene coordination starting from **Ic2** was only 0.4 kcal/mol, and formation of the **Ic3a** intermediate was exothermic by 6.3 kcal/mol. A related study by Vrieze and co-workers [44] on the insertion reaction of CO into Pd–C bonds of complexes containing terdentate nitrogen ligands proposed that one of the terminal N of the chelate ligand is substituted by the incoming CO within the reaction mechanism [44]. Another study in a different system analogously proposed the breakage of one labile palladium–pyridine bond in alkyne hydrogenation to coordinate an additional molecule present in the reaction media, such as hydrogen or an alkyne molecule [45].

Once the square planar intermediate **Ic3a** is formed, a small conformational change (associated to the change of the N–C–C–N dihedral angle) gives rise to intermediate **Ic3b,** which is lower in energy (by 0.6 kcal/mol). In both intermediates **Ic3a** and **Ic3b**, coordination of the olefin is perpendicular to the plane containing the metal center and the other ligands. The next step corresponds to insertion of the alkene into the Pd–H bond through transition state **ts3**. This process has been systematically studied computationally for the second-row metal complexes, including a palladium monohydride species [46]. The insertion process involves rotation of the olefin concomitantly to the insertion process itself (see Fig. 12b), producing the intermediate **Ic4a**, in which there is an agostic interaction between the metal and the recently formed C–H bond, as expected after the insertion process [47a]. This step is thermodynamically favorable by 8.8 kcal/mol, with an energy barrier of 5.0 kcal/mol. Along with **Ic4a,** there is another conformer, **Ic4b**, which is 0.8 kcal/mol lower in energy.

An alternative pathway for forming the intermediate **Ic4b** starts from the **Ic2bis** structure. In this case, the process occurs in a single step; the transition state **ts2bis** reveals a simultaneous hydride migration to the ethylene molecule and breaking of the coordination of the N(amine) ligand. The energy barrier for this process is 9.6 kcal/mol. This pathway is energetically less favorable than the two-step pathway starting form the **Ic2** intermediate, in which the highest barrier is 5.0 kcal/mol. These results are in agreement with the conclusion reached by Thorn and Hoffmann [48] that ethene insertion into a M–H bond is more difficult in a trigonal bipyramidal structure than in a square planar structure [48].

The existence of direct hydride migration concomitantly with the N(amine) leaving when starting from the **Ic2bis** structure led us to consider an analogous process starting from the **Ic2** structure (see the dashed arrow in Fig. 11). Although we extensively searched this direct process in the potential surface, we could not locate the associated transition state. In any case, this process is expected to be energetically similar to that starting from **Ic2bis**, which is higher than the stepwise process previously shown.

3.3.3. Second hydrogen transfer closing the catalytic cycle

The next step in the proposed reaction mechanism is the second hydrogen transfer process yielding the product, ethane. The possibility of alkyl protonation by the acid formed in the first step, as suggested in the literature [30,31], has been analyzed

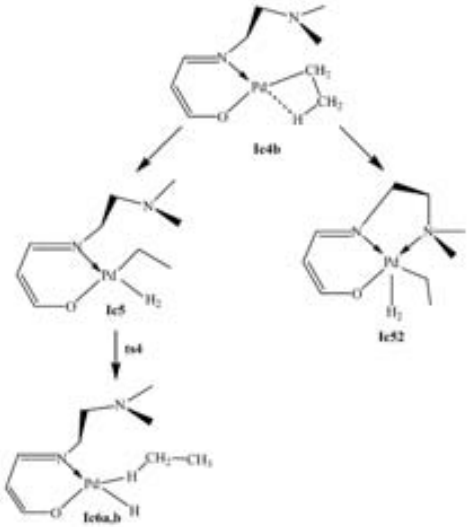

Fig. 13. Different ways of coordination of H_2 to the **Ic4b** intermediate and evolution of **Ic5**.

for the Au^{III} system and found to be energetically prohibitive [20]; therefore, we did not consider this pathway here. Instead, we investigated H_2 molecule coordination to the catalyst at intermediate **Ic4b**. The two alternatives considered for this H_2 coordination are shown in Fig. 13. In the first of these, the **Ic4b** intermediate evolves by breaking the weak agostic interaction between the metal and the C–H bond and coordinating the dihydrogen molecule into the vacant site forming the **Ic5** intermediate, an exothermic process by 4.0 kcal/mol. In the second pathway, the N(amine) of the Schiff base complex coordinates again to the vacant site and H_2 coordinates to the complex, forming a penta-coordinated structure, **Ic52**. Extensive exploration of the potential energy surface around the coordination mode supposed for the **Ic52** intermediate was performed without success; thus, calculations suggest that when it exists, this penta-coordinated intermediate will be very high in energy.

Consequently, the reaction mechanism was considered to go through intermediate **Ic5**. After the dihydrogen molecule coordination, the next step corresponds to hydrogenolysis to give the hydride intermediate **Ic6a** (see Fig. 13) and ethane, which remains coordinated to the complex by means of an agostic interaction between the metal and one of the C–H bonds. H_2 activation goes through a four-centered metathesis-like transition state (**ts4** in Fig. 14) with an activation energy of 12.1 kcal/mol. An analogous hydrogenolysis step also has been found to be favorable for the chain termination process in ethylene polymerization by means of the diimine–palladium [47b] and diimine–nickel [47c], and also in a hydride-exchange process [49].

The final step in the catalytic cycle involves the conformational change of a side chain of the N(amine) ligand, fa-

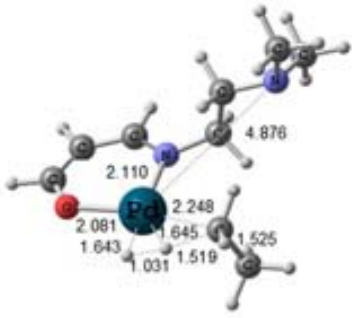

Fig. 14. Optimised geometry of the transition state for the hydrogenolysis of H_2 (**ts4**). Distances in Å.

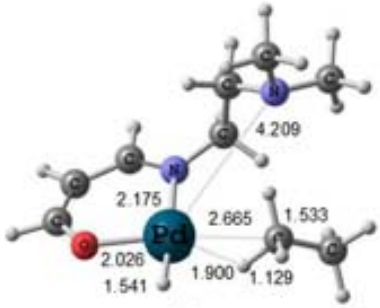

(a)

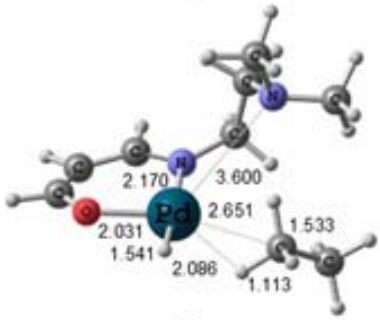

(b)

Fig. 15. Optimised geometry of the transition states for (a) conformational change of the aminic chain (**ts5**) and (b) N(aminic) coordination to Pd with ethane release occurring concomitantly (**ts6**). Distances in Å.

cilitating its coordination to palladium, concomitantly with product (ethane) release. The conformational change of the aminic chain (producing intermediate **Ic6b**) has a barrier height of 2.9 kcal/mol, and the process is endothermic by only 2.3 kcal/mol. The optimized geometry of the transition state for this process, **ts5**, is shown in Fig. 15. The simultaneous co-

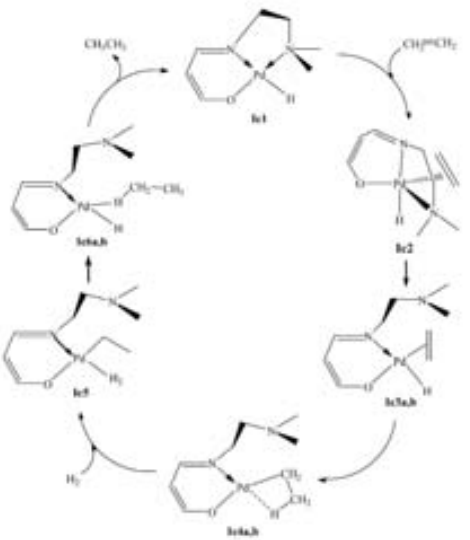

Fig. 16. Proposed catalytic cycle without the initial H_2 activation. Letters written after the intermediate labels correspond to different conformers of the same species.

ordination of the N(amine) ligand and the elimination of the ethane molecule through transition state **ts6** (see Fig. 15) has a barrier of only 0.2 kcal/mol. Moreover, this step is exothermic by 33.3 kcal/mol and regenerates the palladium–hydride intermediate **Ic1**, thereby providing an elegant and easy way to close the catalytic cycle. Actually, the final product is a different conformer of the hydride species. Both conformers (see the initial and final catalysts of the energy profile in Fig. 17) are isoenergetic; thus, they have not been distinguished, and both are referred to as **Ic1** in the present work.

3.4. Global reaction mechanism

The complete catalytic cycle, without initial H_2 activation and simplifying some steps that involve conformational rearrangements, is shown in Fig. 16, and the corresponding energy profile is depicted in Fig. 17. The highest energy barrier of the proposed mechanism is 19.2 kcal/mol, which corresponds to the initial activation of H_2 through its heterolytic cleavage over the chlorine ligand. Nevertheless, this process is not within the catalytic cycle; once the hydrogen molecule has been initially activated forming the palladium–hydride intermediate, **Ic1**, this is the active species involved in the catalytic cycle. This should result in an induction period in the kinetic curve, which indeed has been observed experimentally. In Fig. 2a, it can be seen that the induction period is more significant at low temperature and is slightly diminished when the partial pressure of H_2 is increased from 2 to 4 bar (Fig. 2b).

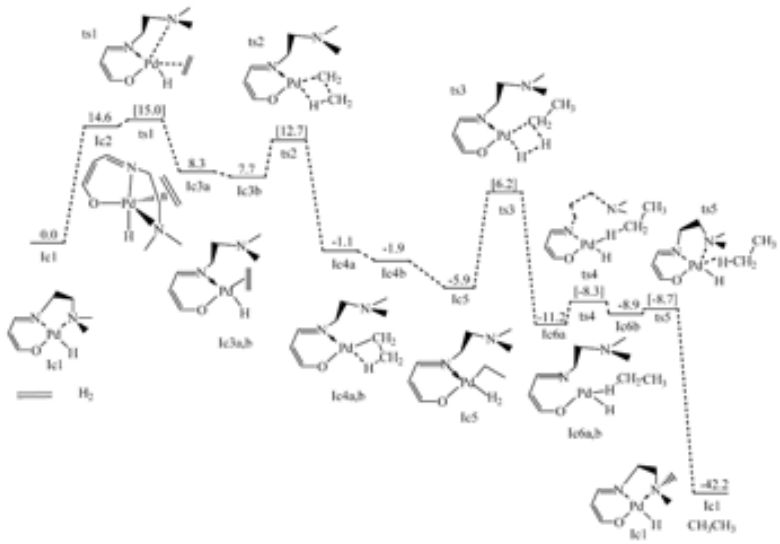

Fig. 17. Calculated energy profile for the proposed mechanism. Energies in kcal/mol.

The second activation of the H_2 molecule, which occurs within the catalytic cycle, occurs in a different (and easier) manner. In this case, the H_2 molecule initially coordinates to a vacant site in the Pd catalyst before undergoing the hydrogenolysis process, which has a lower energy barrier (12.1 kcal/mol). The highest energy barrier step in the catalytic cycle corresponds to N(amine) ligand substitution by the incoming ethylene molecule. This process implies initial ethylene coordination to the catalyst; a new ligand is added to the palladium catalyst, forming a penta-coordinated structure—a process not favorable for a metal center with d^8 electronic configuration. The next step implies N(amine) descoordination to generate again a square planar structure, with an activation barrier of 15.0 kcal/mol for the overall process. Concerning the solvent effects, calculations indicate that its inclusion in the Pd^{II}-catalyzed reaction is important because the energy barrier of the initial step is significantly diminished. Nevertheless, and conversely to the analogous Au^{III} catalyst, in this case both theoretical and experimental results suggest that solvent plays no active role in the reaction mechanism.

4. Conclusion

In the present work, the catalytic performance and the reaction mechanism of a homogeneous and two heterogenized Schiff base complexes of Pd^{II} and Au^{III} in the hydrogenation reactions of diethyl ethylidensuccinates have been analysed and compared by means of kinetic and computational studies. The reaction mechanism for the Pd^{II} catalyst occurs in three main steps: (i) heterolytic activation of hydrogen molecule, generating a Pd–hydride intermediate, (ii) coordination and insertion of the olefin into the catalyst, and (iii) coordination of H_2 molecule, proton transfer to substrate, and regeneration of the Pd–hydride species. Our results demonstrate that the hydrogenation mechanism using Pd^{II} complexes is similar to that of the Au^{III} counterparts, with some significant differences.

For the Pd^{II} complexes, the dihydrogen heterolytic cleavage is more favorable over chlorine than over the oxo group, as for the Au^{III} complexes. Calculations also indicate, in agreement with experimental evidence, that solvent effects are important to speeding-up the reaction rate. Nevertheless, in contrast to the Au^{III} complex, for the Pd^{II} complexes the direct assistance of a solvent molecule does not significantly decreases the energy barrier for the initial heterolytic activation of the hydrogen molecule. This fact is experimentally confirmed by the similar induction periods found for both acetone and ethanol solvents (conversely to the Au^{III} complex).

Regarding the rate-determining step, it is the same for both complexes once the catalytically active species (the hydride intermediate) is formed. This step corresponds to the coordination of the olefin to the catalyst. Nevertheless, whereas for the Pd^{II} complex, the addition of olefin built a pentacoordinated species, for the Au^{III} complex, no five-coordinated complex was found in the reaction mechanism.

The catalytic experiments on the hydrogenation of ethylidensuccinates for the homogeneous catalysts showed similar activity for Pd^{II} and Au^{III}. The TOFs for the supported catalysts increased compared with those for the homogeneous systems for both metals. The hydrogen molecule was heterolytically activated by the metal complex with no oxidative addition

process. This route implies a charge separation that should be facilitated by polar supports, as in fact was noted in the heterogenized catalysts.

Acknowledgments

Financial support for this work was provided by the Spanish MEC (projects MAT2003-07945-C02-01 and -02, and CTQ2005-09000-C02-01, a "Ramón y Cajal" contract to G.U. and FPU fellowships to A.C.-V.), as well as the Auricat EU Network (HPRN-CT-2002-0174), and Generalitat de Catalunya (2005/SGR/00896).

Supplementary material

The online version of this article contains additional supplementary material.

Please visit DOI: 10.1016/j.jcat.2007.12.015.

References

[1] P.N. Rylander, Catalytic Hydrogenation over Platinum Metals, Academic Press, New York, 1967.
[2] A. Yamamato, Organotransition Metal Chemistry, Wiley, New York, 1986.
[3] W.A. Herrmann, B. Cornils, Angew. Chem. Int. Ed. 36 (1997) 1048.
[4] M. Kram, Adv. Catal. 29 (1980) 151.
[5] Z.M. Michalska, D.E. Webster, CHEMTECH 5 (1975) 117.
[6] P.A. Chaloner, M.A. Esteruelas, F. Joó, L.A. Oro, Homogeneous Hydrogenation, Kluwer, Dordrecht, 1994.
[7] G. Dyker, Angew. Chem. Int. Ed. 39 (2000) 4237, and references therein.
[8] (a) G.J. Hutchings, S. Carrettin, P. Landon, J.K. Edwards, D. Enache, D.W. Knight, Y.J. Xu, A.F. Carley, Top. Catal. 38 (2006) 223;
(b) A.S.K. Hashmi, G.J. Hutchings, Angew. Chem. Int. Ed. 45 (2006) 7896.
[9] (a) X. Yao, Ch.-J. Li, J. Am. Chem. Soc. 126 (2004) 6884;
(b) Ch. Wei, Ch.-J. Li, J. Am. Chem. Soc. 125 (2003) 9584.
[10] M. Haruta, Catal. Today 36 (1997) 153.
[11] J. Guzman, B.C. Gates, J. Phys. Chem. B 106 (2002) 7659;
J. Guzman, B.C. Gates, J. Am. Chem. Soc. 126 (2004) 2672.
[12] M. Valden, X. Lai, D.W. Goodman, Science 281 (1998) 1647.
[13] J. Guzman, S. Carrettin, A. Corma, J. Am. Chem. Soc. 127 (2005) 3286.
[14] Q. Fu, H. Saltsburg, M. Flytzani-Stephanopoulos, Science 301 (2003) 935.
[15] A. Abad, P. Concepción, A. Corma, H. García, Angew. Chem. Int. Ed. 44 (2005) 4066.
[16] F. Porta, L. Prati, M. Rossi, G. Scari, J. Catal. 211 (2002) 464.
[17] S. Carrettin, J. Guzman, A. Corma, Angew. Chem. Int. Ed. 44 (2005) 2242.
[18] A. Corma, P. Serna, Science 313 (2006) 332.
[19] (a) C. González-Arellano, A. Corma, M. Iglesias, F. Sánchez, J. Catal. 238 (2006) 497;
(b) C. González-Arellano, A. Corma, M. Iglesias, F. Sánchez, Chem. Commun. (2005) 3451.
[20] A. Comas-Vives, C. González-Arellano, A. Corma, M. Iglesias, F. Sánchez, G. Ujaque, J. Am. Chem. Soc. 128 (2006) 4756.
[21] C. González-Arellano, E. Gutiérrez-Puebla, M. Iglesias, F. Sánchez, Eur. J. Inorg. Chem. (2004) 1955.
[22] C. González-Arellano, A. Corma, M. Iglesias, F. Sánchez, Adv. Synth. Catal. 346 (2004) 1316.
[23] M.J. Frisch, G.W. Trucks, H.B. Schlegel, G. Scuseria, M.A. Robb, J.R. Cheeseman Jr., J.A. Montgomery, T. Vreven, K.N. Kudin, J.C. Burant, J.M. Millam, S.S. Iyengar, J. Tomasi, V. Barone, B. Mennucci, M. Cossi, G. Scalmani, N. Rega, G.A. Petersson, H. Nakatsuji, M. Hada, M. Ehara, K. Toyota, R. Fukuda, J. Hasegawa, M. Ishida, T. Nakajima, Y. Honda, O. Kitao, H. Nakai, M. Klene, X. Li, J.E. Knox, H.P. Hratchian, J.B. Cross, V. Bakken, C. Adamo, J. Jaramillo, R. Gomperts, R.E. Stratmann, O. Yazyev, A.J. Austin, R. Cammi, C. Pomelli, J.W. Ochterski, P.Y. Ayala, K. Morokuma, G.A. Voth, P. Salvador, J.J. Dannenberg, V.G. Zakrzewski, S. Dapprich, A.D. Daniels, M.C. Strain, O. Farkas, D.K. Malick, A.D. Rabuck, K. Raghavachari, J.B. Foresman, J.V. Ortiz, Q. Cui, A.G. Baboul, S. Clifford, J. Cioslowski, B.B. Stefanov, G. Liu, A. Liashenko, P. Piskorz, I. Komaromi, R.L. Martin, D.J. Fox, T. Keith, M.A. Al-Laham, C.Y. Peng, A. Nanayakkara, M. Challacombe, P.M.W. Gill, B. Johnson, W. Chen, M.W. Wong, C. Gonzalez, J.A. Pople, Gaussian 03, Revision C.02, Gaussian, Inc., Wallingford, CT, 2004.
[24] (a) A.D. Becke, J. Chem. Phys. 98 (1993) 5648;
(b) C. Lee, W. Yang, R.G. Parr, Phys. Rev. B 37 (1998) 785;
(c) P.J. Stephens, J.F. Devlin, C.F. Chabalowski, M.J. Frisch, J. Phys. Chem. 98 (1994) 11623.
[25] P.J. Hay, W.R. Wadt, J. Chem. Phys. 82 (1985) 270.
[26] (a) M.T. Cancès, B. Mennucci, J. Tomasi, J. Chem. Phys. 107 (1997) 3032;
(b) M. Cossi, V. Barone, B. Mennucci, J. Tomasi, Chem. Phys. Lett. 286 (1998) 253;
(c) B. Mennucci, J. Tomasi, J. Chem. Phys. 106 (1997) 5151.
[27] (a) K. Fukui, Acc. Chem. Res. 14 (1981) 363;
(b) C. Gonzalez, H.B. Schlegel, J. Chem. Phys. 90 (1989) 2154;
(c) C. Gonzalez, H.B. Schlegel, J. Phys. Chem. 94 (1990) 5523.
[28] (a) A. Corma, C. del Pino, M. Iglesias, F. Sánchez, J. Chem. Soc. Chem. Commun. (1991) 1253;
(b) A. Corma, M. Iglesias, M.V. Martín, J. Rubio, F. Sánchez, Tetrahedron: Asymmetry 3 (1992) 845;
(c) A. Corma, M. Fuerte, M. Iglesias, F. Sánchez, J. Mol. Catal. A Chem. 107 (1996) 225, and references therein;
(d) M.J. Alcón, A. Corma, M. Iglesias, F. Sánchez, J. Mol. Catal. A Chem. 194 (2003) 137.
[29] P. Pelagatti, in: J.G. de Vries, C.J. Elsevier (Eds.), Handbook of Homogeneous Hydrogenation, vol. 1, Weinheim, Wiley–VCH, 2007, p. 71.
[30] (a) G. Henrici-Olivé, S. Olivé, Angew. Chem. Int. Ed. 13 (1974) 549;
(b) G. Henrici-Olivé, S. Olivé, J. Mol. Catal. 1 (1975/6) 121.
[31] D.R. Armstrong, O. Novaro, M.E. Ruiz-Vizcaya, R. Linarte, J. Catal. 48 (1977) 8.
[32] S. Niu, M.B. Hall, Chem. Rev. 100 (2000) 353.
[33] (a) F. Hutschka, A. Dedieu, W. Leitner, Angew. Chem. Int. Ed. 34 (1995) 1742;
(b) F. Hutschka, A. Dedieu, M. Eichberger, R. Fornika, W. Leitner, J. Am. Chem. Soc. 119 (1997) 4432;
(c) A. Milet, A. Dedieu, G. Kapteijn, G. van Koten, Inorg. Chem. 36 (1997) 3223;
(d) A. Dedieu, S. Humbel, J.E. Cornelis, C. Grauffel, Theor. Chem. Acc. 112 (2004) 305.
[34] D.G. Musaev, R.D.J. Froese, K. Morokuma, S. Strömberg, K. Zetterberg, P.E.M. Siegbahn, Organometallics 16 (1997) 1933.
[35] D.G. Musaev, R.D.J. Froese, K. Morokuma, Organometallics 17 (1998) 1850.
[36] D. Sellmann, F. Geipel, M. Moll, Angew. Chem. Int. Ed. 39 (2000) 561.
[37] Y. Masashi, S. Sakaki, J. Am. Chem. Soc. 122 (2000) 3867.
[38] G. Zampella, M. Bruschi, P. Fantucci, L. De Gioia, J. Am. Chem. Soc. 127 (2005) 13180, and references therein.
[39] (a) F. Hutschka, A. Dedieu, J. Chem. Soc. Dalton Trans. 11 (1997) 1899;
(b) M. Ito, M. Hirakawa, K. Murata, T. Ikariya, Organometallics 20 (2001) 379;
(c) C.A. Sandoval, T. Ohkuma, K. Muñiz, R. Noyori, J. Am. Chem. Soc. 125 (2003) 13490;
(d) V. Rautenstrauch, X. Hoang-Cong, R. Churlaud, K. Abdur-Rashid, R.H. Morris, Chem. Eur. J. 9 (2003) 4954;
(e) C.P. Casey, J.B. Johnson, S.W. Singer, Q. Cui, J. Am. Chem. Soc. 127 (2005) 3100;
(f) C. Hedberg, K. Källström, P.I. Arvidsson, P. Brandt, P.G. Andersson, J. Am. Chem. Soc. 127 (2005) 15083.
[40] V.V. Grushin, Chem. Rev. 96 (1996) 2011.
[41] J. López-Serrano, S.B. Duckett, A. Lledós, J. Am. Chem. Soc. 128 (2006) 9596.
[42] Values used in the Gaussian 03 program package.
[43] (a) R.H. Crabtree, P.E.M. Siegbahn, O. Eisenstein, A.L. Rheingold, T.F. Koetzle, Acc. Chem. Res. 29 (1996) 348;

(b) M.J. Calhorda, Chem. Commun. (2000) 801;
(c) J.G. Planas, C. Viñas, F. Teixidor, A. Comas-Vives, G. Ujaque, A. Lledós, M.E. Light, M.B. Hursthouse, J. Am. Chem. Soc. 127 (2005) 15976.
[44] J.H. Groen, A.D. Zwart, M.J.M. Vlaar, J.M. Ernsting, P.W.N.W. van Leeuwen, K. Vrieze, H. Kooijman, W.J.J. Smeets, A.L. Spek, P.H.M. Budzelaar, Q. Xiang, R.P. Thummel, Eur. J. Inorg. Chem. 00 (1998) 1129.
[45] P. Pelagatti, A. Venturini, A. Leporati, M. Carcelli, M. Costa, A. Bacchi, G. Pelizzi, C.J. Pelizzi, Chem. Soc. Dalton Trans. 16 (1998) 2715.
[46] P.E.M. Siegbahn, J. Am. Chem. Soc. 115 (1993) 5803.
[47] (a) N. Koga, S. Obara, K. Kitaura, K. Morokuma, J. Am. Chem. Soc. 107 (1985) 7109;
(b) D.G. Musaev, M. Svensson, K. Morokuma, S. Strömberg, K. Zetterberg, P.E.M. Siegbahn, Organometallics 16 (1997) 1933;
(c) D.G. Musaev, R.D.J. Froese, M. Svensson, K. Morokuma, J. Am. Chem. Soc. 11 (1997) 367.
[48] D.L. Thorn, R. Hoffmann, J. Am. Chem. Soc. 100 (1978) 2079.
[49] I. Demachy, M.A. Esteruelas, Y. Jean, A. Lledós, F. Maseras, L.A. Oro, C. Valero, F. Volatron, J. Am. Chem. Soc. 118 (1996) 8388.

Apèndix B

Annex 2. Treballs no publicats que per motius legals no formen part d'aquesta tesi

B.1 Article VII

A computational study of the olefin epoxidation mechanism catalyzed by cyclopentadienyloxidomolybdenum(VI) complexes.

Aleix Comas-Vives,[a] Agustí Lledós,*[a] and Rinaldo Poli*[b]

[a]*Unitat de Química Física, Departament de Química, Edifici Cn, Universitat Autònoma de Barcelona, 08193 Bellaterra, Catalonia, Spain*

[b]*Laboratoire de Chimie de Coordination, UPR CNRS 8241 liée par convention à l'Université Paul Sabatier et à l'Institut National Polytechnique de Toulouse, 205 Route de Narbonne, 31077 Toulouse Cedex, France*

Abstract

A DFT analysis of the epoxidation of C_2H_4 by H_2O_2 (as a model of *tert*-butylhydroperoxide, TBHP) catalyzed by $[Cp^*MoO_2Cl]$ (**1**) in $CHCl_3$ and by $[Cp^*MoO_2(H_2O)]^+$ (**13**) in water is presented. The calculations were performed both in the gas phase and in solution with the use of the conductor-like polarizable continuum model (CPCM). A low-energy pathway has been identified, which starts with the activation of H_2O_2 to form a hydroperoxido derivative, $[Cp^*MoO(OH)(OOH)Cl]$ (**3**) or $[Cp^*MoO(OH)(OOH)]^+$ (**16a**) with barriers of 24.2 and 28.1 kcal mol^{-1}, respectively, in solution. The latter barrier, however, is reduced to only 1.0 kcal mol^{-1} when one additional water molecule is explicitly included in the calculations. The hydroperoxido ligand in these intermediates is η^2-coordinated with a significant interaction between the Mo center and the β-O atom. The subsequent step is a nucleophilic attack of the ethylene molecule on the activated α-O atom, requiring 12.7 and 14.0 kcal mol^{-1} in solution respectively. The corresponding transformation catalyzed by the peroxido complex $[Cp^*MoO(O_2)Cl]$ (**8**) in $CHCl_3$ requires higher barriers for both steps (H_2O_2 activation: 33.7 kcal mol^{-1}; O atom transfer: 26.9 kcal mol^{-1}), which is attributed to both greater steric crowding and to the greater electron density on the metal atom. The isomerization of the hydroperoxido complex **16a** to peroxido derivatives $[Cp^*Mo(O_2)(OH)_2]^+$ (**22**) and $[Cp^*MoO(O_2)(H_2O)]^+$ (**23**) is shown to be favourable in the presence of water. These peroxido derivatives are shown to yield higher barriers for oxygen transfer to the olefin, providing a rationalization for the lower activity of these molybdenum catalysts toward the epoxidation by H_2O_2, relative to TBHP.

Proofs to :
Agustí Lledós
Tel +34-935811716
Fax +34-935812920
E-mail agusti@klingon.uab.es

Introduction

The olefin epoxidation reaction is extremely important as a relatively easy access way to functionalized organic materials from crude oil fractions. The reaction occurs with organic peroxides such as peracids and dioxiranes without the need of a catalyst.[1] The metal-catalyzed version has attracted much attention due to the possibility to perform more selective, notably enantioselective, transformations. Among the possible oxygen delivering agents, H_2O_2 is the subject of the greatest amount of investigations[2] given its low cost and easy availability. However, *tert*-butylhydroperoxide (TBHP) is still heavily used in the research laboratory and industrially because it generally outperforms hydrogen peroxide. Many transition metal catalysts have been used to carry out this transformation, including high oxidation state oxido complexes (methyltrioxidorhenium, dioxido derivatives of Mo and W),[3-6] bis(peroxido) complexes $[(L_1)(L_2)MO(O_2)_2]$ (M = Mo, W),[7] polyoxometallates,[8-10] a variety of oxido complexes generated in situ from Fe and Mn porphyrin, salen, and other coordination compounds.[11-14]

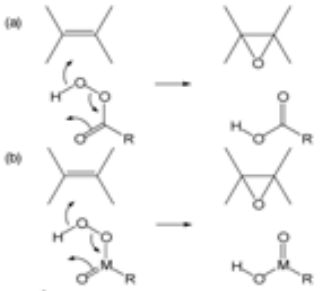

Scheme 1

The mechanism of this reaction has been and continues to be the subject of controversy. In many cases, a mechanism related to that accepted for organic peracids is proposed,[15] see Scheme 1(a). However, this mechanism is easily understood only when H_2O_2 is the oxidant, since the active M-OOH species, Scheme 1(b), can be regenerated from the hydroxido product, M-OH, by simple ligand exchange.[16] It cannot be the operative mechanism for the reactions using TBHP, unless a second oxygen atom transfer takes place to regenerate the active M-OOH species from TBHP and M-OH.

The fact that a large number of peroxido complexes of molybdenum and tungsten have been isolated and fully characterized[17] has led to the consideration that a peroxido ligand is capable of transferring an oxygen atom to the olefin. Two reference mechanisms are based on this idea, usually referred to as the "Mimoun"[18] and the "Sharpless"[19] mechanisms, see Scheme 2. Once again, for the reasons outlined above, these two mechanisms are easily understood only when H_2O_2 is used, less so when TBHP is involved.

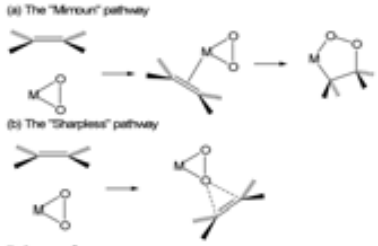

Scheme 2

A number of theoretical investigations have addressed the two competing mechanisms shown in Scheme 2, mostly for Mo,[20-27] but also for other metals,[28, 29] leading to a clear preference for the Sharpless scheme. The need to modify these mechanisms in order to account for the activity of TBHP has been presented by Thiel,[30-32] but to the best of our knowledge no thorough theoretical investigation has followed. Thiel's proposal is outlined in Scheme 3. Essentially, the peroxido ligand serves as a depository of the reactant's proton. The oxidizing agent is activated by coordination and becomes susceptible to nucleophilic attack by the olefin at the electrophilic oxygen atom. Note that this mechanism, proposed by Thiel for the specific oxidation with TBHP (R = *t*Bu), may also operate for H_2O_2 (R = H). Note also that the basic principle is identical to that proposed by Sharpless (exogenous attack of the olefin at an electrophilic

oxygen atom, without coordination). However, the oxygen is not transferred from a coordinated peroxido ligand, rather from the *t*-butylperoxido (or hydroperoxido) ligand. Finally, note that other metal-bonded functionalities may exert, in principle, the same proton depository function (for instance, oxido ligands).

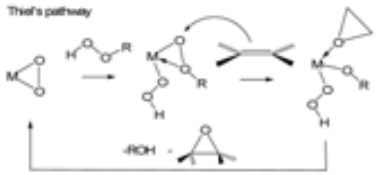

Scheme 3

Extensive experimental studies carried out with $[MoO_2X_2L_2]$-type catalysts and TBHP as oxidant have shown that the source of the oxygen atom for the epoxidation is TBHP and not the catalyst's oxido ligands, ruling out the possible involvement of direct oxygen atom transfer from $Mo(O_2)$ moieties and invalidating both Mimoun and Sharpless mechanisms as originally proposed.[33] Thus, the existence and stability of peroxido complexes must be related to side processes such as the deprotonation of hydroperoxido ligands, Mo-OOH. Indeed, a study by Bergman (the first catalytic study using an organometallic oxido derivative of molybdenum) has shown that the $[Cp^*MoO_2Cl]$/TBHP system is effective for olefin epoxidation, whereas the peroxido analogue, $[Cp^*MoO(O_2)Cl]$, is catalytically inactive.[34] Thus, the peroxido compound cannot be implicated as a catalytic intermediate in the $[Cp^*MoO_2Cl]$-catalyzed epoxidation with TBHP. These findings have later been confirmed by Roesky, who also reported the x-ray structure of the $[Cp^*MoO(O_2)Cl]$ compound.[35] Subsequent studies by Kühn and Romão have shown that related complexes with different cyclopentadienyl ligands, as well as alkyl derivatives of type $[(Ring)MoO_2R]$ (Ring = substituted cyclopentadienyl ligand, R = alkyl) are also catalytically active.[36-38] In a recent collaborative study, some of us have shown that the dinuclear oxido-bridged $[(Ring)_2Mo_2O_5]$ systems are also catalytically active when using TBHP in an organic solvent and are also active with the same reagent under aqueous biphasic conditions. They are inactive, however, when TBHP is replaced by H_2O_2.[39]

Only recently, the use of MeOOH as a model of the *t*BuOOH reagent has been considered in a theoretical study.[33, 40] The activation step of the oxidant reported by this study resembles that proposed by Thiel, except that an oxido ligand is used as the proton depository, see Scheme 4. Hydrogen bonding between the hydroxido proton and the β-O atom of the organoperoxido ligand was found to stabilize this intermediate. However, the subsequent step of the mechanism is quite different than that proposed by Thiel and involves an insertion into the metal-peroxido bond, similar to the pathway proposed by Mimoun (though preliminary olefin coordination does not occur). The most puzzling feature of this mechanism is that the olefin insertion transition state is calculated as 52 kcal/mol higher in energy (63 kcal/mol higher in free energy) than the intermediate, which is itself 16 kcal/mol higher in energy (29 kcal/mol higher in free energy) than the starting materials (catalyst + MeOOH + olefin). This is a prohibitive activation barrier for an efficient catalytic process. For this reason, we think that a new theoretical investigation of the epoxidation mechanism is warranted.

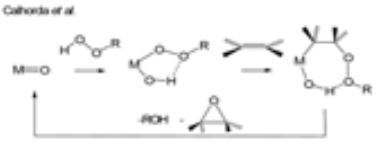

Scheme 4

We have been interested in the aqueous chemistry of the Cp^*Mo^{VI} system[41] and have shown that compound $[Cp^*_2Mo_2O_5]$ self-ionizes in water to yield a 1:1 mixture of $[Cp^*MoO_2(H_2O)]^+$ and $[Cp^*MoO_3]^-$, then evolving to a different ratio by spontaneous hydrolysis or by adjusting the pH with a buffer.[42] While the dinuclear compound may exert the same mechanistic function as $[Cp^*MoO_2Cl]$ (the Cl ligand being replaced by the oxido-bridged Cp^*MoO_3 group), only the cationic

complex is likely to exert a catalytic function among the charged species, since the water ligand can dissociate rather easily[43] and the resulting coordination site may be used for activation of the oxidant. Useful background information comes from our recent computational study of hydration and proton transfer processes for the $Cp^*MoO_2^+$ (aq) system.[43] Therefore, we have decided to examine the mechanism of the olefin epoxidation process by both Bergman's [Cp^*MoO_2Cl] system (which may also serve as a model for [Cp^*MoO_2R], R = alkyl, and [$Cp^*_2Mo_2O_3$]) and the [Cp^*MoO_2]$^+$ cation. Points of interest are:

- indentify a low-energy pathway for oxygen transfer from TBHP (or H_2O_2) to the olefin;
- understand the difference in catalytic activity between the oxido and peroxido derivatives for Bergman's system, [Cp^*MoO_2Cl] and [$Cp^*MoO(O_2)Cl$];
- understand the reason for the better performance of TBHP vs. H_2O_2 as an oxidant and possibly predict the experimental conditions that would favour epoxidation for H_2O_2.

It is to be noted that the [Cp^*MoO_2X] system (X = Cl, CH_3, Cp^*MoO_3) is isoelectronic with the [$MoO_2X_2L_2$] system, see Scheme 5. Thus, the considerations resulting from our calculations on this system may be extrapolated to the more traditional class of [$MoO_2X_2L_2$] catalysts.

Scheme 5

Computational details

Calculations were carried out using the Gaussian 03 package[44] at the DFT level by means of the B3LYP functional.[45-47] For the Mo atom, the LANL2DZ pseudopotential[48] was used with the addition of f polarisation functions.[49] The 6-31G(d) basis set was used for C atoms whereas additional diffuse functions [6-31+G(d)] were added for O and Cl atoms due to their anionic character. For the hydrogen atoms, the 6-31G(d,p) basis set was employed. IRC calculations were made in order to get the two minima linked by every transition-state.[50-52] Solvent effects were included by means of CPCM single point calculations.[53, 54] Additional spheres were included for all the hydrogens except for the Cp* hydrogens by means of the SPHEREONH option. Frequency calculations were made in order to check the presence of one imaginary frequency in transition-state geometries.

Results and Discussion

As a model olefin for our computational study, ethylene was used as the substrate (larger olefins, mostly cyclooctene, have been used for the experimental studies) and H_2O_2 as the oxidant. On the other hand, the full Cp* ligand was maintained in all calculations.

(a) Study of the [Cp^*MoO_2Cl] system, 1.

As stated in the Introduction, compound [Cp^*MoO_2Cl] was the first reported organomolybdenum olefin epoxidation catalyst but a theoretical investigation of the catalytic cycle using this compound has not yet been reported, to the best of our knowledge. In addition, the corresponding peroxido complex, [$Cp^*Mo(O_2)OCl$], **7**, was described as catalytically inactive,[34, 35] but a clear mechanistic interpretation of this phenomenon does not appear to be available. Calculations on this system may also be considered to model the action of other [Cp^*MoO_2X] catalysts (X = CH_3 or Cp^*MoO_3).[36-39] These molecules are excellent epoxidation catalysts provided TBHP is used as the oxidant and the solvent is apolar. Chloroform is frequently used, therefore the calculations have been carried out both on isolated molecules (gas phase) and also by introducing the solvent effect by the CPCM in $CHCl_3$ (ε = 4.9).

On the basis of all previously reported experimental and computational investigations on Mo-catalyzed olefin epoxidation,[2, 20-29, 33, 40] it is rather clear that the first step of the catalytic cycle consists of the activation of the oxidant molecule. Therefore, the first step of our investigation was an analysis of the coordination and activation of the H_2O_2 molecule by **1**. The energy profile is shown in Figure 1 while

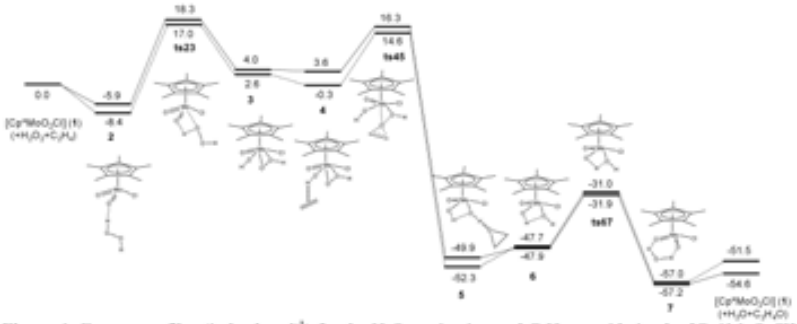

Figure 1: Energy profiles (in kcal mol^{-1}) for the H_2O_2 activation and C_2H_4 epoxidation by [Cp*MoO_2Cl] in the gas phase (dashed lines) and in $CHCl_3$ solution (plain lines). The reference energy corresponds to the separate reagents ([Cp*MoO_2Cl] + H_2O_2 + C_2H_4).

the optimized geometries of the key species are given in Figure 2. The starting species **2** features an H bond between the oxidant as proton donor and an oxido ligand as proton acceptor, slightly stabilizing the system relative to the two separate molecules. The **ts23** transition-state is characterized by nearly equivalent MoO···H distances and H···OOH distances. This structure is quite strained according to the O=Mo-O(H)(OH) angle, 65.8°, explaining the relatively high activation barrier for this proton transfer process (24.2 kcal mol^{-1} in $CHCl_3$ solution). We have found a similar situation in a recent study of the intramolecular proton transfer leading from $[Cp^*MoO(OH)_2]^+$ to $[Cp^*MoO_2(H_2O)]^+$.[43] In that case, we found that the barrier could be dramatically reduced by the proton relay action of a water molecule, which is the reaction solvent, since this allows a reduced angular distortion. In $CHCl_3$, the solvent molecules cannot assure a proton relay mechanism. However, the same role may be exerted by additional H_2O_2 (or *t*BuOOH) molecules and also by the corresponding H_2O (or *t*BuOH) co-product, once this has started to form, as shown in Scheme 6. Nevertheless, we have located the related proton relay mechanism through the H_2O_2 and H_2O activations and surprisingly its assistance does not change significantly the energy barrier, with respective values of 25.0 and 21.9 kcal mol^{-1} in $CHCl_3$. This is probably related to the fact that the more crowded complex does not allow a significantly wider O-Mo-OOH angle even with the water and H_2O_2 assistance. Here the related O-Mo-OOH angles are 80.2° and 74.9, respectively (whereas for the **ts10'11'** structure the O-Mo-OOH angle is more relaxed at 94.8°, and the barrier is much smaller at 1.0 kcal mol^{-1}, *vide infra*).

This step leads to the formation of the activated complex [Cp*MoOCl(OH)(OOH)], **3**. An identical pathway with a similar energy profile may be envisaged for the activation of TBHP. Note that **3** displays a significant interaction between the hydroperoxido β-O atom and the metal center (Mo-O_β = 2.446 Å, *vs.* Mo-O_α = 1.995 Å; and Mo-O_α-O_β = 88.7°), forming what could be formally described as a protonated metal peroxido [Mo(η^2-O_2)] ligand. It also features an H-bond between the OH ligand as a proton donor and the α-O atom of the OOH ligand as a proton acceptor. The nature of this product differs substantially from that obtained in the calculations by Calhorda *et al.*,[40] where the two terminally bonded hydroxido and *tert*-butylperoxido ligands in H-O-Mo-O-O-*t*Bu establish a H-bond between OH as a proton donor and the OO*t*Bu O_β atom as a proton acceptor. It seems that the β-O atom prefers to donate its electrons to the electrophilic Mo center than to engage an H-bond with the OH ligand. Attempts to optimize a structure related to that reported by Calhorda *et al.* did not lead to a stable minimum for this system. Only two additional minima at slightly higher energy in which the β-oxygen is at ca. 2.8 Å from the Mo atom could be located (**3'** and **3"** in Figure 3). In the first one there is a hydrogen-bond but between the OOH ligand as proton donor and the OH

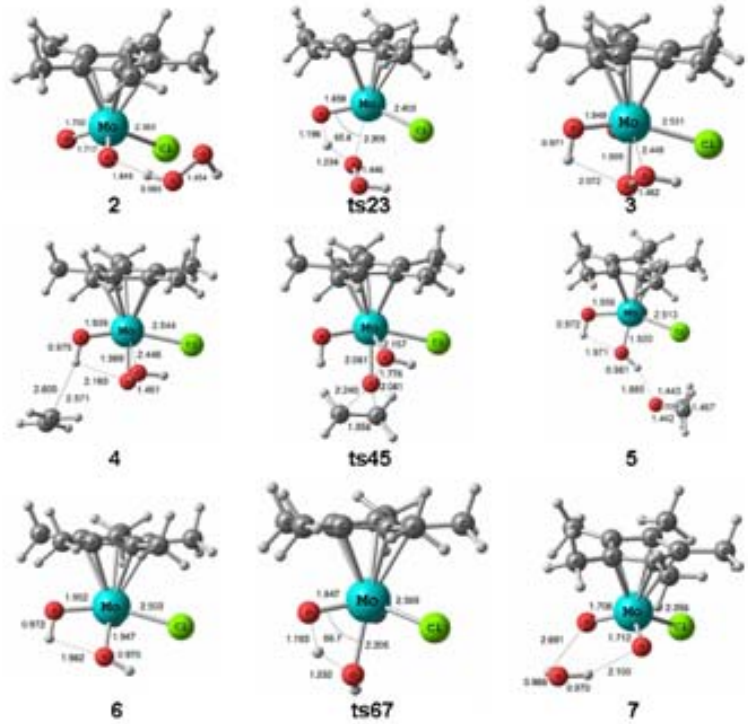

Figure 2: Optimized geometries and main structural data for the systems shown in Figure 1.

ligand as proton acceptor acceptor, whereas in the second one there are no significant H-bonds.

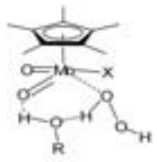

Scheme 6

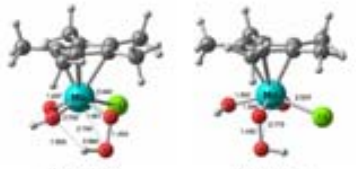

Figure 3: Optimized geometries of systems **3'** and **3''**. The energy values are in kcal mol^{-1} in the gas phase and in $CHCl_3$ (in parenthesis), relative to **3**.

The next step is the oxygen atom transfer from **3** to ethylene. The energy profile is also included in Figure 1 and the transition state geometry is shown in Figure 2. The process starts with the establishment of a weak H-bond between the olefin and the OH ligand (which is worth only 0.4 kcal mol^{-1} of stabilization energy in $CHCl_3$), forming the adduct **4**. The subsequent step is transfer of the hydroperoxido O_α atom to the olefin (**ts45**). The final products, ethylene oxide and [Cp*MoCl(O)(OH)$_2$], **6**, are formed via a H-bonded intermediate **5**. The barrier height (12.7 kcal mol^{-1} in $CHCl_3$), appears as a reasonably small barrier for the rate-determining step of an efficient catalytic cycle and much lower than those estimated earlier for other model systems on the basis of a different mechanism.[33, 40] In order to proceed to a new catalytic cycle, product **6** now needs to eliminate water (or *t*BuOH in the TBHP system). This process presents an energy barrier of 16.7 kcal mol^{-1} in the gas phase

and 16.0 kcal mol^{-1} in $CHCl_3$. Both in the gas phase and $CHCl_3$, the process is exothermic by 9.3 kcal mol^{-1}. Thus, it is easier than the initial activation of the catalyst.

To conclude, this pathway for the oxygen transfer step is quite reasonable once the H_2O_2 has been activated. The rate-limiting step calculated for the isolated system is the H_2O_2 activation according to the energy profile. However, the transition-state energy of **ts45** is very similar to that of **ts23** and entropic effects should disfavour **ts45** respect to **ts23** because two species have been added (H_2O_2 and ethylene) to the system in **ts45** and only one (H_2O_2) in **ts23**. Note that this pathway is also applicable to the oxidation with TBHP, in which case the metal complex after TBHP activation is [Cp*MoCl(O)(OH)(OtBu)]. From the experimental point of view, certain systems (e.g. $[\gamma\text{-}H_2SiV_2W_{10}O_{40}]^{4-}$ with H_2O_2[55] or $MoO_2Cl_2L_2$ compounds with TBHP[56]) show a first order dependence in oxidant, while others (e.g. Mn(TPFPP)Cl with iodosobenzene)[57] show a first order in substrate, suggesting that the nature of the rate determining step is system dependent. For the cyclopentadienyl substituted Mo^{VI} catalyst, no detailed kinetics studies have been reported so far, to the best of our knowledge.

Given the low barriers obtained for the mechanism outlined in Figure 1, we did not consider it worthwhile to explore other pathways, notably those involving the insertion of the ethylene molecule into the Mo-O bond according to the pathway explored by Calhorda *et al.*[40] For clarity, the two key steps are compared in Scheme 7 (the relative energies shown are from the gas-phase calculations). We believe that the β-O atom coordination with formation of the strained three-membered MoOO(H) cycle is important for the activation of the O_α atom. Possibly, the incipient bond formation between the Mo and β-O atoms also contributes to lowering the activation barrier for the oxygen atom transfer to the olefin. This is presumably achieved by lowering the energy of the O-O σ* orbital, which is susceptible to the nucleophilic attack by the external olefin. Indeed, according to a previous study on diperoxo complexes of group 6 metals, the lower the σ* O-O level the smaller the activation energy.[20] A close look at the electronic structure of complex Cp*MoO(OH)(OOH)Cl (**3**) shows that the highest contribution of O-O σ* is in an orbital located at -0.001980 hartrees, much lower than the energy of the orbitals containing the highest O-O σ* contribution for complex Cp*Mo(O_2)(O)Cl (at 0.007610, 0.037480 and 0.043720 hartrees), which will be discussed in more details below. Thus, this would be a qualitative indication that for the former complex the σ* orbital is much more accessible to the olefin nucleophilic attack.

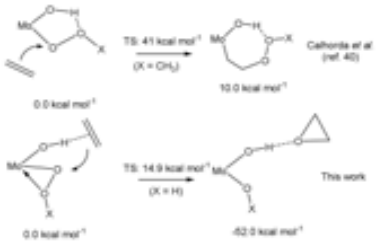

Scheme 7

The mechanism of Figure 1 can therefore be described as a variant of the Sharpless mechanism, where the oxygen atom is transferred from a hydroperoxido (or *tert*-butylperoxido) ligand after activation of the oxidant by protonation of an oxido ligand. It is closely related to the mechanism proposed by Thiel (Scheme 3),[30-32] with the peroxido function being replaced by a simpler oxido function as the proton accepting functionality.

(b) Study of the [Cp*Mo(O_2)OCl] system, 8.

Next, we proceeded to analyze a possible oxygen transfer process from the peroxido complex [Cp*Mo(O_2)(O)Cl] (**8**), which was found catalytically inactive by the Bergman study.[34] If the peroxido ligand in this complex is already sufficiently activated to transfer an oxygen atom to the exogenous olefin substrate, an elementary process leading to the epoxide product and to the dioxide complex **1** can be envisaged. The latter would then need to be transformed back to **8** by interaction with another oxidant molecule (H_2O_2 or TBHP). The lower

energy pathway found for the oxygen atom transfer process involves the attack of ethylene at the *exo* oxygen atom (further away from the Cp* ligand). The transition state **ts81** is illustrated in Figure 4. The relative energy barrier height for this process is 23.3 kcal mol^{-1} in the gas phase and 22.2 kcal mol^{-1} in $CHCl_3$, namely ca. 10 kcal mol^{-1} higher than for the hydroperoxo complex. This result is in good agreement with the experimental observation. A possible reason for the higher oxygen transfer barrier for the peroxido (O_2^{2-}) ligand is the higher energy of the O-O σ* orbital relative to that of the HOO^- ligand in complex **3**, as already commented above. In a previous theoretical work of Rösch *et al.*, it was also concluded that "the hydroperoxo mechanisms is competitive, if not superior to the peroxo mechanisms".[27]

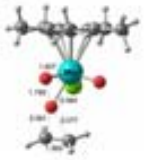

ts81

Figure 4: Optimized geometry and main structural data for system ts81.

The above result is not sufficient to discard the action of complex **8** as a catalyst, because it can still be envisaged that the peroxo ligand serves as the depository of a proton for the activation of another molecule of H_2O_2 (or TBHP) in the same way as shown above for the oxo ligand in **1**, as in the pathway suggested by Thiel (Scheme 3).[30-32] The corresponding energy pathway has also been calculated and is reported in Figure 5, while the relevant optimized geometries are shown in Figure 6. A quick comparison of Figure 5 and Figure 1 shows that the Thiel mechanism (involving compound **8** as the active catalyst) is much less favorable than the mechanism involving compound **1**. Both the H_2O_2 activation and oxygen transfer steps have much greater activation barriers (**ts910** and **ts1112**) than the corresponding steps for complex **1** (**ts23** and **ts45**). The high energy of **ts910** is somewhat unexpected, since the system is geometrically quite similar to **ts23** (*cf.* Figure 2 and Figure 6. The much higher barrier for **ts1112** relative to that of **ts45** may be attributed at least in part to steric compression, as revealed by a greater slip of the Cp* ring in the former transition state. Another important factor may be that the Mo center in the peroxide system is electron richer than in the oxido system (O_2^{2-} is a better electron donor than O^{2-}), raising the energy of the O-O σ* orbital and thus rendering less electrophilic the oxygen atom susceptible to attack by the olefin substrate.

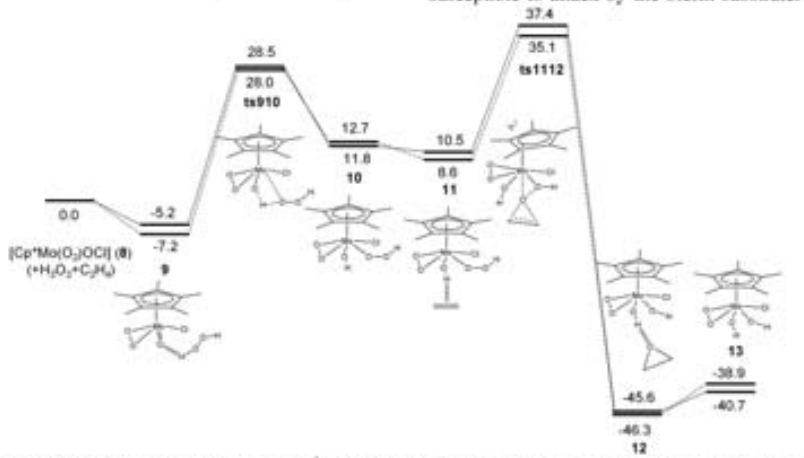

Figure 5: Energy profiles (in kcal mol^{-1}) for the H_2O_2 activation by $[Cp^*Mo(O_2)Cl]$ in the gas phase (dashed lines) and in $CHCl_3$ solution (plain lines). The reference energy corresponds to the separate reagents ($[Cp^*Mo(O_2)OCl] + H_2O_2 + C_2H_4$).

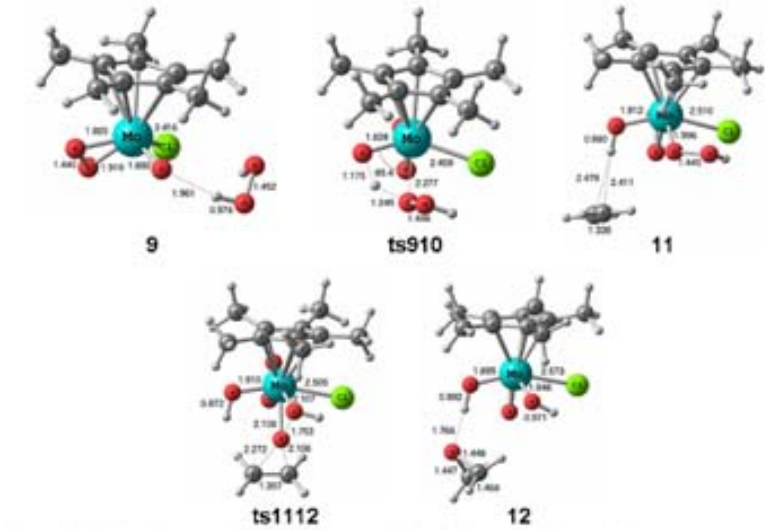

Figure 6: Optimized geometries and main structural data for the systems shown in Figure 5.

Indeed, the molecular orbitals with highest σ* O-O contribution are located at 0.005310, 0.045930 and 0.054900 hartrees for system **10** (Figure 5), *i.e.* much higher than for system **3** (Figure 1). The Mo Mulliken charges are also showing a reduced electrophilicity of **10** relative to **3** (-0.486 and -0.425, respectively).

The above results also give a hint as to why complexes of type Cp^*MoO_2X (Cp^* = substituted cyclopentadienyl ring; X = Cl, alkyl, etc.), as well as isoelectronic $MoO_2X_2L_2$ analogues, are efficient for the epoxidation reaction when using TBHP as the oxidant and much less so when using H_2O_2. The H_2O_2 activation by these systems would give a $Cp^*MoO(OH)(OOH)X$ intermediate such as **3**, which may eliminate water and afford electron-richer peroxido complexes $Cp^*Mo(O_2)(O)X$ such as **8**, the latter being less active catalysts according to the above calculations. This water elimination process has not been investigated computationally for the chloride system, but has been considered for the related cationic system that is discussed in the next section.

(c) Study of the $[Cp^*MoO_2]^+$ system

This investigation was prompted by our knowledge of the speciation of compound $[Cp^*_2Mo_2O_5]$ in an aqueous medium[42, 43] and by our recent finding that the compound catalyzes cyclooctene epoxidation by TBHP (but not H_2O_2) in the presence of water.[39] $[Cp^*_2Mo_2O_5]$ maintains a dinuclear structure in organic solvents, including polar ones such as MeCN and MeOH, but behaves as a weak electrolyte in water producing $[Cp^*MoO_2(H_2O)]^+$ and $[Cp^*MoO_3]^-$. In addition, water dissociation from $[Cp^*MoO_2(H_2O)]^+$ was found to be rapid and reversible.[43] The electron richness of the anionic complex is likely to preclude H_2O_2 (or TBHP) activation and olefin epoxidation catalysis, but the cationic complex, which is isoelectronic with compound **1**, could lead to epoxidation catalysis. Therefore, we have repeated the study described above using this cationic system as a catalyst. In addition to studying the isolated molecules in the gas phase, the calculations were also carried out with the conductor-like polarizable continuum model (CPCM) to simulate the effect of the water solvent (ε = 78.39 at 25°C).[58]

Taking complex $[Cp^*MoO_2(H_2O)]^+$ (**14**) as the starting point, the energy profile in the gas phase (plain line) and water (dashed line) is reported in Figure 7. The dissociation of water from $[Cp^*MoO_2(H_2O)]^+$ to yield the

coordinatively unsaturated $[Cp^*MoO_2]^+$ species has already been reported in our previous study[43] and is shown again here for the purpose of comparison. It requires 39.7 kcal mol^{-1} in the gas phase and only 10.1 kcal mol^{-1} in water.[43] The inclusion of the water solvent effect is remarkable in the absolute energy values and is due to the much greater stabilization of the unsaturated cationic species than its water adduct in a strongly polar medium. There is, therefore, a great difference between this cationic complex in water and the isoelectronic $[Cp^*MoO_2Cl]$ complex in $CHCl_3$: Cl^- dissociation from $[Cp^*MoO_2Cl]$ is very energy demanding (61.1 kcal/mol) in a non-polar solvent such as $CHCl_3$. This dissociation leaves the coordination position in $[Cp^*MoO_2]^+$ available for H_2O_2 binding and activation.

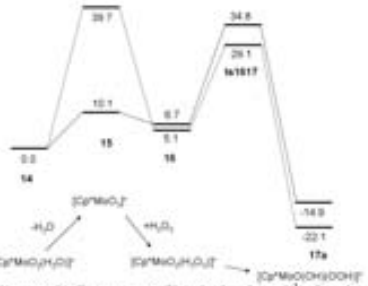

Figure 7: Energy profile (in kcal mol^{-1}) for the activation of H_2O_2 by $[Cp^*MoO_2(H_2O)]^+$ (**14**) in the gas phase (dashed lines) and in water solution (plain lines).

Coordination of H_2O_2 to this unsaturated species shows the same dramatic solvent effect, leading to a substitution product that is only slightly destabilized relative to the aqua complex both in the gas phase and in solution. The isomeric $[Cp^*MoO(OH)(OOH)]^+$ species (**17a**) is even lower in energy, being located at -21.6 kcal/mol from the $[Cp^*MoO_2(H_2O_2)]^+$ in water solution. The optimized geometries are shown in Figure 8. The Mo-O_β distance of 2.391 Å and the Mo-O_α-O_β angle of 89.2° suggest a significant interaction between Mo and O_β, similar and even to and even stronger that that experienced by complex **3**.

The intramolecular proton transfer leading from **16** to **17a** requires a rather high activation, 28.1 kcal mol^{-1} in water solution. In this activation, one proton of the H_2O_2 molecule migrates to one oxo ligand, whereas the O-O-H moiety becomes covalently bonded to the Mo atom. The migrating proton is located approximately midway between the two oxygen atoms in the transition state **ts1617** (also shown in Figure 8). Note that this transition state is related to that obtained for the H_2O_2 activation by **1**, **ts23** (Figure 2). However, the Mo-H_2O_2 bond is already fully formed in the precursor to **ts1617**, whereas it is in the process of being established in **ts23**. The O-Mo-O angle involving the donating and accepting O atoms in **ts1617** has quite significantly narrowed relative to **16**. This is most probably the main reason for such a high activation barrier, by analogy with the recently calculated and closely related intramolecular proton transfer process leading from $[Cp^*MoO(OH)_2]^+$ to $[Cp^*MoO_2(H_2O)]^+$.[43] Following the same strategy of this previous study, we considered the explicit inclusion of additional water molecules in the calculations, since these may act as proton relay and allow lower energy pathways because of reduced molecular distortions.[43, 59-62]

Figure 8: Optimized geometries and main structural data for the systems in Figure 7.

Indeed, we find that one water molecule suffices to dramatically decrease

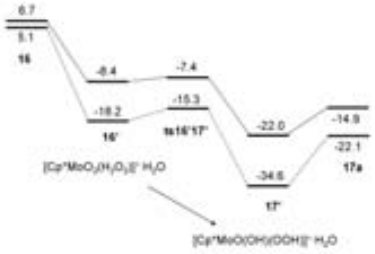

Figure 9: Energy profile (in kcal mol^{-1}) for the activation of H_2O_2 by $[Cp^*MoO_2(H_2O)]^+$ in the presence of an additional H_2O molecule in the gas phase (dashed lines) and in water solution (plain lines).

the barrier to only 1.0 kcal/mol in solution (**ts16'17'**), see Figure 9. Entropic effects would probably increase this barrier. In any case, due to the large difference between the assisted and non-assisted processes, the water-assisted pathway should be the preferred one. The additional water lowers the energy of both starting (**16** to **16'**) and final (**17a** to **17'**) systems through the establishment of a hydrogen bond. Thermodynamically, the process is exothermic by 13.6 kcal mol^{-1} in water solution. The related optimized geometries are shown in Figure 10. The geometry of the related transition state **ts16'17'** is relaxed, the O-Mo-OOH angle being 94.8°. An analysis of the various O-H distances shows that the donating O-H bond has already largely broken, whereas the incipient O-H bond has not yet formed to a great extent. Therefore, the transition state may be more correctly described as having a $[Cp^*MoO_2(OOH)]\cdot(H_3O^+)$ character. To conclude this part, the calculations suggest that the H_2O_2 activation process is very facile. The slowest step is the H_2O dissociation from **14**, which requires only 10.1 kcal mol^{-1} in solution, considering a dissociative mechanism. For the oxidation system where the oxidant is TBHP, a similar energetic pathway is expected, since the *t*Bu group plays the role of a spectator group, located on the β-O atom, far away from the metal center.

We now turn to the oxygen transfer step from the activated oxidant to the olefin. Starting from **17a**, we were able to locate two pathways with practically equivalent activation barriers, where the transferred oxygen atom is the β-O atom in one case (transition state **ts1819**) and the α-O atom in the other case (transition state **ts2122**). The energy profiles of these two pathways are comparatively shown in Figure 11. The first pathway starts with an H bonding interaction between the ethylene π electron density and the hydroperoxido proton, leading to the **18** structure accompanied by a significant stabilization. Concerning the second pathway, first an endoergic (8.7 kcal mol^{-1} in the gas phase, 7.2 kcal mol^{-1} in solution) reorientation of the O-O-H group from a perpendicular to a parallel arrangement (**17b**) takes place, followed by the formation of a stabilizing hydrogen-bond between the ethylene and the O-H group.

The optimized geometries of the two transition states for the oxygen transfer processes are presented in Figure 12. The transition state **ts1819** features a 1,2-shift of the hydroperoxido proton from the β-O atom to the α-O atom, while the former establishes the covalent interaction with the olefin carbon atoms. Like for the case of compound **1** (Figure 1), olefin attack is exogenous and occurs without formation of

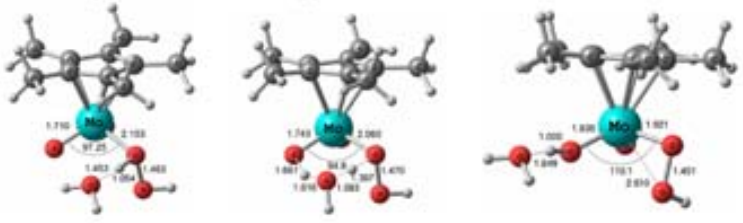

16' ts16'17' 17'

Figure 10: Optimized geometries and main structural data for the systems of Figure 9.

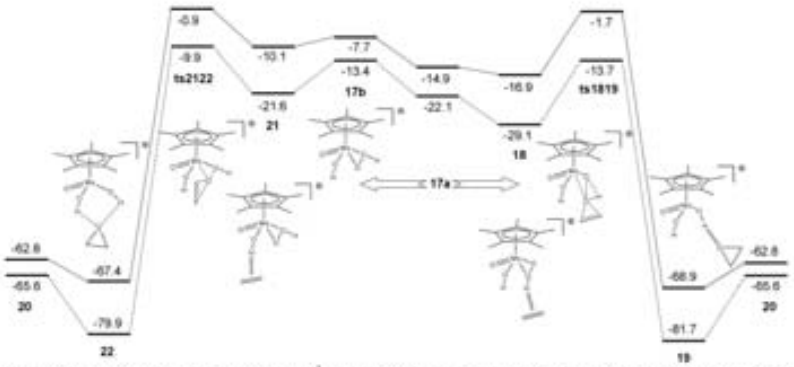

Figure 11: Energy profiles (in kcal mol^{-1}) for the oxygen atom transfer from **17a** to ethylene in the gas phase (dashed lines) and in water solution (plain lines).

metal-carbon bonds. At this stage, the Cp* ring has severely slipped to adopt an essentially η^3-coordination mode. The **ts2122** structure, on the other hand, features an olefin exogenous electrophilic attack at the α-O atom, again without formation of metal-carbon bonds, while the Mo center strengthens its interaction with the β-O atom. The transition state **ts2122** is closely related to that of the oxygen atom transfer starting from the neutral system **1** in Figure 1 (**ts45**). The barrier height (14.0 kcal mol^{-1} in water respects to **17a**) is also close to the barrier leading to **ts45** (12.7 kcal mol^{-1} in $CHCl_3$). The two pathways in Figure 11 lead to the same products, $[Cp^*Mo(O)(OH)_2]^+$ (**20**) and ethylene oxide, with only slightly different features: **ts1819** leads to a H-bonded intermediate **19** where the epoxide binds one OH ligand, whereas **ts2122** leads to a configuration **22** where both OH ligands act as (weaker) proton donors in H bonding. These products are slightly stabilized relative to the separate species, as shown in Figure 11. The regeneration of the starting complex **14** by intramolecular proton transfer, assisted by additional water molecules, occurs by a low-energy pathway, as shown in our previous study.[43] Clearly, both pathways are energetically viable, having relatively low activation barriers of 15.2 (for **ts1819** from **18**) and 14.0 (for **ts2122** from **17a**) kcal mol^{-1} in solution. It should be remarked, however, that only one of these two pathways, namely that going through transition state **ts2122**, can be adapted to the oxidation with TBHP, whereas the pathway involving the 1,2 proton shift in transition state **ts1819** will certainly become much more difficult when the proton is replaced by a *t*Bu group.

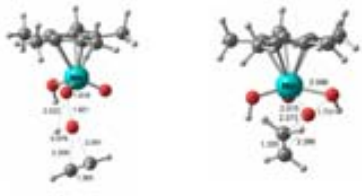

ts1819 **ts2122**

Figure 12: Optimized geometries and main structural data for the transition states **ts1819** and **ts2122**.

We now wish to analyze the possible formation of other isomers of **17a** and **17b** that may be conceived by transfer of the second H_2O_2 proton to either the oxido ligand, generating the dihydroxido peroxido species $[Cp^*Mo(O_2)(OH)_2]^+$ (**23**) or to the hydroxido ligand, yielding the oxido peroxido aqua species $[Cp^*MoO(O_2)(H_2O)]^+$ (**24**). The reasons for exploring this possibility is that an isomerization leading to peroxo complexes may explain the lack of catalytic activity of this system when H_2O_2 is used as oxidant,[39] since TBHP cannot as easily isomerize by transfer of a *t*Bu group. As argued above, the results that will be presented for the cationic system can probably be at least in part extrapolated to

the neutral chloride system examined in the previous sections.

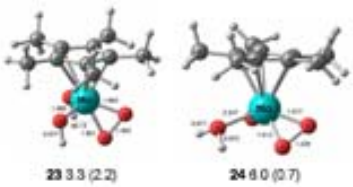

23 3.3 (2.2) **24** 6.0 (0.7)

Figure 13: Optimized geometries and main structural data for complexes **23** and **24**. Gas phase energies (and solution energies in parentheses) are given in kcal mol^{-1} relative to those of isomer **17a**.

Both isomers have been optimized, yielding the geometries and relative energies shown in Figure 13. These two structures are close in energy but slightly less stable than complex **17a** in the gas phase and in solution. In an aqueous medium, a proton may probably be transferred from one oxygen to another through low-energy pathways involving a proton relay mechanism as shown above and in our previous study.[43] It is important to analyze the relative energy of these species in great detail. This is because these systems are closely related, by replacement of an oxido ligand with a peroxido ligand, to the previously studied[43] $[Cp^*MoO(OH)_2]^+$ (**20**) and $[CpMoO_2(H_2O)]^+$ (**14**) isomers. In that case, we know from the experiment that the aqua isomer **14** is more stable than the dihydroxido isomer **20**, since the latter transforms into the former quantitatively. The free energy difference between the two isomers, determined through an indirect kinetics approach, is 6.5 kcal mol^{-1}. Yet, the calculations predicted isomer **20** to be more stable by 10.6 kcal mol^{-1} in the gas phase and by 7.2 kcal mol^{-1} in water solution (CPCM approximation). However, the successive explicit inclusion of additional water molecules in the calculations modified the relative stability toward the correct answer (with only one water molecule, **20** is still more stable than **14**, but only by 4.0 kcal mol^{-1}; with two water molecules, **20** is *less* stable than **14** by 0.4 kcal mol^{-1}). The reason of this trend is the greater acidity of the protons in the aqua ligand of **14**, relative to those of the hydrixido ligands of **20**, thus the resulting H-bonding interaction established with additional water molecules stabilizes **14** relative to **20**. For this reason, we have also carried out calculations on the three isomers after explicitly introducing additional water molecules in the geometry optimizations.

Five different local minima have been optimized with three additional water molecules, as shown in Figure 14. As previously observed for the related **14** and **20** systems,[43] the addition of so many water molecules results in a tendency to deprotonate of the system, thus all optimized minima except **17a(H$_2$O)$_3$-1** can be formally described as ionic species containing the $(H_7O_3)^+$ cation according to a close analysis of the O-H distances. Note that, for all five optimized minima, the strongest H-bonding interaction, either as proton acceptor for the $(H_2O)_3$ cluster in **17a(H$_2$O)$_3$-1** or as a proton donor for the $(H_7O_3)^+$ cluster in all other systems, involves the central oxygen atom (water molecule or H_3O^+ ion, respectively). In **17a(H$_2$O)$_3$-1**, the only H-bonding interaction involves the Mo-OOH ligand as a proton donor. Among the ionized species, the $(H_7O_3)^+$ ion in **17a(H$_2$O)$_3$-2** interacts as a proton donor with one of the oxido ligands of the $[Cp^*MoO_2(OOH)]^-$ anion, assisted by a second weaker interaction between a water molecule and the second oxido ligand, whereas the Mo-OOH proton is not involved. These two structures can be related to **17a**, the second one involving deprotonation of the more acidic Mo-OH ligand, and have a higher relative energy. All other structures feature the $(H_7O_3)^+$ ion acting as a double proton donor to a $[Cp^*MoO(O_2)(OH)]^-$ anion. For **23(H$_2$O)$_3$**, the central H_3O^+ moiety interacts with an oxido ligand, therefore the structure may related to a deprotonated **23**, whereas for **24(H$_2$O)$_3$-1** and **24(H$_2$O)$_3$-2**, the central H_3O^+ moiety interacts with a hydroxide ligand, identifying these systems as deprotonated **24**. Secondary H-bonding interactions are also established by a lateral H_2O molecule of the $(H_7O_3)^+$ cluster, with the peroxido ligand in **23(H$_2$O)$_3$** and in **24(H$_2$O)$_3$-1** and with the oxido ligand in **24(H$_2$O)$_3$-2**. The relative energies of these three species are rather comparable, both in the gas phase and in water.

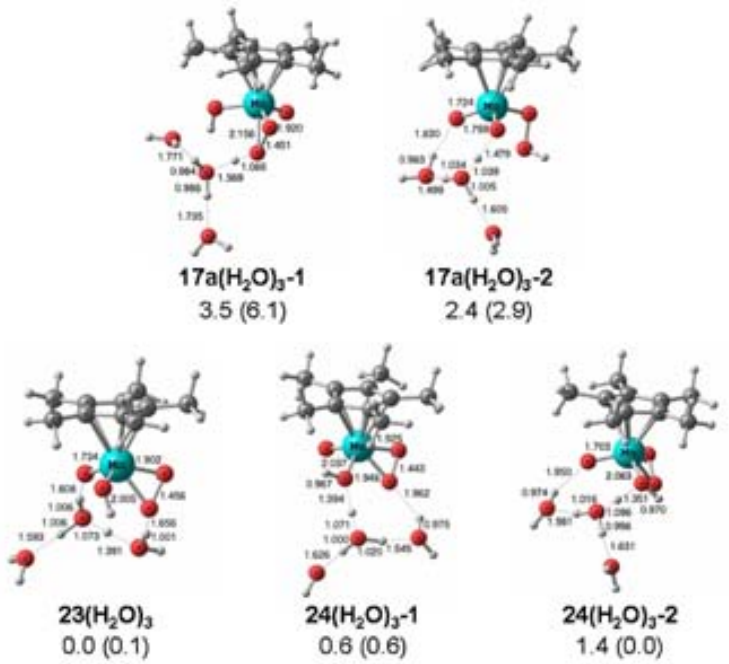

Figure 14: Optimized geometries and main structural data for complexes **17a**$(H_2O)_3$, **23**$(H_2O)_3$ and **24**$(H_2O)_3$. Gas phase energies (and solution energies in parentheses) are given in kcal mol^{-1} relative to those of isomer **23**$(H_2O)_3$.

The trend of relative stabilization by the addition of the water molecules is as expected (**24** > **23** > **17a**), following the order of relative proton acidity (Mo-OH_2 > Mo-OH > Mo-O-OH). These stabilizing effects are less pronounced relative to what was previously observed by addition of water to **14** and **20**.[43] However, compounds **23** and **24** have become more stable than their isomer **17a**, showing that the molecule would prefer to rearrange to yield a deprotonated peroxido ligand in a water-rich environment. According to the arguments presented in a previous section, the deprotonated peroxido ligand is characterized by reduced electrophilicity and greater barriers for oxygen transfer to the olefin substrate. Thus, the lower catalytic activity observed for many systems when using H_2O_2 instead of TBHP, especially in an aqueous environment, can be well rationalized by invoking the generation of more stable and less active peroxido systems.

In order to verify the above statement, we have determined the activation barrier for the oxygen atom transfer to ethylene starting from isomers **23** and **24**. The calculated reaction pathways are rather simple, involving a one-step oxygen atom transfer and resulting in the formation of $[Cp^*MoO_2(OH)_2]^+$ (**20**) or $[Cp^*MoO_2(H_2O)]^+$ (**14**) and ethylene oxide, through transition states **ts2320** and **ts2414**, respectively. The transition state geometries are shown in Figure 15. The energy of **ts2414** is 19.1 kcal mol^{-1} in solution (19.5 kcal mol^{-1} in the gas phase) relative to **24** and C_2H_4 (*cf.* 12.2 kcal mol^{-1} in the gas phase and 14 kcal mol^{-1} in solution for **ts2122** relative to **17a** and C_2H_4) with an energy barrier height of 30.5 and 23.8 kcal/mol in the gas phase and solution respectively respects to the reactant adduct.

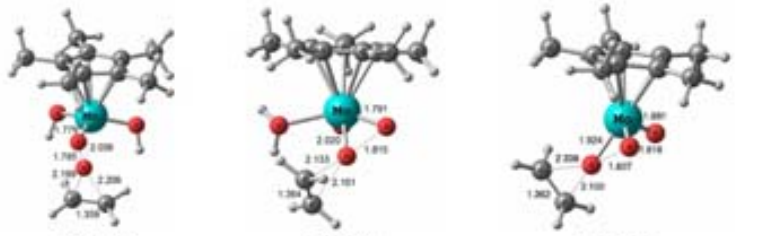

Figure 15: Optimized geometries and main structural data for the transition states of the oxygen atom transfer from $[Cp^*Mo(O_2)(OH)_2]^+$ (**ts2320**), $[Cp^*MoO(O_2)(H_2O)]^+$ (**ts2414**), and $[Cp^*MoO(O_2)]^+$ (**ts2515**).

Thus, this pathway is not competitive with those originating from intermediate **17a** (Figure 11). Transition state **ts2320**, on the other hand, is unexpectedly located at only 10.7 kcal mol^{-1} relative to **17a** and C_2H_4 in the gas phase (12.3 in solution). This is a similar energy barrier than that obtained from the O-OH group as the oxidant group, thus this mechanism appears viable according to this computation study. Nevertheless, when using the TBHP as oxidant, the formation of the less active peroxo complexes (except for the **ts2320** case) is avoided, leading to an overall higher activity.

We have also explored the energetics of water dissociation from species **24**, to yield an unsaturated $[Cp^*MoO(O_2)]^+$ system (**25**), by analogy to the established equilibrium between $[Cp^*MoO_2(H_2O)]^+$ (**14**) and $[Cp^*MoO_2]^+$ (**15**). The H_2O dissociation energy is 33.0 kcal mol^{-1} in the gas phase and 24.4 kcal mol^{-1} in water. The effect of the CPCM for the stabilization of **25** is unexpectedly lower than for the stabilization of **15**, relative to their respective water adducts. Finally, the activation energy for the oxygen atom transfer process from water-free **25** to ethylene (**ts2515**, also shown in Figure 15) was calculated as 20.5 kcal mol^{-1} relative to the separate reactants in water, confirming the expected (*vide supra*) lower activity of the peroxido function. It is possible to envisage that species **25** binds and activates a second H_2O_2 molecule, much the same way as was explored for the peroxido compound **8** in Figure 5, therefore leading to a catalytic cycle operating through the hydroperoxido mechanism. However, the same electronic effect shown to be important for **8** relative to **1** (better donation from O_2^{2-} relative to O^{2-}) is also expected for **25** relative to **15**, raising once again the activation barriers. For this reason, we did not further explore this pathway.

Conclusions

The present study has unveiled a low-energy pathway for olefin epoxidation catalyzed by cyclopentadienyl Mo^{VI} systems. The initial H_2O_2 activation follows the same general path described in other recent computational studies,[33, 40] with protonation of an oxido ligand and generation for a hydroxide hydroperoxido intermediate, but unlike the previous study the latter is found to adopt an asymmetric η^2 coordination mode, with a weak interaction between the β-O atom and the metal center. This interaction is critical for the activation of the α-O atom toward an exogenous nucleophilic attack by the olefin substrate, leading to significantly lower activation barriers for the oxygen atom transfer to the olefin relative to the previous study. This mechanism closely corresponds to what has been proposed by Thiel *et al.*, except that an oxido ligand is the depository of the oxidant proton rather than a peroxido ligand. The study also provides a rationale for the lower activity of peroxido derivatives relative to the oxido analogues, and for the lower activity of H_2O_2 relative to THBP. The former oxidant may undergo isomerization of the reactive hydroperoxido intermediate through proton transfer, leading to less reactive peroxido derivatives. Therefore, the

design of an efficient catalytic system for olefin epoxidation by H_2O_2 should only provide a basic site for transfer of one of the two H_2O_2 protons.

Acknowledgements
We gratefully acknowledge the European Commission for funding this work through the AQUACHEM Research Training Network (Contract n° MRTN-CT-2003-503864). Financial support from the Spanish MEC (Projects CTQ2005-09000-C02-01 and Consolider Ingenio 2010 CSD2007-00006 and FPU fellowship to A.C.-V.), Generalitat de Catalunya (2005/SGR/00896 and LEA project) and CNRS (LEA project) is gratefully acknowledged.

Supporting Information Available
Complete ref 44, absolute energies and Cartesian coordinates of all optimized structures. This material is available free of charge via the Internet at http://pubs.acs.org.

References

1 Schwesinger, J. W.; Bauer, T., In *Stereoselective synthesis*, Helmchen, G.; Hoffmann, R. W.; Mulzer, J.; Schaumann, E., Eds., Houbel Weil Thieme: New York, 1995.
2 Lane, B.; Burgess, K., *Chem. Rev.* **2003,** 103, 2457-2473.
3 Kühn, F. E.; Santos, A. M.; Herrmann, W. A., *J. Chem. Soc., Dalton Trans.* **2005**, 2483-2491.
4 Freund, C.; Abrantes, M.; Kühn, F. E., *J. Organomet. Chem.* **2006,** 691, 3718-3729.
5 Kühn, F. E.; Santos, A. M.; Abrantes, M., *Chem. Rev.* **2006,** 106, 2455-2475.
6 Freund, C.; Herrmann, W.; Kühn, F. E., *Topics Organomet. Chem.* **2007,** 22, 39-77.
7 Dickman, M. H.; Pope, M. T., *Chem. Rev.* **1994,** 94, 569-584.
8 Mizuno, N.; Yamaguchi, K.; Kamata, K., *Coord. Chem. Rev.* **2005,** 249, 1944-1956.
9 Nardello, V.; Aubry, J.-M.; De Vos, D. E.; Neumann, R.; Adam, W.; Zhang, R.; Ten Elshof, J. E.; Witte, P. T.; Alsters, P. L., *J. Mol. Catal. A* **2006,** 251, 185-193.
10 Bregeault, J.-M.; Vennat, M.; Salles, L.; Piquemal, J.-Y.; Mahha, Y.; Briot, E.; Bakala, P. C.; Atlamsani, A.; Thouvenot, R., *J. Mol. Catal. A* **2006,** 250, 177-189.
11 Katsuki, T., *Coord. Chem. Rev.* **1995,** 140, 189-214.
12 Dalton, C. T.; Ryan, K. M.; Wall, V. M.; Bousquet, C.; Gilheany, D. G., *Topics Cat.* **1998,** 5, 75-91.
13 Mcgarrigle, E. M.; Gilheany, D. G., *Chem. Rev.* **2005,** 105, 1563-1602.
14 Rose, E.; Andrioletti, B.; Zrig, S.; Quelquejeu-Etheve, M., *Chem. Soc. Rev.* **2005,** 34, 573-583.
15 Sheldon, R. A.; Kochi, J., *Metal-catalyzed organic reactions*. ed.; Academic Press: New York, 1981.
16 Faller, J. W.; Ma, Y., *J. Organometal. Chem.* **1989,** 368, 45-56.
17 Wilkinson, G.; Gillard, R. D.; Mccleverty, J. A. (eds.); *Comprehensive Coordination Chemistry*; Pergamon Press: Oxford, 1988.
18 Mimoun, H.; Seree De Roch, I.; Sajus, L., *Tetrahedron* **1970,** 26, 37-50.
19 Sharpless, K. B.; Townsend, J. M.; Williams, D. R., *J. Am. Chem. Soc.* **1972,** 94, 295-6.
20 Di Valentin, C.; Gisdakis, P.; Yudanov, I. V.; Rösch, N., *J. Org. Chem.* **2000,** 65, 2996-3004.
21 Yudanov, I. V.; Di Valentin, C.; Gisdakis, P.; Rösch, N., *J. Mol. Catal. A* **2000,** 158, 189-197.
22 Deubel, D. V.; Sundermeyer, J.; Frenking, G., *J. Am. Chem. Soc.* **2000,** 122, 10101-10108.
23 Deubel, D. V.; Sundermeyer, J.; Frenking, G., *Inorg. Chem.* **2000,** 39, 2314-2320.
24 Deubel, D. V., *J. Phys. Chem. A* **2001,** 105, 4765-4772.
25 Deubel, D. V.; Sundermeyer, J.; Frenking, G., *Eur. J. Inorg. Chem.* **2001**, 1819-1827.
26 Deubel, D. V.; Frenking, G.; Gisdakis, P.; Herrmann, W. A.; Rösch, N.; Sundermeyer, J., *Acc. Chem. Res.* **2004,** 37, 645-652.
27 Gisdakis, P.; Yudanov, I. V.; Rösch, N., *Inorg. Chem.* **2001,** 40, 3755-3765.
28 Bühl, M.; Schurhammer, R.; Imhof, P., *J. Am. Chem. Soc.* **2004,** 126, 3310-3320.
29 Salles, L.; Piquemal, J. Y.; Thouvenot, R.; Minot, C.; Bregeault, J. M., *J. Mol. Catal. A* **1997,** 117, 375-387.

[30] Thiel, W. R.; Priermeier, T., *Angew. Chem., Int. Ed. Engl.* **1995,** 34, 1737-1738.

[31] Thiel, W. R., *J. Mol. Catal. A* **1997,** 117, 449-454.

[32] Thiel, W. R.; Eppinger, J., *Chem. Eur. J.* **1997,** 3, 696-705.

[33] Kühn, F. E.; Groarke, M.; Bencze, E.; Herdtweck, E.; Prazeres, A.; Santos, A. M.; Calhorda, M. J.; Romão, C. C.; Gonçalves, I. S.; Lopes, A. D.; Pillinger, M., *Chem. Eur. J.* **2002,** 8, 2370-2383.

[34] Trost, M. B.; Bergman, R. G., *Organometallics* **1991,** 10, 1172-1178.

[35] Chakraborty, D.; Bhattacharjee, M.; Krätzner, R.; Siefken, R.; Roesky, H. W.; Usón, I.; Schmidt, H.-G., *Organometallics* **1999,** 18, 106-108.

[36] Abrantes, M.; Santos, A.; Mink, J.; Kühn, F.; Romão, C., *Organometallics* **2003,** 22, 2112-2118.

[37] Zhao, J.; Santos, A. M.; Herdtweck, E.; Kühn, F. E., *J. Mol. Catal. A* **2004,** 222, 265-271.

[38] Zhao, J.; Herdtweck, E.; Kühn, F. E., *J. Organomet. Chem.* **2006,** 691, 2199-2206.

[39] Martins, A. M.; Romão, C. C.; Abrantes, M.; Azevedo, M. C.; Cui, J.; Dias, A. R.; Duarte, M. T.; Lemos, M. A.; Lourenço, T.; Poli, R., *Organometallics* **2005,** 24, 2582-2589.

[40] Veiros, L. F.; Prazeres, A.; Costa, P. J.; Romão, C. C.; Kühn, F. E.; Calhorda, M. J., *J. Chem. Soc., Dalton Trans.* **2006**, 1383-1389.

[41] Poli, R., *Chem. Eur. J.* **2004,** 10, 332-341.

[42] Collange, E.; Garcia, J.; Poli, R., *New J. Chem.* **2002,** 26, 1249-1256.

[43] Jee, J.-E.; Comas-Vives, A.; Dinoi, C.; Ujaque, G.; Van Eldik, R.; Lledós, A.; Poli, R., *Inorg. Chem* **2007,** 46, 4103-4113.

[44] Frisch, M. J., *et al.*, *Gaussian 03, Revision D.01*, ed.; Gaussian, Inc.: Wallingford CT, 2004.

[45] Becke, A. D., *J. Chem. Phys.* **1993,** 98, 5648-5652.

[46] Lee, C. T.; Yang, W. T.; Parr, R. G., *Phys. Rev. B* **1988,** 37, 785-789.

[47] Stephens, P.; Devlin, F.; Chabalowski, C.; Frisch, M., *J. Phys. Chem.* **1994,** 98, 11623-11627.

[48] Hay, P. J.; Wadt, W. R., *J. Chem. Phys.* **1985,** 82, 270-283.

[49] Ehlers, A. W.; Boehme, M.; Dapprich, S.; Gobbi, A.; Hoellwarth, A.; Jonas, V.; Koehler, K. F.; Stegmann, R.; Veldkamp, A.; Frenking, G., *Chem. Phys. Lett.* **1993,** 208, 111-114.

[50] Fukui, K., *Acc. Chem. Res.* **1981,** 14, 363-8.

[51] Gonzalez, C.; Schlegel, H. B., *J. Chem. Phys.* **1989,** 90, 2154-61.

[52] Gonzalez, C.; Schlegel, H. B., *J. Phys. Chem.* **1990,** 94, 5523-5527.

[53] Barone, V.; Cossi, M., *J. Phys. Chem. A* **1998,** 102, 1995-2001.

[54] Cossi, M.; Rega, N.; Scalmani, G.; Barone, V., *J. Comput. Chem.* **2003,** 24, 669-681.

[55] Nakagawa, Y.; Mizuno, N., *Inorg. Chem.* **2007,** 46, 1727-1736.

[56] Valente, A. A.; Moreira, J.; Lopes, A. D.; Pillinger, M.; Nunes, C. D.; Romao, C. C.; Kühn, F. E.; Goncalves, I. S., *New J. Chem.* **2004,** 28, 308-313.

[57] Collman, J. P.; Zeng, L.; Wang, H. J. H.; Lei, A.; Brauman, J. I., *Eur. J. Org. Chem.* **2006**, 2707-2714.

[58] Weast, R. C., *CRC Handbook of Chemistry and Physics*. 57th ed.; CRC Press: Cleveland, Ohio, 1976.

[59] Lledós, A.; Bertrán, J., *Tetrahedron Lett.* **1981,** 22, 775-778.

[60] Sambrano, J. R.; Andres, J.; Gracia, L.; Safont, V. S.; Beltran, A., *Chem. Phys. Lett.* **2004,** 384, 56-62.

[61] Prabhakar, R.; Blomberg, M. R. A.; Siegbahn, P. E. M., *Theoret. Chem. Acc.* **2000,** 104, 461-470.

[62] Hratchian, H. P.; Sonnenberg, J. L.; Hay, P. J.; Martin, R. L.; Bursten, B. E.; Schlegel, H. B., *J. Phys. Chem. A* **2005,** 109, 8579-8586.

Table of contents (TOC):

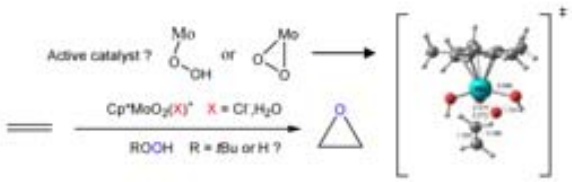

B.2 Article VIII

Modelling catalysis in water

DOI: 10.1002/anie.200((will be filled in by the editorial staff))

The Wacker Process: Inner- or Outer-Sphere Nucleophilic Addition? First Principles Molecular Dynamics Answers**

Aleix Comas-Vives, András Stirling, Agusti Lledós and Gregori Ujaque**

((Dedication----optional))

The Wacker process is paradigmatic because it has been the first organometallic catalytic oxidation industrially applied.[1,2] This process involves the oxidation of ethylene to acetaldehyde in aqueous solvent. Its catalytic cycle as currently understood is shown in Scheme 1. The mechanism has been shown to depend on the reaction conditions, in particular by the concentration of [Cl⁻] and $[CuCl_2]$.[3-5] The most controversial reaction step is the hydroxypalladation of ethene. The debate relies on the mode of the water nucleophilic attack on ethene: (a) via an inner-sphere mechanism from a coordinated water to palladium (*syn*-addition), or (b) via an outer-sphere mechanism of a water molecule from the bulk (*anti*-addition). To contrast the reactivity of the free and coordinated water toward the alkene is crucial in understanding the mechanism and may help to develop other aqueous phase processes, a key challenge in green chemistry.

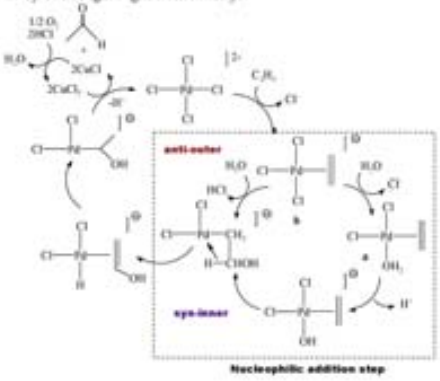

Scheme 1. Catalytic cycle of the Wacker Process

Several stereochemical studies support the outer-sphere attack,[5-8] whereas other kinetic and isotope effect studies[9,10] support the inner-sphere mechanism. Molecular orbital analysis by Eisenstein and Hoffmann showed that η^2 to η^1 ethylene slipping was the driving force toward the external nucleophilic attack.[11] Fujimoto and Yamasaki supported trans addition for hydroxide.[12] Siegbahn has also tackled the Wacker process theoretically,[13-15] by combining explicit (up to four water molecules) and implicit models, supporting the outer-sphere mechanism.[15] Very recently, Eshtiagh-Hosseini raised comparable results using a similar model,[16] although some of their conclusions have been questioned later.[17] Goddard and co-workers also studied this process,[17,18] nicely rationalizing the dependence of the addition mode on reaction conditions on the basis of theoretical calculations; an empirical correction was included in the calculations to obtain reasonable energy barriers for those steps where a proton is released to the medium (forming a hydronium species).[18]

Although a great deal of chemical and mechanistic insight have been obtained from these computational studies the inherent limitations of simplified solvent models in treating the reactive bulk medium prevent to formulate a convincing picture for the mechanisms. In particular, a proper description of the aqueous medium is crucial since solvent molecules may actively participate in the process. The straightforward simulation strategy is to explicitly include the solvent molecules into the model and follow the reactions by purely quantum chemical method. The aim of this work is to study the nucleophilic addition step by means of first principles molecular dynamics combined with metadynamics. This framework allows to properly describe the reactivity of the Wacker intermediates as well as the bulk water solvent. Both principal alternatives for the nucleophilic addition step (Scheme 1) have been evaluated: the inner- and outer-sphere mechanisms.

The intermediates, **a** and **b**, with the ethylene coordinated to the catalyst were taken as starting point for the nucleophilic addition. These complexes were placed into a cubic box of 26 water molecules. Car-Parrinello molecular dynamics coupled with metadynamics simulations[19,20] were performed to determine the reactive paths and to obtain the corresponding free energy barriers for the rate limiting step.[21]

Metadynamics employs collective variables (CVs) and efficiently explores the free energy surface defined by the selected CVs. In practice this means that we can dramatically accelerate reactive events and obtain the corresponding activation free energy barriers.[20] We have applied different CVs in several combinations to probe the possible mechanisms. For **a** the selected CVs are: coordination number (CN)[21] of the oxygen of the H_2O ligand with respect to all H-s (**CV1**), CN of the ethene carbons with respect to the oxygen of the H_2O ligand (**CV2**), CN of the Pd atom with respect to the Cl atoms (**CV3**), CN between the carbon atoms of the ethene and all oxygen atoms (**CV4**), CN of the Pd atom with respect to all oxygen atoms (**CV5**) and CN of the Pd atom with respect to the oxygen of the H_2O ligand (**CV6**). For **b**, analogous CVs to **CV3**,

[+] Aleix Comas-Vives, Gregori Ujaque, Agusti Lledós
Unitat de Química Física, Departament de Química,
Edifici Cn, Universitat Autònoma
08193 Bellaterra, Catalonia, Spain
Fax: +34 93-581.29.20
E-mail: gregori@klingon.uab.es

András Stirling
Chemical Research Center of HAS
Pusztaszeri út 59-67, H-1025, Hungary.
E-mail: stirling@chemres.hu

[++] We are grateful to the Spanish MEC (Projects CTQ2008-06866-CO2-01 and Consolider Ingenio 2010 CSD2007-00006, FPU fellowship to A.C.-V.), to Generalitat de Catalunya 2005/SGR/00896) and to the Hungarian Science Foundation OTKA K 68360) . The Red Española de Supercomputación (RES-BSC) is also acknowledged.

Supporting information for this article is available on the WWW under http://www.angewandte.org or from the author.

CV4, and **CV5** were selected: **CV3'**, **CV4'** and **CV5'**. For each metadynamics simulation a set of 2 or 3 CVs has been employed. In all, 6 different combinations of CVs have been compared in order to look into the hydroxypalladation step; the resulting **S1-S6** combinations are depicted in Scheme 2. Note that in a metadynamics simulations the observable reactions are determined by the selected CV sets, thus different sets generate different sequences of reactions steps.

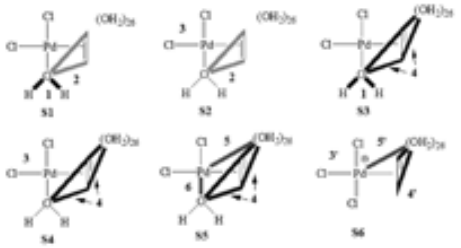

Scheme 2. Selected set of CVs for **a** (**S1** - **S5**) and **b** (**S6**) complexes.

We first summarize the results concerning the chemical activity of the Pd(II) coordination sphere in species **a**.[22] The $CT—H_2O$ exchange requires 14 kcal/mol and 35 kcal/mol activation energy for the first and the second Cl substitution, respectively. The degenerate $H_2O—H_2O$ exchange features a barrier of 25 kcal/mol. We have also found that a coordinated water molecule can easily transfer a proton to the solvent, the corresponding activation energy is 10 kcal/mol. By contrast, the protonation of the ligand H_2O should overcome a barrier of 13 kcal/mol. Taken into account the experimental value of the addition step (22.4 kcal/mol) and the accuracy of the simulations[21] we conclude that these processes can in fact alter the stoichiometry of the catalyst species before the addition reaction takes place and therefore the actual simulations should include these possibilities.

S1 and **S2** simulations were designed to study the intramolecular mechanism. In the first metadynamics simulation for the **a** species (**S1**) we have observed an inner-sphere nucleophilic addition (**CV2**) preceeded by a couple of proton exchanges with the bulk (**CV1**). The coordinated water is rapidly deprotonated forming hydroxyl ligand which then reacted with the ethylene ligand. Figure 1 shows a representative configuration of the TS region. This step yielded the *syn* addition product, with a calculated free energy barrier of 60 kcal/mol, much higher than the experimental value.

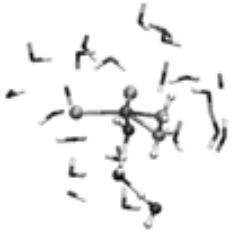

Figure 1. Snapshot of one configuration where the inner-sphere attack one ethene is occurring (S1 simulation).

The **S2** simulation includes the Cl coordination around the Pd(II) ion (**CV3**) together with **CV2** governing the inner sphere attack. The simulations revealed large Cl^- mobility and frequent dissociation from the first solvation shell preceeding the inner-sphere attack. The activation barrier for this latter process was found to be 48 kcal/mol. This barrier is too high in comparison with the experimental free energy barrier for the Wacker process (22.4 kcal/mol). Due to this high barrier, formation of triply hydrated, doubly charged Pd(II) species could occur before the intramolecular addition. This species however rapidly took up a Cl^- anion and released a proton to the solvent. Such a charge separation featuring 35 kcal/mol barrier is highly unfavourable and indicates that this sequence is very unlikely. Clearly, both **S1** and **S2** suggest that the inner-sphere mechanism is not compatible with the exprimental activation energy.

In the following four simulations we probed the outer-sphere (intermolecular) mechanism. The **S3** simulation includes **CV1** and **CV4** steering the proton-exchange of the water ligand and the nucleophilic attack on the ethylene ligand, respectively. The difference between **S1** and **S3** is that *all* H_2O molecules can attack the ethylene ligand. The simulation shows that the first chemically relevant events are proton shuttling between the ligand H_2O and the solution, in accordance with their smaller activation barriers. The intermolecular nucleophilic attack takes place when a "neutral" water molecule is coordinated as a ligand. This step has a free energy barrier of 24 kcal·mol^{-1}, in good agreement with experiment. The C-O bond formation was accompanied by a proton transfer to a neighbour H_2O molecule. Figure 2 displays a representative snapshot of the TS of the outer-sphere attack.

The role of the chlorine ligands was also probed in the outer-sphere route. In simulation **S4** we have employed **CV3** and **CV4**. The outer-sphere attack takes place, after the partial decoordination of a chlorine ligand, having an energy barrier height of 22 kcal·mol^{-1}. One of the protons of the attacking H_2O is again spontaneously released to the medium during the addition. The barrier for the outer-sphere attack in this case is very similar to that obtained in **S3** employing different combination of CVs and agrees nicely with experiment. This indicates that the chlorine mobility does not affect the mechanism of the intermolecular attack.

In simulation **S5** we studied the combined effect of three CVs, namely **CV4**, **CV5** and **CV6**. The motivation behind this choice is to include not only the reaction coordinates responsible for the intra- and intermolecular attacks, but to also foster possible ligand exchanges on the central Pd(II) cation (**CV5** and **CV6**). During the simulation the inner-sphere attack does not occur in line with its high barrier; instead the outer sphere attack could be observed with an energy barrier of 22 kcal/mol in very good agreement with the experimental value and with the previously calculated values. This step gives rise to the *anti* addition product. The simulation yielded other reaction steps with smaller barriers: a $CT—H_2O$ exchange in the early stage of the simulation and a spontaneous proton release from the attacking H_2O molecule to the solvent during the addition reaction. The recoordination of the dissociated Cl^- ion takes place in the trans position with respect to the other chlorine ligand. In addition we also observed a H_2O exchange on the $[PdCl(H_2O)_2(C_2H_4)]^+$ intermediate.

Figure 2. Snapshot of one configuration (**S3** simulation) where the outer-sphere attack on the ethene is occurring. One proton of the attacking water is released to the medium.

From intermediate **b** the unique possible pathway for the nucleophilic attack is the outer sphere mechanism provided that no *cis* Cl^-—H_2O substitution occurs before. A simulation (**S6**) has been carried out involving chlorine coordination (**CV3**$^-$), water coordination (**CV5***) and the nucleophilic attack of a water molecule to the coordinated ethene (**CV4***). The first step observed during the metadynamics run was the substitution of the *trans* chlorine ligand by a water molecule. Subsequently we have seen the nucleophilic attack of a solvent H_2O to the coordinated ethene along with the proton transfer to the medium. Interestingly, nucleophilic attack takes place on the neutral complex. The free energy barrier calculated for the latter process is 19 kcal·mol^{-1}. This value is somewhat lower than that obtained for intermediate **a** but agrees nicely with experiment within the error margin[21] of the simulations.

All the results above clearly indicate the feasibility of the *anti* outer-sphere attack as opposed to the inner-sphere one.[22] Note that the selected CVs do not distinguish between the *syn* and *anti* attacks but only between the inner- and outer-sphere routes. Hence, the *syn* outer-sphere attack can not be discarded as feasible reaction pathway. We note however that the CVs in fact allow both the *syn* and the *anti* directions. Since only the *anti* addition have been observed in the **S3**-**S6** simulations, the *syn* attack has necessarily higher energy barrier.

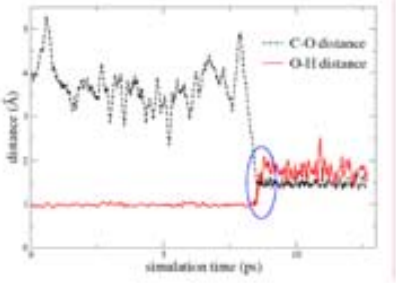

Figure 3. Evolution of the C-O bond and one of the O-H bonds of the reactant H_2O molecule in simulation **S4**. Note that the curves represent configurations taken at every metadynamics step, namely at every 13.6 fs. The blue ellipse indicates the TS region. Similar concerted behaviour has been found for all the other intermolecular mechanism.

The simulations have revealed that the solvent plays an important role in the mechanism. The intermolecular reactions always involved a proton departure from the attacking water to a nearby solvent molecule when the addition to the double bond occurred. This is illustrated in Figure 3 which displays the typical curves of the simultaneous C-O bond formation and proton transfer in simulation **S4**. This concerted behaviour highlights the importance of the second and further neighbour water molecules in the reactions, as the proton transfer is an essential part of the addition reaction and the accompanying charge separation due to the proton transfer benefits from the presence of the polar water medium[12]. This points out that the explicit inclusion of the surrounding bulk water is a key in the simulations to obtain the concerted nature of the two processes in a fairly unbiased manner.

In conclusion, with DFT based molecular dynamics simulation we have followed both the intra- and intermolecular pathways for the nucleophilic attack on the coordinated ethylene ligand. The calculations showed that the ligand sphere of Pd(II) may undergo several changes before reactions on the ethylene ligand occurs. We obtained that the outer-sphere (*anti*) nucleophilic attack is clearly preferred from kinetic point of view to the inner-sphere mechanism. The calculated free energy barrier for the process ranges between 22 and 24 kcal·mol^{-1} which is in very good agreement with the experimental value (22.4 kcalmol^{-1}).[23] The inner-sphere attack is unlikely for its much higher energy barriers. For the case of intermediate **b** $[PdCl_3(CH_2{=}CH_2)]^-$, a free energy barrier of 19 kcal·mol^{-1} has been obtained for the external addition reaction preceded by a *trans* Cl—H_2O substitution. All simulations indicate that the water nuclephilic attack is performed on the neutral complex. The present findings unequivocally support the mechanistic concepts invoking outer-sphere, *anti* addition route for the C-O bond formation. We stress however that further studies are necessary to resolve the apparent conflict between the present findings and some other experimental[3,4] and theoretical proposals.[18] In our opinion the present methodology offers a very efficient framework for such studies and will help in broadening our understanding of this and other aqueous phase catalytic reactions.

Experimental Section

We performed Car-Parrinello molecular dynamics coupled with metadynamics, using the DFT scheme. The HCTH/120 density functional and pseudopotentials with a plane basis set expanded up to 70 Ry were employed. In order to describe solvation, **a** and **b** intermediates were placed with 26 water molecules in simulation cells of 9.86x9.86x9.86 Å. The temperature employed in all simulations was 300 K. The substitution of hydrogen by deuterium allowed us to use a time step of 7 a. u. and 1000 a. u. for the fictitious electronic mass. Further details of the simulations can be found in the Supplementary Information.

Received: ((will be filled in by the editorial staff))
Published online on ((will be filled in by the editorial staff))

Keywords: Wacker Process · Hydroxypalladation · Car-Parrinello Molecular Dynamics · Metadynamics · Aqueous Media

[1] J. Smidt, W. Hafner, R. Jira, J. Sedlmeier, R. Sieber, R. Rüttinger, H. Kojer, *Angew. Chem. Int. Ed.* **1959**, *71*, 176.
[2] J. Smidt, J. Sedlmeier, W. Hafner, R. Sieber, A. Sabel, R. Jira, *Angew. Chem. Int. Ed.* **1962**, *74*, 93.
[3] a) O. Hamed, C. Thompson, P. M. Henry, *J. Org. Chem.* **1997**, *62*, 7082.; b) O. Hamed, P.M. Henry, C. Thompson, *J. Org. Chem.* **1999**, *64*, 7745.

[4] a) N. Gregor, K. Zaw, P. M. Henry, *Organomet.* **1984**, *3*, 1251. b) J. W. Francis, P. M. Henry, *Organomet.* **1992**, *11*, 2832.
[5] J. W. Francis, P. M. Henry, *J. Mol. Catal. A* **1996**, *112*, 317
[6] J. K. Stille, D. E. James, *J. Org. Chem.* **1976**, *108*, 401.
[7] J. E. Backvall, B. Akermark, S. O. Ljunggren, *J. Am. Chem. Soc.* **1979**, *101*, 2411.
[8] J. K. Stille, R. Divakaruni, *J. Org. Chem.* **1979**, *169*, 239.
[9] a) P. M. Henry, *J. Am. Chem. Soc.* **1964**, *86*, 3246.; b) D. J. Nelson, R. Li, C. Brammer, *J. Am. Chem. Soc.* **2001**, *123*, 1564.
[10] M. Kosaki, M. Isemura, Y. Kitaura, S. Shinoda, Y. Saito, *J. Mol. Catal.* **1977**, *2*, 351.
[11] O. Eisenstein, R. Hoffmann, *J. Am. Chem. Soc.* **1981**, *103*, 4308.
[12] H. Fujimoto, T. Yamasaki, *J. Am. Chem. Soc.* **1986**, *108*, 578.
[13] P. E. M. Siegbahn, *Structural Chemistry* **1995**, *6*, 271.
[14] P. E. M. Siegbahn, *J. Am. Chem. Soc.* **1995**, *117*, 5409.
[15] P. E. M. Siegbahn, *J. Phys. Chem.* **1996**, *100*, 14672.
[16] S. A. Beyramabadi, H. Eshtiagh-Hosseini, M. R. Housaindokht, A. Morsali, *Organomet.* **2008**, *27*, 72.
[17] J. A. Keith, R. J. Nielsen, , J. Oxgaard, W. A. Goddard, P.M. Henry, *Organometallics*, **2009**, *28*, 1618.
[18] a) J. A. Keith, J. Oxgaard, W. A. Goddard, *J. Am. Chem. Soc.* **2006**, *128*, 3132. b) J. A. Keith, R. J. Nielsen, J. Oxgaard, W. A. Goddard, *J. Am. Chem. Soc.* **2007**, *129*, 12342.
[19] a) A. Laio, M. Parrinello, *Proc. Nat. Acad. Sci. USA* **2002**, *99*, 12562; b) M. Iannuzzi, A. Laio, M. Parrinello, *Phys. Rev. Lett.* **2003**, *90*, 238302.
[20] Selected application of metadynamics for chemical reactions: a) M. Boero, T. Ikeda, E. Ito, K. Teralura, *J. Am. Chem. Soc.* **2006**, *128*, 16798; b) N. N. Nair, E. Schreiner, D. Marx, *J. Am. Chem. Soc.* **2006**, *130*, 14148; A. Stirling, M. Iannuzzi, M. Parrinello, F. Molnar, V. Bernhart, G. A. Luinstra, *Organometal.* **2005**, *24*, 2533; A. Rodriguez-Fortea, L. Vilà-Nadal, J. Poblet, *Inorg. Chem.* **2008**, *47*, 7745.
[21] See Supporting Information for more information about the metadynamics, the definition of CNs, the parameters used in the simulations, the free energy calculation and the time evolution of of the CVs during the simulations.
[22] With the rate law at low [CT] and [$CuCl_2$] conditions which are the experimental conditions most resembling with our simulations.

Entry for the Table of Contents (Please choose one layout)

Layout 1:

Modelling Catalysis in Water

Aleix Comas-Vives, András Stirling, Agustí Lledós, Gregori Ujaque

_____ Page – Page

The Wacker Process: Inner- or Outer-Sphere Nucleophilic Addition? First Principles Molecular Dynamics Answer

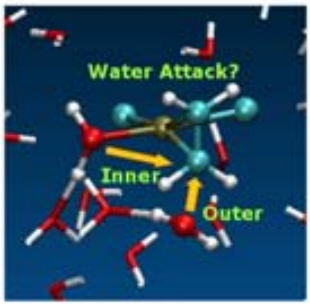

Two modes for the nucleophilic addition of water to a Pd-coordinated alkene have been proposed: *syn*-inner and *anti*-outer sphere mechanisms. Both processes have been evaluated by placing $PdCl_2(H_2O)(C_2H_2)$ complex in a box of water molecules. The calculated Gibbs energy barriers for the outer mechanism are in good agreement with experiment, whereas those for the inner mechanism are significantly higher. The nucleophilic addition has been also evaluated for the $[PdCl_3(C_2H_2)]^-$ complex with similar results.

SUPPORTING INFORMATION

The Wacker Process: Inner- or Outer-Sphere Nucleophilic Addition? First Principles Molecular Dynamics Answers

Aleix Comas-Vives,[1] András Stirling,[2,*] Agustí Lledós[1] and Gregori Ujaque[1,*]

[1]*Unitat de Química Física, Departament de Química, Edifici Cn, Universitat Autònoma de Barcelona, 08193 Bellaterra, Catalonia, Spain*

[2]*Chemical Research Center of HAS, Pusztaszeri út 59-67, H-1025, Hungary.*

Contents

1. Description of the MD methodology

All molecular dynamics calculations have been performed within the Car-Parrinello framework[1]. We have used periodic models of the solutions placed in a cubic unit cell with dimensions of 9.86 Å × 9.86 Å × 9.86 Å. The HCTH/120 exchange-correlation functional[2] has been used. Only the valence electrons have been treated explicitly and the interaction between the ionic core and valence electrons has been included via norm-conserving Troullier-Martins type pseudopotentials[3]. In particular for Pd we have generated a pseudopotential including the semicore 4s and 4p states as well and core radii of 1.31, 1.37, and 1.25 Å were used for the pseudization of the *s*, *p* and *d* channels, respectively. The pseudopotentials have been tested on small molecules and complexes against all-electron calculations. The electronic orbitals were expanded in a plane-wave basis set up to a kinetic energy cutoff of 70 Ry. The fictitious electronic mass was 1000 a.u. in the simulations and the replacement of the hydrogen atoms with deuterium allowed a time step of 0.169 fs. The simulation temperature was in all cases 300 K. The initial configurations for the simulations have been obtained from equilibration procedure: 6 water molecules have been replaced by the Pd(II) complex in

a previously equilibrated water system of 32 H_2O molecules, then it has been kept at 600 K for 1 ps and then it was carefully cooled down to 300 K. For the simulations we have used the CPMD program package[4].

2. Description of the metadynamics methodology

In metadynamics[5] we select a set of collective variables (CVs) s_α. In order to describe a chemical reaction the selected CVs must distinguish between reactants and products. In our study we have coupled the metadynamics with ab initio MD within the Car-Parrinello framework[1]. The complete system of the ionic, electronic and CV degrees of freedom is described by the following equation:

$$L = L_{CP} + \frac{1}{2}\sum_\alpha M_\alpha \dot{s}_\alpha^2 - \frac{1}{2}\sum_\alpha k_\alpha \left(s_\alpha(R) - s_\alpha\right)^2 - V(t,s)$$

L_{CP} is the Car-Parrinello Lagrangian; the first additional term represents the fictitious kinetic energy of the s_α values, where M_α is the corresponding fictitious mass parameter. The second additional term represents a restraining potential that forces the ionic degrees of freedom to follow the motion of the CVs. We have used M_α and k_α values equal to 50 amu bohr^2 and 5 au, respectively, in all the simulations. These parameters ensure the adiabatic separation of the CV movements from the fictititous electronic degrees of freedom of the CP Lagrangian and the necessary correlated motion of the CVs and the auxiliary variables. $V(t,s)$ is a history dependent potential term which enhances the sampling of the configurational space, encouraging the system to visit unexplored regionsof this space. In practice it is a sum of repulsive hill-like (Gaussian) potential terms deposited at given time intervals:

$$V(t,s) = \sum_{t_i < t} h \exp\left(-\frac{s(t) - s(t_i)}{2\left[w(t_i)\delta s\right]^2}\right)$$

Concerning the hill size, preliminary calculations were performed at larger hill heights and widths, with subsequent refinements. All the calculations have finally employed a maximum hill width (δs) of 0.05 and hill heights (h) of 0.314 kcalmol^{-1} except for the **S1** simulation where a hill height of 0.628 kcal mol^{-1} was used. The nonspherical nature of the free energy basins was taken into account by employing anisotropic scaling factors ($\mathbf{w}$) which were recalculated on the fly at given periods during the simulations as built in the metadynamics routine of the CPMD package. The hills were deposited after 80 MD time steps (13.6 fs) in all the simulations. We estimated a 2.6 kcal/mol error bar for the calculated activation free energies when using the smaller Gaussian height[6]. During the metadynamics simulations we explore the free energy surface spanned by the selected CVs. As the simulation proceeds we gradually explore this surface by reconstructing it from the deposited Gaussian hills:

$$F(s) = -\lim_{t \to \infty} V(t, s) + \text{constant}$$

For every elementary step we can therefore determine the corresponding activation free energy irrespective of the order of the reaction steps. In this study the activation free energy values are reported relative to the free energy level of the initial species.

For the nucleophilic addition steps we have checked that the predicted transition state structures indeed connect the corresponding minima in dynamical sense; we have performed commitment analysis by selecting representative configurations from the TS regions and then started unbiased MD simulations employing random atomic velocities taken from the 300K Boltzmann distribution. These simulations produced trajectories which arrived into the two free energy minima in almost equal times: this indicates that the selected CV-s indeed identified the proper TS between the the reactant and product states.

3. Description and parameters used for the selected CVs

In this work, the selected CVs have been coordination numbers (CN) [7]. We have used two types of CNs. The first type (labelled as COOR_RF) is defined as a continuous function of the distance between atoms A and i (R_{Ai}) as:

$$CN_A = \sum_{i=1}^{n_A} \frac{1-\left(\frac{R_{Ai}}{d_0}\right)^p}{1-\left(\frac{R_{Ai}}{d_0}\right)^q}$$

where A corresponds to the reference atom, i runs over n_B atoms coordinated to the reference atom, and d_0 represents a reference distance (the ideal d_0 value is close to the distance in the transition state). p and q determine the decay of the CN curve. A particular case (BNSWT) is when n_B is 1, which corresponds to the mutual coordination of A and B. The other type of CN (TOT_COOR) is a more generalized form of the coordination concept:

$$CN_{AB} = \sum_{i=1}^{N_A} \sum_{j=1}^{N_B} \frac{1-\left(\frac{R_{ij}}{d_0}\right)^p}{1-\left(\frac{R_{ij}}{d_0}\right)^q}$$

Here i and j are the atoms belonging to the two atomic groups A and B for which CN_{AB} is defined whereas R_{ij} is the interatomic distance between atoms i and j.

The specific parameters for every CV were the followings:

CV1: d_0 = 1.7 Å; p= 10; q= 60. (COOR_RF)

CV2: d_0 = 2.2 Å; p= 6; q= 16. (COOR_RF)

CV3: d_0 = 3.4 Å; p= 6; q= 16 (COOR_RF)

CV4: d_0 = 2.2 Å; p= 6; q= 16. (TOT_COOR)

CV5: d_0 = 3.1 Å; p= 25; q= 100. (COOR_RF)

CV6: d_0 = 3.6 Å; p= 8; q= 40. (BNSWT)

CV3': d_0 = 3.6 Å; p= 6; q= 22. (COOR_RF)

CV4': d_0 = 2.2 Å; p= 6; q= 16. (TOT_COOR)

CV5': d_0 = 3.1 Å; p= 25; q= 100. (COOR_RF)

4. Time evolution for every set of CVs

In this section, the time evolution for the CVs during the simulations (**S1**, **S2**, **S3**, **S4**, **S5** and **S6**), are depicted as function of the time (in ps).

S1 simulation:

Figure 1. Time evolution of the **S1** set of CVs.

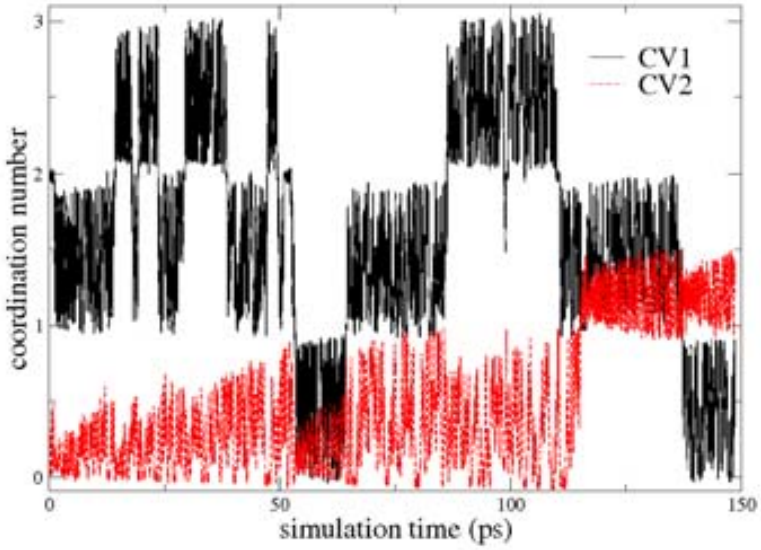

S2 simulation:

Figure 2. Time evolution of the **S2** set of CVs.

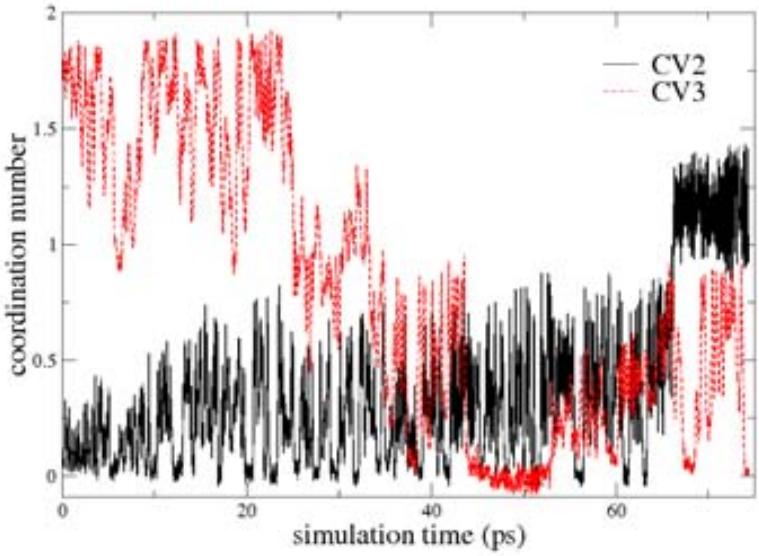

S3 simulation:

Figure 3. Time evolution of the **S3** set of CVs.

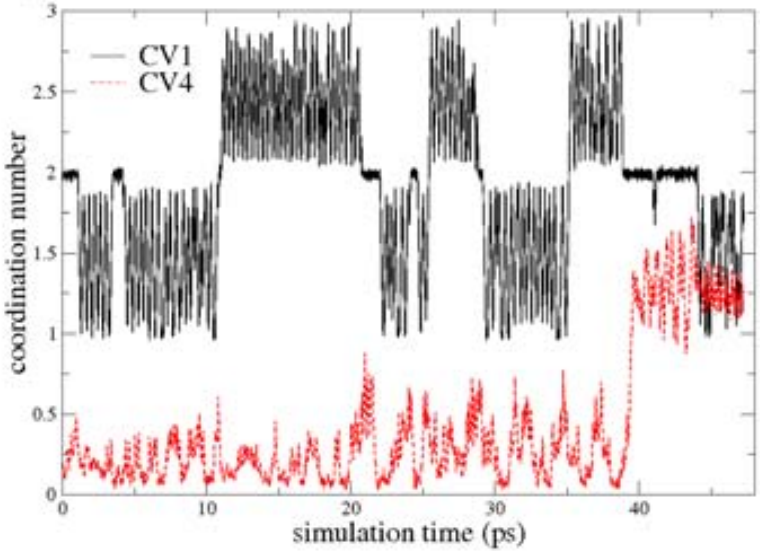

S4 simulation:

Figure 4. Time evolution of the **S4** set of CVs.

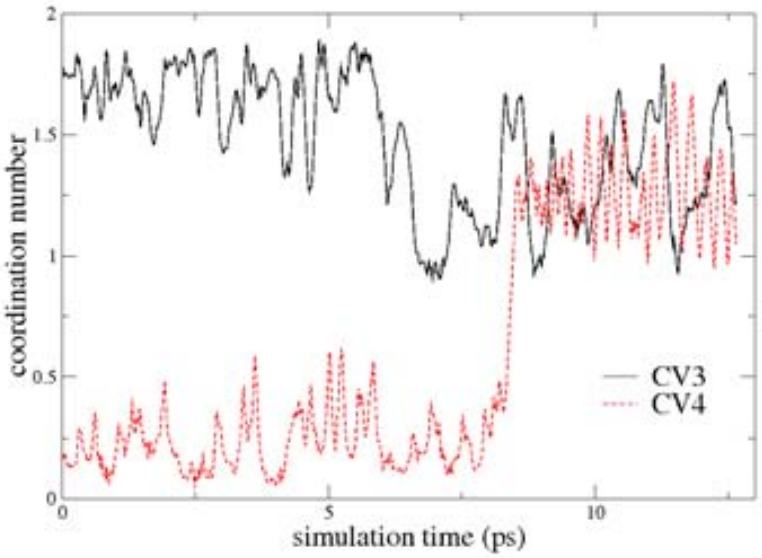

S5 simulation:

Figure 5: Time evolution of the s5 set of Cvs.

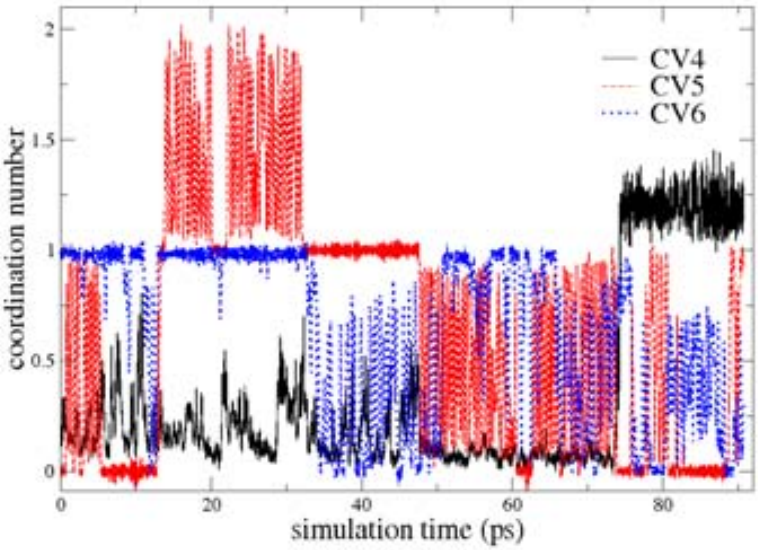

S6 simulation:

Figure 6. Time evolution of the **S6** set of CVs.

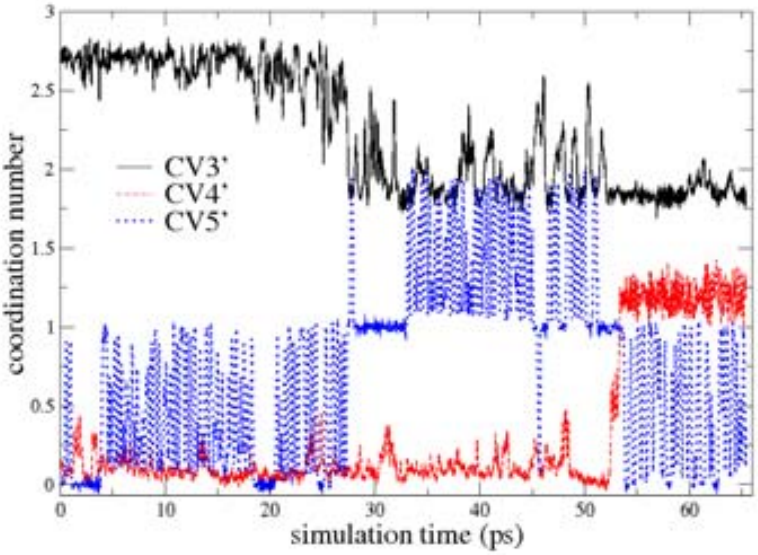

References

[1] R. Car, M. Parrinello, *Phys. Rev. Lett*. **1985**, *55*, 2471.

[2] A. D. Boese, N. Doltsinis, N. C. Handy, M. Sprik, *J. Chem. Phys*. **2000,** *112*, 1670.

[3] N. Troullier, J. L. Martins, *Phys. Rev. B* **1991**, *43*, 1993.

[4] CPMD v3.11. Copyright IBM Corp 1990-2007, Copyright MPI für Festkörperforschung Stuttgart 1997-2001.

[5] a) A. Laio, M. Parrinello, *Proc Natl. Acad. Sci. USA* **2002**, *20,* 12562; b) M. Iannuzzi, A. Laio, M. Parrinello, *Phys. Rev. Lett*. **2003**, *90,* 238302.

[6] A. Laio, A. Rodriguez-Fortea, F. L. Gervasio, M. Ceccarelli, M. Parrinello, *J. Phys. Chem. B* **2005**, *109*, 6714.

[7] M. Sprik, *Faraday Discuss*. **1988**, *110*, 437.